People's Democratic Republic of Algeria

Ministry of Higher Education and Scientific Research

Mentouri Brothers University of Constantine 1

Faculty of Natural and Life Science

Department of Applied Biology

Ph.D. School in Microbial and Bioprocess Biotechnology

in cotutelle with the University of Naples Federico II (Italy)

Department of Chemical Sciences

Ph.D. School in Chemical Sciences (XXXIII Cycle)

Order N°: 108/D3C/2021

Serial N°: 06/Bio/2021

A thesis submitted in fulfilment of the requirements for the degree of

Doctor of Philosophy

Potential bio-control substances produced by fungi and plants of different Mediterranean Basin ecosystems

Ph.D. Thesis

Presented by Roukia Zatout

In front of the committee:

President:

Khedara Abdelkrim — Pr. Mentouri Brothers University of Constantine 1

Supervisors:

Noreddine Kacem Chaouche — Pr. Mentouri Brothers University of Constantine 1

Antonio Evidente — Pr. University of Naples, Federico II

Examiners:

Marina Della Greca — Pr. University of Naples, Federico II

Lucia Panzella — Pr. University of Naples, Federico II

Rihab Boushaba — Pr. Salah Boubnider University, Constantine3

Academic year 2021-2022

Acknowledgments

First of all, I would like to thank ALLAH for all his support and guidance at every stage of my life and in this work.

I would like to thank my Algerian and Italian supervisors: Prof. Noreddine Kacem Chaouche, Prof. Antonio Evidente. I am grateful for their assistance, support, guidance, candidness, and encouragement that they provided to me throughout the duration my studies.

I would also like to extend my appreciation to Prof. Angela Lombardi coordinator of PhD school 33 Cycle, University of Naples Federico II.

My special thanks are to Prof. Alessio Cimmino and Dr. Marco Masi of University and University of Naples Federico II for their valuable suggestions, constructive discussions, and continuous encouragement.

I would too like to thank to all the members of my two laboratories: Laboratoire de Mycologie, de Biotechnologie et de l'Activité Microbienne (LaMyBAM), Université des Frères Mentouri, Constantine1 (Algeria), especially to Radia Cherfia for her help and support.

Laboratory Bioactive Natural Substance (SNAB), University of Naples Federico II, especially to Roberta Di Lecce.

The most important of all, I would like to thank my family, especially my mom and dad for their unconditional love and supports. You never said that I couldn't do anything, always supported my decisions, and had faith in my abilities. I love you.

I owe a great deal of thanks to other my family members for support and encouragement.

I am also grateful to my all my friends, especially to Nassima for standing by me in all stages of my life.

My partner Mohamed deserves specially honours for his immense support and encouraging me throughout the during all these years education.

Table of Contents

List of Tables

List of Figures

List of Abbreviation

AC	Absolut configuration
ACN	Acetonitrile
Ac_2O	Acetic anhydride
ANOVA	Univariate Analysis of Variance
A431	Epidermoid carcinoma
BLASTn	Basic Local Alignment Search Tool
CA	California
$CDCl_3$	Deuterated Chloroform
CH_2Cl_2	Dichloromethane
$CHCl_3$	Chloroform
C_6H_6	Benzene
CNR	National Research Council
COSY	Homonuclear Correlation Spectroscopy Sequence
$CDCl_3$	Deuterated Chloroform
DEPT	Distortionless Enhancement by Polarization Transfer
DFT	Density-functional theory
DMAP	4-Dimethylaminopyridine
DMSO	Dimethyl sulfoxide
DNA	Deoxyribonucleic Acid
ECD	Electronic Circular Dicroism
ESIMS	Electrospray ionization mass spectrometry
EtOAc	Ethyl Acetate
EtOH	Ethanol
FT-IR	Fourier Transform Infrared
GFFP	Glass fiber filter paper
H	Hours
^1H NMR	Proton Nuclear Magnetic resonance
H_2O	Water
HaCaT	Cultured Human Keratinocyte (cells)
HCl	Hydrochloric acid
HeLa B	Cervix adenocarcinoma
H1299	Nonsmall cell lung carcinoma
HMBC	Heteronuclear Multiple Bond Correlation
^1H NMR	**^{1}** Proton Nuclear Magnetic resonance
HPLC	High Performance Liquid Chromatography
HRESIMS	High resolution electrospray ionization mass spectrometry
HSQC	Heteronuclear Single Quantum Correlation
H_2SO_4	Sulfuric acid
IFAS	Institute of Food and Agricultural Sciences
i-PrOH	Iso-Propanol
IR	Infrared
ITS	Internal Transcriber Spacer
LC-MS	Liquid Chromatography Mass Spectrometry
LC/MS-MS	Liquid Chromatography tandem Mass Spectrometry
kcal/mol	Kilocalories per mole
MM	Molecular Mechanics

Me_2CO	Acetone
MeCN	Acetonitrile
MeOH	Methanol
MRM	Multi Reaction Monitoring
LC-MS	Liquid Chromatography Mass Spectrometry
MHz	Mega hertz
m/z	Mass over charge
$NaHCO_3$	Sodium hydrogen carbonate
Na_2SO_4	Sodium sulfate
NaOCl	Sodium hypochlorite
NOESY	Nuclear Overhauser Effect Spectroscopy
^{13}C NMR	Carbon-13 Nuclear Magnetic resonance
ORD	Optical rotatory dispersion
PCR	Polymerase Chain Reaction
PDA	Potato Destrose Agar
R_f	Retardation factor
RP-18	Liquid Chromatography Mass Spectrometry
rDNA	Ribosomal DNA
SDW	Steril Distilled Water
SMD	solvent model for acetonitrile
TLC	Thin Layer Chromatography
TOF	Time Of Flight
UK	United Kingdom
USA	United States of America
UV	Ultraviolet
WHO	World Health Organization
VCD	Vibrational Circular Dicroism
WI	Wisconsin
G	Gram
g/mL	Grams per milliliter
g/L	Grams per litre
^{1}H	Proton
Hz	Hertz
J	Coupling constant
mM -	Multiplet
min	Minutes
mg	Milligram
MHz	Megahertz
mL	Millilitres
µg	Microgram
µL	Microlitre
µM	Micrometre
mm	Millimetre
mol/L	Moles per litre
m/z	Mass to charge ratio
n.t	Not tested
NMR	Nuclear Magnetic Resonance
pH	Potential hydrogen

ppm	Parts per million
V	Volume
WHO	World Health Organisation
µL	Micro-litre
µm	Micro-meter
°C	Degrees celsius
δ	Chemical shift value in ppm
%	Percent
S	singlet
br s	broad singlet
dd	double doublet
ddd	doublet of double doublet
q	quartet
m	multiplet

General introduction

General introduction

Agriculture plays a central role in increasing food availability, needed to feed the ever-growing human population in the world that will reach almost 10 billion by 2050. This sector, therefore, has also an essential role in improving health outcomes (FAO, 2017; Evidente *et al*., 2019). Moreover, the agriculture is considered a key factor to improve both food and nutrition security, supporting livelihoods and contributing to the overall economy. It has also a direct impact on deforestation, air and water pollution and foodborne diseases.

Despite the significant progress made by the introduction of new technologies in agricultural practices (Mintesno, 2016; Tilman *et al*., 2011; FAO, 2017; Evidente *et al*., 2019), the biotic and the abiotic stresses are major constraints for plant growth, crop yield, food quality, and global food security right from the seed germination stage till the harvesting one.

The biotic agents responsible for infectious plant diseases include fungi, bacteria, viruses, nematodes, insects, weeds, and parasitic higher plants. On the other hand, the biotic stress is totally different from the abiotic one, which is imposed on plants by non-living factors such as salinity, sunlight, temperature, cold, floods and drought that have negative impacts on crop plants. Both stresses can determine heavy losses in the quality and the quantity of agrarian production (Oerke, 2006; Gull *et al*., 2019; Kenawy *et al*., 2019; Suryadi, 2019). Different biological, physical and/or chemical methods have been used to control crop losses caused by pests in the field (pre-harvest losses) and during the storage (postharvest losses) (Droby *et al*., 1989; Wilson and Wisniewski, 1989; Sharma *et al*., 2009). However, the main control method is the massive use of chemical pesticides with heavy environmental impact and consequent risk for human and animal health due to their transmission along the food chain (Tscharntke *et al*., 2012).

An alternative to chemical pesticides could be the use of natural compounds-based pesticides, which are eco-friendly and ideal for sustainable agricultural production with minimal damage to the environment and with no risk for human and animal health. Furthermore, these natural products play important roles in the ecology of many different types of organisms whose study can lead to the discovery of novel natural products with bioactivities of practical importance (Cutler, 1988; Rosegrant and Cline, 2003; Godfray *et al*., 2010; Cimmino *et al*., 2015a; Evidente *et al*., 2019).

The main aims of the present thesis have been the isolation as well as the chemical and the biological characterization of bioactive metabolites; with potential herbicidal and fungicidal activities; produced by fungi and plants of different Mediterranean Basin ecosystems in comparison by two phytopathogenic fungi; *Dreschlera gigantea* and *Macrophomina phaseolina*.

Chapter 1: Collection, extraction, and purification of bioactive metabolites from *Agaricus litoralis*

1.1- Introduction

Wild edible macrofungi have a long history of uses for their medicinal and nutritional properties (Wu *et al*., 2019; Zeb and Lee, 2021). Indeed, they have been consumed by people for thousands of years (Poucheret *et al.,* 2006; Zhang *et al*., 2015); for that, they considered one of the most prominent functional foods, whereby they are collected in the wild or in the cultivated worldwide (An-Qi *et al*., 2020).

In fact, many studies have demonstrated that macrofungi are good producers of a broad spectrum of high- and low-molecular-weight bioactive compounds such as polysaccharides, proteins, fats, phenolic compounds, and vitamins; possess strong biological activities (Badalyan and Rapior, 2020; Niego *et al*., 2021).

Due to the specific climatic conditions and the high floristic diversity, the forested area of Algeria is one of the northern Africa regions with higher edible macrofungi diversity. Despite of these later credible importances, only a few reports are known (Benazza-Bouregba, 2017). In fact, too little works have been carried out on the chemical composition and the bioactive compounds of the wild edible macrofungi in Algeria, especially in Djebel el Ouahech's forests of Constantine region. Thus, the two main aims of this chapter were; first of all to collect and to identify the edible wild macrofungi, in particular *Agaricus* spp. from the forests of Djebel el Ouahech of Constantine region- Algeria, and secondly, to isolate phytotoxic compounds from these reliably identified species.

1.2- Literature review

1.2.1- Macrofungi

Macrofungi are an important section of Fungi Kingdom, containing the most diverse eukaryotic and heterotrophic organisms on the earth (Boa, 2004; Mueller *et al.*, 2007). They play a critical role in the lives of plants, animals, and also human beings; yet their diversity is underestimated (Govorushko *et al.*, 2019; Hongyun *et al.*, 2020).

Larger fungi, usually referred to as macrofungi or macromycetes, including gilled fungi, jelly fungi, coral fungi, stink fungi, bracket fungi, puffballs, truffles, and birds nest (Enow, 2013). The most of macrofungi produce fleshy and colloidal fruiting bodies representing sexual reproductive structures; however, little macrofungi species, represent the asexual reproductive stage. Indeed, the most of these macrofungi belonging to the Basidiomycota or Ascomycota

phylum while the others, with a few numbers, are Zygomycota. Their fruiting bodies may be located above or below ground (Mueller *et al*., 2007; Govorushko *et al*., 2019).

Ecologically, the macrofungi are either saprophytes, parasites or symbiotics. The major of these later ones, symbiotics, are ectomycorrhizae that cannot be reproduced independently. Instead, their host partners are needed to help their dispersion and reproduction (Al-Thani, 2010). Nearly 14 000 macrofungal species have been identified worldwide, in which more than 2000 edible and/or medicinal macrofungi have been characterized (Meenu and Xu, 2019; Hongyun *et al*., 2020) such as *Agaricus* genus.

1.2.1.1- *Agaricus*

Agaricus L. is a genus of saprobic fungi within the order Agaricales (Basidiomycota) including more than 500 species worldwide particularly in the Asian countries, North America, Europe as well as in some part of Africa (Chang and Miles 1989; Zhao *et al*., 2011; Karunarathna *et al*., 2014; Gui *et al*., 2015; Kerrigan 2016; Zhao *et al*., 2016; Chen *et al*. 2019; An-Qi *et al*. 2020). This genus is common in various habitats, such as grassland and forests (Callac and Chen 2018). The species of *Agaricus* is characterized by a stipe detachable from the pileus provided with one or several annuli and free lamellae that produce brown basidiospores, odour often faint or fungoid, cheilocystidia frequently absent or hardly different from immature basidia (Parra 2008; Zhao *et al*., 2011). However, during the past decade, the taxonomy of *Agaricus* has been well developed using DNA-based phylogenetic methods (Zhao *et al*., 2011; Zhao *et al*., 2016; He *et al*., 2018; Parra *et al*., 2018; Chen *et al*., 2019). Later, the current taxonomic system includes six subgenera and 24 sections (Chen *et al*., 2017; Callac and Chen 2018; He *et al*., 2018; Parra *et al*., 2018). *A. litoralis* is one of *Agaricus* genus.

1.2.1.2- *Agaricus litoralis*

A. litoralis (Fig. 1), also known as the coastal mushroom, is a species of *Agaricus* genus mushroom. It was first described by Wakefield and A. Pearson as *Psalliota litoralis* in 1946 (Møller, 1950). The *A. litoralis* species grows most often in grassy places, dunes, steppes, it native throughout Europe (Scandinavia, Spain, Italy, France, Germany and Great Britain), along the coasts (England and Denmark), but is rarely found in most areas except for southern Europe. While it may be quite common locally, such as on Öland island (Cappelli, 1984; Courtecuisse and Duhem, 1994). *A. litoralis* is a white or grey-white mushroom with a compact cap that may

reach a width of up to 12 centimeters. Its cap is often depressed when older and rests of the *annulus* may occur on the outer rim. While rose-coloured at a young age, the *gills* become dark brown, as the mushroom grows older. Besides, the stem reaches 5–6 centimetres in height and 1.5–2 centimeters in width. It is often remarkably shorter than the cap. Its spores are usually dark brown and egg-shaped. The mushroom is saprotrophic; it feeds on decaying matter and prefers herbaceous dry grasslands (Møller, 1950; Cappelli, 1984; Parra, 2008).

Figure 1. *Agaricus litoralis*, Sociedad Micológicas (2017).

1.2.2- Fungi as a source of bioactive compounds

Fungi are one of the richest sources of secondary metabolites that have the potential for the discovery of new drugs and agrichemicals, including all important categories of natural products, terpenes, phenylpropanoids, polyketides, alkaloids, etc. (Dewick, 2009; Deshmukh *et al*., 2014; Cimmino *et al*., 2015; Evidente *et al*., 2019). These fungal metabolites could be used to formulate natural bio-pesticides (herbicides, fungicides, bactericides, insecticides, etc.) and several studies have already been conducted to understand the role of bioactive fungal metabolites and therefore to use them against specific diseases. As a result, many new phytotoxins, fungicides, antibiotics, and plant growth regulators, have been previously reported (Durbin, *et al.,* 1989; Strobel *et al*., 1991; Ballio *et al*., 1991; Décamps and Tabacchi, 1994; Evidente and Motta, 2001; Evidente and Motta, 2002; Evident *et al.*, 2019).

1.2.3- Bioactive metabolites produced by macrofungi

Macrofungi may play important roles in regulating the human gut microbiome (Giannenas *et al*., 2011; Chang *et al*., 2015; Li *et al*., 2019). This characteristic opens up new prospects for the application of macrofungi and their bioactive ingredients.

Macrofungi produce natural compounds with a broad spectrum of biological activities including; antimicrobial, antifungal, antiviral, anti-inflammatory, antioxidant, antidiabetic, antithrombotic, antitumor, anticancer, anticomplementary, anticoagulant, hypolipidemic, hepatoprotective, immunostimulant and immunological properties; which made them suited for their use in food, cosmetics, biomedicine, agriculture, environmental protection and wastewater management (Chang and Miles, 1989; Ha, Gerhauser *et al.*, 2000; Loria-Kohen *et al*., 2014; Kozarski *et al*., 2015; Abdullah, 2017).

The most important biologically active substances present in macrofungi are phenolics compounds, secondary metabolites that originate from the pentose phosphate, shikimate, and phenylpropanoid pathways. They have an aromatic ring bearing one or more hydroxyl groups (Balasundram, Sundram and Samman, 2006; Palacios *et al*., 2011). Phenolics play important roles in the ecology of many different types of organisms. Phytotoxins are one example of phenolics with a potential application in agriculture as natural herbicides, fungicides, bactericides, insecticides, etc.

1.3- Materials and Methods

1.3.1- Collection of Macrofungi

Fresh macro-fungi were collected during December 2017 and May 2018 from the forest of Djebel el Ouahch of Constantine region in the eastern of Algeria, which covers an area of 66,535 ha. It is included between 36°14'20, 19 "and 36°33'55,81" north latitude and between 6°38'0,82 "and 6°58'37,65" East of longitude (Boudy, 1955). A voucher specimen was deposited at the Herbarium of Université de Montpellier 2, Institut de Botanique, France. The fruiting bodies were dried under shade. The dried fruiting bodies were cut into small pieces using scalpels then crushed using a pistil and a motor to obtain a tiny powder.

1.3.2- Identification of *Agaricus* spp.

1.3.2.1- Morphological identification of *Agaricus* spp.

The morphological identification of macro-fungi was carried out at the Laboratory of Mycology, Biotechnology and Microbial Activity (LaMyBAM), Department of Applied Biology, University of the Mentouri Brothers, Constantine 25000, Algeria. The basidioma were photographed immediately in their natural habitat. General characters of fleshy mushroom were recorded in the field, like locality, date of collection, habitat, altitude, odour and color. The description was made from macrocharacters (shape, size and color of pileus, lamellae, ring, and stipe) (Cappelli 1984, Zhao *et al*., 2011, Courtecuisse and Duhem, 2013).

1.3.2.2- Molecular identification of *Agaricus* spp.

DNA extraction, amplification, and sequencing

Molecular identification was carried out at ALVALAB, Oviedo 33006, Spain. Total DNA was extracted from dry specimens employing a modified protocol based on Murray and Thompson (1980). PCR reactions (Mullis and Faloona, 1987) included 35 cycles with an annealing temperature of 54 ºC. Primers ITS1F (5'-TCC GTA GGT GAA CCT GCG G-3') and ITS-4 (5'-TCC TCC GCT TAT TGATAT GC3'), were employed to amplify the ITS rDNA region (White *et al*., 1990; Gardes and Bruns, 1993). PCR products were checked in 1% agarose gels, and amplicons were sequenced with one or both PCR primers. Chromatograms were checked searching for putative reading errors, and these were corrected. The obtained sequences were deposited in GenBank.

1.3.2.3- Phylogenetic analyses

***Phylogenetic Maximum Likelihood (ML) tree of Agaricus* spp.**

The phylogenetic tree was constructed using the Maximum Likelihood method and Tamura-Nei model (Tamura and Nei, 1993). The tree with the highest log likelihood (-1743.10) is shown. The percentage of trees in which the associated taxa clustered together is shown next to the branches. Initial tree(s) for the heuristic search was (were) obtained automatically by applying Neighbor-Join and BioNJ algorithms to a matrix of pairwise distances estimated using the Tamura-Nei model, and then selecting the topology with superior log likelihood value. The tree is drawn to scale, with branch lengths measured in the number of substitutions per site. This analysis involved 19 nucleotide sequences. There was a total of 650 positions in the final dataset. Evolutionary analyses were then conducted in MEGA X (Kumar *et al*., 2018).

1.3.3- Extraction and purification of secondary metabolites from *Agaricus* spp.

Fungal material (500 g) was extracted with MeOH-H_2O (1:1, v/v) under stirred conditions at room temperature for 24 h. The extract was centrifuged, and the supernatant was evaporated under reduced pressure to eliminate the methanol, however, the aqueous phase was extracted by EtOAc (3 × 400 mL), dried with Na_2SO_4 then evaporated under reduced pressure (Kimura and Tamura 1973).

The organic extract (170 mg) was purified by column chromatography on silica gel, eluted with $CHCl_3$-*i*-PrOH (8:2, v/v) affording 10 groups of homogeneous fractions. The residue (36 mg) of the third fraction was purified by preparative TLC eluted with $CHCl_3$-$_i$-PrOH (85:15, v/v), yielding the main metabolite as white solid (**1**, 5 mg, Fig. 5).

1.3.4- Phytotoxic assay

The phytotoxic activity of the crude extract and pure compound were assayed by the tomato leaf cutting and the leaf puncture with some modification, as reported in a previous work (Evidente *et al*., 1995; Fukushima *et al*., 1998; Andolfi *et al*., 2014).

1.3.4.1- *Tomato leaf cutting assay*

Tomato cuttings were taken from 21-day old seedlings, the tomato (*Lycopersicon esculentum* L.) leaves were placed in a tube containing 1 mL of compound solution. The EtOAc extract was dissolved in 40% of MeOH in sterile distilled water (SDW) and tested at 1 mg/mL.

Each treatment was repeated three times. The tomato leaves were also placed in a tube containing 1 mL of MeOH in distilled H_2O (4%) that was used as negative control. The results were observed after 28 h.

1.3.4.2- *Leaf puncture assay*

The phytotoxic activity of tyrosol was assayed by a leaf puncture on seven agrarian plants: eggplant (*Solanum melongena* L.), fig (*Ficus carica* L.), apricot (*Prunus armeniaca* L.), peach (*Prunus persica* (L.) Batsch), lemon (*Citrus limon* (L.) Osbeck), cucurbita (*Cucurbita* L.) and grapevine leaves (*Vitis vinifera* L.), as well as on two wild plant leaves: willow oak (*Quercus phellos* L.) and blackberry (*Rubus fruticosus* L.). All these plants were tested at 1 mg/mL.

The compound was dissolved in MeOH and diluted with distilled H_2O and brought up to a final concentration of 1 mg/mL; (the MeOH concentration was 4%). Droplets of the test solutions (20 µL) were applied on the axial side of leaves that had previously been needle punctured, an

additional droplet (20 µL) of MeOH in distilled H_2O (4%) were applied on leaves as controls. Each treatment was repeated twice, and the leaves were observed after 28 h.

1.4- Results and Discussions

1.4.1- Taxonomy of *Agaricus* spp.

The samples identification was based on their morphological observation and molecular analyses.

1.4.1.1- Macroscopic characteristics

Pileus 7–15 cm of diameter, at first hemispherical then plano-convex at maturity, surface whitish, then quickly grey-ochraceous-brownish, sometimes light brown, broken into brown scales at disc when mature; margin first involuted then appendiculate, entire, distinctly exceeding the lamellae when young. Lamellae free, tight, pale, then flesh-coloured, finally dark brown at maturity. Stipe short, robust, ventricose, almost smooth, with the base usually prolongated by one or more rhizoids. Annulus membranous, white, fragile, persistent, rather ample, upper side striate, lower side smooth, often torn and appendiculate at pileus margin. Contexts compact, thick, whitish, slightly reddening when cut especially towards stipe base. Odour of bitter almond. Taste mild, fungoid with printed brownish spore (Figure 2).

These precious characteristics can suggest the genus *Agaricus* to our macrofungus (Chang and Miles 1989; Zhao *et al*., 2011; Callac and Chen 2018).

1.4.1.2- Molecular identification

The DNA sequence analysis of the IST region were used for molecular identification of the studied macrofungus;

The BLAST result was obtained by comparing partial nucleotide sequences to the GenBank database (Table 1). The sequences matched those of *Agaricus litoralis*; % identity 99.72 (i.e. JF727867.1) from France. The phylogenetic analysis (Figure 3) confirms the monophyly of the clade encompassing the Algerian sequence and the MW165560.1 sequence identified as *A. litoralis* in GenBank.

This is the first published record of *Agaricus litoralis* in Djebel el Ouahch forest (Constantine, East Algeria). *Agaricus litoralis* is a rare species in Algeria, growing on grass- and herb-rich dry meadows, on grazed, and steppe dry meadows with plenty of juniper bushes.

Wakefield and Pearson first described this species as *Psalliota litoralis* (Pearson, 1946) in Britain. It has mostly been reported from Europe, especially Scandinavia and Great Britain, but also under other names (*Agaricus spissicaulis* F.H. Møller from Denmark, *Agaricus maskae* from the Czech Republic (Møller, 1950; Pilát 1954). While, it may be quite common locally, such as on Öland and Gotland islands, it is rarely found in most areas except southern Europe. The genus *Agaricus* is significantly diversified in Europe and poorly documented so far in the Mediterranean regions. Ist species *Agaricus litoralis*, morphologically similar to *Agaricus arvensis* and *Agaricus crocodilinus*, has been already collected but misidentified in North Africa (Malencon and Bertault, 1970; El Kholfy *et al*., 2011) reported it from Morocco (as *Agaricus spissicaulis*).

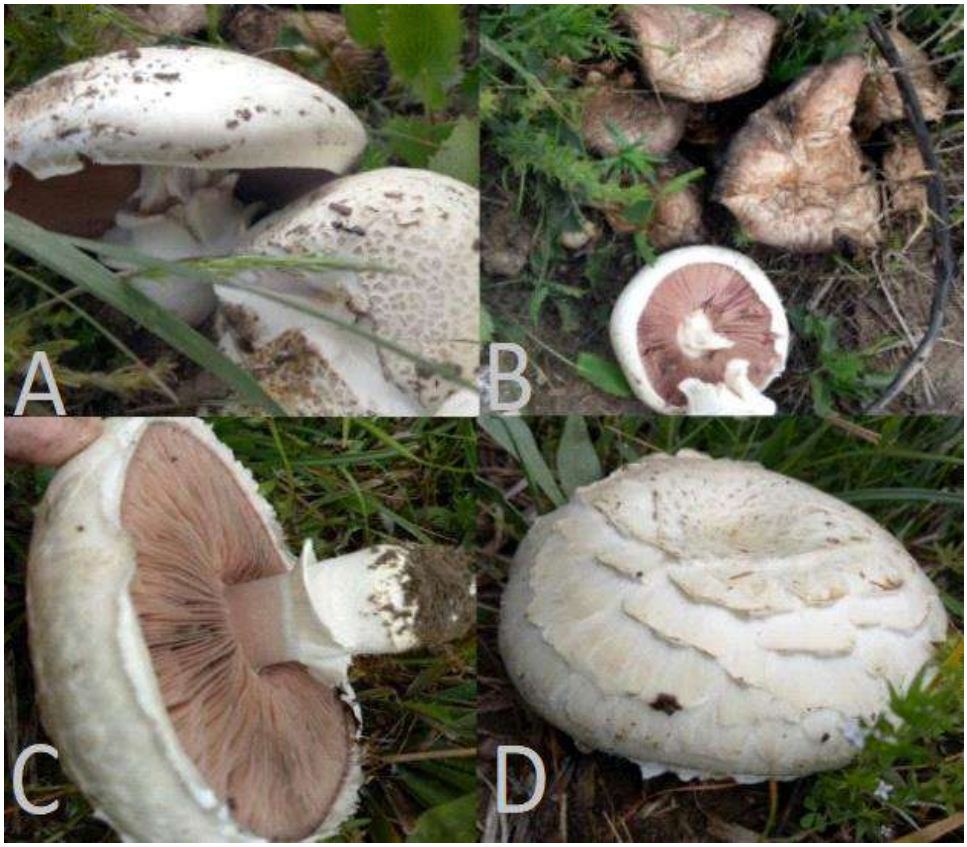

Figures 2. **A-D** *Agaricus litoralis* (Zatout, 2018); A. Basidiomata in the field; B. Mature basidiomata; C. Lamellae and stipe with annulus; D. Pileus surface.

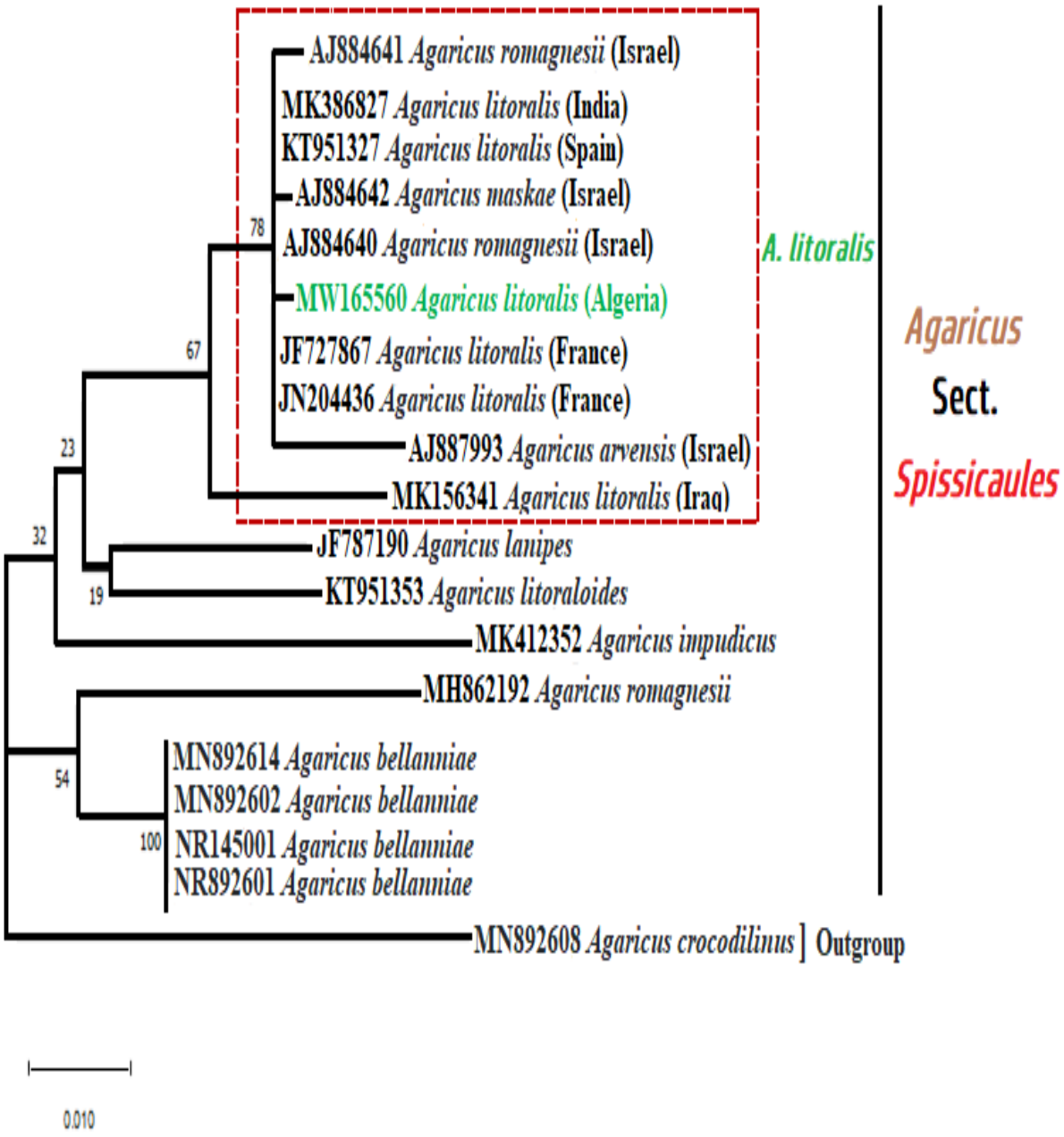

Figure 3. Phylogenetic Maximum Likelihood (ML) tree of *Agaricus litoralis*.

Table 1. List of used specimens in molecular phylogenetic studies and their GenBank accession numbers. The strain of the current study is in bold.

Species name	Specimen or strain Id	GenBank accession No	Origin	References
Agaricus romagnesii	792	AJ884641	Israel	Didukh *et al*., 2005
Agaricus litoralis	YM-19	MK386827	India	Farooq *et al*., 2019
Agaricus litoralis	LAPAG420	KT951327	Spain	Zhao *et al*., 2016
Agaricus maskae	816	AJ884642	Israel	Didukh *et al*., 2005
Agaricus romagnesii	791	AJ884640	Israel	Didukh *et al*., 2005
Agaricus litoralis	**ZRDO25**	**MW165560**	**Algeria**	**this study**
Agaricus litoralis	CA829	JF727867	France	Callac and Moinard, 2011
Agaricus litoralis	CA120	JN204436	France	Callac and Moinard, 2011 Zhao *et al*., 2012
Agaricus arvensis	15	AJ887993	Israel	Didukh *et al*., 2005
Agaricus litoralis	RA44	MK156341	Iraq	Rukaibaa *et al*., 2018
Agaricus lanipes	CA406	JF797190	France	Callac and Moinard, 2011
Agaricus litoraloides	ZRL2011249	KT951353	China	Zhao *et al*., 2016
Agaricus impudicus	GLM:GLM-F39352	MK412352	Germany	Eberhardt and Schuessler, 2019
Agaricus romagnesii	CBS 623.89	MH862192	India	Vu *et al*., 2019
Agaricus bellanniae	S.D. Russell MycoMap #1591	MN892614	USA	Russell, 2019
Agaricus bellanniae	S.D. Russell MycoMap #964	MN892602	USA	Russell, 2019
Agaricus bellanniae	RWK_2008	NR145001	USA	Kerrigan, 2016
Agaricus bellanniae	S.D. Russell MycoMap #1698	MN892601	USA	Russell, 2019

1.4.2- Structural identification of secondary metabolites from *Agaricus litoralis*

The EtOAc extract obtained from *A. litoralis* was purified by combination of column chromatography and TLC, as detailed in the Experimental Section, yielding a known metabolite which was identified as tyrosol (Figure 5). Its chemical structure was confirmed by comparing its spectroscopic analysis (^{1}H-NMR and ESI MS) data with those reported in literature (Kimura and Tamura 1973; Capasso *et al*., 1992; Cimmino *et al*., 2017; Masi *et al*., 2020).

1.4.2.1- Tyrosol (1)

Tyrosol, obtained as an amorphous solid, had: ^{1}H NMR (400 MHz, in $CDCl_3$) δ 7.10 (d, *J*=8.2 Hz, H-2 and H-6), 6.79 (d, *J*=8.2 Hz, H-3 and H-5), 3.82 (t, *J*=6.6 Hz, H2-8), 2.80 (t, *J*=6.6 Hz, H2-7); ESIMS (+) *m/z* 299 $[2M+Na]^+$, 161 $[M+Na]^+$. These data agree with those previously reported (Kimura and Tamura 1973; Capasso *et al*., 1992; Cimmino *et al*., 2017; Masi *et al*., 2020).

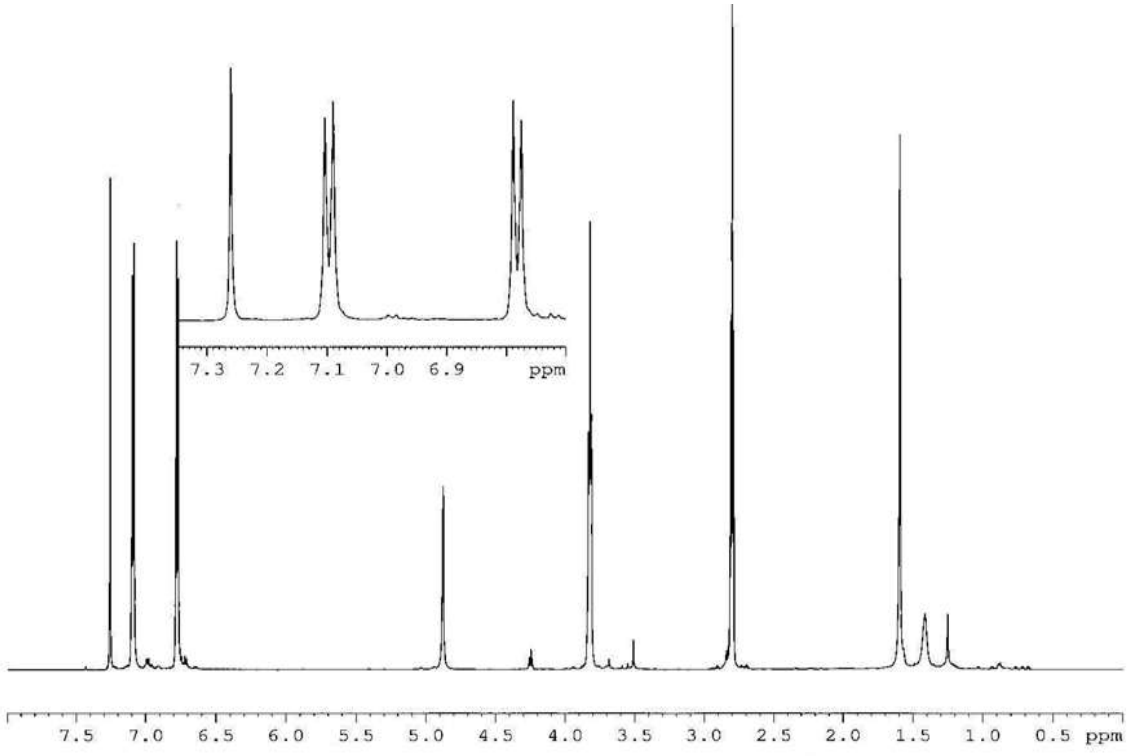

Figure 4. ^{1}H NMR spectrum recorded in $CDCl_3$ at 400 MHz.

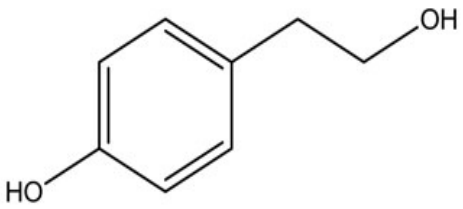

Figure 5. Structure of tyrosol (**1**) isolated from *Agaricus litoralis*.

Tyrosol, is a ubiquitous secondary metabolite that has been found in plants (Capasso *et al*.,1992), bacteria (Bouallagui and Sayadi, 2006), and fungi (Masi *et al*., 2018a). Moreover, tyrosol has been considered well-known metabolite that has various biological activities (Di Benedetto, 2007), including the phytotoxicity.

1.4.3- Phytotoxic assay

Two bioassays were used to investigate the phytotoxic activity of *A. litoralis* organic extract and tyrosol. The EtOAc extract was tested at 1 mg/mL by tomato cuttings bioassay and using a leaf puncture assay on tomato (*Lycopersicon esculentum* L.) leaves. In both bioassays, the EtOAc extract obtained from *A. litoralis* exhibited strong phytotoxicity activity.

The phytotoxic activity of tyrosol was evaluated at 1 mg/mL by leaf puncture assay on seven agrarian plants (eggplant, fig, apricot, peach, lemon, cucurbita and grapevine) and two wild plants leaves (willow oak and blackberry). In fact, tyrosol was active in this assay by causing a necrosis in all plants except willow oak in wild plants leaves. This compound showed the highest toxic effect on grapevine, apricot, peach, cuccurbita and blackberry, while moderately toxic on the eggplant leaves. Tyrosol also appeared with low phytotoxicity on fig and lemon leaves (Fig. 6 and Table 2).

Recently, tyrosol was also identified as a phytotoxic metabolite produced by several fungi which act as pathogens for agrarian (Evidente *et al*., 2019), and forest plants (Masi *et al*., 2018a).

In fact, its phytotoxic activity on faba bean, legume, tomato (Evidente *et al*., 2010), grapevine (Reveglia, 2019), marigold, pricklysida and lamb's quarters was previously reported (Venkatasubbaiah *et al*., 1992; Gamboa-Angulo, 2001). Tyrosol has showed different biological activities and is also reported as a quorum sensing molecule in *Candida albicans*, controlling growth, morphogenesis, and biofilm formation (Albuquerque and Casadevall, 2012).

Table 2. Level of toxicity induced 28 h after treatment on leaves of different agrarian and wild plants by tyrosol compound produced by *Agaricus litoralis*.

Compound	**Level of toxicity** [a]								
Tyrosol	Apricot	Grapevine	Cucurbita	Lemon	Peach	Fig	Willow-oak	Eggplant	Blackberry
	3	3	3	1	3	1	0	2	3

[a] Severity scale: 0. no symptoms; 1. wilting; 2. necrotic spots; 3. severe necrotic; 4. severe necrosis and shrivelling.

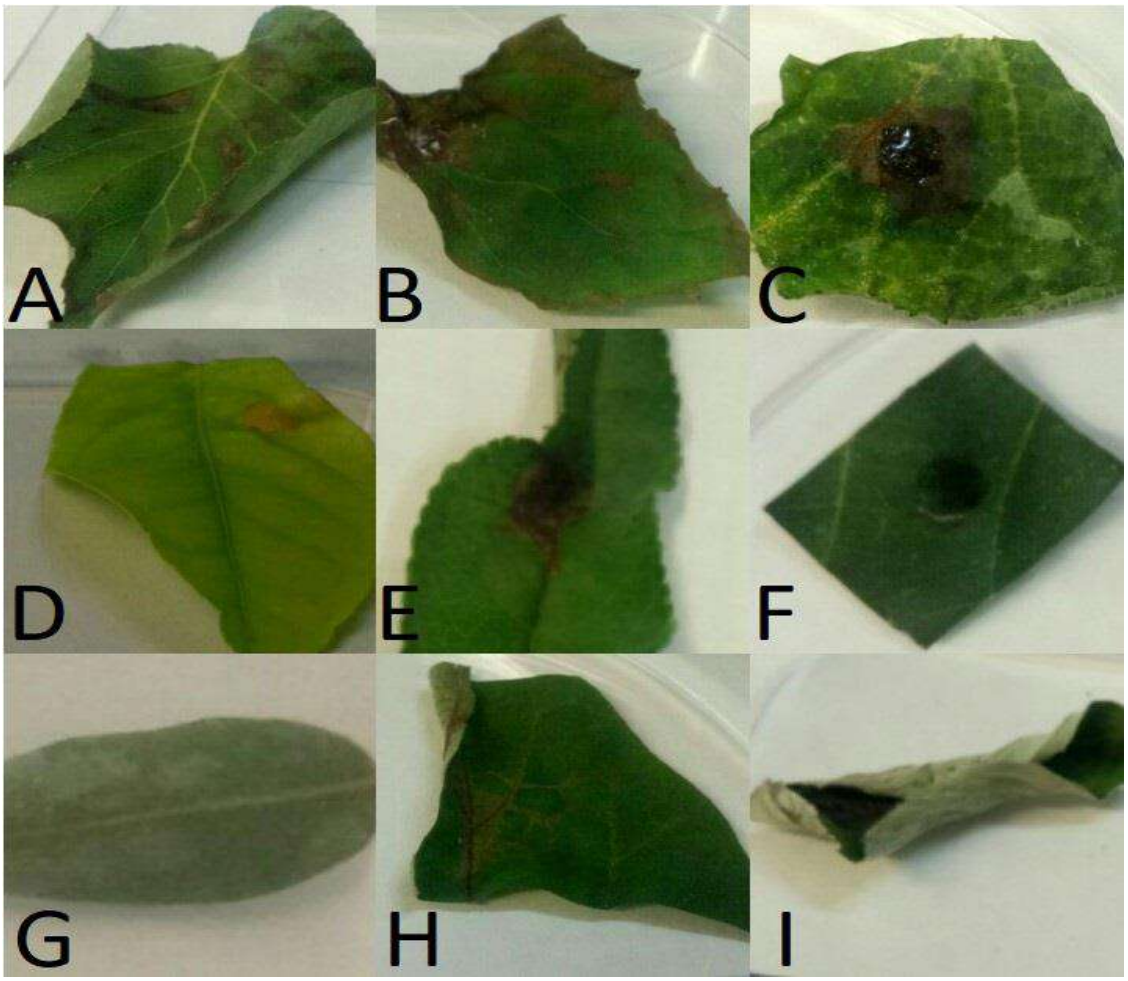

Figures 6. A – I Phytotoxic effect of tyrosol on leaves of different agrarian and wild plants at a concentration of 1 mg/mL after 28 h. (A) apricot; (B) grapevine; (C) cucurbita; (D) lemon; (E) peach; (F) fig; (G) willow oak; (H) eggplant; (I) blackberry.

Chapter 2: Collection, extraction, and purification of bioactive metabolites from *Dittrichia viscosa*

2.1- Introduction

Weeds are one of the main reasons affecting modern agriculture and their management is one of the most troublesome, expensive and labor-consuming of the agricultural practices (Boari *et al*., 2021).

The broomrapes (*Orobanche* and *Phelipanche* spp.) are obligate, chlorophyll-lacking, root parasitic weeds that obtain all their nutrient resources by attacking crops inflicting high yield losses in many parts of Europe, Asia, and Africa. *Orobanche cumana* is one of the most virulent broomrape weeds highly specialized attacking sunflower. *Phelipanche ramosa* and *Orobanche minor* have broader host ranges infecting not only many crops, but also their associated non-parasitic weeds and other wild plants. The underlying cause in such host range variation is often due to adaptation to the specific germination stimulants exuded by roots of their hosts (Fernández-Aparicio *et al*., 2009; Fernández-Aparicio *et al*., 2011). Moreover, when the crop plant is already infected by these weeds the use of herbicides is the only option, but the repetitive use of traditional chemical herbicides can reduce the health value of crops and increase the risk of emergence of herbicide resistances in the weed. Therefore, there is need for a diversification on efficient alternatives to conventional broomrape control to achieve sustainable plant protection programs (Fernández-Aparicio *et al*., 2016; Perotti *et al*., 2020). *Dittrichia viscosa* (L.) Greuter, a native and spontaneous Mediterranean plant, produces several bioactive compounds, some of which have phytotoxic and allelopathic effects causing inhibition of seed germination and plant growth, or necrosis of leaves (Andolf *et al*., 2013; Boari *et al*., 2021). For exmaple, four bi- and tri-cyclic sesquiterpene lactones named inuloxins A, B, C and D, together with the known a-costic acid isolated from *Dittrichia viscosa*, with potential herbicidal activity against the parasitic weeds *O. crenata*, and *C. campestris*. In addition, a-costic acid had a suppressive effect on the dodder seed germination but had a stimulating action on the broomrape seed germination. Considering its interesting activity, further studies are planned on of the absolute configuration (AC) of inuloxins A, B, C and D. The aims of this chapter are to: extraction, and purification of bioactive metabolites from *Dittrichia viscosa;* identification of the already known metabolites; chemical and biological characterization of new metabolites; assignment of relative and absolute configurations; preparation of hemisynthetic derivatives of some metabolites; biological activities.

2.2- Literature review

2.2.1- Plants as source of bioactive compounds

Plants produce a vast and diverse assortment of secondary metabolites. These substances are often differentially distributed among limited taxonomic groups within the plant kingdom. Estimation of the amount of identified plant species is now around 374,000, including 295,383 species of flowering plants (Christenhusz and Byng, 2016).

The primary metabolites, in contrast, such as phytosterols, acyl lipids, nucleotides, aminoacids, and organic acids, are found in all plants and perform metabolic roles that are essential and usually evident (Hussain *et al*., 2012). Although noted for the complexity of their chemical structures and biosynthetic pathways, secondary metabolites based natural products have been widely perceived as biologically insignificant and have historically received little attention from most plant biochemists (Parsaeimehr *et al*., 2011; Hussain *et al*., 2012).

The study of secondary metabolites in plants is an important source for the discovery of bioactive compounds with a wide range of applications such as drugs or agrochemicals (Grindberg *et al*., 2011).

2.2.1.1- *Dittrichia viscosa*

Dittrichia viscosa (L.) Greuter (sin. *Inula viscosa* (L.) Aiton) (Figure. 6) is an evergreen, belonging to the Compositae family (*Asteraceae*). The name *Dittrichia* comes from the German botanist Manfred Dittrich, who reclassified this genus, while the name *viscosa* is a Latin word meaning sticky to touch, mainly referring to the sticky exudate from the glandular hairs of the plant (Anderberg, 1991; Brullo and De Marco, 2000; Pelser *et al*., 2010).

D. viscosa is a highly branched, small shrub common throughout the Mediterranean Basin, native to the coasts of southern Europe (France, Spain, Greece, Italy, Bulgaria) and Turkey, the Middle East (Israel, Jordan and Syria) as well as northern Africa (Algeria, Egypt, Libya). It is well adapted to disturbed open situations and dry ecosystems.

In fact, it is established in the Azores, Belgium, and Great Britain. In Western Australia it is considered a serious environmental weed marked for eradication and prohibited import to Australia (DPIPWE, 2011; Sladonja *et al*., 2021).

It is a perennial shrub plant, has long, narrow leaves that are pointed at both ends. These leaves, linear-lanceolate, are rough and green in colour with the upper part richly covered with hairs and glands. The sticky exudate from the glandular hairs diffuses an unpleasant smell. This sticky exudate contains essential oil. The pyramidal inflorescence is composed of numerous flower heads with golden-yellow flowers. Flowering occurs in autumn, while the fruits consist of achenes. The species is very resistant to adverse abiotic conditions common in degraded environments like frequent cutting, fire, drought, and nutrient poor soil (Parolin *et al*., 2014). It is important as food for the caterpillars of certain butterflies, moths as well several parasitoids of economically important pests (Kavallieratos *et al*., 2002).

Figure 7. *Dittrichia viscosa*

2.2.2- Metabolites from *Dittrichia viscosa*

Dittrichia viscosa is a species known for the presence of several classes of metabolites that are responsible of the biological properties such as flavonoids, sesquiterpene lactones and acids and triterpenoids (Lauro *et al*., 1990; Grande *et al*., 1992; Staurianakou *et al*., 2004; Gum *et al*., 2007; Dor and Hershenhorn *et al*., 2012; Sladonja *et al*., 2021).

The most typical metabolites of this species are the sesquiterpene acids and lactones. Among these, α-costic acids showed different activities while sesquiterpene, inuviscolide and tomentosin induced apoptosis of human melanoma cells (Rozenblat *et al*., 2008) as well as manifesting anti-inflammatory, antioxidant, antibacterial and antifungal activity (Schinella *et al*., 2002; Abrham *et al*., 2010). Moreover, α-costic acid and inuloxins A-D (Figure. 8)

isolated from leaves, aerial parts, and whole plants of *D. viscosa* plant have demonstrated the ability to inhibit *Orobanche crenata* and *Cuscuta campestris* seed germination. Successively, inuloxin A and α-costic acid induced significant germination of *O. cumana* seeds while inuloxin C induced a phytotoxic effect on four broomrapes being the length of radicles exposed to this compound shorter and with light brown patches (Andolfi *et al*., 2013; Cimmino *et al*., 2014).

Considering that the absolute configuration (AC) of naturally occurring compounds is close related to their biological activity (Evidente *et al*., 2011; Evidente *et al*., 2013) the AC of inuloxin A, the main germacrane sesquiterpene isolated from *D. viscosa*, was determined by chiroptical and computational methods (Santoro *et al*., 2015). The same methods were successively used to assign the AC to the eudesmanolide inuloxin C (Johnson *et al*., 2018). Studies were carried out to investigate the potential fungicidal from *D. viscosa* against some pathogens of agricultural interest, including cucumber, tomato, potato, wheat and sunflower (Wang *et al*., 2004).This plant has also allelopathic potential and, in particular, its extracts caused phytotoxic effects on several species, inhibiting roots and causing root anatomical abnormalities (Aşkin Çelik and Aslantürk, 2010).

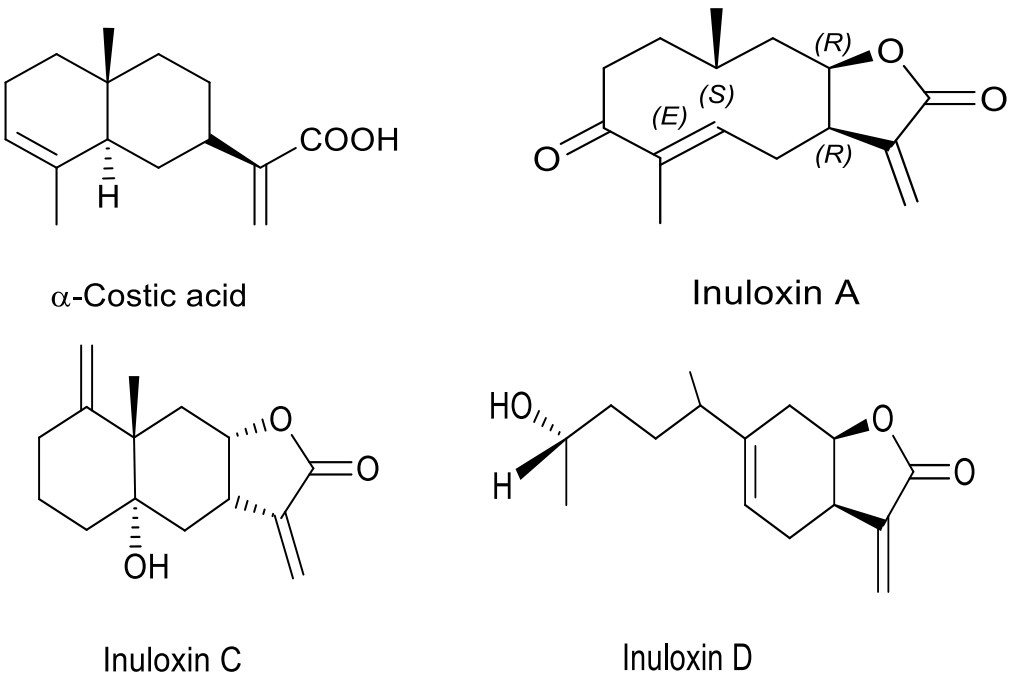

Figure 8. Some metabolites produce by *Dittrichia viscosa*

2.3- Materials and Methods

2.3.1- Collection of *Dittrichia viscosa*

The *D. viscosa* species was collected fresh in Southern Italy. A voucher specimen was deposited at the Colletion of Istituto di Scienze delle Produzioni Alimentari, CNR, Bari, Italy. After harvesting, leaves were detached from the stems and dried in a ventilated oven at 50 °C for two days. The plant material was then grinded to obtain a tiny powder by using a lab mill and packaged in plastic bags under vacuum until its use.

2.3.2- General Experimental Procedures

Optical rotation was measured in $CHCl_3$ solution by a P-1010 digital polarimeter (Jasco, Tokyo, Japan). IR spectra were recorded as deposit glass film on a Thermo Nicolet 5700 FT-IR spectrometer (Madison, WI, USA). UV spectra were measured in MeOH on a V-530 spectrophotometer (Jasco, Tokyo, Japan). ^{1}H and ^{13}C NMR spectra were recorded at 400 and 100 MHz, respectively, in $CDCl_3$ by Bruker spectrometers (Karlsruhe, Germany). The same solvent was used as internal standard. Carbon multiplicities were determined by DEPT spectra (Berger and Braun, 2004). DEPT, COSY-45, HSQC, HMBC and NOESY experiments (Pretsch *et al*., 1987) were performed using Bruker microprograms. HR ESIMS and ESIMS were recorded using LC/MS ESIMS-TOF system (Agilent 6230B, HPLC 1260 Infinity) (Milan, Italy). The HPLC separation were performed using a Phenomenex LUNA (C18 (2) 5u 150 x 4.6 mm) (Torrance, CA, USA). Analytical, preparative and reverse phase TLCs were carried out on silica gel (Merck, Kieselgel 60, F254, 0.25, 0.5 mm and RP-18 F254s respectively) plates (Merck, Darmstadt, Germany). The spots were visualized by exposure to UV radiation, or by spraying first with 10% H_2SO_4 in MeOH, and then with 5% phosphomolybdic acid in EtOH, followed by heating at 110°C for 10 min. Column chromatography was performed using silica gel (Kieselgel 60, 0.063-0.200 mm) (Merck, Darmstadt, Germany).

2.3.3- Extraction, and Purification of secondary metabolites from *Dittrichia viscosa*

Plant material (450 g) was extracted (1 × 1 L) with H_2O/MeOH (1:1, v/v) under stirred conditions at room temperature for 24 h. The suspension was then centrifuged, and the supernatant was extracted by CH_2Cl_2 (3 × 400 mL). The organic extracts were combined, dried with Na_2SO_4 and evaporated under reduced pressure, giving a brown–red oily residue (17 g) (Andolfi *et al*., 2013). This latter was chromatographed by silica gel column eluted

with $CHCl_3$-*i*-PrOH (95:5, v/v), obtaining nine groups of homogeneous fractions. The second and third fractions, contained the main metabolites. The residues of these two fractions were combined and purified by a RP-18 column at medium pressure, using system solvent B, giving three fractions. The two lesser polar fractions, both obtained as homogeneous yellow oil, contained the main metabolite identified as α-costic acid (**2**, 400 mg, Figure 9) and another oily homogeneous metabolite, which was named inuloxin A (**3**, 105 mg, Figure 9). The residue (1.1 g) of fifth fraction was further purified in the same conditions above reported giving seven homogeneous fraction groups. The residue (36.8 mg) of the first fraction of the latter column was purified by preparative TLC using EtOAc-*n*-hexane (6:4, v/v) giving both inuloxins E and D as pure oils (**6**, 11.6 mg, *Rf* 0.65 and **5**, 5.8 mg, *Rf* 0.48, Figure 9) and inuloxin C (**4**, 11.0 mg, *Rf* 0.40, Figure 9).

2.3.3.1- Preparation of Hemisynthetic Derivatives of Inuloxin D

2.3.3.1.1- *4*-O-*Acetyl Derivative of Inuloxin D* (7)

Inuloxin D (**5**, 2 mg), dissolved in pyridine (40 µL), was converted in its corresponding acetyl ester (**7**) by acetylation with Ac_2O (40 µL). The reaction was carried out under stirring for 1 hour at room temperature. It was stopped with MeOH and the azeotrope that was formed by addition of C_6H_6 was evaporated under nitrogen stream. The residue was then purified by TLC eluted with $CHCl_3$/*i*-PrOH (98:2, v/v) yielding (7, 1.2 mg) as an amorphous oil.

2.3.3.1.2- *4*-O-*Azidopentanoyl Ester of Inuloxin D* (8)

Then, 5.0 mg of DCC and 15 µL of 5-azidopentanoic acid were added to a solution of inuloxin D (**5**, 2.0 mg) in pyridine (100 µL). The mixture was kept under stirring at room temperature 24 h and reaction stopped by addition of C_6H_6 and MeOH and was dried under nitrogen stream. The residual oil was then purified by TLC eluted with $CHCl_3$, affording 5-azidopentanoyl ester of inuloxin D (**8**, 1.5 mg).

2.3.3.1.3- *4*-O-*Mesyl Ester of Inuloxin D* (9)

Mesyl chloride (25 µL) was added to inuloxin D (**5**, 2.0 mg), which was dissolved in CH_2Cl_2 (300 mL) and pyridine (40 µL). The reaction was carried for 2 hours at room temperature. It was stopped with MeOH, and the azeotrope formed by addition of C_6H_6 was evaporated under nitrogen stream. The residue was then purified by TLC eluted with $CHCl_3$ yielding (**9**) (1.2 mg) as an amorphous oil.

2.3.3.1.4- *4*-O-*p*-*Bromobenzoylester of Inuloxin D* (10)

DMAP (5.0 mg) and *p*-bromobenzoyl chloride (5.0 mg) were added to inuloxin D (**10**, 2.0 mg), which was dissolved in anhydrous MeCN (100 µL). The reaction mixture was left under stirring for 4 hours. It was then quenched with a 1N $NaHCO_3$ and extracted with CH_2Cl_2. The residue obtained after solvent evaporation was purified by preparative TLC and was eluted with $CHCl_3$ to afford the *p*-bromobenzoyl ester of inuloxin D (**5**, 0.9 mg).

2.3.4- Biological assays

2.3.4.1- Germination Induction Bioassays

Germination activity of inuloxin D, inuloxin E and inuloxin D derivatives was assayed on *Orobanche cumana*, *Orobanche minor* and *Phelipanche ramosa*. Seeds were surface sterilized by immersion in 0.5% (*w/v*) NaOCl and 0.02% (v/v) Tween 20, and sonication for 2 min, and then rinsed thoroughly with sterile distilled water, and dried in a laminar air flow cabinet. Approximately 100 seeds of each broomrape species were placed separately on 9 mm diameter glass fiber filter paper disks (GFFP) moistened with 50 µL of sterile distilled water. Subsequently, GFFP disks were placed inside sterile 10 cm Petri dishes, sealed with parafilm, and conditioned for 7 days at 22 °C in the dark.

Tested samples, dissolved in acetone, were diluted with sterilized distilled water to a final concentration of 10^{-4} M. The final concentration of acetone was adjusted to 0.70% (v/v). GFFP disks containing conditioned seeds were transferred inside laminar flow cabinet to sterile filter paper to remove excess water, and then transferred to a new 10 cm sterile Petri dish. For each broomrape species, 50 µL-aliquots of each test solution were applied to three disks containing conditioned seeds. Seeds treated with distilled water (containing 0.70% acetone) or the synthetic strigolactone GR24 were included as controls for comparison. The seeds were incubated in the dark at 22 °C for 7 days prior to examination for germination. Seeds with an emerged radicle were scored as germinated using a stereoscopic microscope at 30 × magnification, and the percentage of germination was established for each dish.

2.3.4.2- Germination and Growth Inhibition Bioassays

The inhibitory activity of inuloxins D and E on seed germination and radicle growth of *O. cumana*, *O. minor*, and *P. ramosa* was assayed as reported previously (Fernández-Aparicio *et al*., 2013). A solution of the GR24 (10^{-6} M) was prepared in sterile distilled water.

Immediately before use, stock solutions of each inuloxin prepared in acetone were diluted in the GR24 solution to 10^{-4} M of each toxin while keeping constant the GR24 concentrations and acetone in order to allow comparisons.

Broomrape seeds were surface sterilized and conditioned, as described above. Fifty microliter aliquots of each inuloxin-GR24 were applied to each GFFP disk containing the seeds. Petri dishes were sealed with Parafilm and were stored in the dark at 22 °C for 7 days to promote germination and radicle growth. The percentage of seeds germination and radicle growth were established for GFFP disk in order to score levels of inuloxin-mediated inhibition. The germination percentage was determined by scoring the number of seeds with an emerged radicle through the seed coat in a total 100 seeds per disc. Radicle length was measured in 15 randomly selected germinated seeds from each disc.

2.3.5- Statistical analysis

The bioassays were performed twice with three replicates. Percentage data were approximated to normal frequency distribution by means of angular transformation (180/π × arcsine (sqrt [%/100])) and were subjected to analysis of variance (ANOVA) using SPSS software for Windows, version 21.0 (SPSS Inc., Chicago, Illinois, USA). The significance of mean differences between each treatment against its respective control was evaluated by the two-sided Dunnett test. The Null hypothesis was rejected at the level of 0.05.

2.3.6- Absolute configuration of inuloxin D

ECD, VCD and ORD were measured for 4-*O*-acetyl derivative (**7**) which was obtained by common acetylation of Inuloxin D (**5**) with pyridine and acetic anhydride as detailed previously reported (Fernández-Aparicio *et al*., 2011). ECD spectra were measured using Jasco J810 spectrometer in MeCN solvent with 1 cm path length at concentration $4.4x10^{-5}$ M. VCD spectra were measured using Chiral IR instrument in deuterated chloroform solvent with 100 μm path length at concentration $3.07x10^{-1}$ M. ORD was measured using Autopol IV polarimeter in $CHCl_3$ solvent with 0.5 dm path length at concentration $3.55x10^{-3}$ g/mL at six discrete wavelengths (633, 589, 546, 436, 405, and 365 nm).

The initial conformational searches were undertaken within a 20 kcal/mol energy window using CONFLEX program (Frisch *et al*.,16) for diastereomers of (**7**). Subsequent geometry optimizations and spectral calculations were undertaken with Gaussian 16 (Scalmani *et al*.,2010). All the conformers of diastereomers of (**7**) obtained with CONFLEX were optimized at PM6 level. All unique conformers obtained in PM6 optimization were then

optimized at B3LYP/ 6-31G* level. The unique conformers of diastereomers of (**7**) were optimized further at B3LYP/ 6-311++G(2d,2p) level. The lowest energy (within 2 kcal/mol) unique conformers of (**7**) at this level were further optimized at B3LYP/ 6-311++G(2d,2p) level with polarizable continuum model (PCM) (Tomasi *et al*., 2005; Polavarapu *et al*., 2021) for $CHCl_3$ solvent. ECD, VCD, and ORD calculations for these conformers of (**7**) were then carried out at B3LYP/ 6-311++G(2d,2p) / PCM($CHCl_3$) level, except for ECD calculations which utilized the CAM-B3LYP functional and PCM for CH_3CN. The specific optical rotation (SOR) predicted at 633, 589, 546, 436, 405, and 365 nm was used to generate ORD. The quantitative comparison between experimental and calculated ORD is obtained (Polavarapu *et al*., 2017) by calculating the root mean square deviation (RMSD) as follows:

$$\mathrm{RMSD} = \sqrt{\frac{\sum_{i}\left(Y_{i,calc} - Y_{i,obs}\right)^2}{N}}$$

where $Y_{i,calc}$ and $Y_{i,obs}$ are, respectively, the calculated and experimental SORs at *i*th wavelength and N is the number of discrete wavelength data points and the summation runs over discrete wavelength data points. To assess the differences between ECD predictions performed with PCM ($CHCl_3$) and PCM (CH_3CN), geometry optimizations and ECD predictions were also undertaken at CAM-B3LYP/ 6-311++G(2d,2p)/ PCM (CH_3CN) level for all conformers of diastereomer **2C**. Since no significant differences were found in these calculations, ECD calculations for diastereomers **2A**, **2B**, and **2D** were undertaken at CAM-B3LYP/ 6-311++G(2d,2p)/ PCM (CH_3CN) level using the optimized geometries and Gibbs energies at B3LYP/ 6-311++G(2d,2p)/ PCM ($CHCl_3$) level.

ECD and VCD spectral analyses were undertaken using CDSpecTech program (Covington and Polavarapu, 2016; Covington and Polavarapu, 2017) which implements the Tanimoto's similarity function (Tanimoto 1958; Cheng *et al*., 1996) as proposed by Shen *et al*., 2010 and designated here as *Sim*XXX function, where XXX represents the type of spectrum (XXX = VA, VCD, VDF, EA, ECD, EDF etc). VDF and EDF, respectively, represent vibrational and electronic dissymmetry factors. *Sim*XXX (XXX = VCD, VDF, ECD, EDF) ranges from −1 to +1, where +1 is perfect agreement of experimental spectrum with predicted spectrum for the AC used in calculations. *Sim*EA and *Sim*VA range from 0 to 1 but do not provide information on AC. The closer the value is to +1, the better the similarity between experimental and calculated spectra. CDSpecTech is a freely available program which directly reads the output

files from Gaussian program and simulates the chiroptical spectra. In addition, this program calculates the above-mentioned similarity values as a function of frequency / wavelength scale factor and incorporates various options, as detailed by Polavarapu *et al*., 2017 and Covington *et al*., 2017.

2.4- Results and Discussion

2.4.1- Structural identification of secondary metabolites from *Dittrichia viscosa*

The organic extract of the aerial part of *D. viscosa*, obtained as described in the experimental section, was fractioned by a combination of column and TLC chromatography to afford four known metabolites identified as α-costic acid, inuloxins A, C and D (**2-5**, Figure 9) and another new sesquitepenoid, named inuloxin E (**6**, Figure 9).

2.4.1.1- *α*-costic acid (2) *α*-costic acid was obtained as a homogeneous yellow oil, had: $[\alpha]^{25}_{D}$ +48.6° (*c* 1.0, $CHCl_3$); IR ν_{max} 3450, 1680, 1657, 1613 cm^{-1}]; The ^1H NMR spectrum is very similar to that reported in the literature (Andolfi *et al*., 2013). ESIMS (+) *m/z* 235$[M+H]^+$, 189 $[M\text{-}COOH]^+$. These data agree with those previously reported (Shtacher and Kashman, 1970; Andolfi *et al*., 2013).

2.4.1.2- Inuloxin A (3)

Inuloxin A was obtained as an oily homogeneous, had: $[\alpha]^{25}_{D}$ +8:5 (*c* 1.9); ^1H NMR spectrum is similar to that reported in the literature (Andolfi *et al*., 2013). ESIMS (+) *m/z* 519 $[2M+Na]^+$, 287 $[M+K]^+$, 271.1321 [calcd. for $C_{15}H_{20}NaO_3$ 271,1310, $M+Na]^+$, 249 $[M+H]^+$, 231 $[M+H\text{-}H2O]^+$. These data agree with those previously reported (Shtacher and Kashman, 1970; Andolfi *et al*., 2013).

2.4.1.3. Inuloxin C (4)

Inuloxin C was obtained as an oily homogeneous, had: $[\alpha]^{25}D$ +13.1 (*c* 0.3); IR ν_{max} 3428, 1758, 1662, 1635, 1152 cm^{-1}; UV λ_{max} nm (log ε) 262 (1.07); ^{1} H NMR spectrum is similar to that reported in the literature (Andolfi *et al*., 2013); ESIMS (+) *m/z* 519 $[2M+Na]^+$, 287 $[M+K]^+$, 271.1319 [calcd. for $C_{15}H_{20}NaO_3$ 271.1310, $M+Na^+$], 253 $[M+Na–H_2O]^+$. These data agree with those previously reported: (Shtacher and Kashman, 1970; Andolfi *et al*., 2013).

2.4.1.4- Inuloxin D (5)

$[\alpha]^{25}_{D}$+81.8 (c 0.2). The ^{1}H NMR spectrum is similar to that reported in the literature (Andolfi *et al*., 2013). HR ESIMS (+) *m/z*: 251.1658 [calcd. for $C_{15}H_{23}O_3$ 251.1647, $M+H]^+$, 233 $[M+H-H_2O]^+$.

2.4.1.5- Inuloxin E (6)

Inuloxin E was obtained as a pure oil, had: $[\alpha]^{25}D$ + 21.4 (*c* 0.4); IR ν_{max} 1762, 1714, 1660 cm^{-1} (Figure 16); UV λ_{max} nm (log ε) end absorbtion. ^{1}H and ^{13}C NMR (Figure 10 and Figure 11) are reported in Table 3; ESIMS (+), *m/z* 519 $[2M + Na]^+$, 271.1321 ($C_{15}H_{20}NaO_3$, calcd 271.1310 $[M + Na]^+$), 249 $[M + H]^+$.

2.4.1.5.1- *$NaBH_4$ Reduction of Inuloxin E*

Inuloxin E (**6**, 2 mg), dissolved in MeOH (1.0 mL), was added $NaBH_4$ (2 mg) and the reaction was performed under stirring at room temperature for 30 min. The mixture was neutralized with 0.1 M HCl, extracted with CH_2Cl_2 (3 × 30 mL), and dried (Na_2SO_4). The oily residue was purified by TLC, using petroleum ether/acetone (8:2, v/v) for elution to give the main metabolite inuloxin D (**5**) as an oil (0.8 mg, Rf 0.37). Inuloxin D spectroscopic and optical data similar to these previously reported in literature (Andolfi *et al*., 2013).

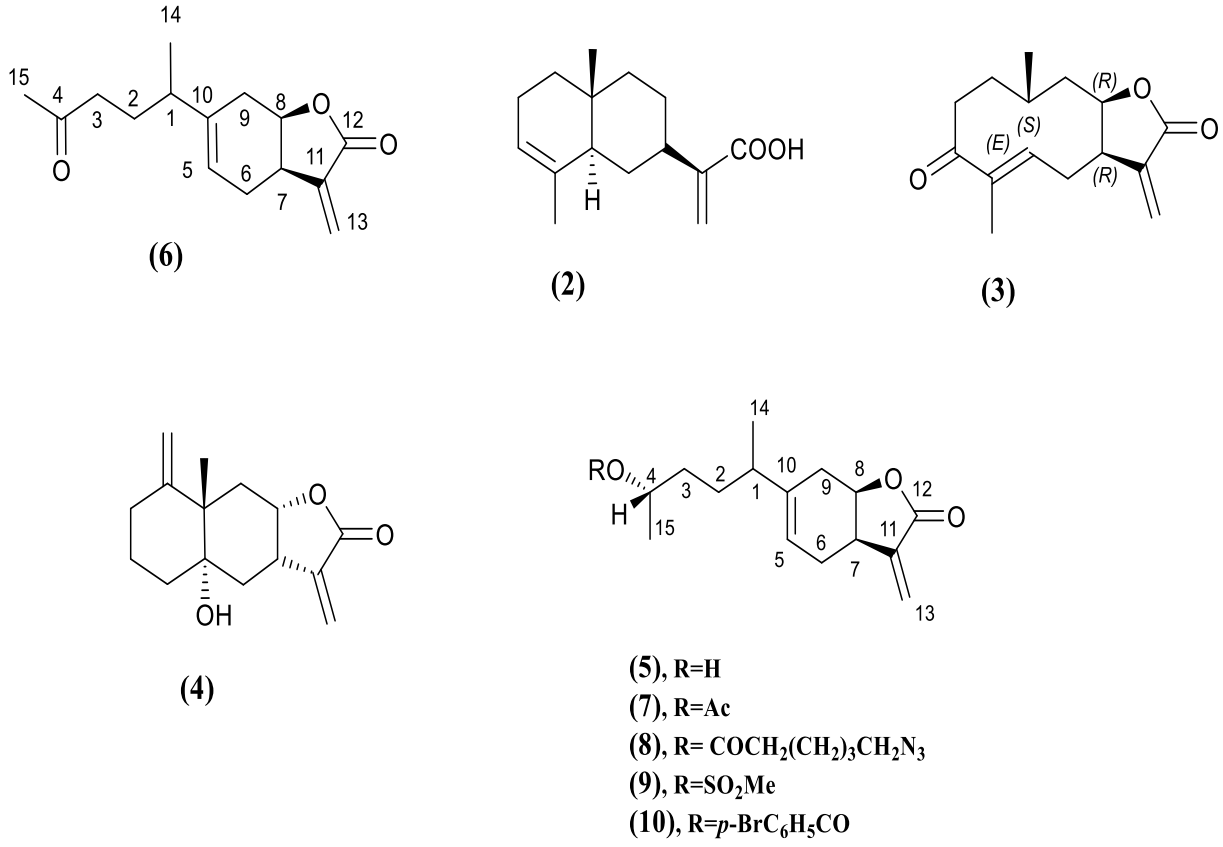

Figure 9. Structures of secondary metabolites isolated from *D. viscosa* (**2** and **10**).

2.4.1.5.2- *Structural characterizationof inuloxin E*

Inuloxin E (**6**) had a molecular formula of $C_{15}H_{20}O_3$ as deduced from its ESIMS spectrum consistent with six hydrogen deficiency. The preliminary ^{1}H and ^{13}C NMR investigation (Figure 10 and Figure 11) showed that it was very close to inuloxin D from which it differed for lacking of two hydrogens. Its ^{1}H NMR spectrum (Figure 10, Table 3) showed the signal pattern of benzofurane moiety as in (**5**). In fact, the protons of an exocyclic methylene and that of a trisubstituted olefinic groups resonating as two doublets (J = 3.2 Hz) and a broad double doublet (J = 8.8 and 5.3 Hz) at δ 6.28 and 5.54 and 5.46, respectively (Pretsch *et al*., 1987). This latter is coupled in the COSY spectrum (Figure 57, Table 13) (Berger and Braun, 2004) with the two protons of the adjacent methylene group (H_2C-6) which appeared as two multiplet at δ 2.43 and 2.18 being also coupled with the proton of the adjacent methine carbon (HC-7) appearing as multiplet at δ 3.34. Being the proton of one of the head-bridge carbons of the junction between the cyclohexene and the furanone ring, H-7 was coupled with the proton (H-8) of the other head-bridge carbon (C-8), which resonated as doublet of double doublets (J = 11.8, 8.4 and 2.7 Hz). H-8 also coupled with the protons of the adjacent

methylene group (H_2C-9), appearing both as doublet of double doublets (J = 13.0, 6.0 and 2.7 and 13.0, 11.0 and 8.4 Hz), at δ 2.02 and 1.89. The signals of the side chain significant differed from those of inuloxin D. In particular, the signals of H-1 and H_2-2 appeared as multiplets at δ 2.37 and 2.26, which is very similar to the value observed in (**5**) as well, the doublet (J = 6.9 Hz) of the secondary methyl group (Me-14), which resonated at δ1.16. Instead, a significant downfield shift (Δδ 1.06 and 0.78) was observed for of the protons of C-3 resonating as two multiplets at δ 2.56 and 2.26, while the signal of H-4 is missing. Finally, the terminal methyl group (Me-15) appeared as a singlet downfield shifted (Δδ 0.93) at δ 2.17 (Breitmaier and Voelter, 1987).

These finding are consistent with a 1-methyl-4-oxopentyl side chain attached at C-10 of the pentahydrobenzofuranone of (**6**) as also supported from the HMBC couplings observed in the HMBC spectrum (Figure 14, Table 3) (Berger and Braun, 2004) between C-1 with H-5, H_2-6 and H_2-9 and between C-10 with H-1 and Me-14. The couplings observed in the HSQC spectrum (Figure 13, Table 3) (Berger and Braun, 2004) allowed to assign the chemical shifts to all the protonated carbons and in particular the signals at δ 122.1, 120.1, 79.3, 42.6, 42.1, 36.7, 35.4, 30.4, 29.9, 26.6, and 20.9 were assigned to C-13, C-5, C-8, C-3, C-7, C-9, C-1, C-2, C-15, C-6 and C-14 (Ellestad *et al*., 1972). The ^{13}C NMR spectrum (Figure 11, Table 3) also showed the signals of one ketone and one lactone carbonyls at δ 208.0 (C-4) and 170.2 (C-12) and those of two quaternary olefinic carbons at δ 144.5 (C-10) and 139.0 (C-11), which were assigned by the correlations, observed in the HMBC spectrum (Figure 14, Table 3) between C-4 with H_2-3 and Me-15, C-12 and H-7, H-8 and H_2-13, C-10 and H-1, H_2-6, H_2-9 and Me-14 and C-11 with H_2-6, H-7, H-8 and H_2-13.

Thus, the chemical shifts to all the protons and corresponding carbons of (**6**) were assigned, as reported in Table 3, and inuloxin E was formulated as 3-methylene-6-(1-methyl-4-oxo-pentyl)-3a,4,7,7a-tetrahydro-3*H*-benzofuran-2-one.The structure assigned to (**6**) was further supported by the absence of any signal due to hydroxy group in the IR spectrum (Figure 16) and by the other couplings observed in the HMBC spectrum (Figure 14, and reported in Table 3. The ESIMS spectrum showed that its sodiated $[2M + Na]^+$ at *m/z* 271.1321, while its ESIMS showed the sodiated dimeric cluster protonated $[M + H]^+$ forms at *m/z* 519 and 249, respectively.

Considering the value (J = 8.4 Hz) for the coupling constant measured between H-7 and H-8 in comparison with the same value recorded in **(5)**, a *cis*-junction could be attributed between

the two rings of the pentahydrobenzofurane moiety. This was confirmed by the data obtained from NOESY experiment (Berger and Braun, 2004). In fact, in the NOESY spectrum (Figure 15), the significant correlation between H-7 and H-8 was observed together with the expected coupling between the two protons of the exocyclic olefinic methylene group H_2C-13 and the protons of H_2C-6a with both H-5 and H-7. A further support to the structure assignment of inuloxin E was obtained by the reduction of (**6**) with sodium borohydride.

The main product obtained was identified as inuloxin D by comparison of its spectroscopic and optical rotation data with those previously reported for the natural (**5**) (Andolfi *et al*., 2013), suggesting that there was stereoselectivity in reduction reaction. These results were not a surprise as stereoselective reduction of the ketone group of some naturally occurring compounds with sodium borohydride was already observed (Ellestad *et al*., 1972; Steyn *et al*., 1982; Evidente *et al*., 1997; Evidente *et al*., 2011; Cala *et al*., 2018).

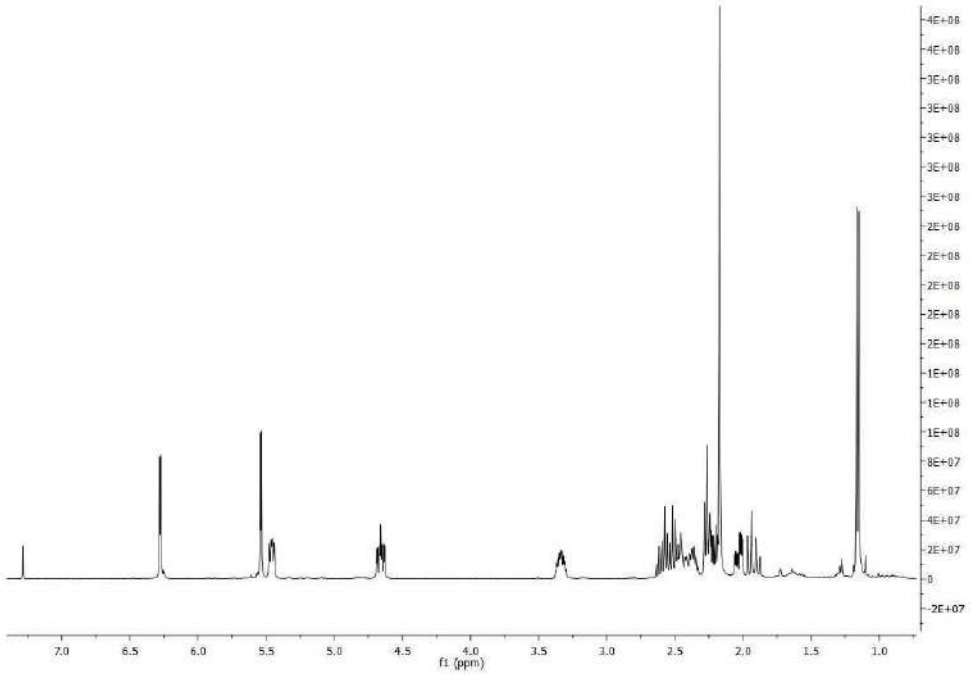

Figure 10. ^{1}H NMR spectrum of inuloxin E (**6**) ($CDCl_3$, 400 MHz).

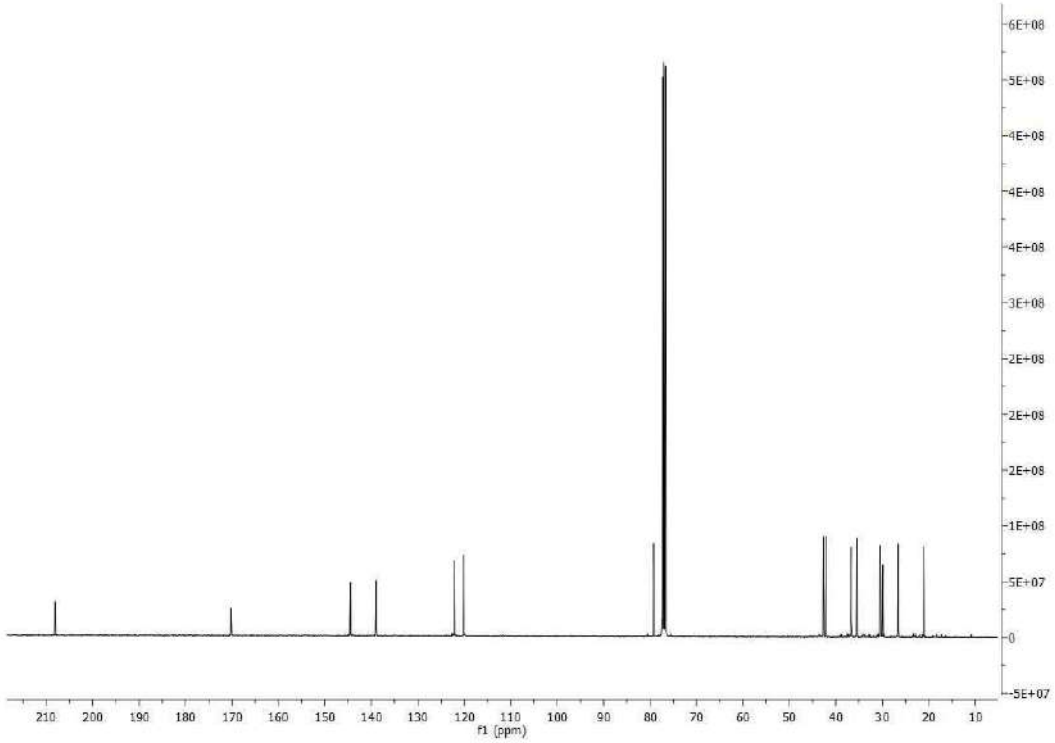

Figure 11. ^{13}C NMR spectrum of inuloxin E (**6**) ($CDCl_3$, 100 MHz).

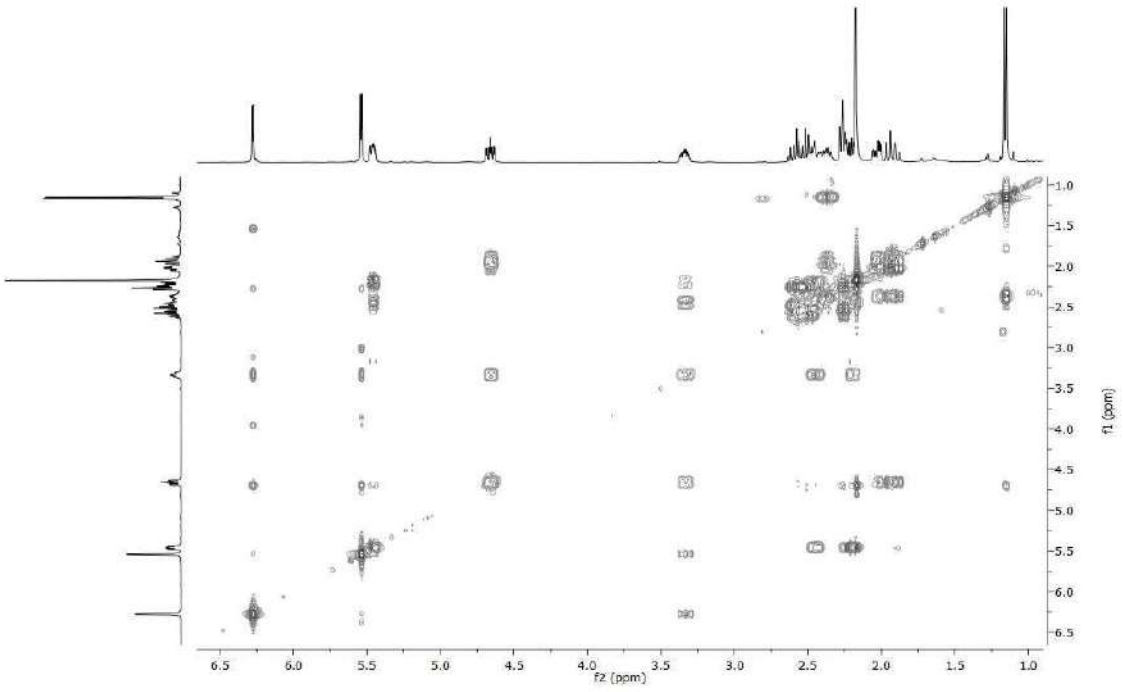

Figure 12. COSY spectrum of inuloxin E (**6**) ($CDCl_3$, 100 MHz).

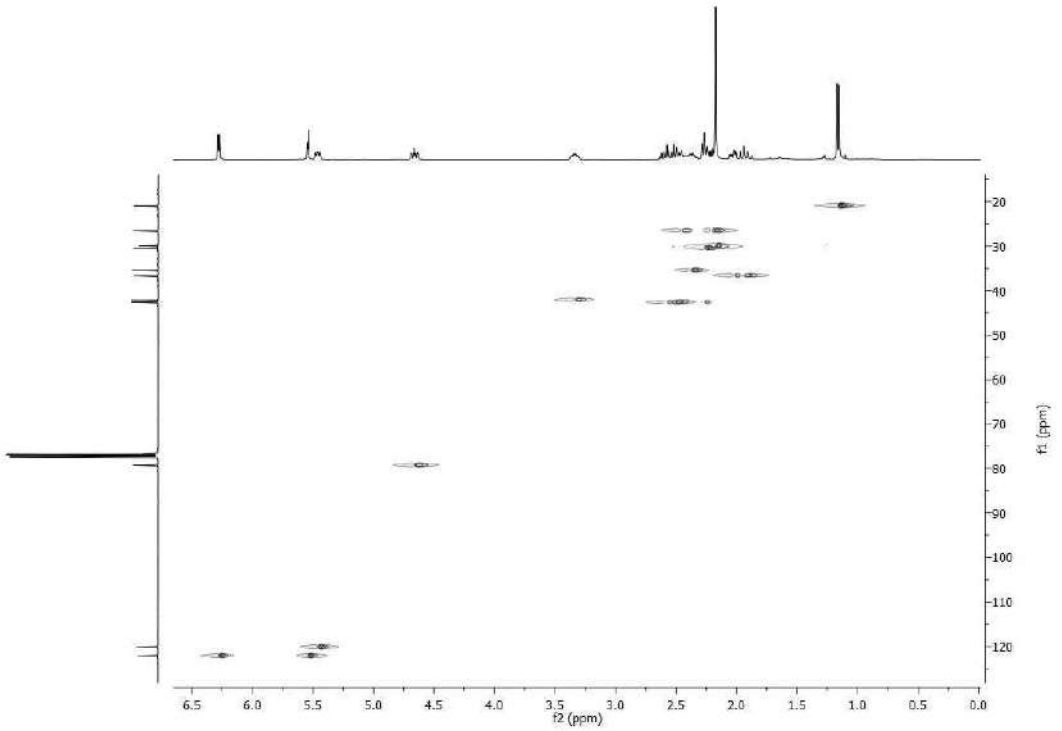

Figure 13. HSQC spectrum of inuloxin E (**6**) ($CDCl_3$, 400/100 MHz).

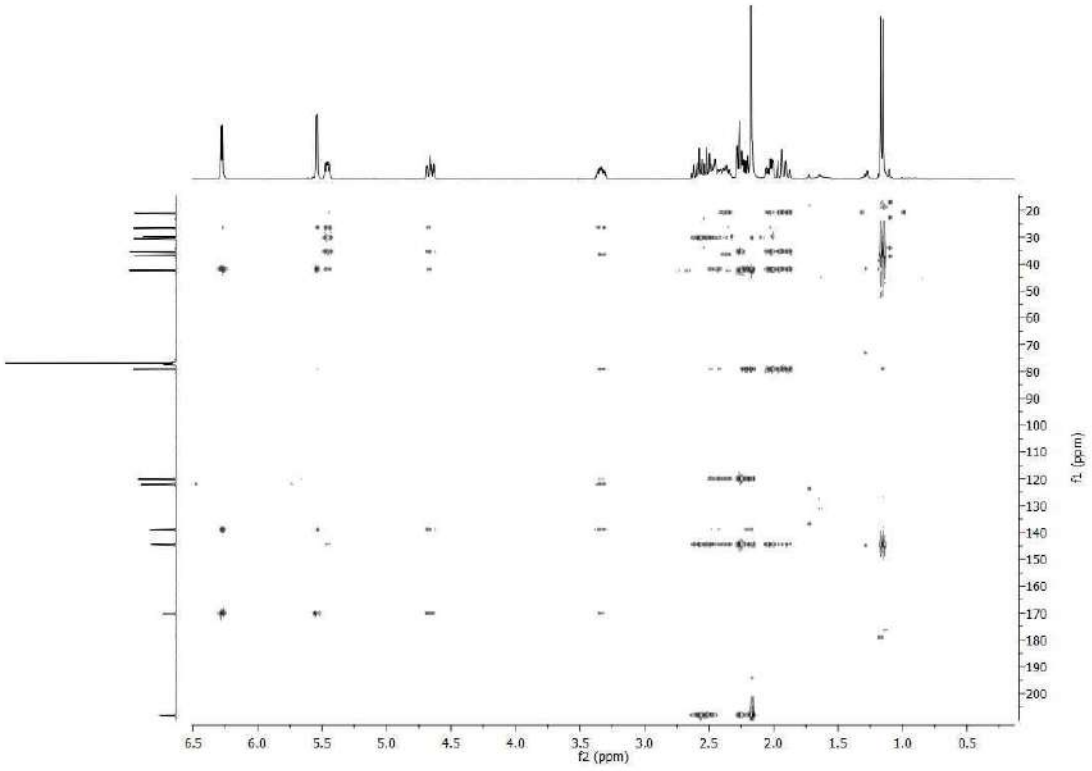

Figure 14. HMBC spectrum of inuloxin E (**6**) ($CDCl_3$, 400/100 MHz).

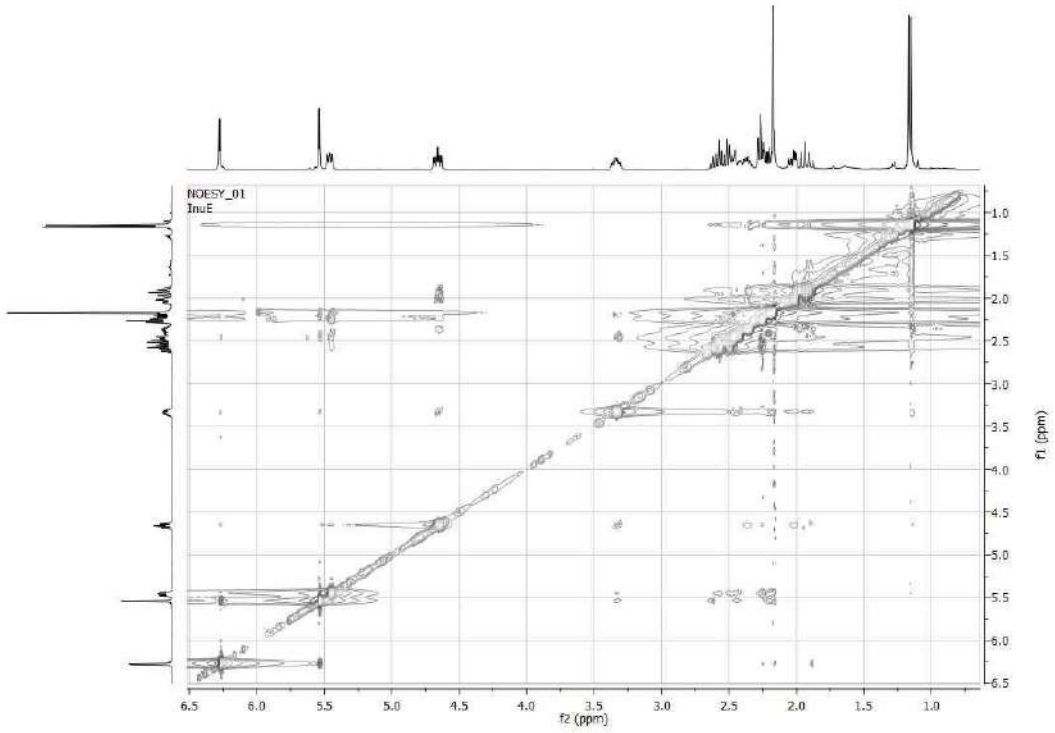

Figure 15. NOESY spectrum of inuloxin E (**6**) ($CDCl_3$, 100 MHz).

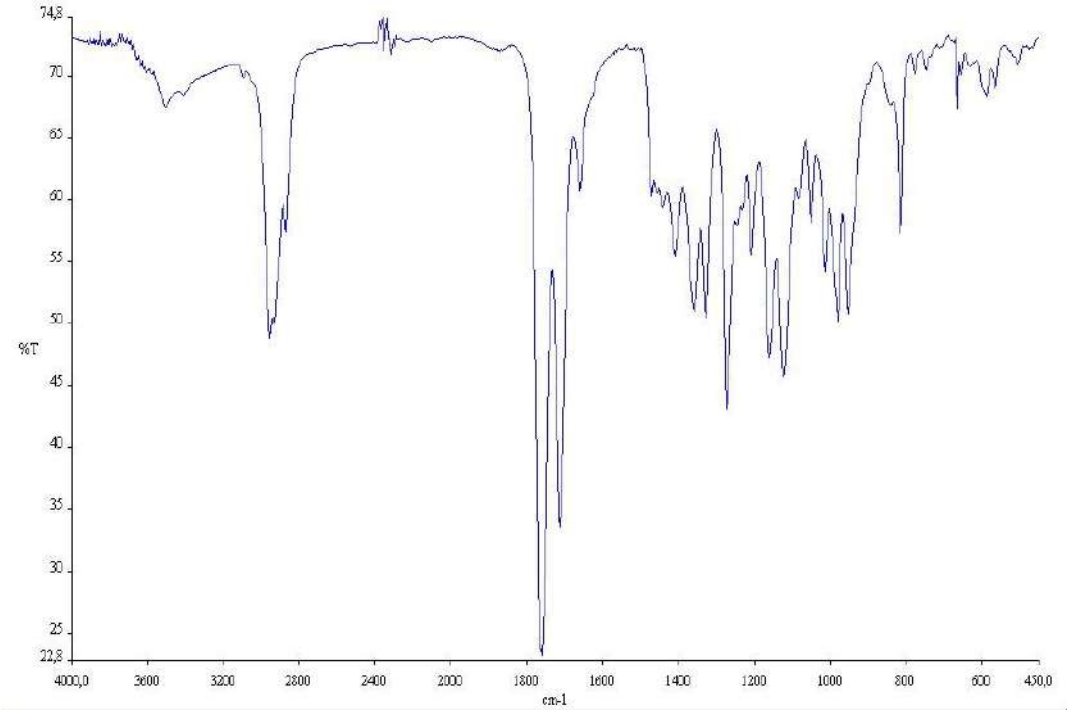

Figure 16. IR spectrum of inuloxin E (**6**).

Table 3. ^{1}H and ^{13}C NMR data of inuloxin E (**6**) [a,b]

Position	δC[c]	δH (*J* in Hz)	HMBC
1	35.4 d	2.37 m	H_2-6, H-5, H_2-9, H-8, Me-14
2	30.4 t	2.26 m (2H)	H-3A, H-5,
3	42.6 t	2.56 m 2.26 m	H_2-2
4	208.0 s		H_2-3, Me-15
5	120.1 d	5.46 br dd (8.8, 5.3)	H_2-6
6	26.6 t	2.43 m 2.18 m	H-5, H-7, H-8
7	42.1 d	3.34 m	H-5, H_2-6, H-8 picc, H_2-9, H_2-13,
8	79.3 d	4.66 ddd (11.8, 8.4, 2.7)	H_2-6, H-7, H_2-9
9	36.7 t	2.02 ddd (13.0, 6.0, 2.7) 1.89 ddd (13.0, 11.0, 8.4)	H-1, H-7
10	144.5 s		H-1, H_2-6, H_2-9, Me-14
11	139.0 s		H2-$_6$, H-7, H-8, H_2-13
12	170.2 s		H-7, H_2-13, H-8,
13	122.1 t	6.28 d (3.2) 5.54 d (3.2)	H-7
14	20.9 q	1.16 d (6.9)	H_2-9, H-1, H-5
15	29.9 q	2.17 s	

[a] The chemical shifts are in δ values (ppm) from TMS. [b] 2D ^{1}H, ^{1}H (COSY) ^{13}C, ^{1}H (HSQC) NMR experiments delineated the correlations of all the protons and the corresponding carbons. [c] Multiplicities were assigned by DEPT spectrum.

2.4.2- Hemisynthesis and chemical characterization of inuloxin D derivatives

2.4.4.1- *4*-O-*Acetyl Derivative of Inuloxin D* (7)

Derivative (**7**) had: *Rf* 0.75; ^{1}H NMR data: are reported in Table 14; ESIMS (+), *m/z* 315 $[M + Na]^+$, 293 $[M + H]^+$.

2.4.4.2- *4*-O-*Azidopentanoyl Ester of Inuloxin D* (8)

Derivative (**8**) had: *Rf* 0.70; ^{1}H NMR data: are reported in Table 14; ESIMS (+), *m/z* 398 $[M + Na]^+$, 376 $[M + H]^+$.

2.4.4.3- *4*-O-*Mesyl Ester of Inuloxin D* (9)

Derivative (**9**) had: ^{1}H NMR data: are reported in Table 14; ESIMS (+), *m/z* 351 $[M + Na]^+$, 329 $[M + H]^+$.

2.4.4.4- *4*-O-*p*-*Bromobenzoylester of Inuloxin D* (10)

Derivative (**10**) had: ^{1}H NMR data are reported in Table 14; ESIMS (+), *m/z* 454 and 452 $[M + Na]^+$ 432 and 430 $[M + H]^+$.

Inuloxins E and D were assayed in comparison with four different ester derivatives prepared from inuloxin D (**7**-**10,** Figure 9). In particular, the acetyl derivative of **5** (**7**) was prepared by usual acetylation and its ^{1}H NMR spectrum (Table 4) differed from that of the parent compound essentially for the downfield shift (Δδ 1.04) of H-4, resonating as a multiplet at δ 4.84, and the presence of the singlet of the acetyl group at δ 2.06. Its ESIMS showed the sodiated $[M + Na]^+$ and protonated $[M + H]^+$ forms at *m/z* 315 and 293. The 4-*O*-azidopentanoyl ester of **5** (**8**) prepared by dehydratation between (**5**) and the 5-azidopentanoyl acid showed a ^{1}H NMR spectrum (Table 14) which differed from that of (**5**) for downfield shift (Δδ 1.10) of H-4, resonating as a multiplet at δ 4.90, and for the signal system of the azidopentanoyl residue observed at δ 2.36 (t, J = 6.9 Hz, CH_2-2'), 1.79-1.62 (CH_2-3' and CH_2-4'), 3.33 (t, J= 6.9 Hz, CH_2-5'). The ESI-MS spectrum showed the sodiated $[M + Na]^+$ and protonated $[M + H]^+$ forms at *m/z* 398 and 376. The 4-*O*-mesyl ester of **5** (**9**) was prepared by reaction of inuloxin D with mesyl chloride. Its ^{1}H NMR spectrum (Table 4) differed from that of (**5**) for downfield shift (Δδ 1.02) of H-4, resonating as a multiplet at δ 4.82, and the presence of the singlet of the mesyl group at δ 3.04. Its ESI MS showed the sodiated $[M + Na]^+$ and protonated $[M + H]^+$ forms at *m/z* 351 and 329. Finally, the *p*-bromobenzoyl ester of **5** (**10**) was prepared by reaction between inuloxin D and *p*-bromobenzoyl chloride. The ^{1}H NMR spectrum (Table 4) differed from that of (**5**) or the downfield shift (Δδ 1.30) of H-4, resonating as a multiplet at δ 5.10, and the presence of the two doublets (J = 8.7 Hz) of the *p*-Br-substituted benzoyl residue at δ 7.90 and 7.59. Its ESI MS showed the typical isotopic sodiated $[M + Na]^+$ and protonated $[M + H]^+$ forms at *m/z* 454 and 452 and 432 and 430, respectively.

Table 4. ^{1}H NMR data of Inuloxin D (**5**) and Its Derivatives (**7**-**10**)

Position	2 [a]	3 [b]	4 [c]	5 [d]	6 [e]
	δH, (*J* in Hz)	δH, (*J* in Hz)	δH, (*J* in Hz)	δH, (*J* in Hz)	δH, (*J* in Hz)
1	2.39 m	2.36 sextet (6.6)	2.40 m	2.36 sextet (6.6)	2.36 sextet (6.9)
2	2.06 m	2.06 (2H) m	2.06 (2H) m	2.05 (2H) m	2.06 (2H) m
	2.04 m				
3	1.52 m	1.74 m	1.79 m	1.86 m	1.76 m
	1.48 m	1.53 m	1.62 m	1.66 m	1.65 m
4	3.80 m	4.84 m	4.90 m	4.82 m	5.10 m
5	5.52 dd (8.7, 4.9)	5.47 dd (9.2, 5.2)	5.46 dd (9.2, 5.4)	5.54 dd (9.2, 5.2)	5.42 dd (8.9, 5.4)
6	2.48 m	2.45 br dd (14.2, 5.2)	2.45 br dd (13.8, 5.4)	2.47 br dd (13.8, 5.2)	2.42 br dd (14.2, 5.4)
	2.21 m	2.19 ddd (14.2, 9.2, 4.5)	2.19 ddd (13.8, 9.2, 4.5)	2.22 ddd (13.8, 9.2, 5.4)	2.13 ddd (14.2, 8.9, 4.6)
7	3.36 m	3.38 m	3.38 m	3.38 m	3.35 m
8	4.66 ddd (11.8, 8.6, 2.9)	4.67 ddd (11.8, 8.3, 2.7)	4.67 ddd (11.5, 7.7, 2.4)	4.46 ddd (11.8, 8.6, 2.5)	4.66 ddd (11.6, 8.8, 2.5)
9	2.01 m	1.96 (2H) m	1.96 (2H) m	1.96 (2H) m	2.01 m
	1.98 m				1.93 m
13	6.27 d (3.2)	6.28 d (2.9)	6.28 d (2.9)	6.29 d (2.9)	6.26 d (3.0)
	5.55 d (3.2)	5.55 d (2.9)	5.55 d (2.9)	5.56 d (2.9)	5.51 d (3.0)
14	1.16 d (6.9)	1.15 d (6.6)	1.15 d (6.7)	1.16 d (6.9)	1.12 d (6.9)
15	1.24 d (6.2)	1.25 d (6.2)	1.25 d (6.4)	1.46 d (6.1)	1.35 d (6.6)

[a] These data are the same already reported in Andolfi *et al*., 2013; bthe singlet of the acetyl group was present at δ 2.06; [c] the signal system of the azidopentanoyl residue were observed at δ 2.36 (t, *J*= 6.9 Hz, CH_2-2'), 1.79-1.62 (CH_2-3' and CH_2-4'), 3.33 (t, J= 6.9 Hz, CH_2-5'); [d] the singlet of the mesyl group resonated at δ 3.04; ethe two doublets (*J*= 8.7) of the *p*-Br-substituted benzoyl residue were observed at δ 7.90 and 7.59.

3.4.3- Biological assays

3.4.3.1- Germination induction bioassays

The stimulation activity of inuloxins D and E was studied in three species of broomrape weeds: *O. cumana*, *O. minor* and *P. ramosa* (Figure 17). None of those inuloxins were active inducing germination of *O. minor* and *P. ramosa*, two broomrape species known for their low level of specialization in root exudate recognition (Fernández-Aparicio *et al*., 2009; Fernández-Aparicio *et al*., 2011).

On the contrary, both inuloxins induced germination of the highly selective seeds of *O. cumana*. In *O. cumana*, the effect of inuloxin D was stronger than that induced by inuloxin E and therefore, four ester derivatives above reported were prepared from inuloxin D and tested in all broomrape species (Table 5).

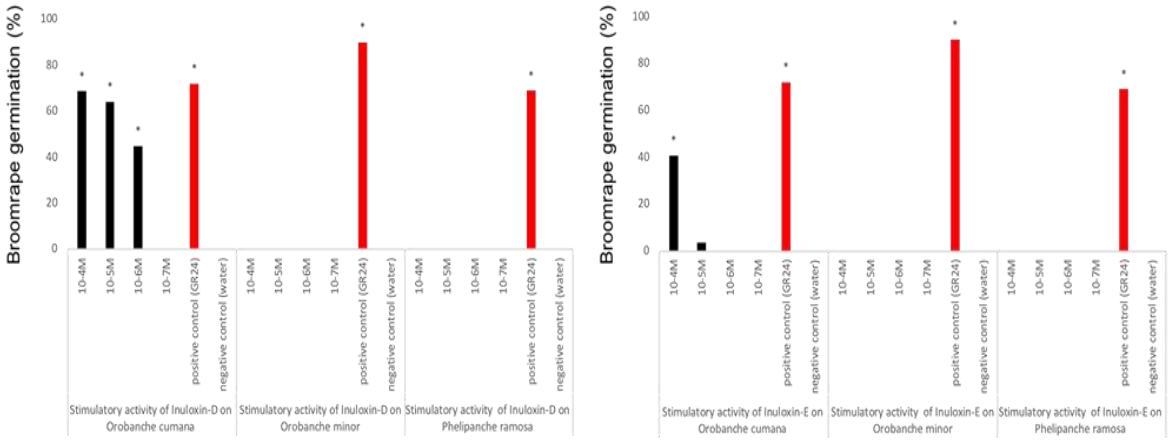

Figure 17. *Orobanche cumana*, *Orobanche minor* and *Phelipanche ramosa* germination induced by inuloxin D (left panel), and inuloxin E (right panel). The asterisk (*) indicates differences at the 0.05 level compared with the negative control (seeds induced to germinate with water).

The structural modifications made in inuloxin D did not carry induction activity on *O. minor* and *P. ramosa* seeds inducing their germination. The germination level of *O. cumana* was reduced in (**8** and **10**), at all concentrations tested in comparison with inuloxin D. At 10^{-4} M the levels of *O. cumana* germination induced by (**7** and **9**), were comparable with that induced by (**5**), however at lower concentrations, the germination activity was reduced in these derivatives in comparison with inuloxin D.

3.4.3.2- Germination and Growth Inhibition Bioassays

The inhibition activity of inuloxin E and inuloxin D in seeds of three species of broomrape weeds: *O. cumana*, *O. minor* and *P. ramosa* was studied by mixing these metabolites with GR24, a synthetic germination stimulant active in the three broomrape weeds studied in this work. No inhibitory action was observed in inuloxin D and inuloxin E as the germination activity of GR24 mixed with each inuloxin was not different from that induced by GR24 control. This effect was observed for *O. cumana* and also for the species *O. minor* and *P. ramosa*, and therefore confirmed that the effect reported in Figure 18for *O. minor* and *P. ramosa* is lack of stimulatory activity and not inhibitory action. Interestingly, *O. cumana* and

P. ramosa seeds that germinated with GR24 mixed with inuloxin D developed shorter radicles (Figure 19). This inhibition of radicle growth was not observed in seeds of *O. minor*. Inuloxin E did not inhibit the radicle growth in any of the broomrape species tested.

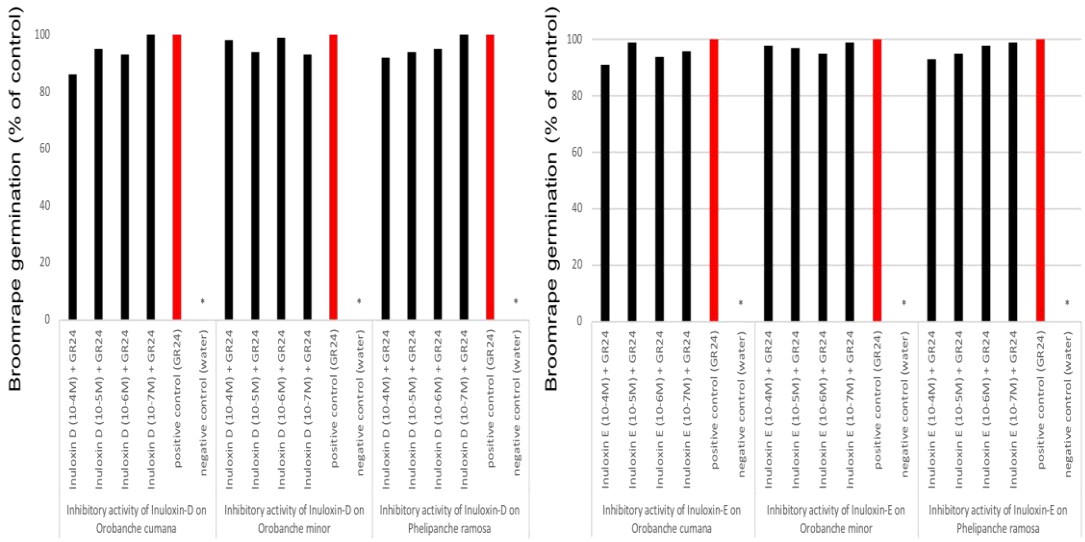

Figure 18. Inhibition of Orobanche cumana, Orobanche minor and Phelipanche ramosa germination tested by application of GR24 alone or GR24 mixed with inuloxin D (left panel) and inuloxin E (right panel). Data is expressed as percentage referred to the control GR24. The asterisk (*) indicates differences at the 0.05 level compared with the positive control (seeds induced to germinate with only GR24).

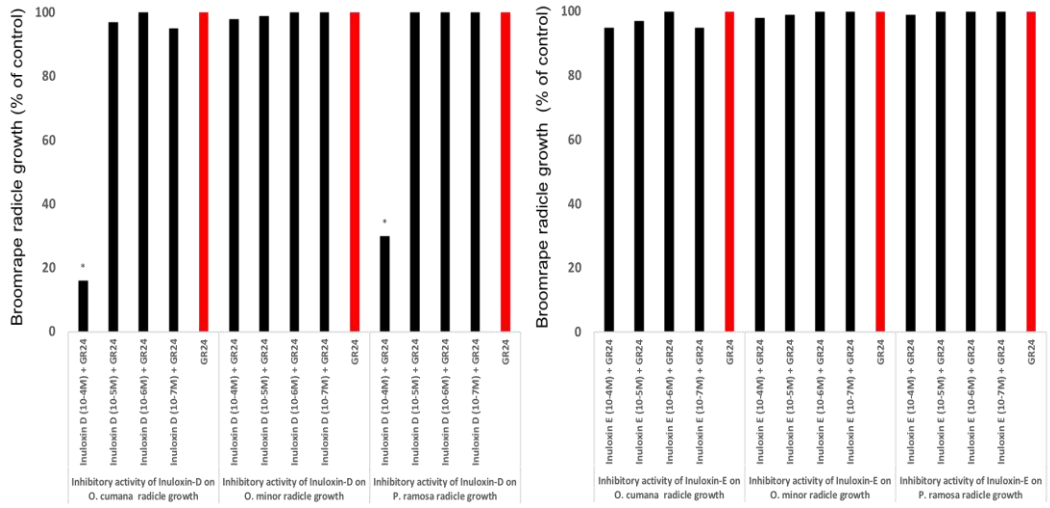

Figure 19. *Orobanche cumana*, *Orobanche minor* and *Phelipanche ramosa* radicle growth in the presence of GR24 alone or GR24 mixed with inuloxin D (left panel) and inuloxin E (right

panel). Data is expressed as percentage referred to the control GR24. The asterisk (*) indicates differences at the 0.05 level compared with the positive control (GR24).

Table 5. Induction of Seed Germination of three Broomrape Species *O. cumana*, *O. minor* and *P. ramosa* by Inuloxin D Derivatives (7-10).

Broomrape Seed Germination (%)				
Inuloxin D derivative	**Concentracion**	***O. cumana***	***O. minor***	***P.ramosa***
7	10^{-4}M	57.8	0.0	0.0
	10^{-5}M	14.9	0.0	0.0
	10^{-6}M	2.3	0.0	0.0
	10^{-7}M	0.0	0.0	0.0
8	10^{-4}M	64.7	0.0	0.0
	10^{-5}M	29.4	0.0	0.0
	10^{-6}M	4.2	0.0	0.0
	10^{-7}M	0.0	0.0	0.0
9	10^{-4}M	26.4	0.0	0.0
	10^{-5}M	0.0	0.0	0.0
	10^{-6}M	0.0	0.0	0.0
	10^{-7}M	0.0	0.0	0.0
10	10^{-4}M	18.6	0.0	0.0
	10^{-5}M	3.5	0.0	0.0
	10^{-6}M	0.0	0.0	0.0
	10^{-7}M	0.0	0.0	0.0
GR24	1	64.0	80.4	68.1
control -	0	0.0	0.0	0.0

2.4.4- Absolute configuration of inuloxin D

Since there is no possibility for intramolecular hydrogen bonding in (**5**), conformational search is less complicated. Nevertheless, there are large number of conformers due to the flexibility of side chain containing C1-C4. For each diastereomer, the numbers of conformers within 2 kcal/mol electronic energy difference, that have been used for final vibrational frequency and spectral calculations, are listed in Table 16. The lowest energy conformer of each diastereomer of **(5)** has the following populations, based on Gibbs energy: **2A**: 22%; **2B**: 21%; **2C**:15%; **2D**:14%. It is important to note that since the lowest energy conformer of each diastereomer accounts for only less than 25% of the total population, multiple conformers can be regarded as important for generating the population weighted spectra.

Moreover, the population weighting using Gibbs and electronic energies did not significantly alter the final result.

As mentioned earlier, ECD calculations were undertaken for **2C** at both CAM-B3LYP/ 6-311++G(2d,2p)/ PCM (MeCN) and B3LYP/6-311++G(2d,2p)/PCM ($CHCl_3$) levels, using Gibbs energies at the respective optimized geometries, for population weighting. These calculations reveal that there are no significant differences between their results. *Sim*EA, *Sim*ECD, and *Sim*EDF values are 0.94, 0.41, and 0.87 for calculation with PCM($CHCl_3$) and 0.94, 0.40, and 0.85 for calculation with PCM (CH_3CN) (Table 16). For these reasons, ECD calculations for the other three diastereomers of **(5)** were carried out using the geometries optimized with PCM ($CHCl_3$), carrying out ECD calculations with PCM(CH_3CN) and using Gibbs energies at the optimized geometries for population weighting.

Since predicted ECD spectra for all diastereomers show relatively strong matches with experimental ECD spectra, having the negative-positive-negative pattern of Cotton Effects (CEs), it is hard to discern qualitatively if any one particular diastereomer can be favored for assigning the AC. Quantitative analysis using the similarity between calculated and experimental spectra provides discrimination to a certain extent (Table 6). *Sim*EDF magnitude, greater than 0.8, is nearly equal for all diastereomers, a problem that can occur when there are only few bands for comparison. The magnitude of *Sim*ECD follows the order: *ent*-**5D** (0.54) > *ent*-**5A** (0.48) > **5B** (0.46) > **5C** (0.40). However, due to limited number of ECD bands available for comparison between experimental and predicted spectra, care should be exercised in placing excessive reliance on these *Sim*ECD values. As will be seen later, the conclusion based on ECD analyses will be contradicted by VCD and ORD analyses.

Table 6. Notation for stereoisomers of **(5)** and the number of investigated conformations

Stereoisomer	No. of conformers[a]
16A (1S,4S,7S,8S)	35
ent-16A (1R,4R,7R,8R)	
16B (1S,4S,7R,8R)	37
16C (1R,4S,7R,8R)	40
16D (1R,4S,7S,8S)	42
ent-16D (1S,4R,7R,8R)	

[a] The numbers of conformers for the two enantiomers are expected to be same.

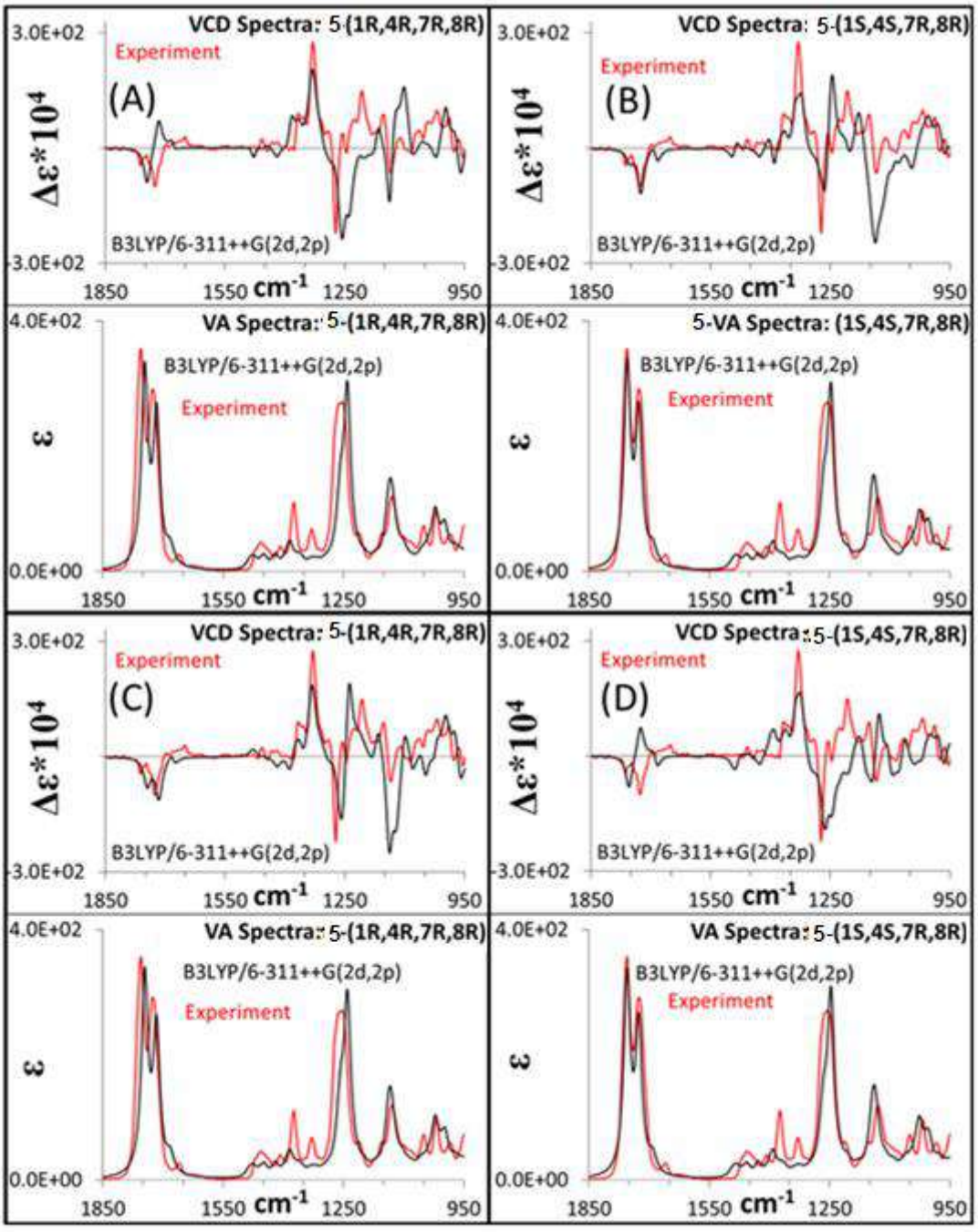

Figure 20. VA and VCD of (1*R*,4*R*,7*R*, 8*R*), *ent*-**5A**, (panel A), (1*S*,4*S*,7*R*, 8*R*), **5B**, panel (B), (1*R*,4*S*,7*R*, 8*R*), **16C**, (panel C), and (1*S*,4*R*,7*R*, 8*R*), *ent*-**5D**, (panel D). Experimental spectra were measured in chloroform. VA and VCD spectra are simulated with populations weighted using Gibb energies at B3LYP/6-311++G(2d,2p)/PCM(Chloroform) level. Band positions are scaled by 0.985, 0.99, 0.985, and 0.99 for panels A-D which corresponds to the x-axis scale factor that yields the maximum *Sim*VCD value. Predicted intensities of VA and VCD spectra have been multiplied by 0.4 and 2 respectively to appear on the same scale as the corresponding experimental spectra. VCD spectrum predicted for **16A** has been inverted to obtain the spectrum

for **16**-(1*R*,4*R*,7*R*,8*R*). VCD spectrum predicted for **5D** has been inverted to obtain the spectrum for **16**-(1*S*,4*R*,7*R*, 8*R*).

The predicted VA and VCD spectra for the diastereomers of (**5)** are compared with corresponding experimental spectra in Figures 65. As can be seen in these figures, VA spectra for all four diastereomers appear qualitatively identical. VCD spectra of diastereomers show some qualitative differences, but it is difficult to judge which diastereomer predicted spectra best match the experimental spectra. Therefore, quantitative similarity overlap analysis is useful at this stage. The similarity analyses for quantitative comparison of experimental and calculated VCD spectra included the 1800-950 cm^{-1} region (Table 6). Among the four non-enantiomeric diastereomers considered, the magnitudes of *Sim*VCD follow the order 0.37(**5C**) > 0.30(**5B**) > 0.23(*ent*-**5A**) > 0.22(*ent*-**5D**); those of *Sim*VDF values follow the order 0.52(**5C**) > 0.45(*ent*-**5A**) > 0.42(**5B**) > 0.40(*ent*-**5D**). The magnitudes of both *Sim*VCD and *Sim*VDF are the largest for **5C**. The magnitude of *Sim*VCD for **5C** is near the confidence threshold, but those of other diastereomers are well below the confidence threshold (Polavarapu *et al*., 2017). Thus, VCD analysis clearly favors the (1*R*,4*S*,7*R*,8*R*) diastereomer for assigning the AC of (S**6)**. This type of quantitative similarity analysis renders itself as an indispensable tool for determining the AC in situations where visual comparison does not point to an obvious preference.

Experimental ORD measurements revealed very small SOR values, with a sign switch at shorter wavelength (Fig. 21). The sign reversal at the shorter wavelength is not reproduced in the calculations for any of the diastereomers, but positive signs observed in the experiment at longer wavelengths are reproduced in the predicted values for *ent*-**2A** and *ent*-**2D** and for the diastereomers **2B** and **2C**. Quantitative analysis (see Equation 1) indicates that the RMSD values for **2A**-**2D** are, respectively, 272, 320, 244 and 370. Based on these RMSD values, **2C** is the preferred diastereomer for the AC assignment.

To summarize the analyses, VCD and ORD data favor the (1*R*,4*S*,7*R*,8*R*) diastereomer (**6C**) for assigning the AC of (**5)**. Thus, the AC of (**5)**, acetylated inuloxin D, and by extension Inuloxin D, can reasonably be assigned as (1*R*,4*S*,7*R*,8*R*), while that of inuloxin E can reasonably assigned as (1*R*,7*R*,8*R*) (Fig. 22).

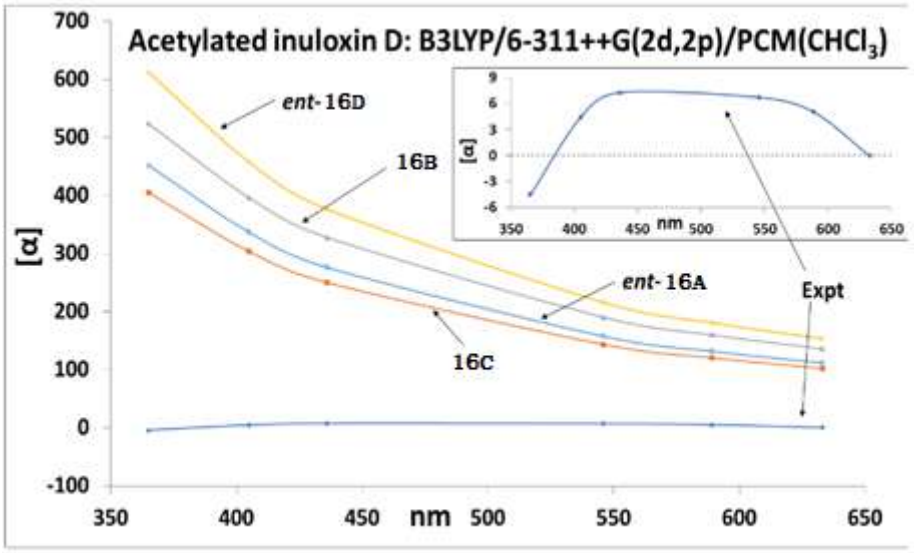

F**igure 21**. Comparison of experimental ORD to those calculated for four diastereomers of acetylated inuloxin D. ORD predicted for 2**6A** have been inverted to obtain the spectra for *ent*-**6A**; ORD predicted for **6D** have been inverted to obtain the spectra for *ent*-**6D**. The inset shows experimental ORD on an expanded y-axis scale.

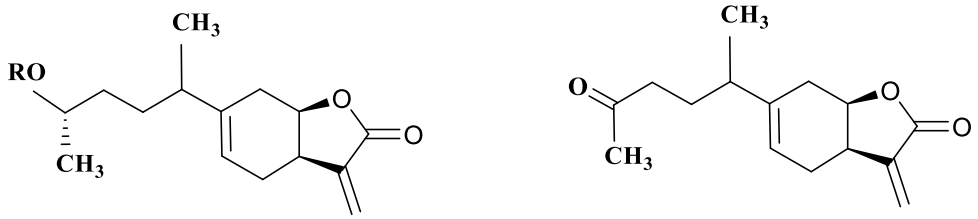

(5), **R=H**
(7), R=Ac

(6)

Figure 22. Inuloxin D **(5)**, acetylated inuloxin D (**7)**, and inuloxin E (**6)**, with assigned AC

Chapter 3: Production, extraction, and purification of bioactive metabolites from two phytopathogenic fungi (*Drechslera gigantea*) and (*Macrophomina phaseolina*)

3.1- Introduction

Phytopathogenic fungi constitute one of the main infectious diseases of crop plants, playing an important role in the persistent and significant annual crop losses with consequent heavy economic problems. Considering the social and economic impact of the plant diseases. Phytopathogenic fungi are controlled by synthetic fungicides to avoid losses in agrarian production (Yourman and Jeffers, 1999; Paulitz and Bélanger, 2001; Ribera and Zuñiga, 2012; Evidente *et al*., 2019). However, the extensive use of these pesticides has resulted in a series of environmental and ecological problems, such as the increase in resistant weed populations, soil compaction, and water pollution, which seriously affect the sustainable development of agriculture. Therefore, there is a great demand for novel natural fungicides (Tscharntke *et al*., 2012; Cimmino *et al*., 2015a; Peng *et al*., 2021). Thus, many studies were warried out of phytotoxins produced from phytopathogenic fungi and the knowledge of plant pathogenesis processes can help to find the best and rapid remedial to control plant diseases. Considering these results, it seems of interest to find new bioactive metabolites produce by two phytopathogenic fungi *Dreschlera gigantea* and *Macrophomina phaseolina*, when growth in liquid cultures.

The aim of this chapter has been the isolation and the chemical and biological characterization of bioactive metabolites with potential herbicidal and fungicidal activity produced by two phytopathogenic fungi from Argentina: *D. gigantea* and *M. phaseolina*.

3.2- Literature review

3.2.1- Phytopathogenic fungi

3.2.1.1- *Drechslera gigantea*

D. gigantea (Heald and Wolf) (Figure 23A) is a cosmopolitan fungal pathogen found throughout North and South America, Japan, and other regions (Evidente *et al*. 2006., Sivanesan, 1992). It causes a zonate eye-spot disease of many commonly cultivated turfgrasses and weeds, including crabgrass (*Digitaria* spp.), quackgrass (*Agropyron repens*) and bermuda grass (*Cynodon dactylon*) (Farr *et al*., 1989; Strobel *et al*., 1991; Sivanesan, 1992; Evidente *et al*., 2006a). Under severe levels of disease, the leaf spots may coalesce, causing leaf lesions and leaf blight. Infected leaves may be killed. The *D. gigantea* alone and in combination with two other grass pathogens, *Exserohilum longirostratum* and *E. rostratum*

is effective for grass management under field conditions (Chandramohan and Charudattan, 2001; Chandramohan *et al*., 2002). Typically, symptoms of *D. gigantea* leaf blight (Figure 24B) appears within about one week after the fungus is sprayed on the grass foliage and the disease progresses steadily over the following two to three weeks. The treated foliage is killed, and the control lasts for 10 weeks or more. Rhizomes are not killed, and the grasses will re-grow after a period of mycoherbicide-caused suppression. Moreover, some evaluations have confirmed that these fungi are effective for grass management under field conditions (Chandramohan *et al*., 2002; Evidente *et al*., 2006a).

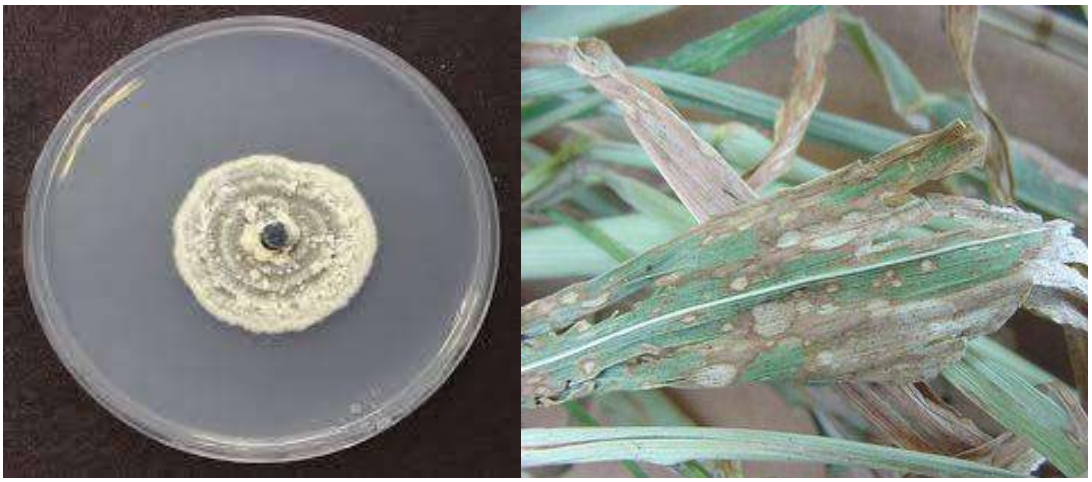

Figure 23. A. Colony of *D. gigantea* growing on PDA after 7 days (Lane *et al*., 2020). **B.** leaf blight (*Drechslera gigantea*) (Bachi, 2009).

3.2.1.2- *Macrophomina phaseolina*

M. phaseolina (Tassi) Goid. (Figure 24A), is a fungal pathogen in the *Botryosphaeriaceae* family found all over the world specially in tropical and subtropical countries with arid to semi-arid climates in Africa, Asia, North and South America, and Europe. It causes stem canker, seedling blight, charcoal rot, wilt, leaf blight (Figure 24B), stem blight and pre-emergence and post-emergence damping-off, dry root rot and stem rot of forest trees, fruit trees and weed species. In fact, *M. phaseolina* attacks a wide range of hosts in more than 500 cultivated and wild plant species (Kaur *et al*., 2012; Abbas *et al*., 2020). Major cultivated hosts include peanut (*Arachis hypogaea*), cabbage (*Brassica oleracea*), pepper (*Capsicum annuum*), chickpea (*Cicer arietinum*), soybean (*Glycine Max*), sunflower (*Helianthus annuus*), sweet potato (*Ipomoea batatas*), alfalfa (*Medicago sativa*), sesame (*Sesamum*

indicum), potato (*Solanum tuberosum*), sorghum (*Sorghum bicolor*), wheat (*Triticum aestivum*), and corn (*Zea mays*), among others.

M. phaseolina continues to cause huge economic losses in many crops and this prompt researcher on the identification and characterization of genetic variability within their epidemiological and pathological niches (Kaur, 2012; Chavan *et al*., 2019). Among the several and economical important crop infected there is also soybean (*Glycine max* L.), a Leguminosae which is one of the most important culture in the world for its utilization in agro-food and as biobased oil industry. It is not only used for human consumption, but also to produce low-cost, high protein produced in bulk as ingredients for remanufacture and formulated to-day in several different foods (Lusas *et al*., 1995). Soyabean was also genetically modified, and it represent the 40% of the total production in the world and it is essentially cultivated in Asia, Brazil, USA, India, and Argentina (Pagano and Miransari, 2016). The genus *Macrophomina* was first established by Petrak (1923) with the description of *M. philippinensis. M. phaseolina* was also identified on *Zea mays* (Vörös – Manninger, 1973), *Glycine max* (Érsek, 1979).

From 1987 to 1991 Simay, found this fungus in *Solanum tuberosum, Helianthus tuberosus, Phaseolus vulgaris, Vicia faba,* Allium sativum, moreover it was also identified in *Beta vulgaris, Cannabis sativa, Valeriana officinalis* (Simay, 1993), *Capsicum annuum* (Fischl *et al*., 1995), *Citrullus lanatus* (Békési *et al*., 1995) *Prunus armeniaca* (Vajna-Rozsnyai, 1995) and *Picea pungens* (Fischl *et al*., 2008).

Figure 24. A. Colony of *M. phaseolina* growing on PDA after 7 days (Lane *et al*., 2020). **B.** Leaf blight symptoms caused by *Macrophomina phaseolina*.

3.2.2- Bioactive metabolites produced by phytopathogenic fungi

Phytopathogenic fungi produce several bioactive metabolites that have a high functional diversity. They could be involved in the interaction with the host, virulence, biotic or abiotic stress protection and in some cases, they could be involved in symbiotic relationships (Nielsen *et al*., 2017, Ebert *et al*., 2019).

3.2.2.1- Metabolites from *Drechslera* species

Drechslera is a fungal genus well-known to produce numerous phytotoxic secondary metabolites. Most of the phytopathogenic *Drechslera* species and their phytotoxins, have been widely studied as agents of very severe diseases of cereal crops such as rice, maize, and sorghum, by causing brown spot lesions on the leaves (Au *et al*., 2000; Bury *et al*., 2013; Evidente *et al*., 2006a; Fayzalla *et al*., 2010). Ophiobolin A was the first and most representative compound isolated from *Drechslera* species (Figure 25). This metabolite was the main phytotoxin produced by the rice pathogen *Helminthosporium orizae* (or *Cochliobolus orizae*, or *Drechslera orizae*, or *Bipolaris orizae*). (Nozoe *et al*., 1965; Canonica *et al*., 1966). Successively, several ophiobolins close to ophiobolin A were isolated from different fungi and showed different biological activities as reviewed by *Au et al*., (2000) and to the most recent one by Masi *et al*., (2019).

Ophiobolin A was isolated from *Drechslera sorghicola* together with 3-anhydroophiobolin A and their 6-epimers (Figure 3). When tested by leaf spot assay on several plants, ophiobolin A and its 6-epimer resulted to be more phytotoxic than their anhydrous derivatives (Pena-Rodriguez and Chilton, 1989). A new macrolide named (-)-dihydropyrenophorin was isolated from *Drechslera avenae*, the causal agent of leaf blotch of oats. Its phytotoxic activity depended on the plant species used and from its concentration (Sugawara and Strobel, 1986). From *Drechslera tritici-repentis* the causal agent of reddish-brown spots on wheat (*Triticum vulgare*) were isolated two spirocyclic γ-lactams named triticones A and B. When assayed on wheat they showed phytotoxicity on both leaf and protoplasts (Sugawara *et al*., 1988). De-*O*-methyldiaporthin is a new isocoumarin, isolated from the liquid culture of *Drechslera siccans* a fungus pathogenic on oats (*Aoena sativa*), perennial ryegrass (*Lolium perenne*) and Italian ryegrass (*Lolium multiflorum*). When tested on host plants no symptoms appeared but when tested on corn (*Zea mays*), crabgrass (*Digitaria ischaemum*), and soybean (*Glycine max*) necrotic lesions were observed (Hallock *et al*., 1993). Ophiobolin A together with 3-anhydrous and 6-*epi*-ophiobolin A (Figure 25), and ophiobolin I (Figure 25). was also

isolated from *Drechslera gigantea*, as mycoherbicide against *Digitaria sanguinalis* (Evidente *et al*., 2006a). From the same culture filtrates were also isolated a new ophiobolin, named ophiobolin E (Figure 25), together with ophiobolins B and J (Figure 25) and its 8- epimer that was isolated for the first time (Figure 25). When assayed by the leaf puncture assay on four different weeds, only ophiobolins B and J resulted to be toxic, with ophiobolin B highly toxic on *Bromus* sp. and *Hordeum marinum* leaves (Evidente *et al*., 2006b). The possibility to have a good amount of ophiobolin A allowed wider range of studies. Thus, ophiobolin A showed to have strong anticancer activity against different human cancer cells (Bury *et al*., 2013; Locato *et al*., 2015). When assayed on several dicotyledon weeds, ophiobolin A showed to be the most phytotoxic among the tested compounds and the hydroxy group at C-3, the stereochemistry at C-6, and the aldehyde group at C-7 appeared to be very important structural features to impart this phytotoxicity (Evidente *et al*., 2006a).The tridimensional structure of ophiobolin A, which is closely related to its biological activity was determined by X-ray diffractometric analysis (Andolfi *et al*., 2006). On the basis of the biological activity reported by Au *et al*., (2000), ophiobolin A was assayed for its growth-inhibitory activity in both plant and mammalian cells inducing cell death in *Nicotiana tabacum* L. cv. Bright Yellow 2 (TBY-2) cells, showing typical features of apoptosis-like cell death, and inhibited eight cancer cell lines growth by 50% after 3 days. Ophiobolin A also showed significant antitumor activity on B16F10 mouse melanoma model with lung pseudometastases when assayed at 10 mg/kg and inhibited the proliferation and migration of glioblastoma multiforme (GBM) GBM cells, likely by inhibiting big conductance Ca2þ-activated Kþ channel (BKCa) channel activity. The ophiobolin A induced paraptosis-like cell death in GBM cells, which correlated with the cytoplasmatic vacuolization, possibly brought about by the swelling and fusion of mitochondria and/or the endoplasmic reticulum (ER) (Bury *et al*., 2013). These results induced to try to increase the efficacy of ophiobolin A by its formulation and thus chemoembolization particles for its delivery were synthesized and tested to investigate cell death mechanism on a Rhabdomyosarcoma cancer (RD), which is the most common soft tissue sarcoma in children. The use of ophiobolin A onto RD cells in culture showed a 70% reduction in cell (Morrison *et al*., 2014).

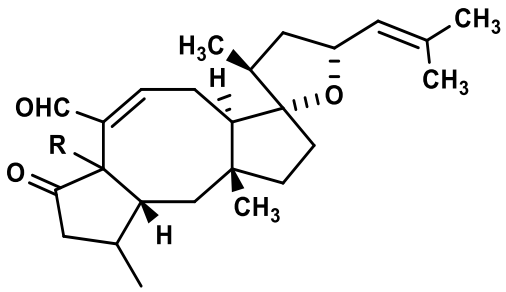

Ophiobolin A, R=βH
6-*epi*-Ophiobolin A, R=αH

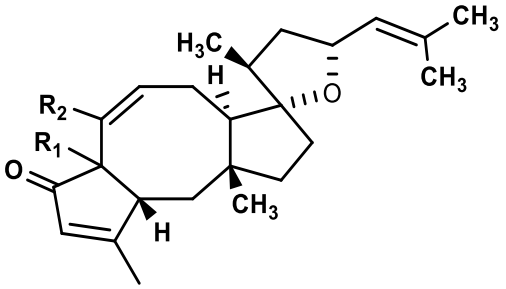

3-Anhydro-6-*epi*-ophiobolin A, R_1=αH, R_2=CHO
Ophiobolin I, R_1=βH, R_2=CH_2OH

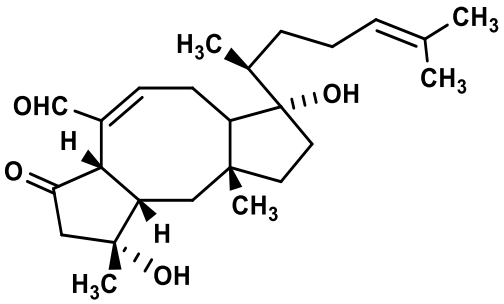

Ophiobolin B

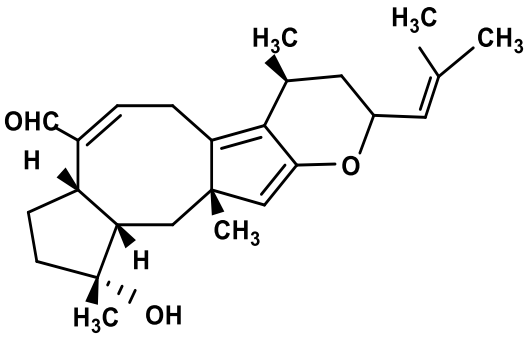

Ophiobolin E

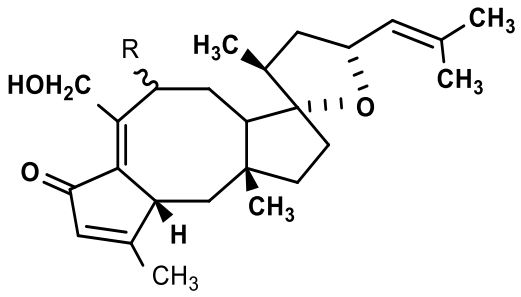

Ophiobolin J, R=βOH
8-*epi*-Ophiobolin J, R=αOH

Figure 25. Some metabolites produced by *Drechslera gigantea*.

3.2.2.2. Secondary metabolites produced by *Macrophomina phaseolina*

M. phaseolina has been reported to produce different secondary metabolites (Salvatore *et al*., 2020) (Figure 26). In fact, studies were carried out to investigate the phytotoxins produced by the pathogen and potentially involved in charchoal rot disease (Evidente *et al*., 2019). Phaseolinone, an eremophilane sequiterpenoids, which inhibits the seed germination of black gram (*Phaseolus mungo* L.), was firstly isolated from culture filtrates of *M. phaseolina* and

its structure was determined by spectroscopic and chemical methods (Dahr *et al*., 1982). Its absolute stereochemistry was assigned by comparison of its ECD and ^{1}H NMR data with those of phomenone another eremophilane sesquitepenoid isolated from *Phoma exigua*, and other *Phoma* sp. as *Phoma destructiva* Plowr responsible of a wilt tomato disease (*Lycopersicon esculentum* Mill.) (Capasso *et al*., 1984). Successively, phaseolinone was isolated in India from the couture filtrates of *M. phaseolina* together with asperlin, isoasperlin, phaseolinic acid and acetylphomalactone. All the metabolites were able to cause nonspecific leaf necrosis on several plants but only phaseolinone induced disease symptoms in plants similar to those caused by the pathogen (Bhattacharya *et al*., 1992).When *M. phaseolina* was grown in Mississippi, phaseolinone was not produced but the main phytotoxin appeared to be (-)-botryodiplodin (Ramezani *et al*., 2007), a mycotoxin previously isolated from *Botryodiplodia theobromae*, a fungus that causes rot in tropical fruits (Sen Gupta *et al*., 1966). (-)-Botryopdiplodin was synthetized as racemic mixture and as a pure enantiomer (Mukaiyama *et al*., 1974; Andrey *et al*., 2003; Nouguier *et al*., 2003) and its availability allowed to study its role in plant disease (Abbas *et al*., 2020).Recently, the metabolites produced by a strain of *M. phaseolina* isolated from *Eucalyptus globulus* were investigated and identified as the well-known fungal metabolites (3*R*,4*S*)-botryodiplodin, succinic acid, tyrosol, (*R*)-mellein, and *cis*-(3*R*,4*R*)-4-hydroxymellein and azelaic acid. However, no biological activities were reported for these metabolites (Salvatore *et al*., 2020). Soybean is becoming a crop very important for the agriculture in Argentina. However, the growing conditions under monoculture and no-tillage system have favored the occurrence and the severity of a large number of diseases, which constitute a serious constraint to production and the quality of the legume. Thus, many studies were carried out to develop method based on their biocontrol. Some bacteria were evaluated in dual in vitro test for their antifungal activity combined with manganese phosphate. Two strains were selected as *Pseudomonas fluorescens* and *Bacillus subtilis*. Consequently, greenhouse experiment demonstrates that greatest reductions in soybean disease severity induced by *M. phaselina* were achieved when strain *P. fluorescens* was applied singly or when strain *B. subtilis* was combined with manganese phosphite, achieving 82% of control in both cases (Simonetti *et al*., 2015). Recently, a strain of *Pseudomonas donghensis* SVBP6, isolated from an agricultural plot in Argentina, showed a broad spectrum and diffusible antifungal activity. From its culture filtrates the main antifungal metabolite was isolated and identified as 7-hydroxytropolone which showed significant antifungal activity against *M. phaseolina*. This result is very important for its potential practical application as natural fungicide easily to

synthesize and biofomulate and as a precursor for novel bioactive tropolonoid compounds (Muzio *et al*., 2020).

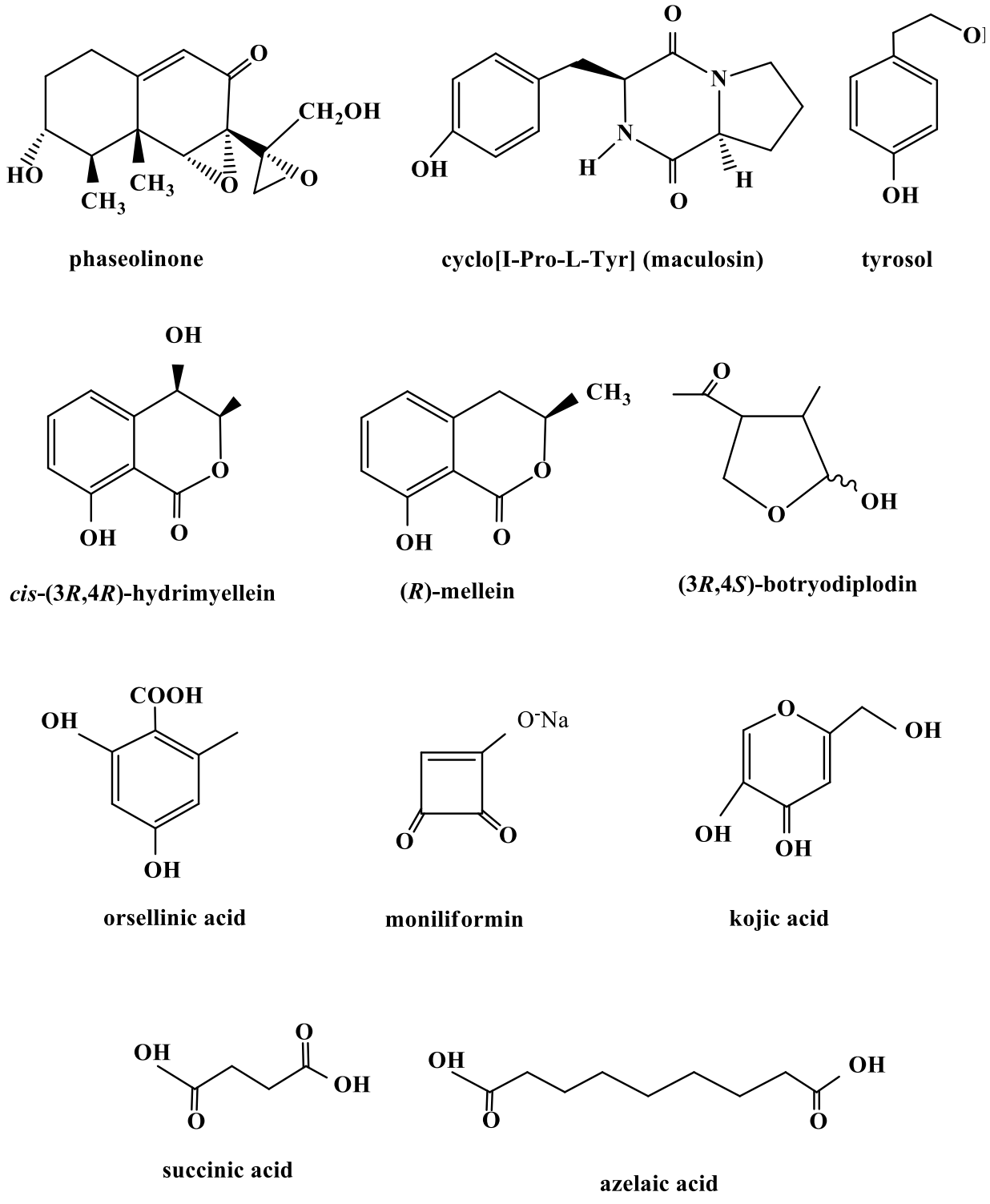

Figure 26. Some metabolites produced by *Macrophomina phaseolina*.

3.3- Materials and Methods

3.3.1- Production, extraction, and purification of bioactive metabolites from *Dreschlera gigantea*

3.3.1.1- Production of *Dreschlera gigantea*

The *D. gigantea* N. 7004 strain was isolated from Prof. R. Charudattan, during extensive field surveys in Florida, from naturally infected large crabgrass (*Digitaria sanguinalis*) (Chandramohan and Charudattan, 2001). It was stored in PDA slants both in the Biological Control of Weeds Collection at the Plant Pathology Department, University of Florida/IFAS, Gainesville, FL, USA (N. LCLF-1). The fungus was grown and maintained on Petri dishes containing PDA (potato-dextrose-agar, Oxoid, England), Roux bottles (1 l) containing a mineral-defined medium (350 ml) (Pinkerton and Strobel, 1976), were seeded with mycelial fragments obtained from colonies actively growing on PDA plates. The cultures were incubated at 25 °C in the dark for 10 days, then filtered and lyophilized by Dr. M. Vurro.

3.3.1.2- General Procedures

Optical rotations were measured in a MeOH solutions on a Jasco P-1010 digital polarimeter (Jasco, Tokyo, Japan); IR spectra were recorded as a glassy film on a Perkin-Elmer Spectrum One FT-IR spectrometer (Madison, WI, USA). UV and ECD spectra were recorded at room temperature on a JASCO J815 spectropolarimeter (Jasco, Tokyo, Japan), using 0.5 mm cells and concentrations of about 4.5×10^{-3} M for 1 and 2.5×10^{-3} M for 2. ^{1}H and ^{13}C NMR spectra were recorded at 400 and 100 MHz, respectively, in $CDCl_3$ by Bruker spectrometers (Karlsruhe, Germany). The same solvent was used as internal standard. Carbon multiplicities were determined by DEPT (Distortionless Enhancement by Polarization Transfer) spectra (Berger and Braun, 2004). DEPT, COSY-45 (Correlated Spectroscopy), HSQC (Heteronuclear Single Quantum Correlation), HMBC (Heteronuclear Multiple Quantum Correlation) and NOESY (Nuclear Overhauser Effect Spectroscopy) experiments (Berger and Braun, 2004), were performed using Bruker microprograms. Chemical shifts are in δ (ppm). Coupling constants (*J*) are in Hertz. The following symbols were used: *s*=singlet; *br s*: broad singlet; *d*: doublet; *dd*: double doublet; *ddd*: doublet of double doublet; *t*: triplet; *q*: quartet; *m*: multiplet.

High resolution electrospray ionization mass spectrometry (HRESIMS), electrospray ionization mass spectrometry (ESIMS) and liquid chromatography mass spectrometry (LC/MS) analyses were performed using the LC/MS Timeof-flight (TOF) system AGILENT

(Agilent Technologies, Milan, Italy) 6230B, HPLC 1260 Infinity. The HPLC separations were performed with a Phenomenex LUNA column (C18 (2) 5µm 150 x 4.6 mm) (Torrance, CA, USA). Column chromatography was performed using silica gel (Kieselgel 60, 0.063-0.200 mm) (Merck, Darmstadt, Germany). Analytical, preparative and reverse phase TLCs were carried out on silica gel (Merck, Kieselgel 60, F_{254}, 0.25, 0.5 mm and RP-18 F254s, respectively) plates (Merck, Darmstadt, Germany). The spots were visualized by exposure to UV radiation, or by spraying first with 10% H_2SO_4 in MeOH, and then with 5% phosphomolybdic acid in EtOH, followed by heating at 110°C for 10 min.

3.3.1.3- Extraction, and Purification of secondary metabolites from *Drechslera gigantea* culture filtrate

The lyophilized material obtained from the culture filtrates (4 L) was dissolved in distilled water (400 mL, final pH 4.5) and extracted with EtOAc (3 × 400 mL) (Sugawara *et al*., 1993). The organic extracts were combined, dried with Na_2SO_4, filtered, and evaporated under reduced pressure obtaining a brown oil residue (1.2 g). This latter was chromatographed on silica gel eluted with $CHCl_3$-*i*-PrOH (96:4, v/v) obtaining eleven groups of homogeneous fractions. The residue of the third fraction (540 mg) was crystallized with EtOAc-*n*-hexane (1:5, v/v) giving white crystals of ophiobolin A (**11**, 448.2 mg, Figure 27). The residue obtained from the mother liquors of crystallization (91.8 mg) was further purified by TLC, eluted three times with $CHCl_3$-*i*-PrOH (98:2, v/v), yielding five bands. The first and fifth bands resulted to be two homogeneous amorphous solids identified as 3-anhydrous-6-*epi*-ophiobolin A (**13**, 13.2 mg, Figure 27) and 6-*epi*-ophiobolin A (**12**, 7.9 mg, Figure 27). From the second band, further amount of (**12**, 24.5 mg) was obtained as a white crystalline solid. The residues of third (3.4 mg) and fourth (2.6 mg) bands were further purified on TLCs, eluted with *n*-hexane-EtOAc (65:35, v/v) and petroleum ether-acetone-EtOAc (75:15:10, v/v/v), yielding an amorphous solid, which being new as below reported, was named drophiobolin B (**16**, 1.9 mg, Figure 27).

The residue of the seventh fraction (36.0 mg) of the first column, was further purified by two successive steps on TLC, using as eluent first EtOAc-*n*-hexane (5.5:4.5, v/v) and then $CHCl_3$-*i*-PrOH (94:6, v/v), yielding another amorphous solid identified as ophiobolin I (**14**, 8.9 mg, Fig. 27). The residue of the ninth fraction was further purified on reverse phase TLC using as eluent acetone-H_2O (75:25, v/v) and then on TLC eluted with $CHCl_3$-*i*-PrOH (95:5, v/v) yielding another amorphous solid, which being new as below reported, was named drophiobolin A (**15**, 1.2 mg, Fig. 27).

3.3.1.4- Computational Details

Preliminary conformational analyses were performed by Spartan02 (Wavefunction, Inc., Irvine CA, 2002) package employing MMFF94s molecular mechanics force field with Monte Carlo searching and fixing arbitrarily ACs (2*S*,6*R*,10*R*,11*R*,14*S*,15*S*) and (2*S*,6*R*,10*R*,11*R*,15*S*,15*S*) for the two epimers **2a** and **2b** of **(15**) and (2*R*,10*R*,11*R*,14*S*,15*S*,17*R*) for (**16**). All possible conformers were searched, considering the degrees of freedom of the system within an energy window of 30 kcal/mol. The minimum energy conformers found by molecular mechanics were further fully optimized by using the DFT at the DFT/B3LYP/TZVP level taking into account the solvent effect by using the IEFPCM implicit model with acetonitrile as solvent by Gaussian09 package (Frisch *et al*., 2009). All conformers are real minima, no imaginary vibrational frequencies have been found, and the free energy values have been calculated and used to get the Boltzmann population of conformers at 298.15 K. The DFT/ B3LYP/ TZVP/ IEFPCM (MeCN) geometries were employed as input geometries for calculation of UV and ECD spectra at the TDDFT/ CAM-B3LYP/ 6-311++G(2d,2p)/ IEFPCM (MeCN) level of theory.

The theoretical UV and ECD spectra were obtained as average over the conformer Boltzmann populations. The ECD spectra were obtained from calculated excitation energies and rotational strengths, as a sum of Gaussian functions centered at the wavelength of each transition, with a parameter σ (width of the band at 1 / 2 height) of 0.3 eV. To guarantee origin independence and to evaluate the quality of the molecular wave functions employed, theoretical ECD spectra were obtained both in the length and velocity representation, using the lowest 30 states.

The velocity/length calculated spectra were almost coincident, indicating a good level of calculation. Therefore, in all figures, only the velocity-form predicted spectra are reported. Calculated spectra have been redshifted by 10 nm, for compounds (**2a** and **2b**), and by 12 nm for compound (**16**). In addition, the intensity of coumpounds (**2a** and **2b**) have been scaled by 30 units and that of compound (**16**) by 4 units.

3.3.1.5- Biological assays

3.3.1.5.1- *Phytotoxic assay*

The phytotoxic activity of drophiobolins A and B and ophiobolin A was tested at 10^{-3} and 10^{-4} M by leaf-puncture assay on weeds (*Digitaria sanguinalis* L. and *Chenopodium album* L) and cultivated plant (*Lycopersicon esculentum* L.), as previously reported (Liu *et al*., 2019).

The compounds were dissolved in a small amount of MeOH and then diluted to the desired concentration with distilled water (final concentration of MeOH 2%).

3.3.1.5.2- *Cytotoxic activity MTT assay*

The effect of drophiobiolins A and B on cell viability was evaluated on human immortalized Hacat skin keratinocytes and tumor derived A431 (epidermoid carcinoma), H1299 (nonsmall cell lung carcinoma), and HeLa B (cervix adenocarcinoma) cell lines. Drophobiolins A and B cytotoxicity were compared to that of ophiobolin A. Cells were seeded at 10^4 in 96 well plates. Twenty-four hours later, the medium was changed and supplemented with drophobiolins A, B and ophiobolin A (from 0.5 µM to 10 µM) in DMSO. After 24h of incubation cell viability was determined by MTT assays. Aliquots (10 µl) of MTT solution 1:10 (stock solution 5 mg/ml) were added to each well containing 100 µl of medium and incubated with cells for 4 h. After incubation, the medium was removed and 150 µl aliquots of DMSO were added to each well to solubilize the formazan crystals.

Optical density was measured after 4 h with an ELISA reader (Bio-Rad) in a dual-wavelength mode (570 and 630 nm) filter using an iMark microplate reader (Bio-Rad) and calculated as follows: Absorbance (570 nm) − Absorbance (630 nm). The cell viability was calculated as (Absorbance of test sample) / (Absorbance of control).

All experiments were performed three times in triplicates and presented as mean ± standard deviation calculated using GraphPad Prism8 software. Analysis of variance was performed by one-way ANOVA and multiple comparisons. $*P < 0.5$ when compared with the control.

3.3.2- Production, extraction, and purification of bioactive metabolites from *Macrophomina phaseolina*

3.3.2.1- Production of *Macrophomina phaseolina*

The *M. phaseolina* 2013-1 strain was obtained from infected soybean roots growing in Pergamino, Buenos Aires province, Argentina and maintained on potato dextrose agar (PDA) in Petri dish. The isolate was deposited in the fungal culture collection of the Plant Pathology Department of the University of Buenos Aires (FAUBA, Argentina). Later, the isolate was grown under stationary conditions in 2 L flasks containing 1 L of PDB. Each flask was inoculated with 15 mycelial plugs and incubated at 25 °C in the dark for 15 days. Then, the mycelial mats were removed by centrifugation (7000 rpm for 30 min) and successive

filtration of the supernatant using 0.22 μm pore diameter membranes (Whatman, Maidstone, UK).

3.3.2.2- General Procedures

A P-1010 digital Jasco polarimeter was used to measure the optical rotations in MeOH; a PerkinElmer Spectrum 100 FT-IR spectrometer (Madison, WI, USA) was employed to record IR spectra as glassy film; a Jasco V-530 spectrophotometer was utilized to acquire UV spectra in MeCN solution; UV and ECD spectra were recorded at room temperature on a JASCO J815 spectropolarimeter(Jasco, Tokyo, Japan), using 0.1 mm cells and concentrations of ca. 1.7×10^{-2} M in MeOH. ^{1}H and ^{13}C NMR spectra were recorded in $CDCl_3$, also used as internal standard, at 400/100 MHz on a Bruker spectrometer. COSY-45, HSQC, and HMBC experiments were performed using a Bruker microprogram. HRESI and ESI mass spectra and liquid chromatography (LC)/MS analyses were carried out using the LC/MS TOF system Agilent 6230B, HPLC 1260 Infinity. A Phenomenex LUNA (C18 (2) 5u 150 × 4.6 mm column) was utilized to perform the HPLC separations. Preparative and analytical TLC were performed on silica gel (Merck, Kieselgel 60 F254, 0.50 and 0.25 mm, respectively) plates, while column chromatography (CC) was performed on silica gel (Merck, Kieselgel 60, 0.063−0.200 364 mm); the spots were visualized by exposure to UV light and/or by spraying with 10% H_2SO_4 in MeOH and with 5% phosphomolybdic acid in EtOH, followed by heating at 110 °C for 10 min. Sigma-Aldrich Co. (Milan, Italy) supplied all the reagents and the solvents.

3.3.2.3- Extraction and Purification of secondary metabolites from *Macrophomina phaseolina* culture filtrates

The culture filtrates (4 L), showing significative phytotoxic activity on tomato (*S. lycopersicum* L.), were combined, and concentrated under vacuum at room temperature to 400 mL. Then, the culture was acidified to pH 2 with formic acid and extracted exhaustively with EtOAc (3 × 400 mL). The combined organic extracts were dried with Na_2SO_4, filtered, and evaporated under reduced pressure (Sugawara *et al*., 1993). The organic residue (109.7 mg) was chromatographed on silica gel eluted with EtOAc-MeOH-H_2O (85:10:5, v/v/v) obtaining eight groups of homogeneous fractions. The residue of the second fraction (8.3 mg) was purified on TLC eluted with CH_2Cl_2-MeOH, (1:1, v/v), yielding guignardone A (**17**, 3.6 mg, Figure 37) as an amorphous solid. The residue of the seventh fraction (20.2 mg) was further purified on TLC eluted with $CHCl_3$-EtOAc-MeOH-H_2O (2:2:1, v/v/v) yielding

phaseocyclopentenones A (**18**, 10.2 mg, Figure 37) and B (**19**, 7.5 mg, Figure 37) as two yellowish oils.

3.3.2.3.1- *3,5-Di-O-Acetyl Derivative of Phaseocyclopentenone A* (20)

Phaseocyclopentenone A (**9**, 1 mg) was acetylated with pyridine (20 μL) and Ac_2O (20 μL). The reaction was left at room temperature in the dark for 48 h and stopped by evaporation under a N_2 stream. The residue (1.2 mg) was purified by TLC, eluted with CH_2Cl_2-MeOH (9:1, v/v) to afford (**20**) as a homogeneous compound.

3.3.2.4- Computational Details

Molecular mechanics and preliminary density functional theory (DFT) calculations were run with Spartan'18 (Wavefunction, Inc., Irvine CA, 2018), with standard parameters and convergence criteria. Final DFT and time-dependent DFT (TDDFT) calculations were run with Gaussian'16 (Frisch *et al*., 2009) with default grids and convergence criteria. First, the conformational space of phaseocyclopentenone A (**18**) and phaseocyclopentenone B (**19**) was sampled with the Monte Carlo algorithm using Merck molecular force field (MMFF).

All conformers thus found were first optimized at the ωB97X-D /6-31G(d) level in vacuo, then at the ωB97X-D /6-311+G(d,p) level including SMD solvent model for acetonitrile. The procedure led to four conformers for phaseocyclopentenone A (**18**) and one conformer for phaseocyclopentenone B (**19**) with sizable population at 300 K. TDDFT calculations were run using B3LYP and CAM-B3LYP functionals (which led to consistent results) with the def2-TZVP basis set and including the IEF-PCM solvent model for MeCN.

The calculations included 48 excited states (roots). ECD spectra were generated by applying a Gaussian band shape with 0.4 eV exponential half-width, from dipole-length rotational strengths. The difference with dipole-velocity values was negligible. The calculated spectra in Figure 37 are plotted with SpecDis; (Bruhn *et al*., 2013) they are red shifted by 10 nm (**18**) or 5 nm (**19**) and scaled by a factor 1.5 to compare with the experimental spectra.

3.3.2.5- Biological assays

3.3.2.5.1- *Phytotoxic assay*

Tomato Cutting Assay

The culture filtrate, the organic extract (at a concentration of 1 mg/mL) and phaseocyclopentenones A and B (**18** and **19**) were assayed on tomato (*S. lycopersicum* L.) cuttings. Tomato cuttings were taken from 21-day-old seedlings, and compounds (**18**) and

(**19**) were assayed at a concentration of 10^{-3} M. Cuttings were placed in the test solutions (2 mL) for 72 h and then transferred to distilled water. MeOH in distilled water (4%) was used as negative control. Three replications were performed for the organic extract and each metabolite. Symptoms were visually evaluated up to 7 days.

Leaf puncture assay

Compounds (**17-19**) were also tested on tomato and soybean (*Glycine max* L.) using the leaf puncture assay at a concentration of 10^{-3} M and 10^{-4} M. Compounds (**17-19**) were first dissolved in MeOH (final concentration: 4%) and sterile distilled water was then added to reach the desired concentration. A droplet (20 µL) of the solutions obtained was applied on the adaxial surface of the plant leaves which were previously punctured with a sterile needle. The leaves were placed on the surface of a water-saturated filter paper in petri dishes. A solution of 4% MeOH in distilled water was used as negative control. The dishes were sealed with parafilm and incubated at 24°C for 7 days in a temperature-regulated chamber. Three replications were performed for each metabolite and plant species. The results were observed after 7 days of treatment.

3.1.2.5.2- *Antifungal Bioassay*

The antagonistic potential of compounds (**17-19**) was tested against two strains of the soybean pathogenic fungi, *Cercospora nicotiane* (Sautua *et al*., 2020) and *Colletotrichum truncatum* (Ramos *et al*., 2013) isolated in Argentina, as inhibition of the mycelial radial growth. In brief, 6 mm diameter mycelial plugs from a 4-day-old culture of *C. nicotianae* or *C. truncatum* was placed in the center of PDA plates.

For each compound, amounts of 50, 100, and 200 µg were dissolved in 20 µL of 4% MeOH and applied on the top of different mycelial plug. Pentachloronitrobenzene 20 µL of 4% MeOH at a concentration of 25 µg/µL were used as negative and positive controls, respectively. The solvent was allowed to evaporate in a laminar flow cabinet, and the plates were incubated at 20°C for 4−7 days or until the growth of the target fungi used as negative control covered the entire plate surface.

Each treatment consisted of three replicates, and the experiment was repeated twice. The results were expressed as the presence or absence of growth (an indication of antifungal activity).

3.4- Results and Discussion

3.4.1- Structural characterization of secondary metabolites from *Dreschslera gigantea*

The organic extract obtained from the culture filtrates of *D. gigantea* was purified, as detailed in the Experimental Section, obtaining four compounds proved to be well-known ophiobolins, ophiobolin A, 6-*epi*-ophiobolin A, 3-anhydro-6-*epi*-ophiobolin A, and ophiobolin I (**11-14,** Figure 27). They were identified by comparing their spectroscopic data (^{1}H NMR and ESIMS) with reported data (Evidente *et al*., 2006). The other two new ophiobolan sesterterpenoids, named drophiobiolins A and B (**15** and **16**, Figures 27). The preliminary ^{1}H and ^{13}C NMR investigation showed that drophiobolin A (**15**) was close to 3-anydrophiobolin A (Kim *et al*., 1984; Pena-Rodriguez and Chilton, 1989) while drophiobiolins B (**16**) appeared close to ophiobolin I (**14**) (Evidente *et al*., 2006b).

3.4.1.1- Ophiobolin A (11)

Ophiobolin A was obtained as white crystals, had: mp 182-185 °, $[\alpha]^{25}_D$ +270° (*c* 0.4), IR ν_{max} 3468 (O-H), 1740 (C=O), 1664 (C=C) cm^{-1}, UV λ_{max} nm (logε) 238 (4.1) [(Nozoe *et al*., 1965): mp 182°, $[\alpha]_D$ +270°, IR ν_{max}($CHCl_3$) 3500, 1743, 1633 cm^{-1}; UV λ_{max}(EtOH) nm (ε) 238 (13800)], [(Li *et al*., 1995): mp 170-172°, $[\alpha]_D$= +265.5° (c=1.0, $CHCl_3$), IR ν_{max} 3500, 1730, 1690, 1660, 1625 cm^{-1}], ^{1}H NMR spectrum is very similar to those previously reported (Sugawara *et al*., 1987; Canales *et al*., 1988; Li *et al*., 1995; Evidente *et al*., 2006). ESIMS *m/z*: 385 $[M+H]^+$, 407 $[M+Na]^+$, 423 $[M+K]^+$. These data agree with those previously reported (Sugawara *et al*., 1988).

3.4.1.2- 6-epi-ophiobolin A (12)

6-*epi*-ophiobolin A was obtained as an homogeneous amorphous solid, had: $[\alpha]^{25}_D$ +44° (*c* 0.1) [(Sugawara *et al*., 1987): $[\alpha]_D$ +46° (*c* 5.3, $CHCl_3$)]; IR ν_{max} 3445 (O-H), 1742 (C=O), 1683 (unsatureated C=O) cm^{-1}, [(Kim *et al*., 1984): IR ν_{max}^{film}: 3450, 1740, 1684, 1640 cm^{-1}]; UV λ_{max} nm (log ε) 235 (4.0); ^{1}H NMR spectrum was very similar to those previously reported (Sugawara *et al*., 1987; Canales *et al*., 1988; Evidente *et al*., 2006). ESIMS (+) *m/z*: 401 $[M+H]^+$, 423 $[M+Na]^+$, 439 $[M+K]^+$. These data agree with those previously reported (Sugawara *et al*., 1987; Evidente *et al*., 2006b).

3.4.1.3- 3-anhydrous-6-epi-ophiobolin A (13)

3-anhydro-6-*epi*-ophiobolin A was obtained as an homogeneous amorphous solid, had: $[\alpha]^{25}_{D}$ +7 (*c* 0.1); IR ν_{max} 1685 (α,β unsaturated C=O), 1645 (C=C) cm^{1}; UV λ_{max} nm (log ε) 225 (3.6), 235 (4.0); ^{1}H NMR spectrum is very similar to those previously reported (Sugawara *et al*., 1987; Canales *et al*., 1988; Evidente *et al*., 2006b) only for the following signals, δ: 2.24 (1H, dd, *J*=6.7 and 3.8 Hz, H-15), 1.99 (1H, dd, *J*=13.2, 2.5 Hz, H-13A), 1.80 (H, m, H-12A), 1.42 and 1.77 (1H each, m H_2C-1); ESIMS (+) *m/z*: 383 $[M+H]^+$, 405 $[M+Na]^+$, 421 $[M+K]^+$. These data agree with those previously reported (Sugawara *et al*., 1987; Evidente *et al*., 2006b).

3.4.1.4- Ophiobolin I (14)

Ophiobolin I, was obtained as a white crystals, had: $[\alpha]^{25}_{D}$ +46.7 (*c* 0.2); IR ν_{max}: 3409 (O-H), 1682 (α,β unsaturated C=O), 1619 (C=C) cm^{-1} [(Li *et al*., 1995): $[\alpha]^{25}_{D}$ +48.6° (*c* 1.0, $CHCl_3$); IR ν_{max} 3450, 1680, 1657, 1613 cm^{-1}]; UV λ_{max} nm (log ε) 225 (4.3) ; ^{1}H NMR spectrum is very similar to those previously reported (Li *et al*., 1995; Sugawara *et al*., 1987; Sugawara *et al*., 1988; Evidente *et al*., 2006b); ESIMS *m/z*: 385 $[M+H]^+$, 407 $[M+Na]^+$, 423 $[M+K]^+$. These data agree with those previously reported (Sugawara *et al*., 1987; Sugawara *et al*., 1988; Evidente *et al*., 2006b).

3.4.1.5- Drophiobolin A (15)

Drophiobolin A was obtained as an amorphous solid, had: IR ν_{max} 3422, 1734, 1615 cm^{-1}; UV λ_{max} (log ε) 275 (3.6) nm; ^{1}H and ^{13}C NMR (Fig. 13 and 14) are reported in Table 3; HR ESIMS (+): *m/z* 1229 $[3\ M+\ Na]^+$, 805 $[2\ M + H]^+$, 425 $[M + Na]^+$, 403.2858 [calcd for $C_{25}H_{39}O_4$ 403.2848 $M + H]^+$, 385 $[M + H - H_2O]^+$, 367 $[M + H - 2x\ H_2O]^+$.

3.4.1.6- Drophiobolin B (16)

Drophiobolin B was obtained as an amorphous solid, had: IR ν_{max} 3421, 1737, 1646, 1614 cm^{-1}; UV λ_{max} (log ε) 276 (3.6) nm; ^{1}H and ^{13}C NMR (Fig. 20 and 21) are reported in Table 3; HR ESIMS (+): *m/z* 819 $[2M + Na]^+$, 797 $[2M + H]^+$, 399.2526 [calcd for $C_{25}H_{35}O_4$ 399.2535, $M + H]^+$, 381 $[M + H - H_2O]^+$.

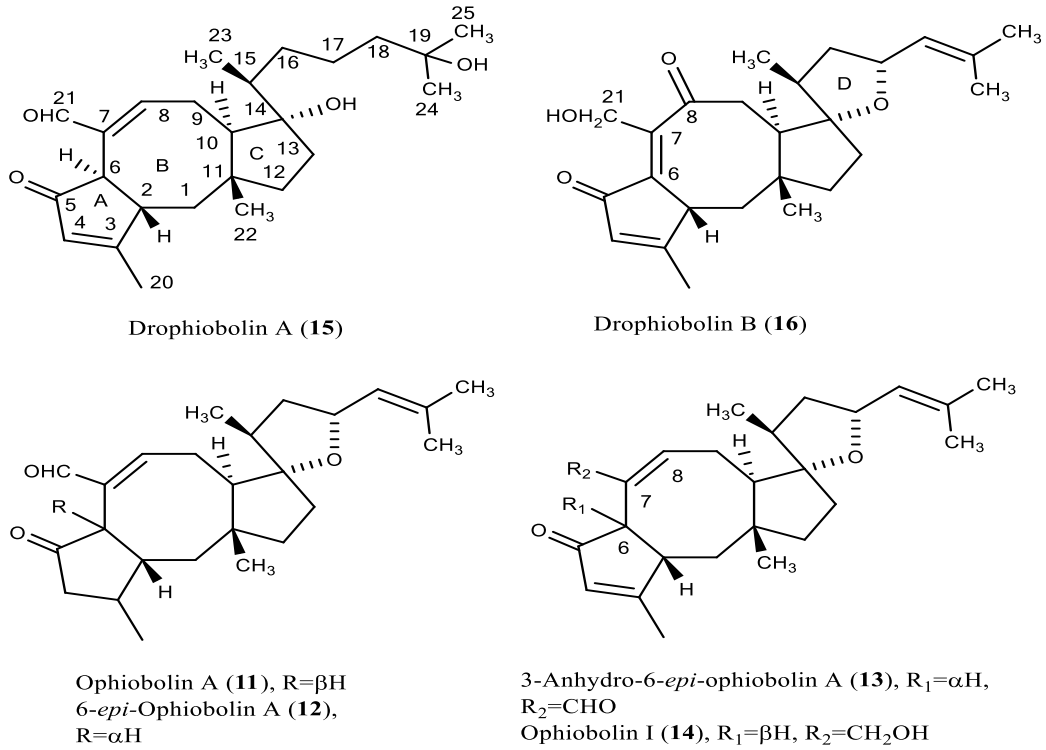

Figure 27. Structures of drophiobolin A and B (**15-16**), ophiobolin A, 6-epi-ophiobolin A, 3-anhydro-6epi- ophiobolin A and ophiobolin I (**11-14**).

3.4.1.7- Structural characterization of drophiobiolin A

Drophiobiolin A (**15**) had a molecular formula of $C_{25}H_{38}O_4$, as deduced from its ESIMS spectrum (Figure 34), which is consistent with seven indices of hydrogen deficiency. The comparison of its ^1H and ^{13}C NMR spectra (Figure 28 and 29), with those of 3-anhydrophiobolin A (**13**) confirmed their structural relation (Kim *et al*., 1984; Pena-Rodriguez and Chilton, 1989). These findings were confirmed by the bands typical for the hydroxyl, carbonyl and olefinic groups and the absorption maxima for an extended conjugated system recorded in the IR (Nakanishi and Solomon, 1977) and UV spectra (Pretsch and Bühlmann, 2000), respectively.

In particular, the ^1H and COSY data (Figure 28 and 30, Table 7) (Berger and Braun, 2004) showed the presence of a singlet, a double doublet (J = 6.3 and 2.4 Hz) and a broad singlet due to the protons of an aldehydic (H-21) and two trisubstituted olefinic (H-8 and H-4) groups at δ 9.33, 6.82 and 6.05, respectively. H-8 coupled with the hydrogens of the adjacent methylene group (H_2C-9) resonating both as a multiplet at δ 2.70 and 2.09 and these, in turn, with the broad double doublet (J = 14.0 and 2.8 Hz) of the adjacent methine hydrogen (H-10) at δ 2.57. H-9A overlapped the multiplet of an allylic proton (H-2) resonating as multiplet at

δ 2.70 which coupled with the two multiplets of the hydrogens of adjacent methylene group (H_2C-1) observed at δ 2.12 and 1.34. These signals accounted for the hydrogen of a suitable pentasubstituted fusacycloctenefuranone system. The multiplets of the hydrogens of two adjacent methylene groups (H_2C-12 and H_2C-13) of the 1,1,2,3,3-pentasubstituted cyclopentane were observed at δ 2.01 and 1.44 and 1.55 and 1.33, while the singlet and the broad singlet of a tertiary (Me-22) and a vinyl methyl (Me-20) groups resonated at δ 0.89 and 2.08 respectively.

Furthermore, the same two spectra also showed the signals of a 1,5-dimethyl-5-hydroxyhexyl side chain which was located at the tertiary hydroxylated carbon (C-14) of the cyclopentane based on the long-range couplings observed in the HMBC spectrum (Figure 32, Table 7) (Berger and Braun, 2004) between C-14 with H-15 and Me-23, which resonated as a multiplet and a doublet (J = 6.7) at δ 1.44 and 0.97, respectively.

H-15 coupled with the two hydrogens of the adjacent methylene groups (H_2C-16) at δ 1.44 and 1.12, with the hydrogens of the adjacent methylene group (H_2C-17) at δ 1.55 and 1.44, which overlapped the multiplets of the residual methylene group (H_2C-18). Finally, the two tail methyl groups Me-24 and Me-25 gave one only overlapped singlet at δ 1.26 (Pretsch and Bühlmann, 2000). The couplings observed in the HSQC spectrum (Figure 31, Table 7) (Berger and Braun, 2004) allowed to assign the chemical shifts to the protonated carbons of the ^{13}C NMR spectrum (Figure 29, Table 7). Consequently, the signals observed at δ 155.9, 130.7, 54.9, 50.2, 49.2, 46.5, 44.6, 41.8, 38.2, 35.7, 33.5, 29.8, 23.3, 23.0, 17.7 and 15.5 in the ^{13}C NMR spectrum were assigned to C-8, C-4, C-10, C-6, C-2, C-1, C-18, C-12, C-15, C-17, C-16, C-24 and C-25 (overlapped signals), C-13, C-22, C-20 and C-23, respectively (Breitmaier and Voelter, 1987). The residual six carbons (one of which was typical of a carbonyl group, two of quaternary olefinic and three quaternary sp^3 carbons) were also assigned based on the long-range couplings observed in the HMBC spectrum (Figure 32, Table 7). In particular, the coupling between the signals at δ 207.5 with H-6, 177.8 with H-1B and Me-20, 141.1 with H-6 and H-21, 88.8 with H-15 and Me-23, 71.4 with Me-24 and Me-25, and 45.2 with H_2-1, H_2-12 and Me-22 allowed to assign them to C-5, C-3, C-7, C-14, C-19 and C-11. Thus, the chemical shifts to all the carbons and corresponding hydrogens of (**15**) were assigned and reported in Table 7. These data appeared consistent with the typical ophiobolan 5-8-5 fused ring system and (**15**) was formulated as 7-hydroxy-7-(6-hydroxy-6-methylheptan-2-yl)-1,9a-dimethyl-3-oxo-3,3a,6,6a,7,8,9,9a,10,10a-decahydrodicyclopenta

[a,d][8]annulene-4-carbaldehyde. The structure assigned to (**15**) was supported by the other correlations observed in the HMBC spectrum (Figure 32, Table 7) and by the data from its ESIMS spectrum (Figure 34) which showed the presence of a trimeric sodium adduct [3 M + Na]$^+$, the protonated dimeric [2 M + H]$^+$, sodium [M + Na]$^+$ and protonated [M + H]$^+$ adducts ions at *m/z* 1229, 805, 425 and 403.2858, respectively. The latter, by two consecutive losses of water, generated the significant fragmentation ions [M + H - H_2O]$^+$ and [M + H - 2 x H_2O]$^+$, at *m/z* 385 and 367.

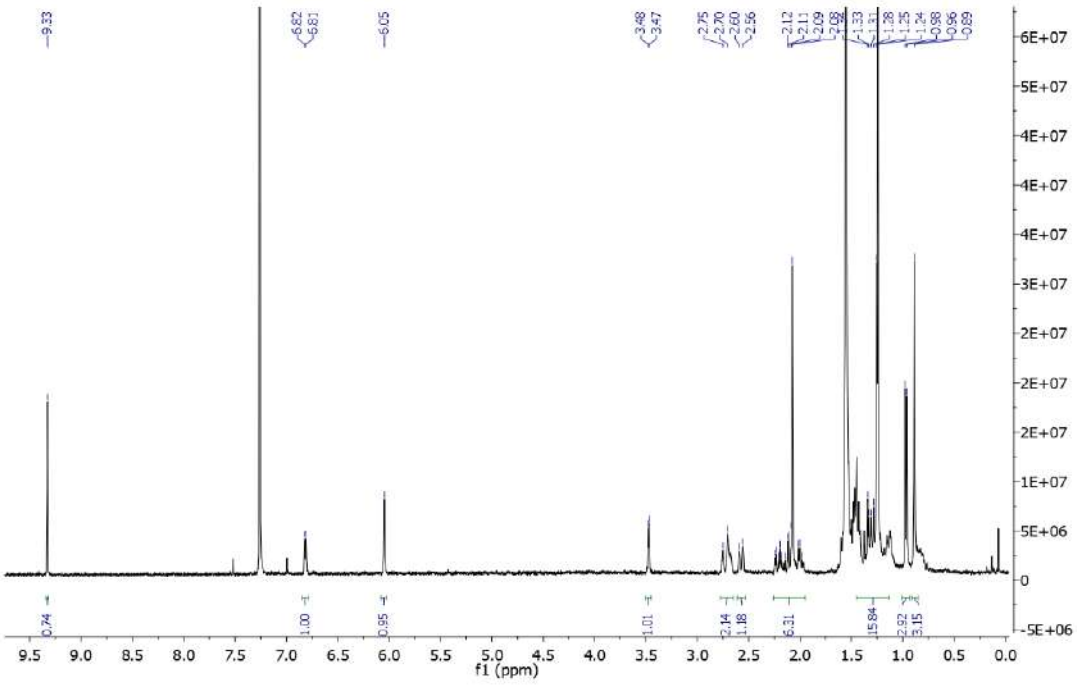

Figure 28. ^{1}H NMR spectrum of drophiobolin A (**15**) ($CDCl_3$, 400 MHz).

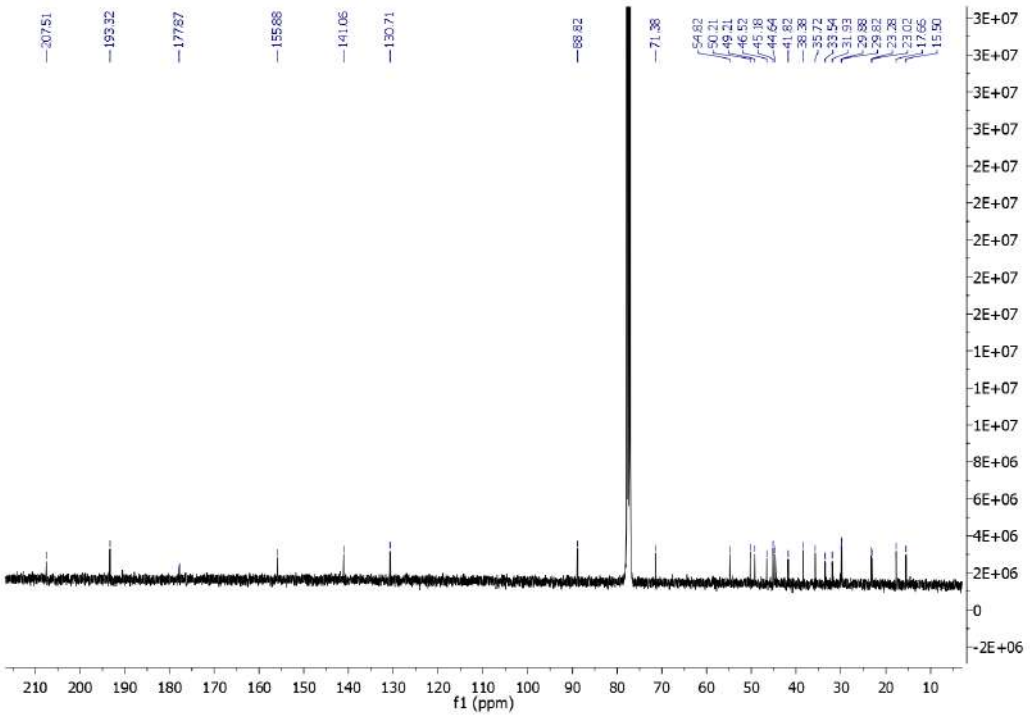

Figure 29. ^{13}C NMR spectrum of drophiobolin A (**15**) ($CDCl_3$, 100 MHz).

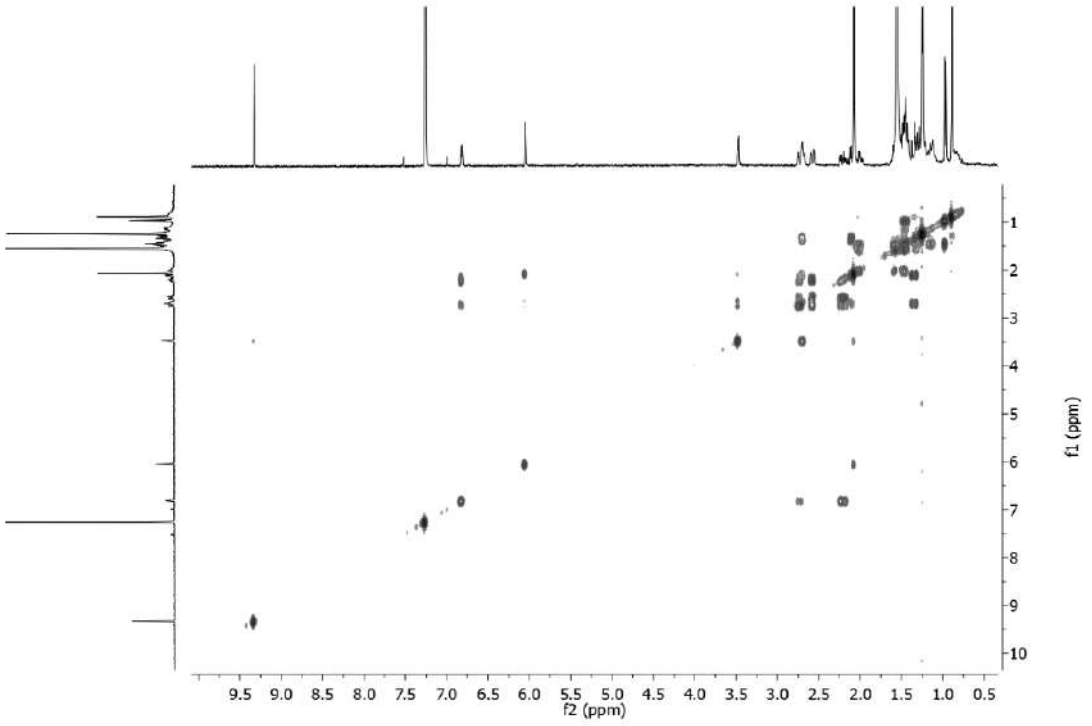

Figure 30. COSY spectrum of drophiobolin A (**15**) ($CDCl_3$, 400 MHz).

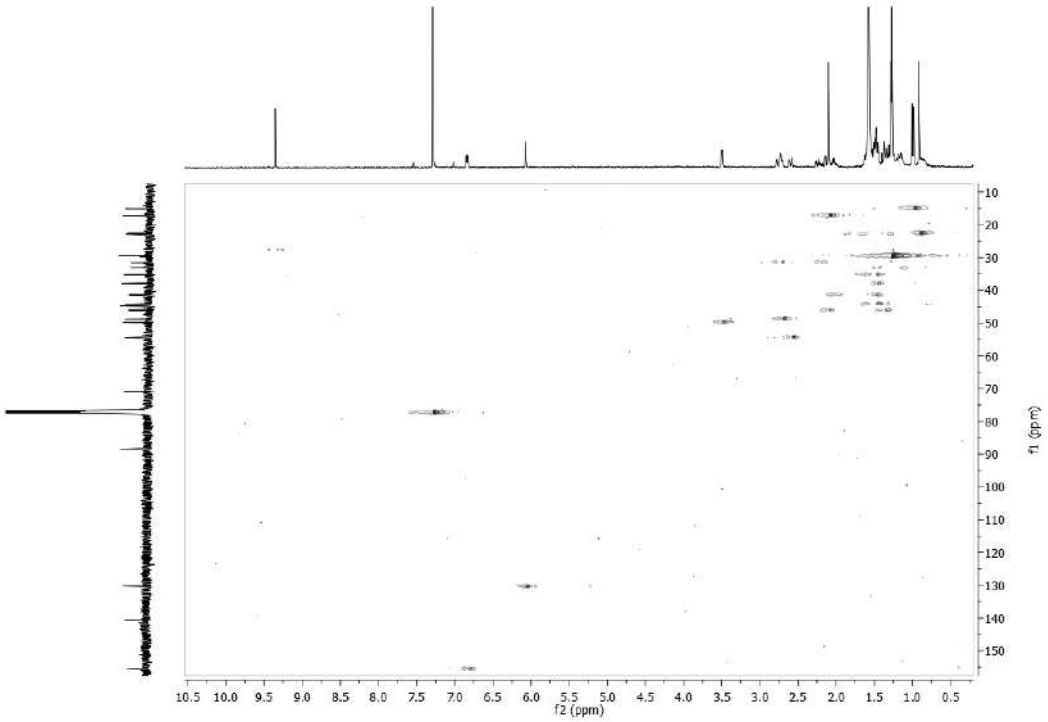

Figure 31. HSQC spectrum of drophiobolin A (**15**) ($CDCl_3$, 400/100 MHz).

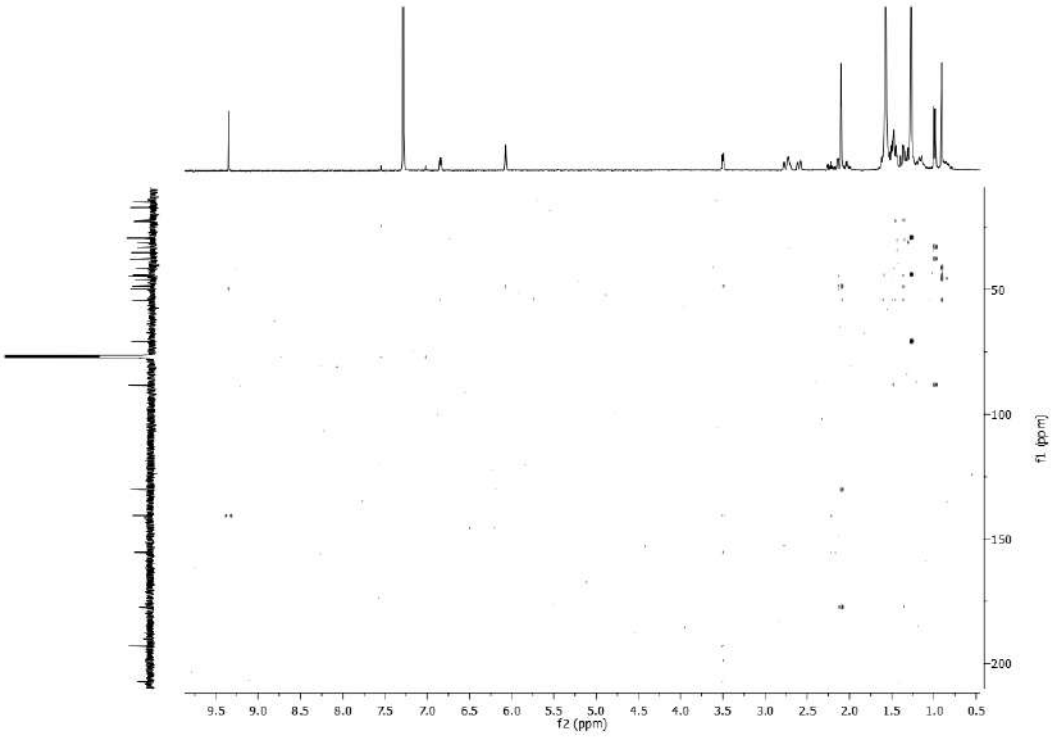

Figure 32. HMBC spectrum of drophiobolin A (**15**) ($CDCl_3$, 400/100 MHz).

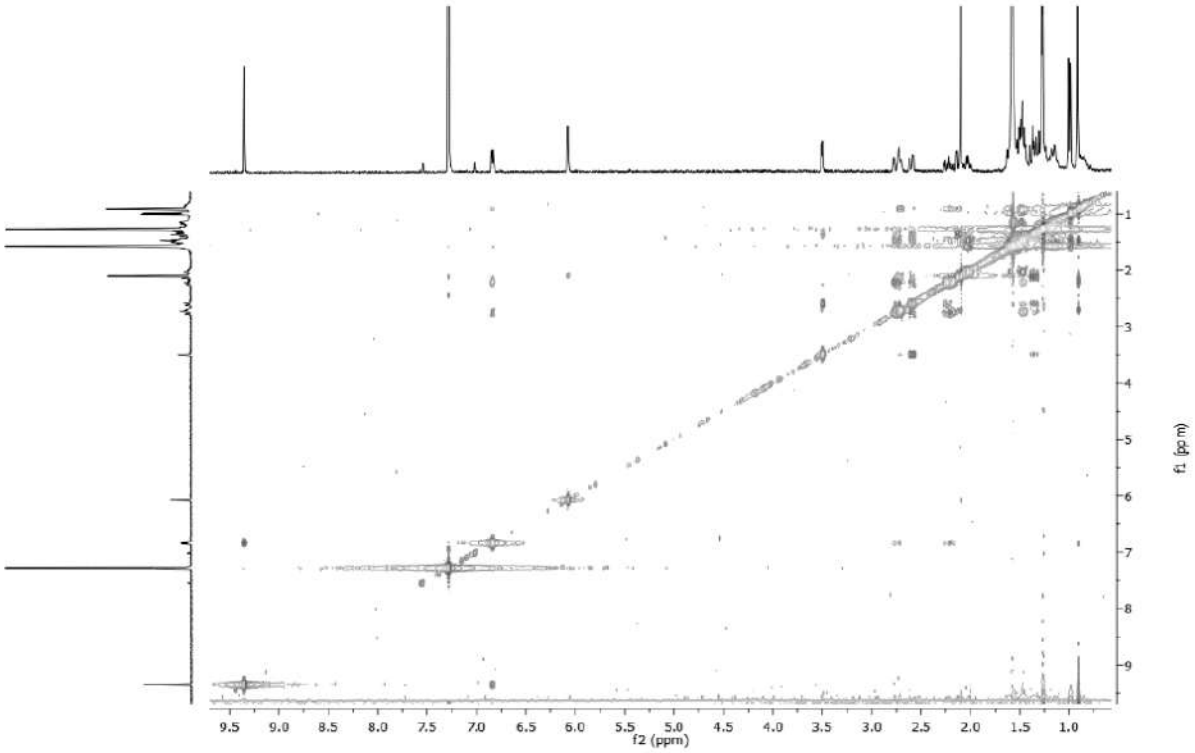

Figure 33. NOESY spectrum of drophiobolin A (**15**) ($CDCl_3$, 400 MHz).

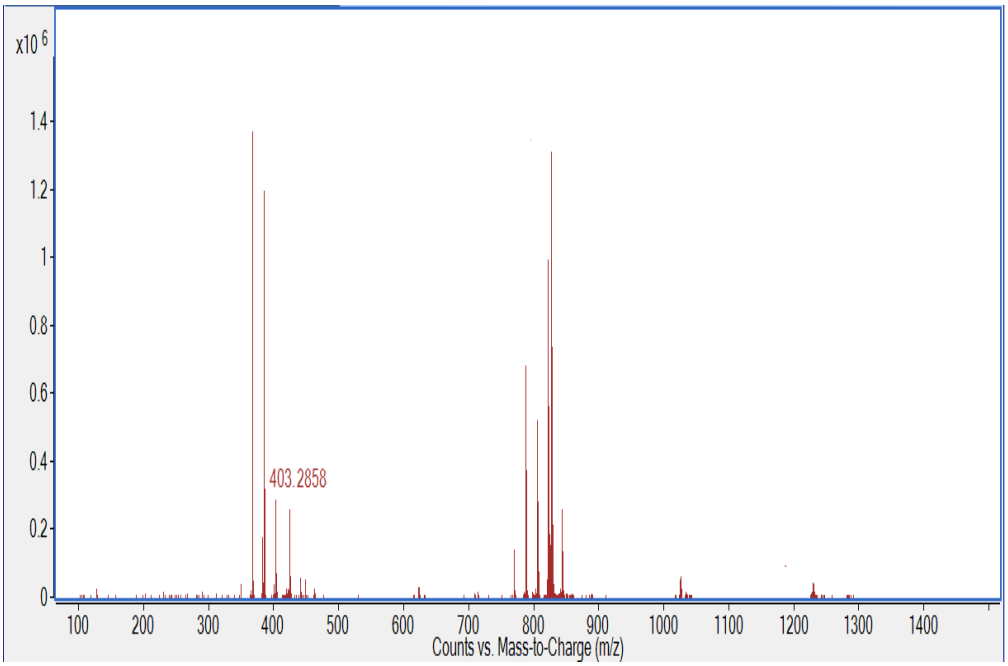

Figure 34. ESI MS spectrum of drophiobolin A (**15**), recorded in positive modality

3.4.1.8- Structural characterization of drophiobiolin B

Drophiobolin B (**16**) had a molecular formula of $C_{25}H_{34}O_4$, as deduced from its ESIMS spectrum (Figure 41), which is consistent with nine indices of hydrogen deficiency. Its ^{1}H NMR and COSY data (Figure 35 and 37) showed the presence of a broad singlet and a double heptet (J = 7.8 and 3.3 Hz) at δ 6.10 and 5.20 due the olefinic hydrogens H-4 and H-18 being the latter coupled with the quartet (J = 7.8 Hz) of the adjacent hydroxylated methine hydrogen (H-17) observed at δ 4.2 and also allylic coupled with the terminal methyl groups of the side chain (Me-24 and Me-25) (Morrison *et al*., 2014). H-17 coupled with only one hydrogen of the adjacent methylene group (CH_2-16) resonates as a quartet a (J = 7.8 Hz) at δ 1.76 while the other appeared as a multiplet at δ 1.73. These latter protons (H_2-16) coupled with of the adjacent methine hydrogen (H-15) resonate as a multiplet at δ 2.11 in part overlapped to the signal of a vinyl methyl group (Me-20) present as a broad singlet at δ 2.11. H-15 also coupled with the hydrogens of the adjacent methyl group (Me-23) and was observed as a doublet (J = 7.8 Hz) at δ 1.05. In the same spectra, a broad singlet and two doublets (J = 1.2 Hz) of the other three vinyl methyl groups (Me-20 and Me-24 and Me-25) were observed at δ 2.11 and 1.73 and 1.68, respectively.

The signals of the AB part of an ABX system corresponding to the hydrohylated methylene group HO-CH_2-21 were observed as two double doublets (J = 14,8 and 4.0 and J = 14.8 and 7.8 Hz) at δ 4.89 and 4.44, which were coupled with the germinal hydroxyl group, the X part, appearing as a broad double doublet (J = 7.8 and 4.0 Hz) at δ 3.63. A double doublet (J =14.4 and 3.3 Hz) and a triplet (J = 14.4 Hz) for the hydrogens of a methylene group α-located to carbonyl group (O=C-8) were observed at δ 2.60 and 2.50 and coupled with of a methine proton (H-10), which being α-located to an oxygentad tertiary carbon, resonated as a double doublet (J = 14.4 and 3.3 Hz) at δ 2.86. In addition, a broad doublet (J = 11.9 Hz) of an allylic methine hydrogen (H-2) was observed at δ 3.07 and coupled with the hydrogens of the adjacent methylene group (CH_2-1) resonating as a double doublet (J = 13.9 and 2.1 Hz) and a multiplet at δ 1.94 and 1.28, with the latter in part overlapped with the signal of one of the hydrogens of CH_2-12. The allylic coupling (< 1 Hz) between H-2 and Me-20 was also observed (Pretsch and Bühlmann, 2000). Finally, the singlet of a tertiary methyl group (Me-22) and the multiplets of the hydrogens accounted for two coupled methylene groups (CH_2-13 and CH_2-12) of a pentasubstituted cyclopentane were observed at δ 0.97, 1.70 (2H) and

1.59 and 1.28, respectively. These findings, the absence of the protons H-6 and H-8, and the significant of aldehydic hydrogen, in respect to (**14**), confirmed that (**16**) is close to ophiobolin I (Molinski *et al*., 2012; Nugroho and Morita, 2014; Morita *et al*., 2015; Superchi *et al*., 2018; Mándi., 2019), but differed for the isomerization of the double bond of the octacyclic B ring from C-7⁻C-8 to C-7⁻C-6 and the presence of a carbonyl group at C-8.

Thus, the structure of a $\Delta^{6,7}$-8,O-dehydro ophiobolin I could be suggested for drophiobolin B, which was confirmed by typical band for hydroxyl, carbonyl, and olefinic groups and the absortiom maxima for an extended conjugated system observed in its IR (Nakanishi and Solomon, 1977) and UV spectra (Pretsch and Bühlmann, 2000), respectively.

The ^{13}C NMR data (Figure 36, Table 7) showed, as expected, the presence of the signals for 25 carbons, and the correlations recorded in the HSQC spectrum (Figure 38, Table 7) allowed to assign the signals of the protonated carbons. In particular, the signals at δ 131.8, 126.8, 72.0, 59.3, 51.2, 48.2, 44.6, 42.8, 41.8, 41.4, 36.4, 29.8, 25.9, 20.9, 18.1, 17.4 and 16.1 were assigned to C-4, C-18, C-17, C-21, C-10, C-1, C-2, C-9, C-16, C-13, C-15, C-12, C-24, C-22, C-25, C-20 and C-23, respectively (Breitmaier and Voelter, 1987). The four sp^2 and the two sp^3, one of which is oxygenated, were assigned by the long-range couplings observed in the HMBC spectrum (Figure 39, Table 7). In particular, the coupling between the signal at δ 177.3 and H-2 and Me-20, 146.9 with H_2-9 and H_2-21, 135.5 with H-4, 135.0 with Me-24 and Me-25, 95.5 with H_2-9, H-10 and Me-23 and 43.1 with Me-22 allowed for them to be assigned C-3, C-7, C-6, C-19, C-14, and C-11, respectively. Finally, the signals of the two carbonyls at δ 210.5 and 197.2 were assigned to C-8 and C-5 for the couplings observed in the HMBC spectrum (Figure 39, Table 7) between C-5 with H-4 and Me-20 (Kim *et al*., 1984). Thus, the chemical shifts to the all hydrogens and correspond carbons were attribute and reported in Table 3 and drophiobolin B (**16**) was formulated as 6-(hydroxymethyl)-3',9,10a- trimethyl-5'-(2-methylprop-1-en-1-yl)-3a,4,4',5',10,10a-hexahydro-1*H*,3'*H* spiro [dicyclopenta[*a*,*d*] [8]annulene-3,2'-furan]-5,7(2*H*,9a*H*)-dione.

The structure assigned to (**16**) was supported by the other correlations observed in the HMBC spectrum (Figure 39, Table 7) and by the data from its ESIMS spectrum (Figure 41) which showed the dimeric sodium $[2M + Na]^+$, the protonated dimeric $[2M + H]^+$ adducts, and the protonated $[M + H]^+$ ions at *m/z* 819, 797, and 399.2526. The latter by loss of water generated the significant fragmentation $[M + H - H_2O]^+$ ion at *m/z* 381.

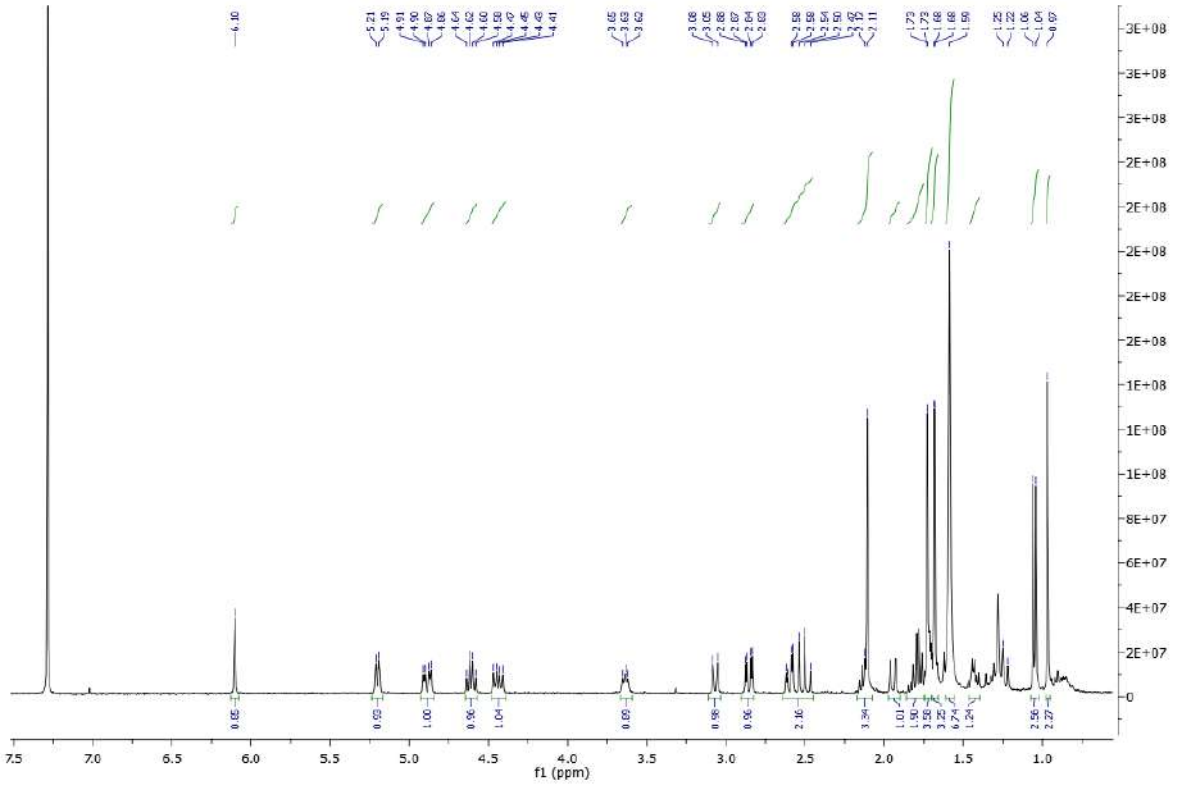

Figure 35. ^{1}H NMR spectrum of drophiobolin B (**16**) ($CDCl_3$, 400)

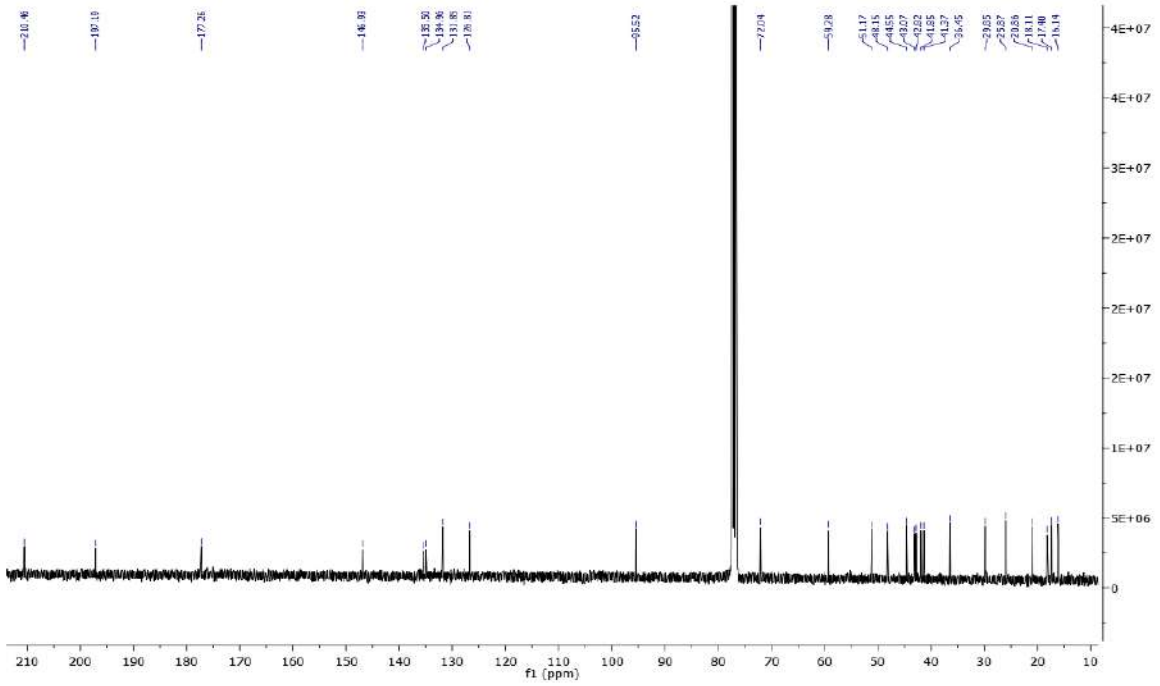

Figure 36. ^{13}C NMR spectrum of drophiobolin B (**16**) ($CDCl_3$, 100 MHz).

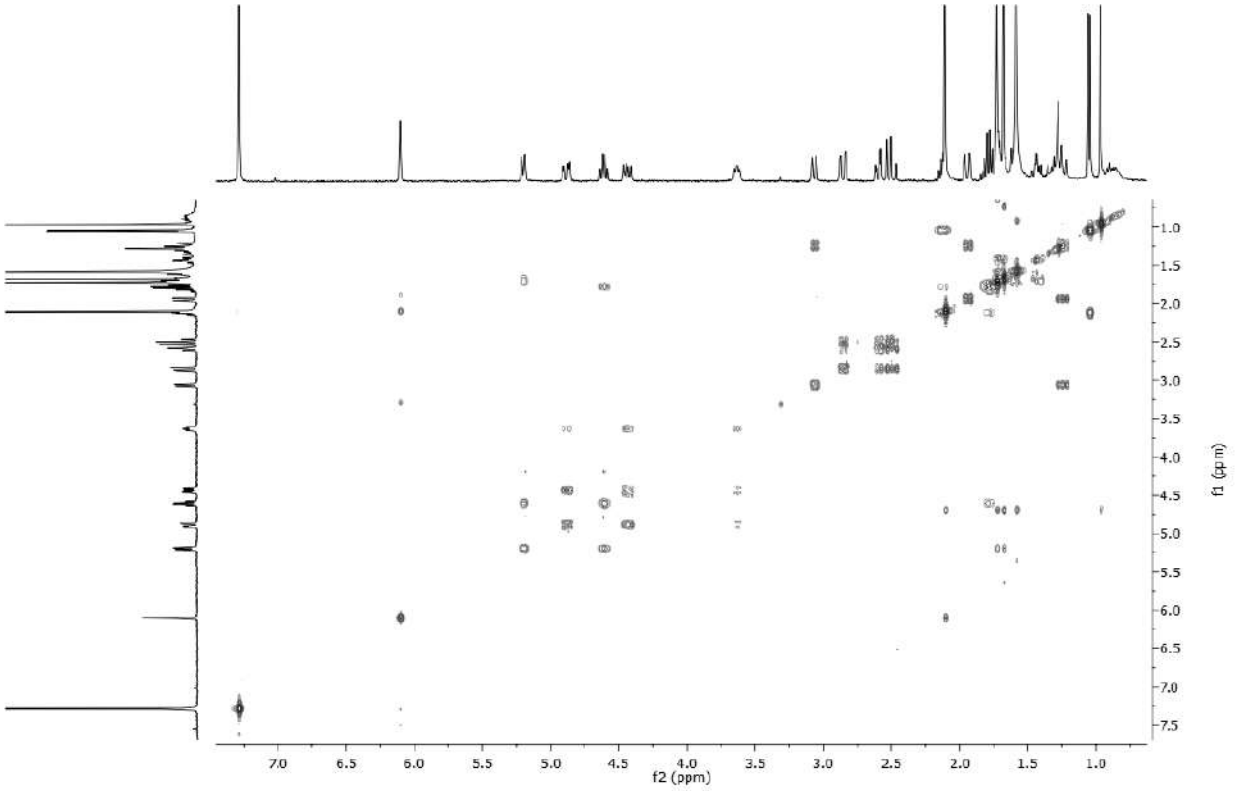

Figure 37. COSY spectrum of drophiobolin B (**16**) ($CDCl_3$, 400 MHz).

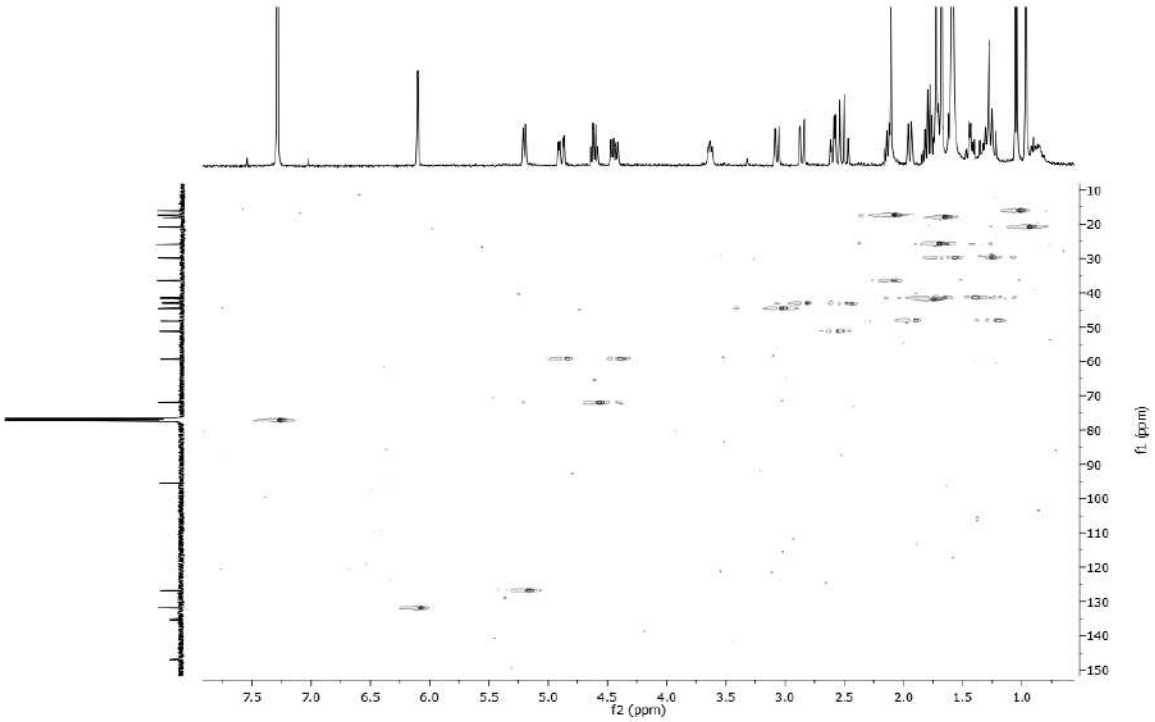

Figure 38. HSQC spectrum of drophiobolin B (**16**) ($CDCl_3$, 400/100 MHz).

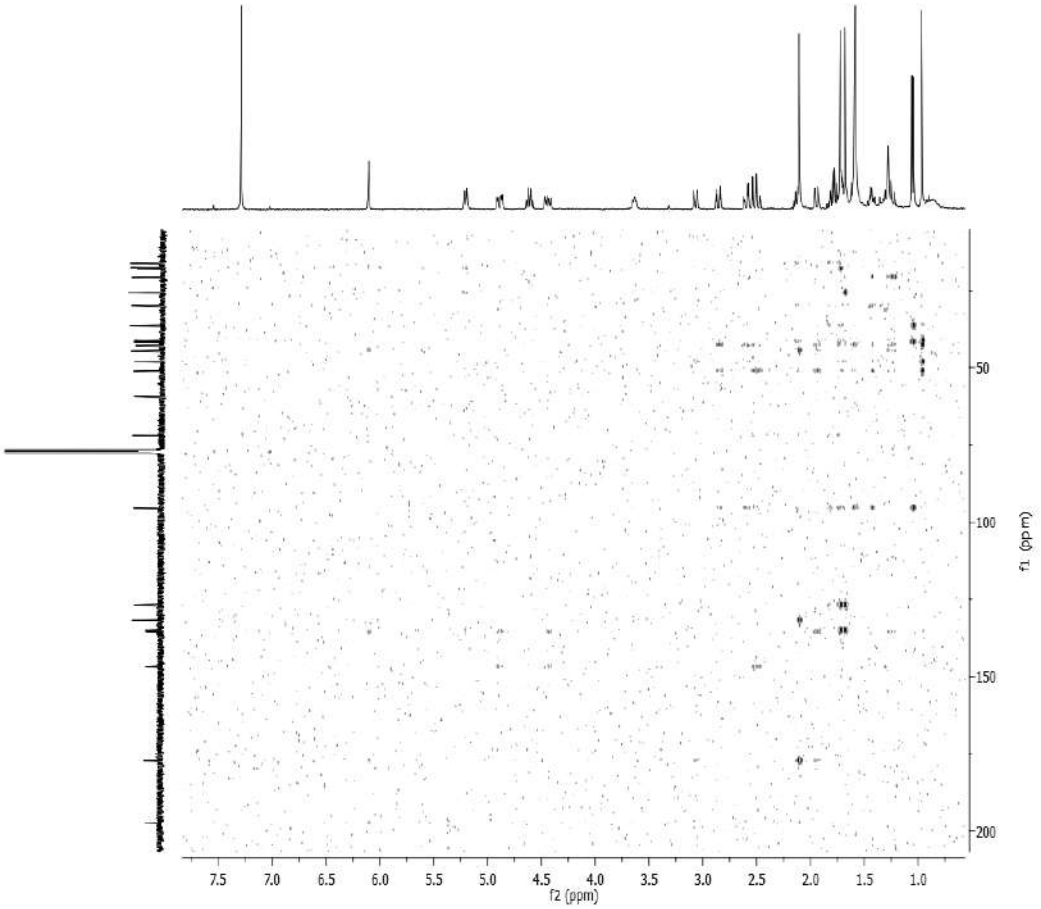

Figure 39. HMBC spectrum of drophiobolin B (**16**) ($CDCl_3$, 400/100 MHz).

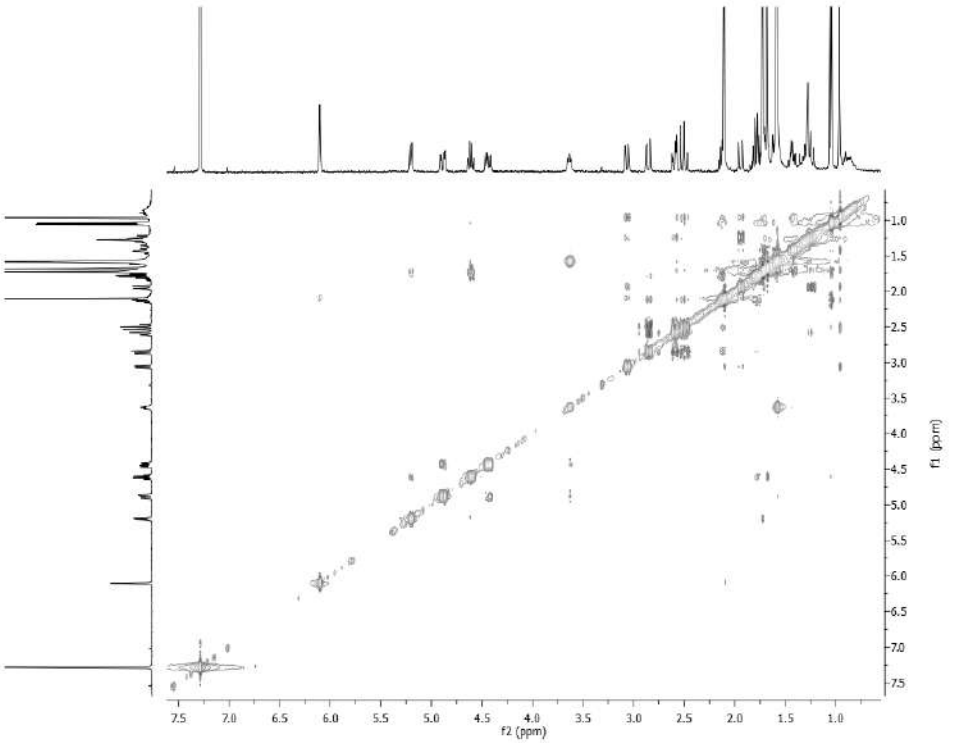

Figure 40. NOESY spectrum of drophiobolin B (**16**) ($CDCl_3$, 400 MHz).

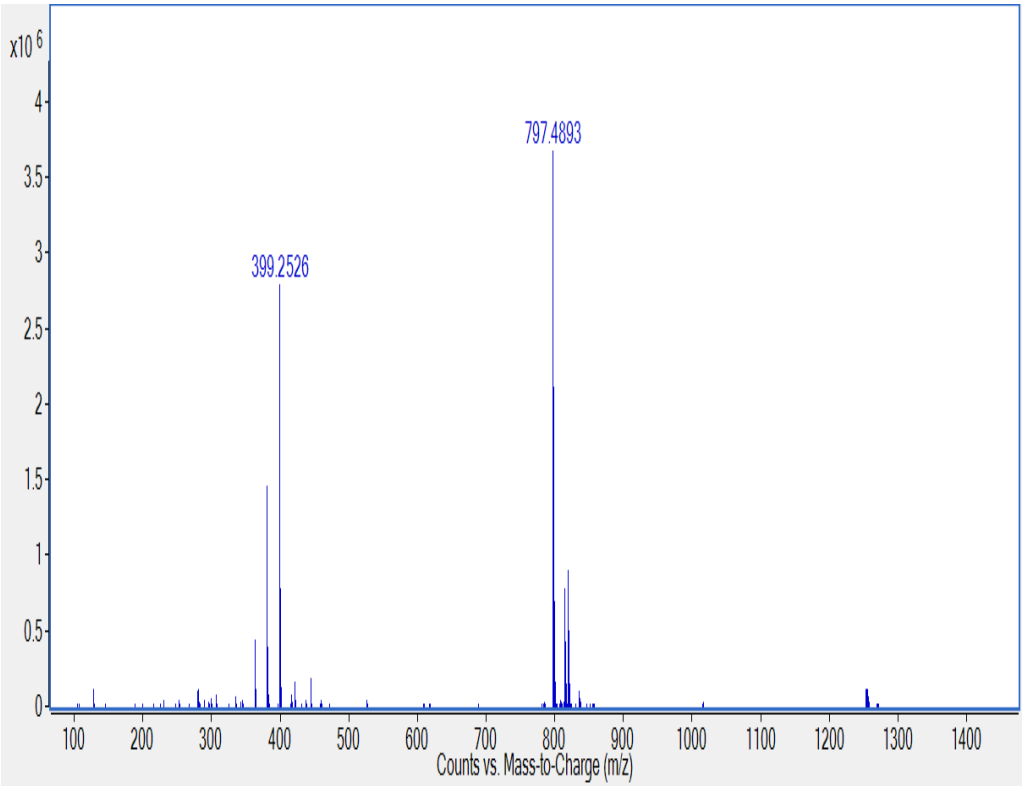

Figure 41. ESI MS spectrum of drophiobolin B (**16**), recorded in positive modality.

Table 7. NMR Data of Drophiobolins A and B (**15** and **16**) [a,b]

	15			**16**		
No.	δ_C [c]	δ_H (*J* in Hz)	HMBC	δ_C [c]	δ_H (*J* in Hz)	HMBC
1	46.5 t	2.12 m 1.34 m	H_3-22	48.2 t	1.94 dd (13.9 and 2.1) 1.28 m[e]	H-2, H_3-22
2	49.2 d	2.70 m[f]	H-6, H-10, H_3-20	44.6 d	3.07 br d (11.9)	H_3-20
3	177.8 s		H-1B, H_3-20	177.3 s		H-2, H_3-20
4	130.7 d	6.05 br s	H_3-20	131.8 s	6.10 br s	H_3-20
5	207.5 s		H-6	197.2 s		H-4, H_3-20
6	50.2 d	3.47 d (4.2)	H-21	135.5 s		H-4
7	141.1 s		H-6, H-21	146.9 s		H_2-9, H_2-21
8	155.9 d	6.82 dd (6.3, 2.4)	H-6, H_2-9	210.5 s		
9	31.9 t	2.70 m[f] 2.09 m	H-8	42.8 t	2.60 dd (14.0 and 3.3) 2.50 t (14.0)	H-10
10	54.9 d	2.57 br dd (14.0, 2.8)	H-8, H_3-22	51.2 d	2.86 dd (14.0 and 3.3)	H_2-9, H-15, H_3-22
11	45.2 s		H_2-1, H_2-12, H_3-22	43.1 s		H_3-22
12	41.8 t	2.01 m, 1.44 m[f]	H_2-13, H_3-22,	29.8 t	1.59 m, 1.28 m[e]	H_2-13
13	23.3 t	1.55 m[f], 1.33 m	H-12B	41.4 t	1.70 m (2H)	H_3-23
14	88.8 s		H-15, H_3-23	95.5 s		H_2-9, H-10, H_3-23
15	38.2 d	1.44 m[f]	H_3-23	36.4 d	2.11 m[e]	H_2-16, H_3-23
16	33.5 t	1.14 m, 1.12 m	H_3-23	41.8 t	1.76 q (7.8), 1.73 m	H-15, H_3-23
17	35.7 t	1.55 m[f], 1.44 m[f]	H-15	72.0 d	4.60 q (7.8)	
18	44.6 t	1.55 m[f], 1.44 m[f]	H_3-24, H_3-25	126.8 d	5.20 d hept (7.8 and 1.2)	H_3-25
19	71.4 s		H_3-24, H_3-25	135.0 s		H_3-24, H_3-25
20	17.7 q	2.08 br s	H-4, H-6	17.4 q	2.11 br s[e]	H-4
21	193.3 d	9.33 s	H-6, H-8	59.3 t	4.89 dd (14.8 and 4.0) 4.44 dd (14.8 and 7.8)	
22	23.0 q	0.89 s	H-13B	20.9 q	0.97 s	H_2-12
23	15.5 q	0.97 d (6.7)		16.1 q	1.05 d (7.8)	H-15, H_2-16
24[d]	29.8 q[f]	1.26 br s[f]		25.9 q	1.73 d (1.2)	H-18, H_3-25
25[d]	29.8 q[f]	1.26 br s[f]		18.1 q	168 d (1.2)	H-18, H_3-24
OH					3.63 br dd (7.8, 4.0)	

[a] 2D ^{1}H, ^{1}H (COSY) and ^{13}C, ^{1}H (HSQC) NMR experiments confirmed the correlations of all the protons and the corresponding carbons. [b] Coupling constants (*J*) are given in parenthesis. [c] Multiplicities were assigned with DEPT. [d] These signals could be exchanged. [e] These signals are in part overlapped. [f] These signals overlapped.

3.4.1.9- Relative and absolute configuration (AC) of drophiobiolin A and B

The relative configuration of drophiobolins A and B (**15** and **16**) was deduced from the correlations observed in the corresponding NOESY spectra (Berger and Braun, 2004). NOESY spectrum of drophiobolin A (**15)** (Figure 33, Table 8) showed the correlation between H-2 and Me-22 and H-6 with H-10, while there were no observed correlations between H-6 with H-2 and H-10 with Me-22. Thus, H-2 and Me-22 were located onto the same side of the molecule and H-6 and H-10 onto the opposite side. This indicates a *trans*-junction between A and B and B and C rings (Cai *et al*., 2019). However, such NOESY analysis did not allow to assign the relative configuration to C-15 and C-14 because, due the rotational freedom of the side chain attached to C-14, compound (**15**) lack of the significant correlation observed in (**16**). Such side chain comes from a reductive opening of the tetrahydrofuran D ring, previously observed also in ophiobolin B (Canonica *et al*., 1966; Evidente *et al*., 2006b; Masi *et al*., 2019). In the NOESY spectrum of drophiobolin B (**16**) (Figure 40, Table 9) significant correlations between H-2 and Me-22, H-10 with H-15, H-17 and Me-23 were observed, while H-10 did not correlate with Me-22. These results allowed to locate H-2, Me-22, Me-23 and H-17 on the same side of the molecule and, H-10, H-15 as well as the ether bridge of tetrahydrofuran D ring, were on the opposite side. Thus, the B/C ring junction is *trans* as in (**15**).

Table 8. NOESY Data of Drophiobolin A (**15**)

Irradiated	Observed	Irradiated	Observed
H-21	H-8	H_2-9	H-8
H-8	H_2-9	H_3-22	H-2, H_2-2A
H-4	H_3-20	H_3-20	H-4
H-6	H-10		

Table 9. NOESY Data of Drophiobolin B (**16**)

Irradiated	Observed	Irradiated	Observed
H-2	H-2A, $H_3$22, H_3-20	H-18	H_3-24
H-10	H-15, H_2-9	H-17	H_3-23, H-16B
H-21A	H-21B, OH	H-4	H_3-20

The AC of drophiobolins A and B (**15** and **16**) was then assigned by comparison of the experimental and TDDFT computed Electronic Circular Dichroism (ECD) spectra (Autschbach, 2012), following a particularly reliable and straightforward approach for the AC assignment in solution to chiral complex natural compounds (Molinski *et al*., 2012; Kong *et al*., 2013; Nugroho and 2014; Evidente *et al*., 2015; Morita *et al*., 2015; Santoro *et al*., 2015; Coronado-Aceves *et al*., 2017; Superchi *et al*., 2018; Mándi., 2019). Accordingly, the UV and ECD spectra of (**15**) were recorded in acetonitrile in the 180-360 nm range (Figure 42).

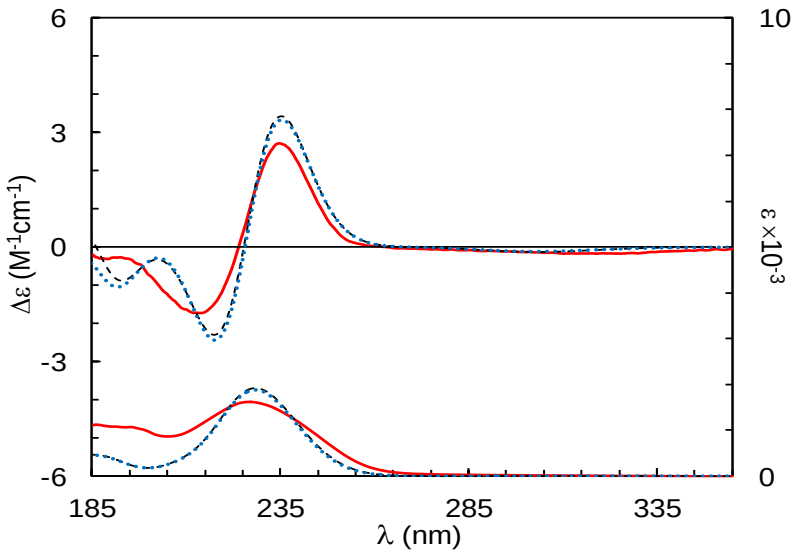

Figure 42. Comparison between experimental (solid red line) and calculated (TDDFT / CAM-B3LYP/ 6-311++G(2d,2p)/ IEFPCM (acetonitrile), ECD and UV spectra for (2*S*,6*R*,10*R*,11*R*,14*S*,15*S*)-**15a** (dashed black lines) and (2*S*,6*R*,10*R*,11*R*,14R,15*S*)-**15b** (dotted blue lines).

The UV spectrum displays an intense broad band at 227 nm allied to the absorption of the two *α,β*-unsaturated carbonyl moieties present on the molecule, while the ECD spectrum displays an intense couplet-like feature centered at 224 nm and constituted by a positive Cotton effect (CE) 235 nm (Δε 2.75) and a negative one at 214 nm (Δε -1.69), followed by a broad weak CE at about 290 nm (Δε -0.07). The ECD couplet can be interpreted as allied to an exciton coupling effect (Harada and Nakanishi, 1983) between the π-π* transitions of the two *α,β*-unsaturated carbonyl chromopheres, i.e., the cyclopentenone and the exocyclic unsaturated aldehyde moieties, while the CE at 290 nm can be ascribed to an overlap of their *n*-π* carbonyl transitions.

Computational conformational analysis of (**15**) was then carried out considering the (2*S**,6*R**,10*R**,11*R**) relative configuration of the A / B / C tricyclic system established by NMR (*vide supra*). NMR analysis provided the relative configuration at C-14 and C-15. The computational analysis was carried out on both epimer at C-14, while the AC at C-15, being undeterminable by ECD analysis, was assumed to be (*S*), as observed in all the reported ophioboline-type molecules. In this case, partial knowledge of the relative configuration, permits avoidance of carrying out computations on all diastereomers (Johnson *et al*., 2018). limiting the investigation to the two epimers at C-14. The conformational analysis was first carried out at the Molecular Mechanics (MM) level on the chosen theoretical models (2*S*,6*R*,10*R*,11*R*,14*S*,15*S*)-**15a** and (2*S*,6*R*,10*R*,11*R*,14*R*,15*S*)-**15b**. The conformers found were then further optimized by density functional theory (DFT) at the DFT /B3LYP /TZVP /IFPCM (acetonitrile) level of theory, considering the solvation effect by IFPCM approach (Tomasi *et al*., 2005) Computations provided eight and five appreciably populated conformers for **15a** and **15b**, respectively (Table 10, Table 11, Figure 43, and Figure 44).

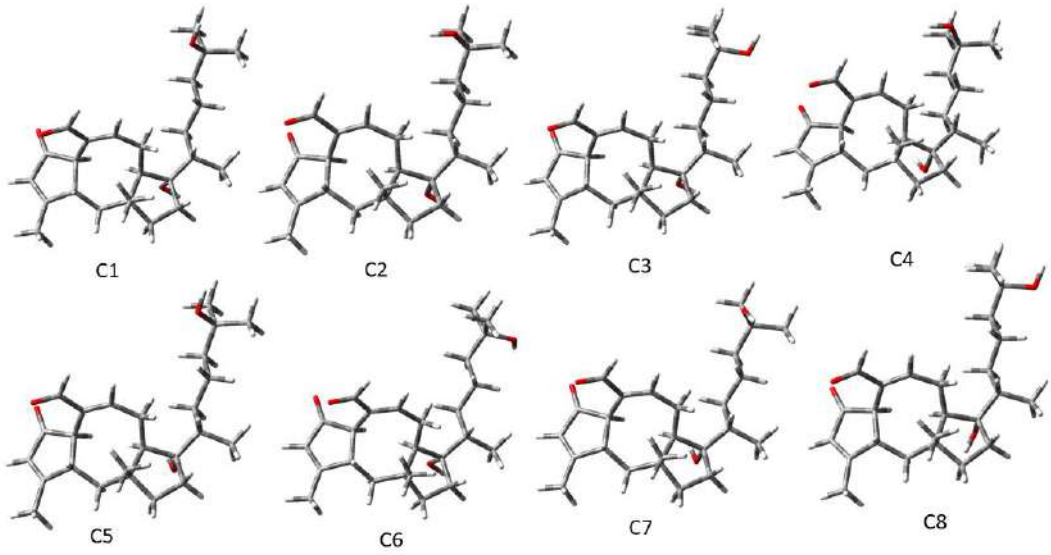

Figure 43. Structures of conformers found of **15a**, FT/B3LYP/TZVP(IEFPCM=Acetonitrile).

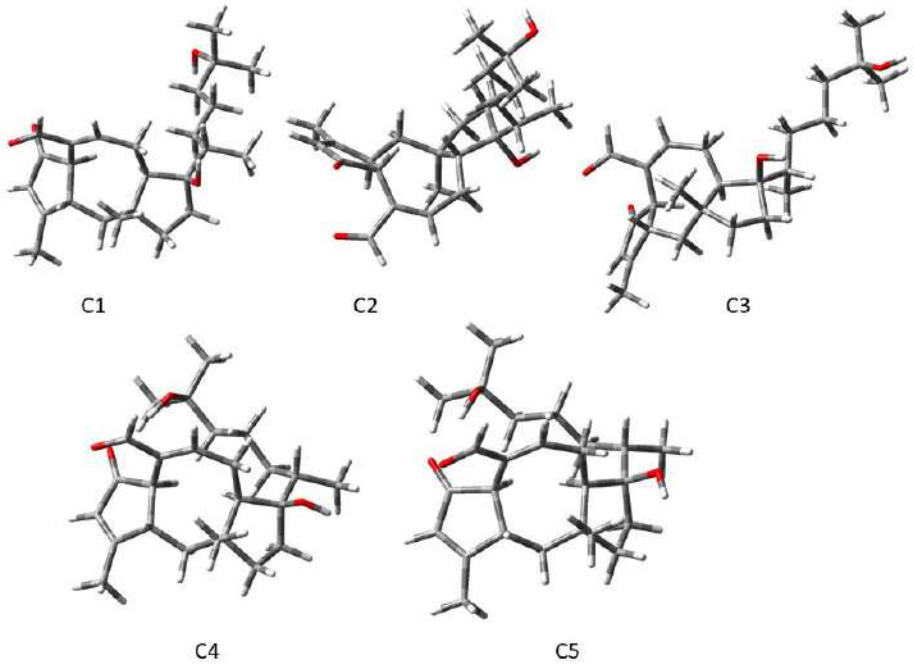

Figure 44. Structures of conformers found of **15b**, DFT/B3LYP/TZVP (IEFPCM=Acetonitrile).

Table 10. Conformers Boltzmann distribution of **15a**.DFT/B3LYP/TZVP (IEFPCM=Acetonitrile).

Conformers	ΔG (Kcal/mol)	% pop
C1	0.000000	23.9
C2	0.276507	15.0
C3	0.300960	14.4
C4	0.314754	14.1
C5	0.356763	13.1
C6	0.544236	9.6
C7	0.734217	6.9
C8	1.242714	2.9

Table 11. Conformers Boltzmann distribution of **15b**. DFT/B3LYP/TZVP (IEFPCM=Acetonitrile)

Conformers	ΔG (Kcal/mol)	% pop
C1	0.000000	48.6
C2	0.122265	39.5
C3	1.094115	7.7
C4	1.617033	3.2
C5	2.291685	1.0

The conformers essentially differed by the conformation of the side chain, being the tricyclic moiety quite rigid. Moreover, as inferred from Figure 45, in both **15a** and **15b** the π-π* electronic transitions allied to the cyclopentenone and the α,β-unsaturated aldehyde chromophores define a positive chirality which, according to the Harada-Nakanishi exciton chirality rule (Harada *et al*., 2012), can allow to predict a positive couplet feature in ECD spectrum, as experimentally observed (Figure 31 and Figure 32) (Pescitelli and Bari, 2017).

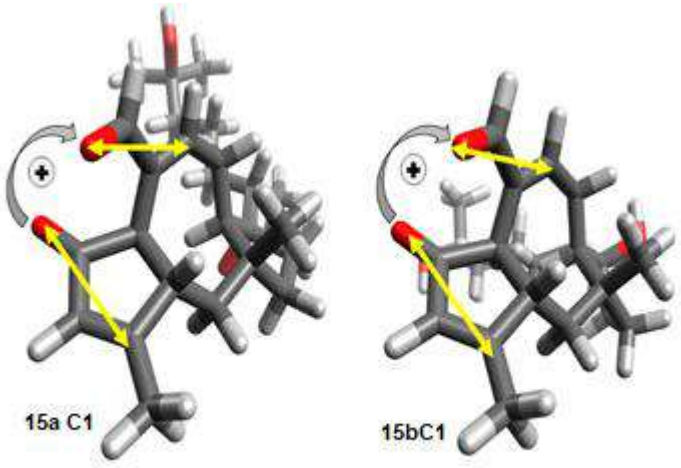

Figure 45. Most stable conformers of epimers **15a** and **15b** indicating the exciton chirality defined by electric transition allied to the two α,β-unsaturated carbonyl chromophores.

This supports the preliminary assignment of the 2*S*,6*R* absolute configuration to the stereocenters of the A/B bycyclic system, and by combining this information with the relative stereochemistry assigned by NMR to C-10 and C-11, the AC to these stereocenters can be also

assigned as 10*R*,11*R*. This stereochemical assignment was further confirmed in a more rigorous way by TDDFT computations. Therefore, UV and ECD spectra for both **15a** and **15b** epimers were calculated on previously found conformers at TDDFT/ CAM-B3LYP/ 6-311++G(2d,2p)/ IFPCM (acetonitrile) level of theory and Boltzmann averaged over conformers populations. As inferred from Figure 42, the UV and ECD spectra of **15a** and **15b** are almost superimposable and then dot not allow a reliable assignment of the AC at C-14. Neither NMR nor ECD analysis helps to assign the correct stereochemistry at this quaternary stereocenter. However, we can suppose that the side chain at C-14 is β as in all the ophibolin-type compound known so far (Masi *et al*., 2019; Cai *et al*., 2019) and then that the AC at that stereocenter is (*S*). The comparison between the ECD experimental spectrum for **(15)** and those computed for **15a** and **15b** (Figure 42) shows agreement for all the three main spectral features observed. In particular, the sign and shape of the couplet-like feature centered at 224 nm and of the broad weak carbonyl band at 290 nm are very well reproduced. Therefore, the (2*S*,6*R*,10*R*,11*R*,14*S*,15*S*) AC can be reliably assigned to the isolated drophobiolin A (**15**).

The AC of drophobiolins B (**16**) was then assigned following the same approach. Accordingly, the UV and ECD spectra of (**16**) were recorded in the 180-360 nm range in acetonitrile (Fig. 46).

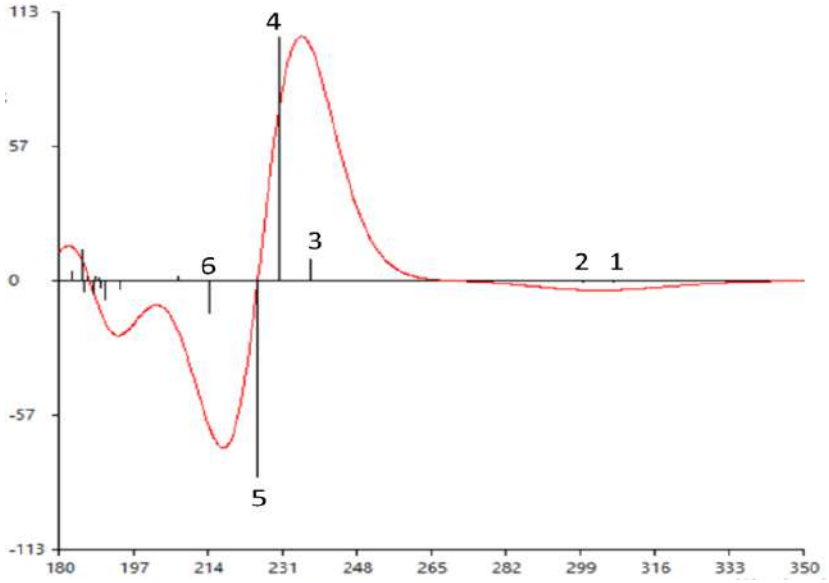

Figure 46. Computed ECD spectra of conformer **16a** displayed the velocity rotational strengths (R_v).

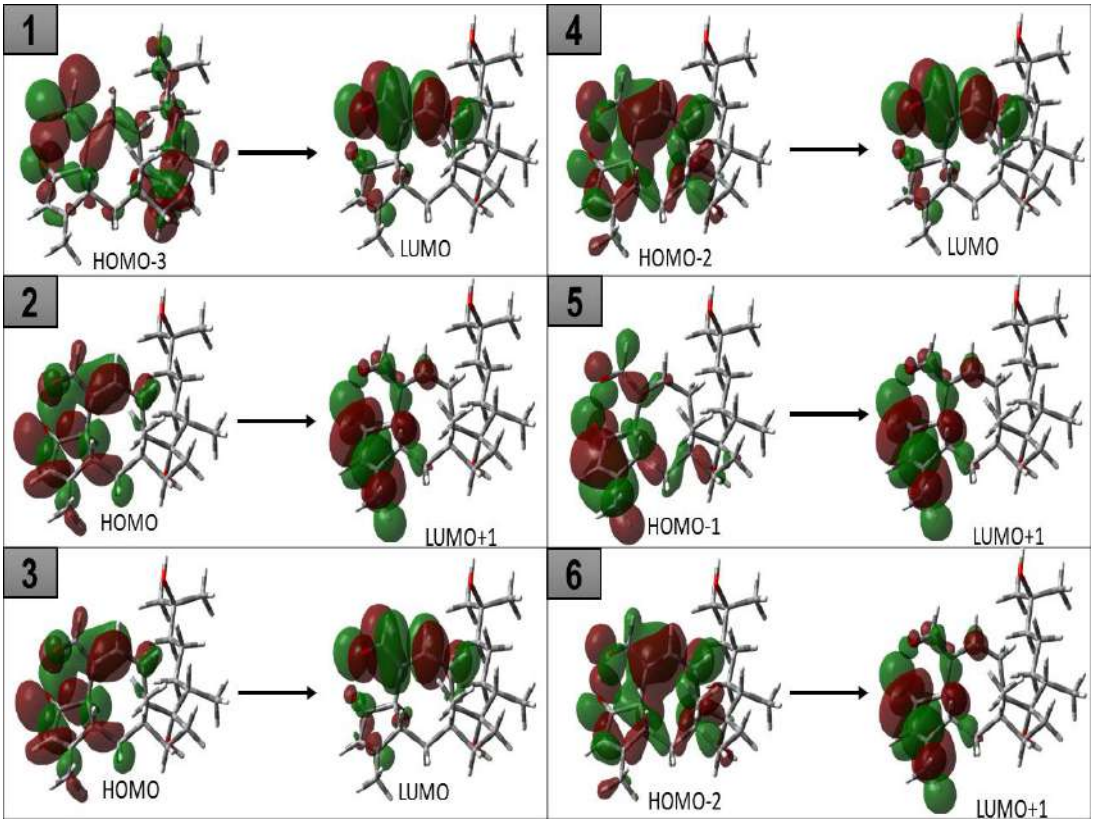

Figure 47. Computed MOs of the main transitions involved in the generation of ECD spectrum of the major populated conformer **15a**. Orbitals displayed with 0.02 isovalue.

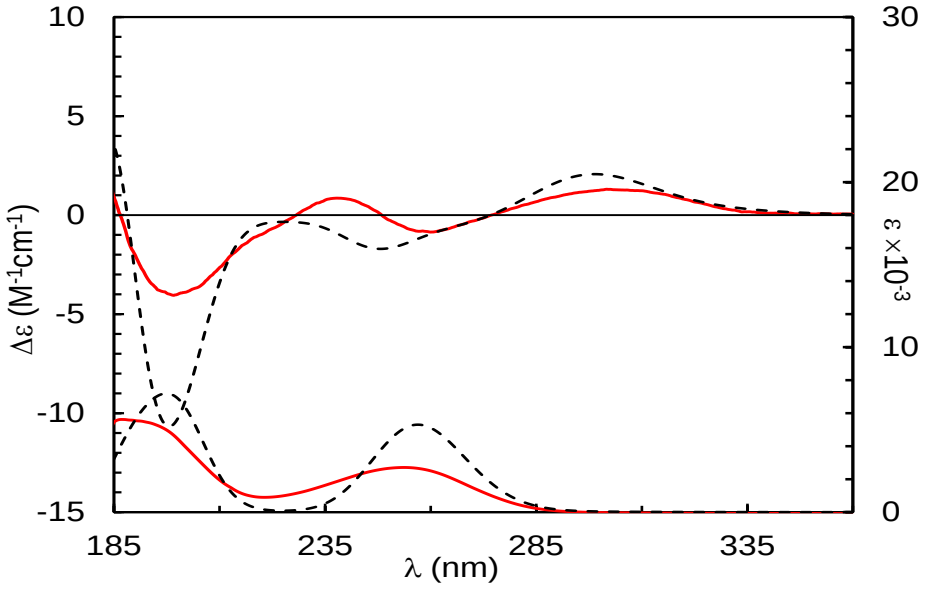

Figure 48. Comparison between experimental (solid red line). and calculated (TDDFT/CAM-B3LYP/ 6-311++G(2d,2p)/ IEFPCM (acetonitrile), ECD and UV spectra for compound (2*R*,10*R*,11*R*,14*S*,15*S*,17*R*)-**16** (dashed black lines).

The UV spectrum displays two intense broad bands at 254 nm and ca. 190 nm allied to the two α,β-unsaturated carbonyl chromophores. The ECD spectrum displays four, alternate in sign, main CEs at 302 nm ($\Delta\varepsilon$ +1.30), 360 nm ($\Delta\varepsilon$ -0.85), 238 nm ($\Delta\varepsilon$ +0.85), 199 nm ($\Delta\varepsilon$ -4.04), respectively. In this case, the NMR analysis provided the relative configuration of all the sterocenters (*vide supra*); therefore, the computational conformational analysis could be carried out on the single (2*R*,10*R*,11*R*,14*S*,15*S*,17*R*)-**16** steroisomer, considering the known (2*R**,10*R**,11*R**,14*S**,15*S**,17*R**) relative configuration. After a first optimization at MM level, the found conformers were refined at DFT/B3LYP/TZVP/IFPCM (acetonitrile) level of theory, obtaining seven appreciably populated conformers (Table 12, Figure 49). Again, the tetracyclic A/B/C/D system appeared to be quite rigid, with the main conformational differences due to rotation of the unsaturated side chain on C-17. The UV and ECD spectra for (2*R*,10*R*,11*R*,14*S*,15*S*,17*R*)-**16** were then calculated on previously found conformers at TDDFT / CAM-B3LYP/ 6-311++G(d,2p)/ IFPCM (acetonitrile) level of theory and Boltzmann averaged over conformers populations. The computed UV and ECD spectra are in very good agreement with the experimental ones, and the main ECD bands are well reproduced in sign, wavelength position, and intensity (Figure 33). The (2*R*,10*R*,11*R*,14*S*,15*S*,17*R*) AC, chosen for the calculation, can be then assigned to the isolated drophobiolin B (**16**). The structure of (**16**) was disclosed while the present article was already prepared and ready for submission; it was a metabolite, named maydispenoids B, isolated from *Bipolaris maydis*, collected from *Anoectochilus roxburghii* (Wall.) and found during a screening for immunosuppressive compounds from fungi (Duan *et al*., 2020).

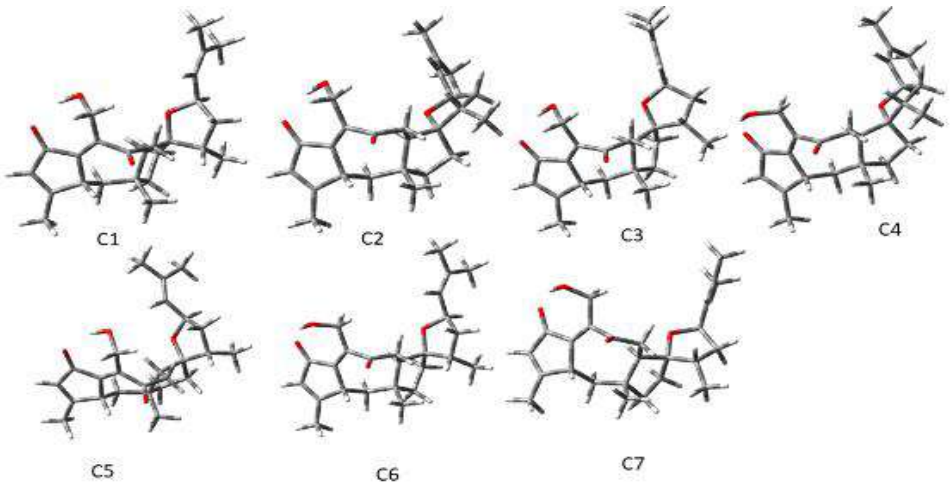

Figure 49. Structures of conformers found of **(16)**, DFT/B3LYP/TZVP (IEFPCM=Acetonitrile).

Table 12. Conformers Boltzmann distribution of **16**. DFT/B3LYP/TZVP (IEFPCM=Acetonitrile).

Conformers	ΔG (Kcal/mol)	% pop
C1	0.000000	37.0
C2	0.094050	31.6
C3	0.758043	10.3
C4	0.885951	8.3
C5	0.990033	7.0
C6	1.415139	3.4
C7	1.615779	2.4

3.4.1.10- Biological assays

3.4.1.10.1- *Phytotoxic assay*

The phytotoxic activity of the drophiobolins A and B, compared to that of ophiobolin A, was tested by leaf-puncture assay on the host weed plant (*Digitaria sanguinalis* L.) and non-host weed (*Chenopodium album* L.) and cultivated (*Lycopersicon esculentum* L.) plants. When tested at 10^{-3} M (Table 13, Figure 35) both (**15** and **16**) showed the same strong phytotoxicity of ophiobolin A on the host plant and tomato. Lower toxicity was observed on *C. album* with respect to (**11**). At 10^{-4} M the toxicity of (**15** and **16**) slightly decreases on all tested plants with (**15**) being inactive on *C. album*.

Table 13. Phytotoxic Activity of Drophiobolins A and B (**15** and **16**) Compared to that of Ophiobolin A (**11**) [a]

	15		**16**		**11**		**Control[b]**
	10^{-3}[c]	**10^{-4}**	**10^{-3}**	**10^{-4}**	**10^{-3}**	**10^{-4}**	
***Digitaria sanguinalis* L.**	3	2	3	2	3	3	0
***Lycopersicon esculentum* L.**	3	2	3	2	3	3	0
***Chenopodium album* L.**	1	0	2	1	3	2	0

[a] Observations were made two days after treatment. Diameter of necrosis on leaves: 3. necrosis > 3 mm; 2. necrosis between 2 and 3 mm; 1. necrosis between 1 and 2 mm; 0. no necrosis. [b] 2%MeOH in distilled water. [c] Molar concentration.

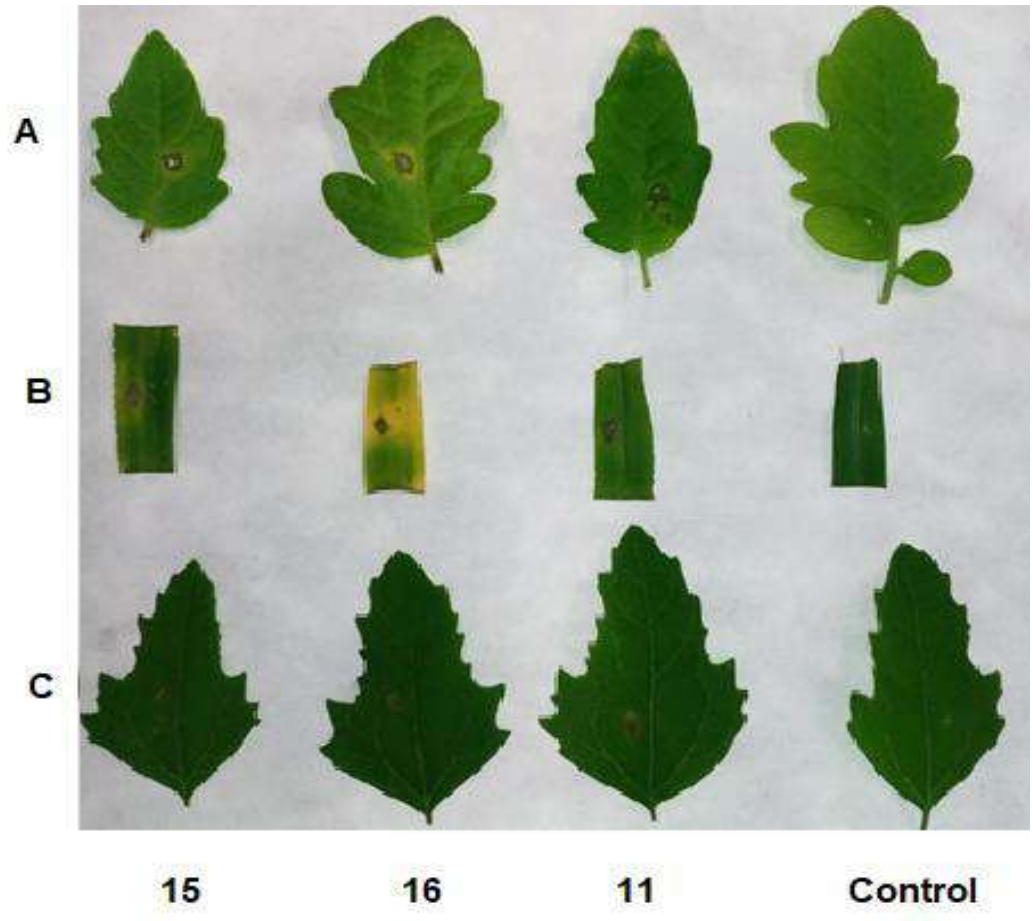

Figure 50. Phytotoxic activity induced by drophiobolins A and B (**15** and **16**), ophiobolin A (**11**) when tested at 10^{-3} M by leaf-puncture assay on cultivated plant (A: *Lycopersicon esculentum* L.) and on weeds (B: *Digitaria sanguinalis* L. and C: *Chenopodium album* L.); control 2% MeOH in distilled water.

3.4.1.10.2- *Cytotoxic activity MTT assay*

The evaluation of the *in vitro* cytotoxicity was performed in A431, Hela B, H1299 cancer cells as well as in Hacat immortalized keratinocytes. The experiments with the new ophiobolins, drophiobolins A and B, were performed in parallel with the already described ophiobolin A. After 24h of treatment, increasing amounts (from 0.5 to 10 μM) of (**15**) or (**16**) slightly reduced cell viability of Hacat (up to 63%) and A431 (up to 72%) while Hela cells viability was significantly reduced (up to 50%, IC_{50} 10 μM) as shown in Figure 50 and Table 10. Ophiobolin A, instead, had dramatic effects on these cell lines (Figure 50). H1299 had a very different behavior being stimulated by drophiobolin A at all concentrations tested while drophiobolin B was ineffective. Interestingly, ophiobolin A that was previously demonstrated

to have strong anticancer effects against glioblastoma (Dasari *et al*., 2015) appeared to be almost ineffective on H1299 lung cancer cells thus showing tumor-cell specificity.

Table 14. Cell viability (%) after 24h of treatment of (**15** and **16**) (from 0.5 µM to 10 µM) compared with ophiobolin A and control (DMSO).

	Control	**Ophiobolin A (11)**			**Drophiobolin A (15)**			**Drophiobolin B (16)**		
µM		0.5	1	10	0.5	1	10	0.5	1	10
Hacat	100%	80%	16%	6%	74%	78%	63%	77%	77%	63%
Hela B	100%	62%	31%	3%	84%	85%	50%	96%	67%	50%
A431	100%	85%	59%	5%	85%	96%	72%	97%	94%	88%
H1299	100%	81%	88%	35%	141%	139%	133%	95%	98%	95%

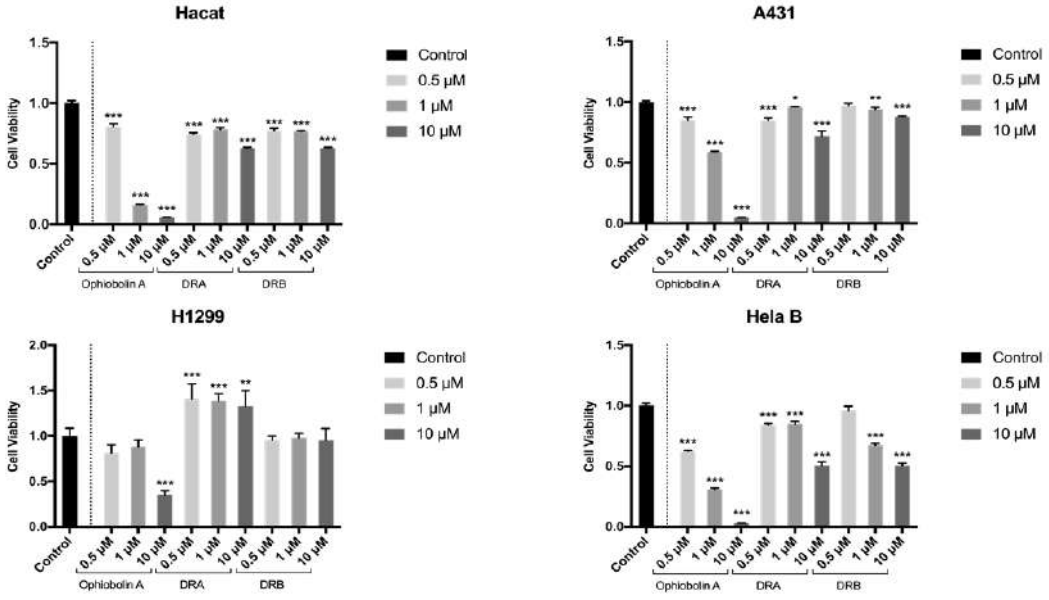

Figure 51. Effects of drophiobolins A or B (DRA and DRB) on cell viability. MTT assay of Hacat, Hela, A431, H1299 cells incubated for 24h with 0.5, 1 and 10 µM drophiobolins A or B were compared with ophiobolin A. Data are expressed as absorbance and presented as mean ± SD of three independent experiments, each done in triplicate. Analysis of variance was performed by one-way Anova and multiple comparisons. **P*< 0.5 when compared with the control.

3.4.2- Structural characterization of secondary metabolites from *Macrophomina phaseolina*

The organic extract of the culture filtrates of *M. phaseolina*, obtained as described in the experimental section, was fractioned by a combination of column and TLC chromatography to afford three pure metabolites (**17**-**19**) that were isolated and identified (Figure 53). A known metabolite identified as guignardone A (**17**, Figure 53) and two new metabolites, named phaseocyclopentenones A and B (**18** and **19**, Figure 53).

The meroterpenoid (**17**) resulted to be isolated for the first time as a metabolite of *M. phaseolina*. It showed the same physical (specific optical rotation) and spectroscopic (^{1}H, ^{13}C, COSY, HSQC and HMBC NMR and ESIMS) properties when compared to those reported after its first isolation from *Guignardia mangiferae*, an endophytic fungus isolated from the *Ilex cornuta* leaves (Yuan *et al*., 2010). The well-known fungal meroterpenoid guignardone A (**17**) was isolated for the first time from *M. phaseolina* which previously showed to produce only the toxic sesquiterpene eremophilane phaseolinone (Dhar *et al*., 1982) and the polyketide botryodiplodin, that is a toxin also produced by other phytopatogenic fungi (Capasso *et al*., 1984; Bhattacharya *et al*., 1992). A preliminary investigation of ^{1}H and ^{13}C NMR spectra of the two specialized metabolites (**18** and **19**), isolated from the Argentina strain of *M. phaseolina* showed that they shared two structural features such as a monosubstituted phenyl and a cyclopentenone residues.

3.4.2.1- Guignardone A (17)

Guignardone A, was obtained as an amorphous solid, had: $[\alpha]^{25}_{D}$ +42 (*c* 0.3 acetone); [(Yuan *et al*., 2006): $[\alpha]^{25}_{D}$ 42 (*c* 0.30 acetone)]; The ^{1}H and ^{13}C COSY, HSQC and HMBC NMR and ESIMS Spectra were very similar to those previously reported (Yuan *et al*., 2010).

3.4.2.2- Phaseocyclopentenone A (18)

Phaseocyclopentenone A was obtained as yellowish oil, had: IR ν_{max}, 3332 (OH); 1719 (C=O), 1676 (C=C); (1597, 1530, 1503 (Ar); UV λ_{max} nm (log ε); 279 (4.54) 248 (4.45); ^{1}H and ^{13}C NMR data, are reported in Table 11; HR ESIMS (+), *m/z* 643 $[2M + Na]^{+}$, 311.0927 $[M+ H]^{+}$ [(calcd for $C_{18}H_{15}O_5$, 311.0919)] 293 $[M + H - H_2O]^{+}$; ESIMS (-), *m/z* 619 $[2M - H]^{-}$; 309.0773 $[M – H]^{-}$ (calcd for $C_{18}H_{13}O_5$, 309.0763).

3.4.2.3- Phaseocyclopentenone B (19)

Phaseocyclopentenone B was obtained as yellowish oil, had: $[\alpha]^{25}_{D}$ + 33 (*c* 0.4); IR *ν*max, 3309 (OH), 1705 (C=O), 1627 (C=C) 1598, 1524, 1496 (Ar); UV λ_{max} nm (log ε), 277 (4.38); ^{1}H and ^{13}C NMR data, are reported in Table 11; HRESIMS (+), *m/z* 555 $[2M + Na]^+$, 533 $[2M + H]^+$ 267.1023 $[M + H]^+$ (calcd for $C_{17}H_{14}O_3$, 267.1021).

3.4.2.4- 3,5-Di-O-Acetyl Derivative of Phaseocyclopentenone A (20)

3,5-Di-*O*-Acetyl Derivative of Phaseocyclopentenone A: had, ^{1}H NMR *δ*: 8.04 (2H, d, *J* = 8.0 Hz, H-2',H-6'), 7.95 (2H, d, *J* = 8.0 Hz, H-2'',H-6''), 7.52 (1H, t, *J* = 8.0 Hz, H-4'), 7.44 (2H, t, *J* = 8.0 Hz, H-3',H-5'), 7.29 (2H, t, *J* = 8.0 Hz, H-3'',H-5''), 7.21 (1H, t, *J* = 8.0 Hz, H-4''), 6.14 (1H, s, H-5), 2.09 (3H, s, MeCO-C3), 1.92 (3H, s, MeCO-C5). ESIMS (+), *m/z* 395 $[M + H]^+$

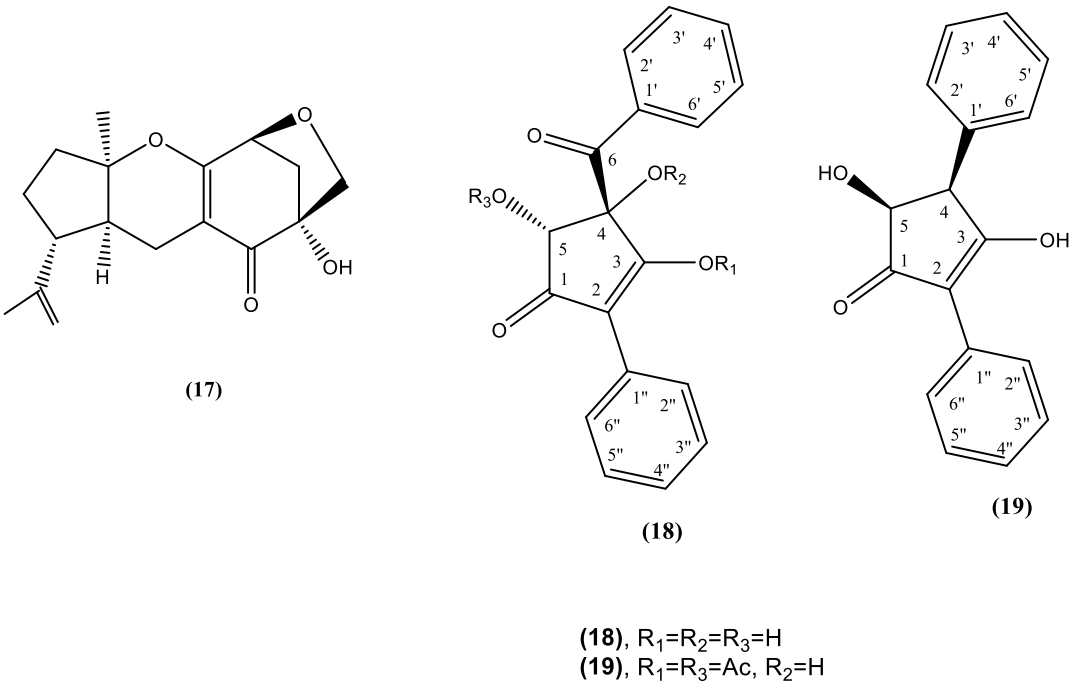

Figure 53. Structures of Guignardone A (**17**), Phaseocyclopentenone A and B (**18** and **19**)

3.4.2.5- Structural characterization of phaseocyclopentenone A

Phaseocyclopentenone A (**18**) had a molecular formula of $C_{18}H_{14}O_5$ as deduced from its ESIMS spectrum (Figure 59) and consistent with twelve hydrogen deficiencies. The presence of the phenyl, benzoyl and cyclopentenone residues was in agreement with the absorption bands for aromatic, double bond and ketone groups and the absorption maxima for conjugated

aromatic systems observed in the IR (Nakanishi and Solomon, 1977) and UV spectra (Pretsch *et al*., 2000), respectively. The IR spectra also showed the presence of bands typical of hydroxy groups (Nakanishi and Solomon, 1977). Accordingly, its ^{1}H and COSY data (Figure 53 and Figure 55) showed the signals consistent with the two afore mentioned residues. In particular, a doublet (J = 8.0 Hz, H-2',6'), a triplet (J = 8.0 Hz, H-3',5') and a triplet (J = 8.0 Hz, H-4') resonating at δ 8.05, 7.43 and 7.53, respectively, accounted for the protons of the benzoyl group (Pretsch *et al*., 2000) as the ketone (C-6) signal observed at δ 200.3 in the ^{13}C NMR spectrum coupled in the HMBC spectrum (Figure 54 and Figure 57, Table 15) (Berger and Braun, 2004) with H-2',6'. In the same spectrum the quaternary sp^2 carbon (C-1') of the same benzene ring at δ 136.7 coupled, as expected with both H-3',5' (Breitmaier and Voelter, 1987). Similar spin systems were observed for the other phenyl group. In fact, a doublet (J = 8.0 Hz, H-2",6"), a triplet (J = 8.0 Hz, H-3",5") and a triplet (J = 8.0 Hz, H-4") were observed at δ 7.83 7.36 and 7.25, respectively. H-3",5" in the HMBC spectrum coupled with the quaternary sp^2 carbon (C-1") of the same ring resonating at δ 130.8. The two phenyl groups and the carbonyl group accounted for nine indices of hydrogen deficiencies and thus three other ones remained to be assigned. These were due to a pentasubstitued cyclopentenone ring. In fact, a quaternary olefinic carbon at δ 115.2 (C-2) coupled in the HMBC spectrum (Figure 57, Table 15) with H-2",6" while the proximate enolic carbon (C-3) appeared at δ 196.6, being also coupled in the HMBC spectrum (Figure 57, Table 15). with the proton (H-5) of a secondary hydroxylated carbon (C-5) resonating as a singlet at δ 4.69. H-5 coupled, in the same spectrum, with the carbonyl (C-1) of the cyclopentenone and the hydroxylated sp^3 quaternary carbon (C-4) present at δ 190.5 and 88.0, respectively (Pretsch *et al*., 2000; Breitmaier and Voelter, 1987). The correlations observed in the HSQC spectrum (Figure 56, Table 15) (Berger and Braun, 2004) allowed to assign the chemical shifts to the protonated carbons. In particular, the signals at δ 132.0, 129.6, 127.7, 127.4, 127.3 and 126.4 were attributed to C-4', C-2',6', C-2",6", C-3",5", C-3',5' and C-4". Thus, the chemical shifts were assigned to the all protons and corresponding carbons as reported in Table 15 and phaseocyclopentenone A (**18**) was formulated as 4-benzoyl-3,4,5-trihydroxy-2-phenylcyclopent-2-enone. The relative configuration at the chiral carbon C-4 and C-5 of (**18**) was assigned by the correlations observed in the NOESY spectrum (Figure 58) (Berger and Braun, 2004). In particular, a diagnostic correlation was observed between H-5 and H-2',6', indicating that H-5 lies on the same side as the benzoyl group suggesting a relative the configuration 4*S**,5*R**. The structure assigned to (**18**) was supported by the other couplings observed in its HMBC spectrum (Figure 57, Table 15) and its ESIMS

spectrum (Figure 59). The latter, recorded in positive modality, showed the dimer protonated adduct $[2M + Na]^+$ and the protonated adduct $[M+ H]^+$ ions at *m/z* 643 and 311.0927. A significant fragmentation peak produced from the protonated adduct by loss of water $[M + H - H_2O]^+$ was observed at *m/z* 293. When the same spectrum was recorded in negative modality the dimer deprotonated adduct and the deprotonated adduct ions were observed at *m/z* 619 and 309.0773, respectively.

The structure of (**18**) was also supported preparing its 3,5-*O*,*O*'-diacetyl derivative (**20**). The ^{1}H NMR of derivative (**20**) differed from that of (**18**) for the downfield shit ($\Delta\delta$ 1.45) of H-5 appearing as singlet at δ 6.14 and the presence of the singlets of the acetyl groups of C-3 and C-4 at δ 2.09 and 1.92. The acetyl groups were located at C-5 and C-3 as in the NOESY spectrum is not observed any correlations between their singlets but that of the acetyl group at C-3 gave a correlation with H-2",6". Thus, the tertiary hydroxy group at C-4 was not acetylated as it is probably engaged in a hydrogen bond with the carbonyl at C-6. Its ESIMS showed the protonated $[M + H]^+$ ion at *m/z* 395.

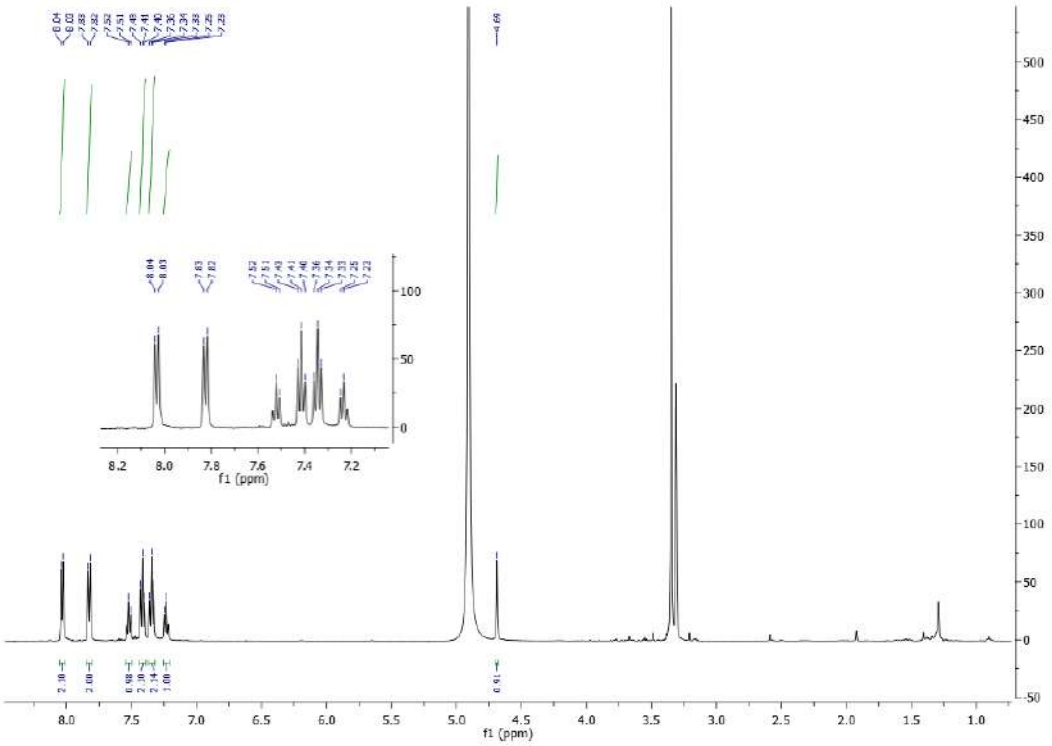

Figure 53. ^{1}H NMR spectrum of phaseocyclopentenone A (**18**) (CD_3OD, 400 MHz).

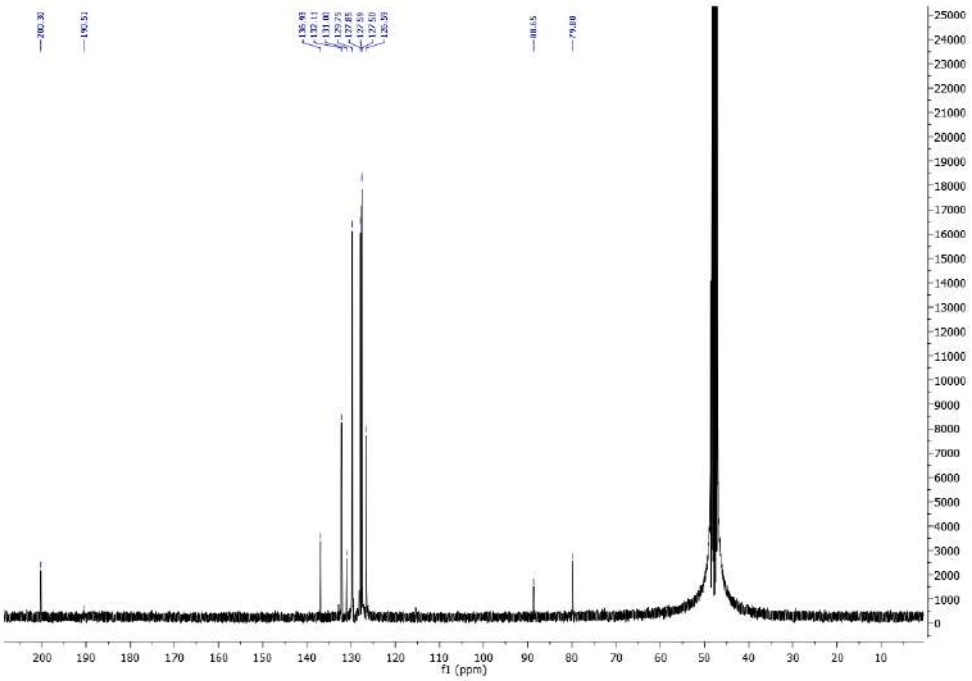

Figure 54. ^{13}C NMR spectrum of phaseocyclopentenone A (**18**) (CD_3OD, 100 MHz).

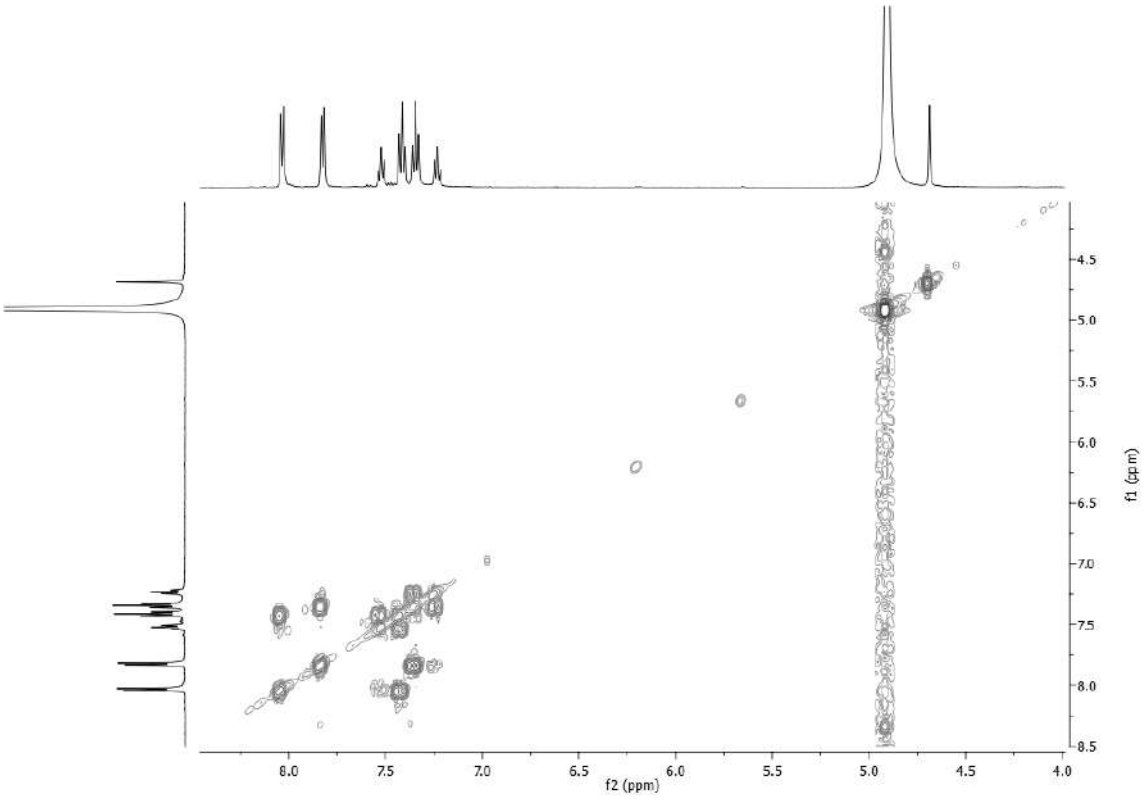

Figure 55. COSY spectrum of phaseocyclopentenone A (**18**) (CD_3OD, 400 MHz).

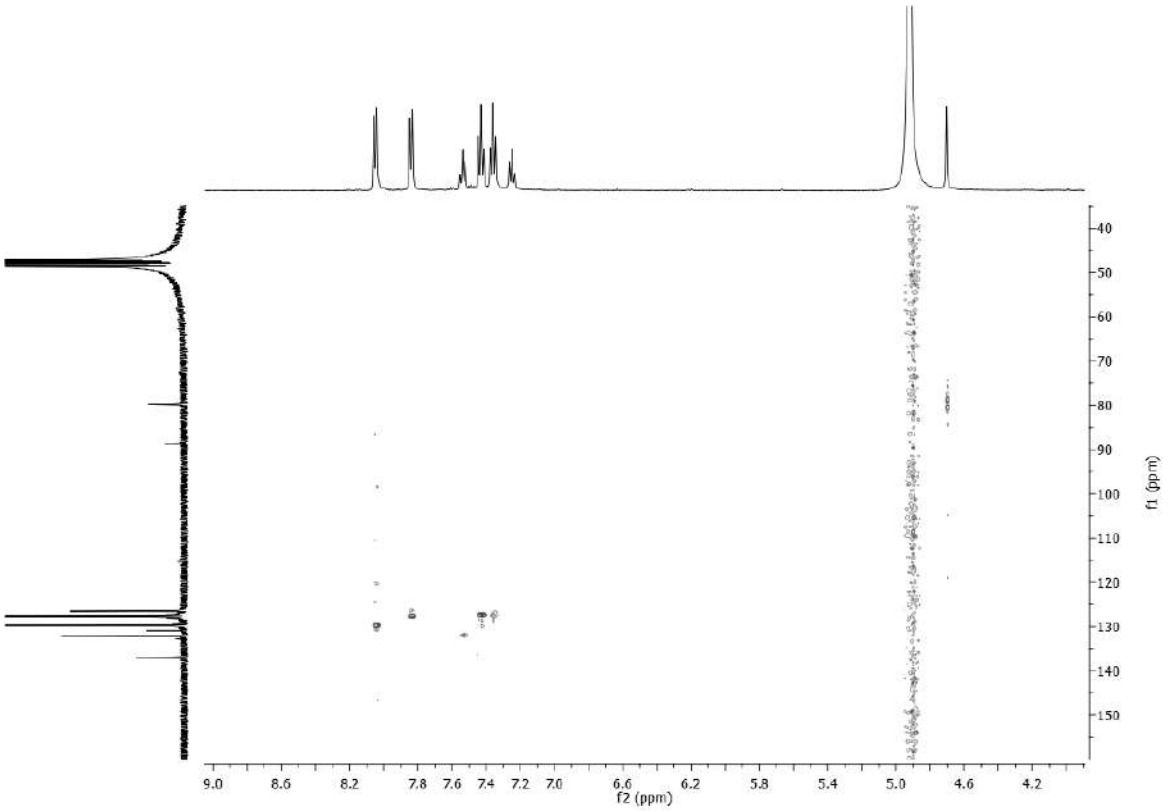

Figure 56. HSQC spectrum of phaseocyclopentenone A (**18**) (CD_3OD, 400/100 MHz).

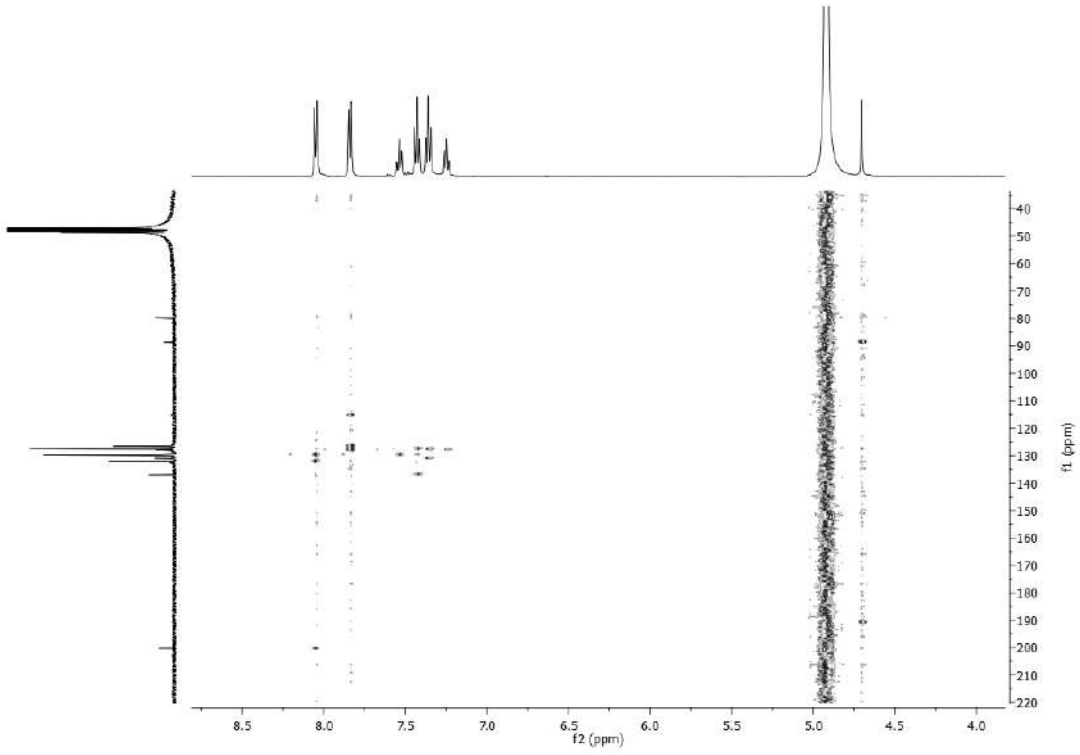

Figure 57. HMBC spectrum of phaseocyclopentenone A (**18**) (CD_3OD, 400/100 MHz).

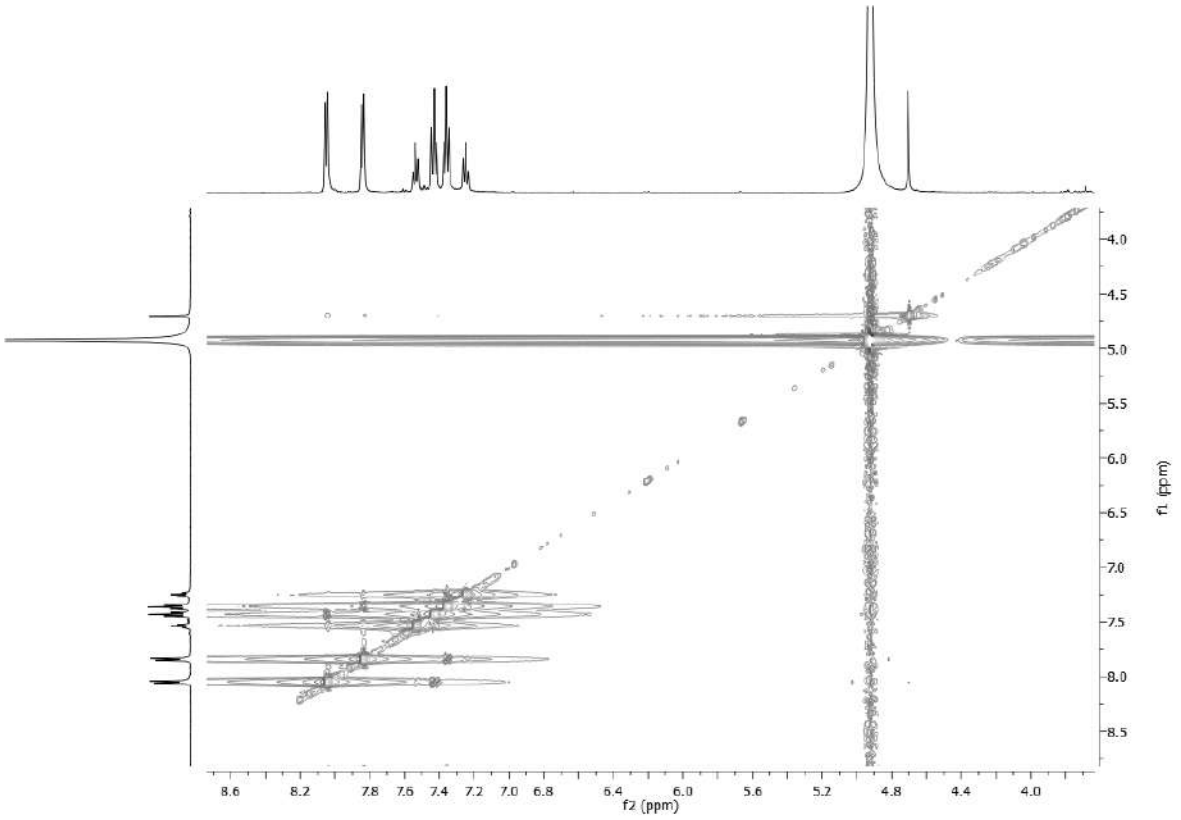

Figure 58. NOESY spectrum of phaseocyclopentenone A (**18**) (CD_3OD, 400 MHz).

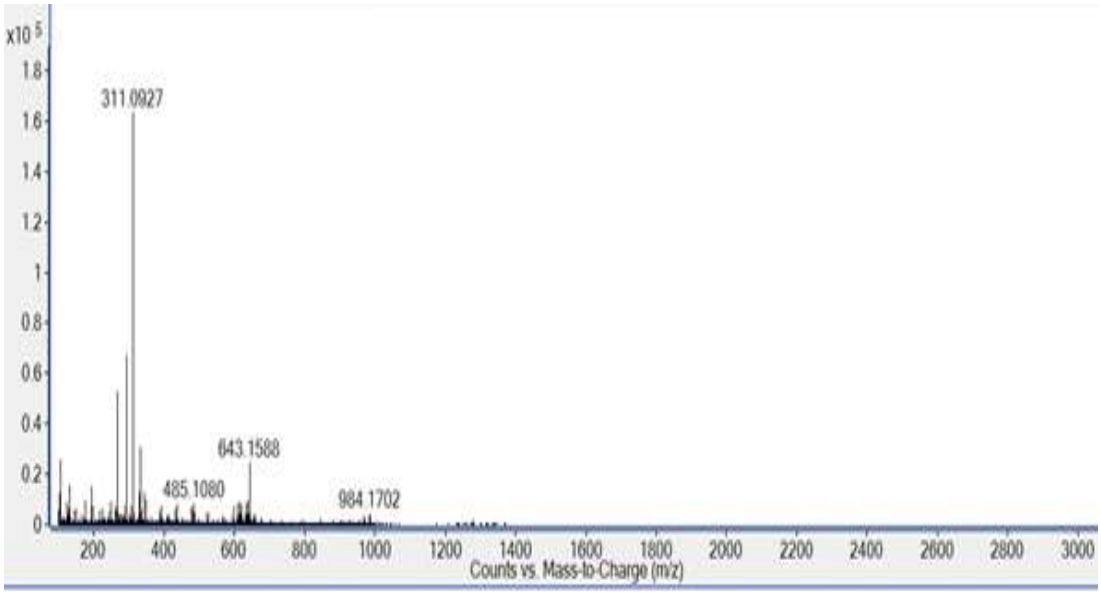

Figure 59. ESIMS spectrum of phaseocyclopentenone A (**18**) recorded in positive modality.

3.4.2.6- Structural characterization of phaseocyclopentenone B

Phaseocyclopentenone B (**19**) (Figure 52) had a molecular formula of $C_{17}H_{14}O_3$ as deduced from its ESIMS spectrum (Fig. 66) and consistent with eleven indices of hydrogen deficiency. As cited above, it contains both the phenyl and cyclopentenone residues as compound (**18**). In fact, the absorption bands for aromatic, double bond and ketone groups and the absorption maxima for conjugated aromatic system were observed in the IR (Nakanishi, and Solomon, 1977) and UV spectra (Pretsch *et al*., 2000), respectively. In addition, the IR spectrum also showed the presence of bands typical of hydroxy groups (Nakanishi, and Solomon, 1977). Thus, based on these preliminary results, (**19**) should differ from (**18**) in respect to the nature of the moiety of the substituents at C-4. In fact, (**19**) showed the presence of another monosubstituted phenyl group instead of the benzoyl and a tertiary hydroxyl residue present in (**18**). As expected, the ^{1}H and ^{13}C NMR data (Figure 60 and Figure 61, Table 15) of (**19**) confirmed by COSY, HSQC and HMBC data (Figure 62, Figure 63 and 64 and, Table 15) supported the suggested structure. In particular, the spectra differed from that of (**18**) for the presence of two coupled doublets (J = 5.9 Hz) observed at δ 4.79 and 4.14 (H-5 and H-4), which accounted for two adjacent methine groups one of which was hydroxylated (Pretsch *et al*., 2000), while their corresponding carbons resonated at δ 71.5 and 55.1 (C-5 and C-4), respectively (Breitmaier and Voelter, 1987). Another difference was the absence of the benzoyl moiety, replaced by a phenyl group. The long-range couplings observed in the HMBC spectrum (Figure 64 and, Table 15) between C-1' and C-2',6' at δ 136.4 and 129.7 with H-4, and between C-2 at δ 115.0 with H-2",6", permitted localization of two phenyl group at C-4 and C-2 respectively. Thus, the chemical shifts were assigned to all the protons and corresponding carbons and reported in Table 15 and phaseocyclopentenone B was formulated as 3,5-dihydroxy-2,4-diphenylcyclopent-2-enone (**19**). The structure assigned to **(19)** was supported by the other couplings observed in its HMBC spectrum (Table 15) and its ESIMS spectrum. The latter, recorded in positive modality, showed the dimer sodium $[2M + Na]^+$ and protonated $[2M + H]^+$ adducts and the protonated adduct $[M+ H]^+$ ions at *m/z* 555, 533 and 267.1023.

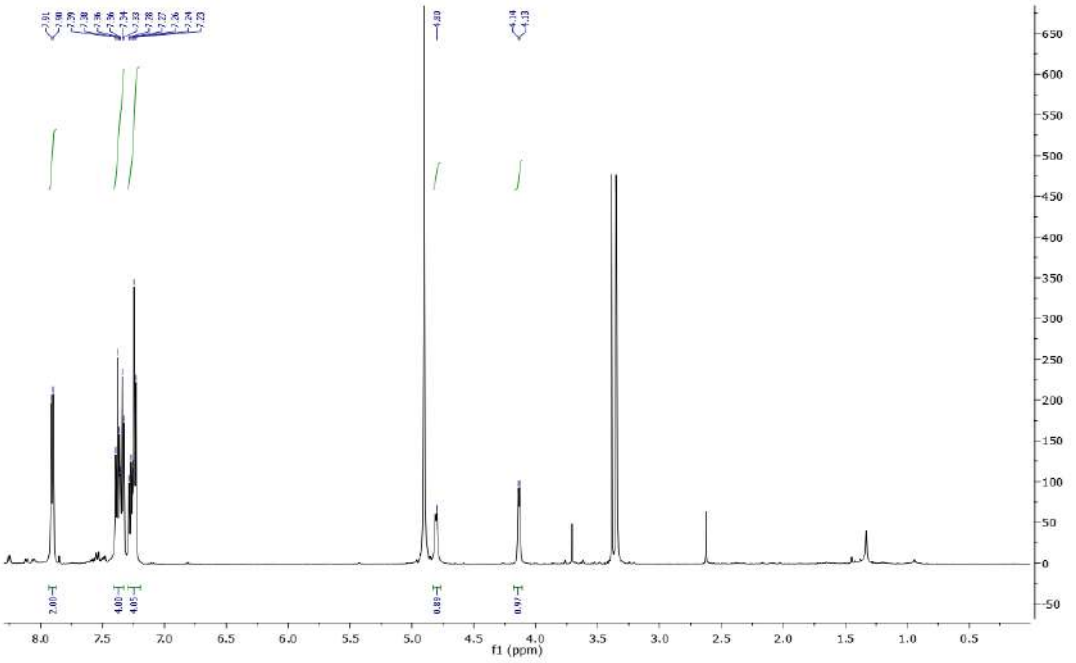

Figure 60. ^{1}H NMR spectrum of phaseocyclopentenone B (**19**) (CD_3OD, 400 MHz).

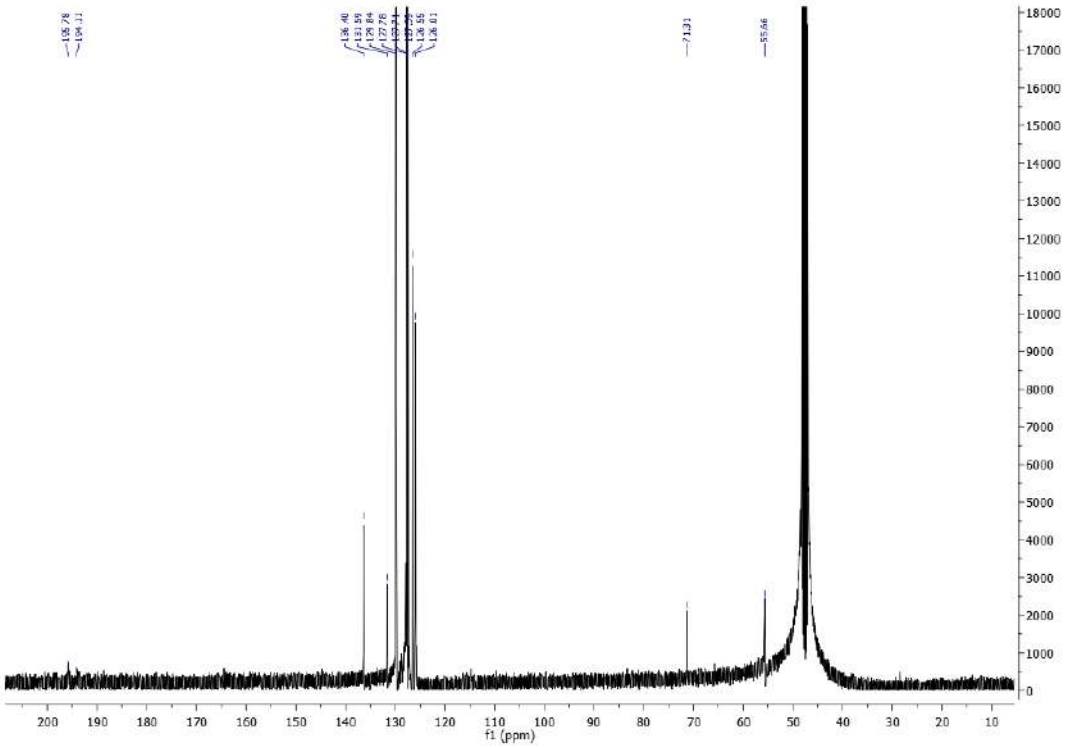

Figure 61. ^{13}C NMR spectrum of phaseocyclopentenone B (**19**) (CD_3OD, 100 MHz).

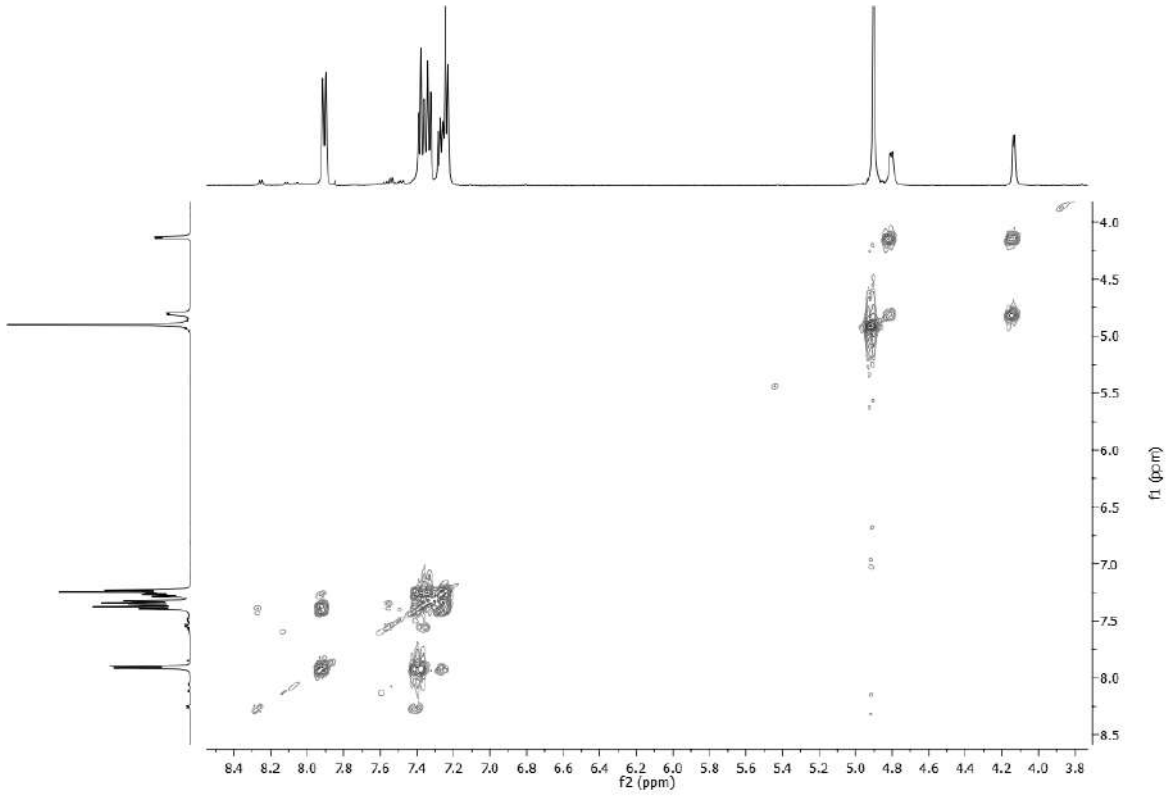

Figure 62. COSY spectrum of phaseocyclopentenone B (**19**) (CD_3OD, 400 MHz).

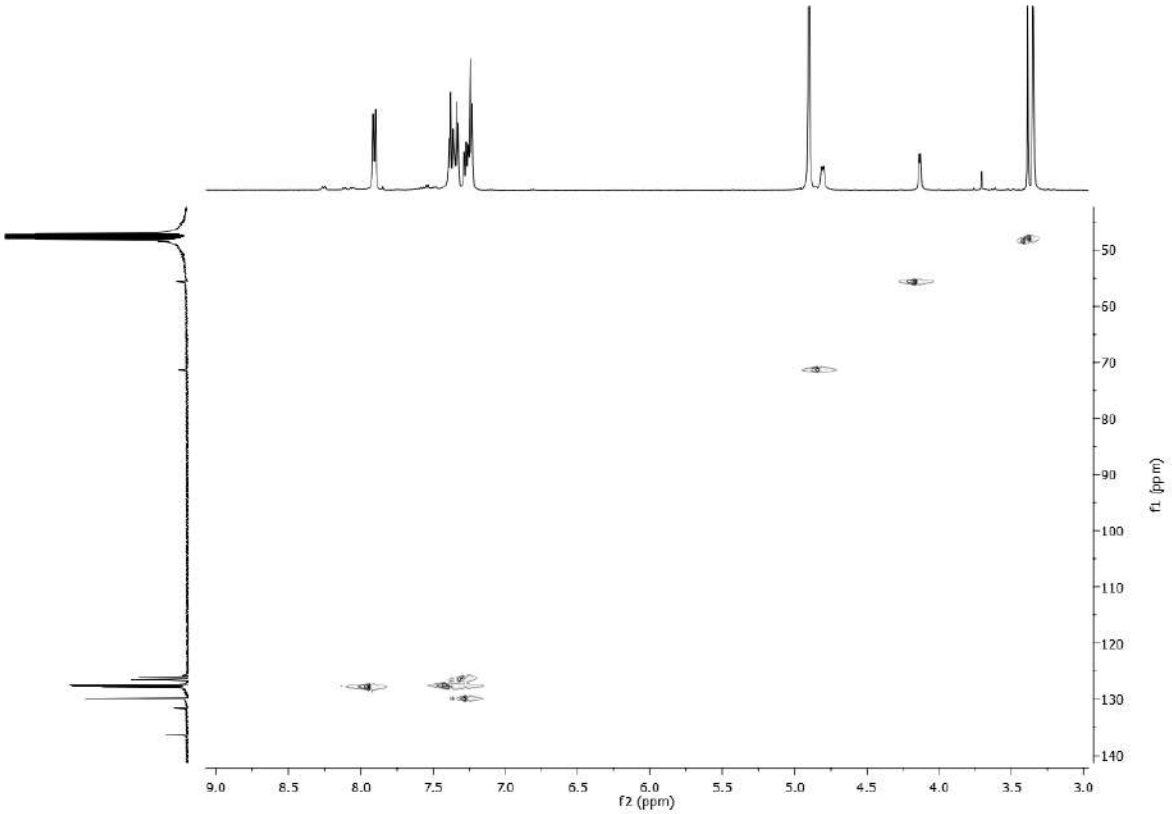

Figure 63. HSQC spectrum of phaseocyclopentenone B (**19**) (CD_3OD, 400/100 MHz).

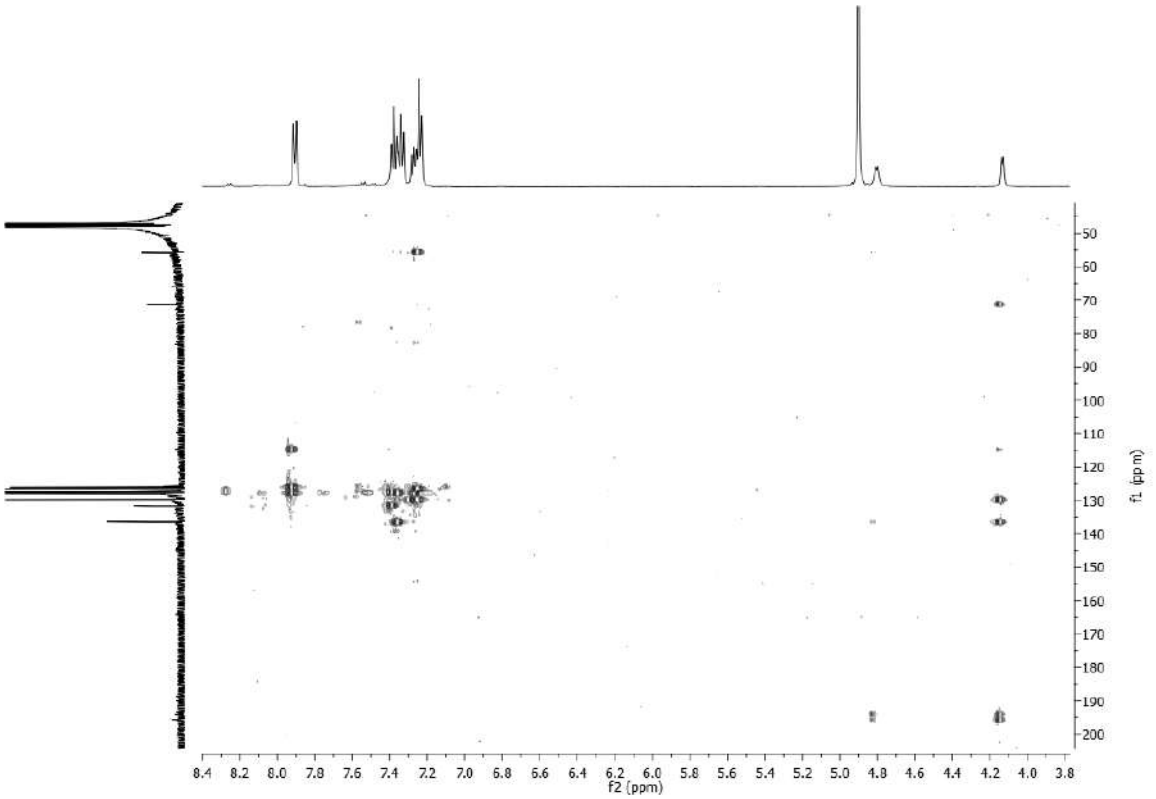

Figure 64. HMBC spectrum of phaseocyclopentenone B (**19**) (CD_3OD, 400/100 MHz).

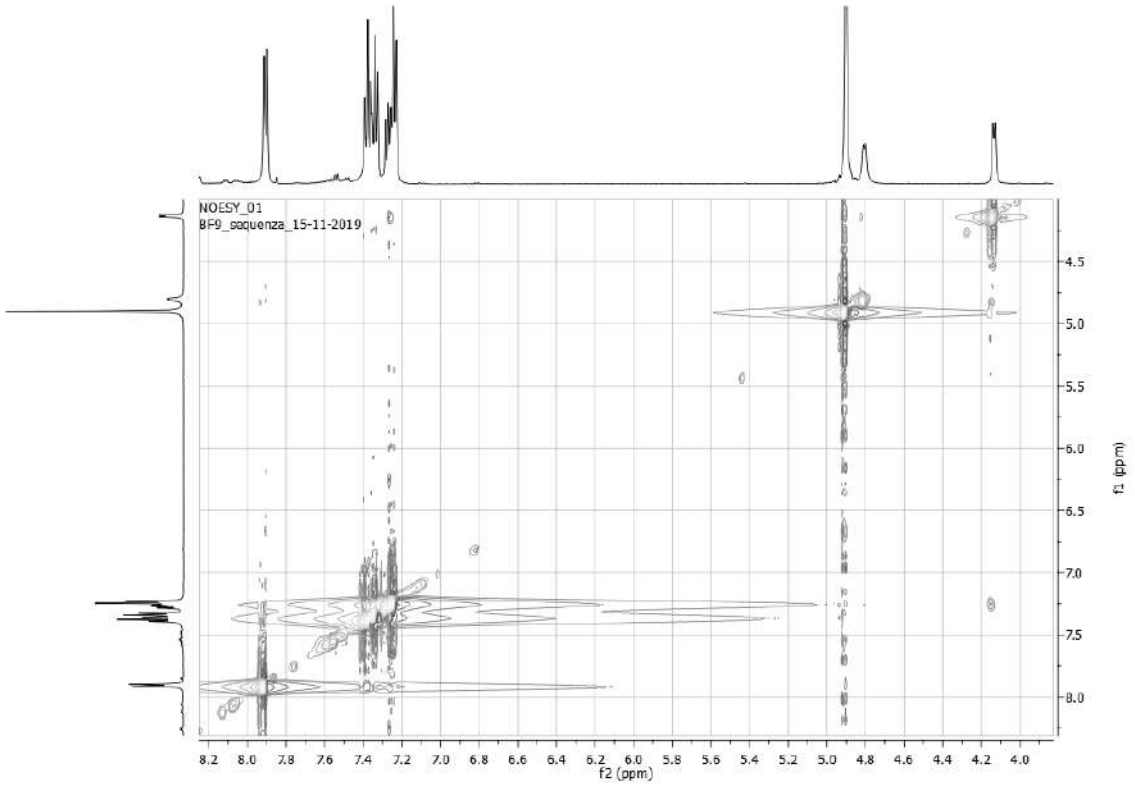

Figure 65. NOESY spectrum of phaseocyclopentenone B (**19**) (CD_3OD, 400 MHz).

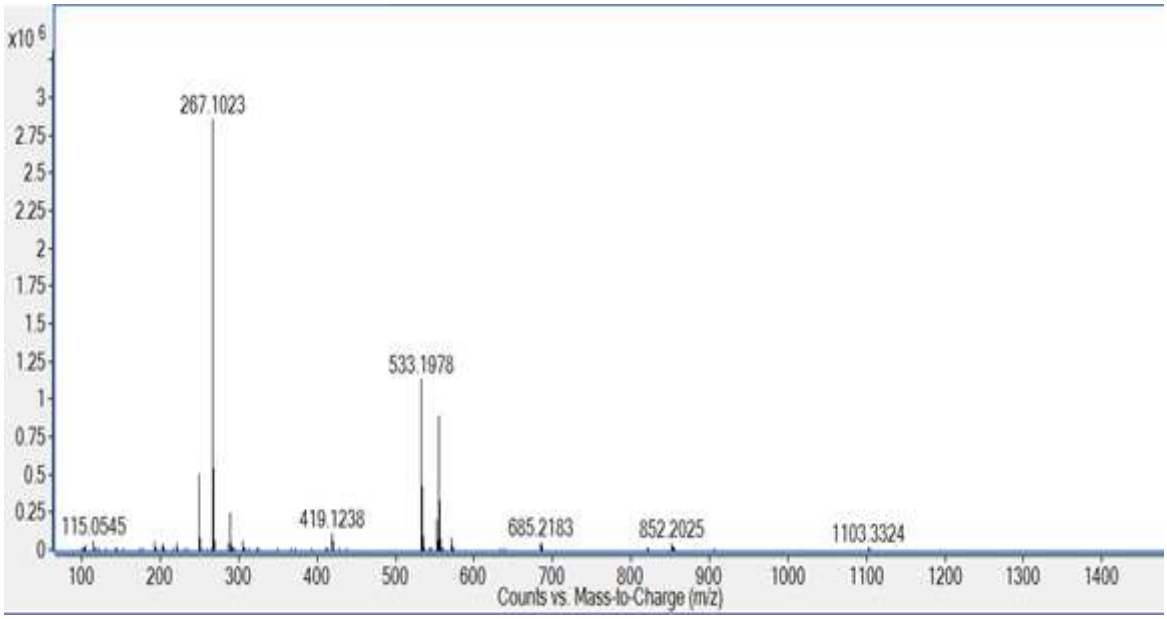

Figure 66. ESIMS spectrum of phaseocyclopentenone B (**19**) recorded in positive modality.

3.4.2.7- Relative and absolute configuration (AC) of phaseocyclopentenone A and B

The relative configuration at carbons C-4 and C-5 was assigned by the correlations observed in the NOESY spectrum between their geminal protons (Berger and Braun, 2004). Thus, H-4 and H-5 were *cis*-positioned, and the relative configuration was (4*R**,5*S**). Both metabolites (**18** and **19**) resisted crystallization, as well as the derivative (**17**). Thus, the AC of phaseocyclopentenones A and B (**18** and **19**) was determined by means of electronic circular dichroism (ECD), using a standardized procedure (Pescitelli and Bruhn, 2016; Superchi *et al*., 2018; Grauso *et al*., 2019). ECD spectra of (**18** and **19**) were recorded in MeCN and simulated using an established procedure which is summarized in the Computational Section. The comparison between experimental and calculated spectra (Figure 67) permitted assignment of the absolute configuration as (4*S*,5*R*)- (**18**) and (4*R*,5*S*)- (**19**).

It must be noticed that the agreement between experimental and calculated spectra is not completely satisfying in the high-energy region of the spectra. This fact should be ascribed to the presence of various chromophores with multiple transitions close in energy, which renders the wavelength region below 250 nm very dense of electronic excitations. This is shown in (Figure 67) for compound (**19**), for which a single strongly preferred conformer was obtained.

Table 15. ^{1}H, ^{13}C NMR and HSQC Data of Macrophenylcyclopentenones A and B (18 and 19) [a,b]

	18			**1**9		
Position	δC[c]	δH (*J* in Hz)	HMBC	δC[c]	δH (*J* in Hz)	HMBC
1	190.5, C		H-5	195.8, C		H-4, H-5
2	115.2, C		H-2",6"	115.0, C		H-2",6", H-4
3	196.6, C		H-5	194.1, C		H-4, H-5
4	88.0, C		H-5	55.1, CH	4.14, d (5.9)	
5	79.7, CH	4.69, s		71.5, CH	4.79, d (5.9)	
6	200.3, C		H-2',6'			
1'	136.7, C		H-3',5'	136.4, C		H-3',5', H-4, H-5
2',6'	129.6, CH	8.05, d (8.0)	H-3',5', H-4'	129.7, CH	7.26, m [d]	H-3',5', H-4
3',5'	127.3, CH	7.43, t (8.0)	H-2',6'	127.4, CH	7.40, t (7.7)	
4'	132.0, CH	7.53, t (8.0)	H-2',6', H-3',5'	126.5, CH	7.29, t (7.7)	H-2',6'
1''	130.8, C		H-3",5"	131.5, C		H-3",5"
2'',6''	127.7, CH	7.83, d (8.0)	H-4"	127.8, CH	7.93, d (8.0) [g]	H-4"
3'',5''	127.4, CH	7.36, t (8.0)	H-2",6"	127.4, CH	7.40, t (8.0)	
4''	126.4, CH	7.25, t (8.0)	H-2",6"	126.0, CH	7.26 m[d]	H-2",6"

[a] The chemical shifts are in δ values (ppm) from TMS. [b] 2D ^{1}H, ^{1}H (COSY) ^{13}C,^{1}H (HSQC) NMR experiments delineated the correlations of all the protons and the corresponding carbons. [c] Multiplicities were assigned by DEPT spectrum. [d] These signals are overlapped.

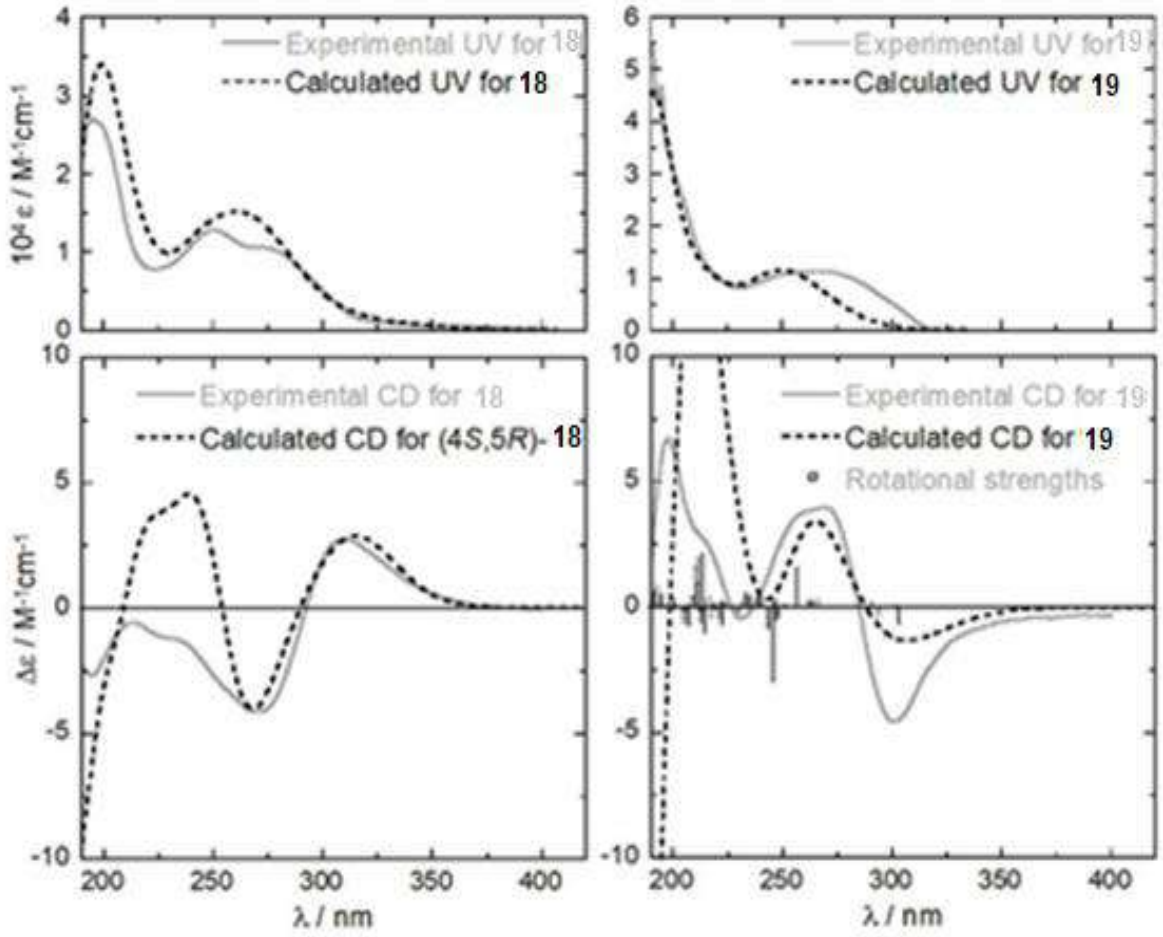

Figure 67. Experimental UV and ECD spectrum of **18** and **19** measured in acetonitrile (solid gray lines) compared with the spectra calculated on (4*S*,5*R*)-**18** and (4*R*,5*S*)-**19** at the B3LYP/def2-TZVP//ωB97X-D/6-311+G(d,p) level. The vertical bars in the bottom right spectrum represent calculated rotational strengths (in arbitrary units).

3.4.2.8- Biological assay

3.4.2.8.1- *Phytotoxic assay*

The phytotoxic activity was tested using two different bioassays. The culture filtrate, the organic extract (at a concentration of 1 mg/mL) and compounds (**18** and **19**) (at a concentration of 10^{-3} M) were tested on tomato (*S. lycopersicum* L.) by cutting assay. A strong phytotoxicity was observed testing the culture filtrate and the organic extract and phaseocyclopentenone B (**19**) which caused strong wilting while slight symptoms were detected for plants treated with compound (**18**). Compounds (**18** and **19**) were also tested by leaf puncture assay on tomato and on soybean (*Glycine max* L.), together with guignardone A (**17**) (which was obtained in lower amount), at a concentration of 10^{-3} and 10^{-4} M. Compounds (**17**-**19**) showed phytotoxicity on tomato at both concentrations while no activity was observed on the host plant (Table 16).

Compound (**17**) induced marked necrosis compared to that of compounds (**18** and **19**) especially at the highest concentration (Figure 68).

These results demonstrated the importance of the substituents present at C-4 and C-5 in compounds (**18** and **19**) to impart the phytotoxicity but also a different mechanism of action in the two bioassays. This is the first report on the phytotoxic activity of guignardone A also in respect to the other related meroterpenoids belonging to the same group of natural compounds.

3.4.2.8.2- *Antifungal bioassay*

Assayed against *Colletotrichum truncatum* and *Cercospora nicotianae*, two fungi pathogenic to soybean, the metabolites (**17-19**) did not exhibit any antifungal activity.

Table 16. Phytotoxic Activity of Compounds (**17-19**) [a]

Bioassay	**Plant**	**17**		**18**		**19**		**Control**[b]
		10^{-3}[c]	10^{-4}	10^{-3}	10^{-4}	10^{-3}	10^{-4}	
Leaf puncture assay	*Solanum lycopersicum* L.	2	1	2	2	3	3	0
	Glycine max L.	0	0	0	0	0	0	0
Cutting assay	*S. lycopersicum* L.	1	n.t.[d]	3	n.t.	n.t	n.t.	0

[a] Observations were made seven days after treatment. Intensity of necrosis on leaves in the leaf puncture assay: 3. severe necrosis; 2, intermediate necrosis; 1. slight necrosis; 0. no necrosis. Intensity of wilting symptoms in cutting assay: 3. complete wilting; 2. intermediate symptoms; 1. slight symptoms; 0. no symptoms. [b] 4% MeOH in distilled water. [c] Molar concentration. [d] Not tested.

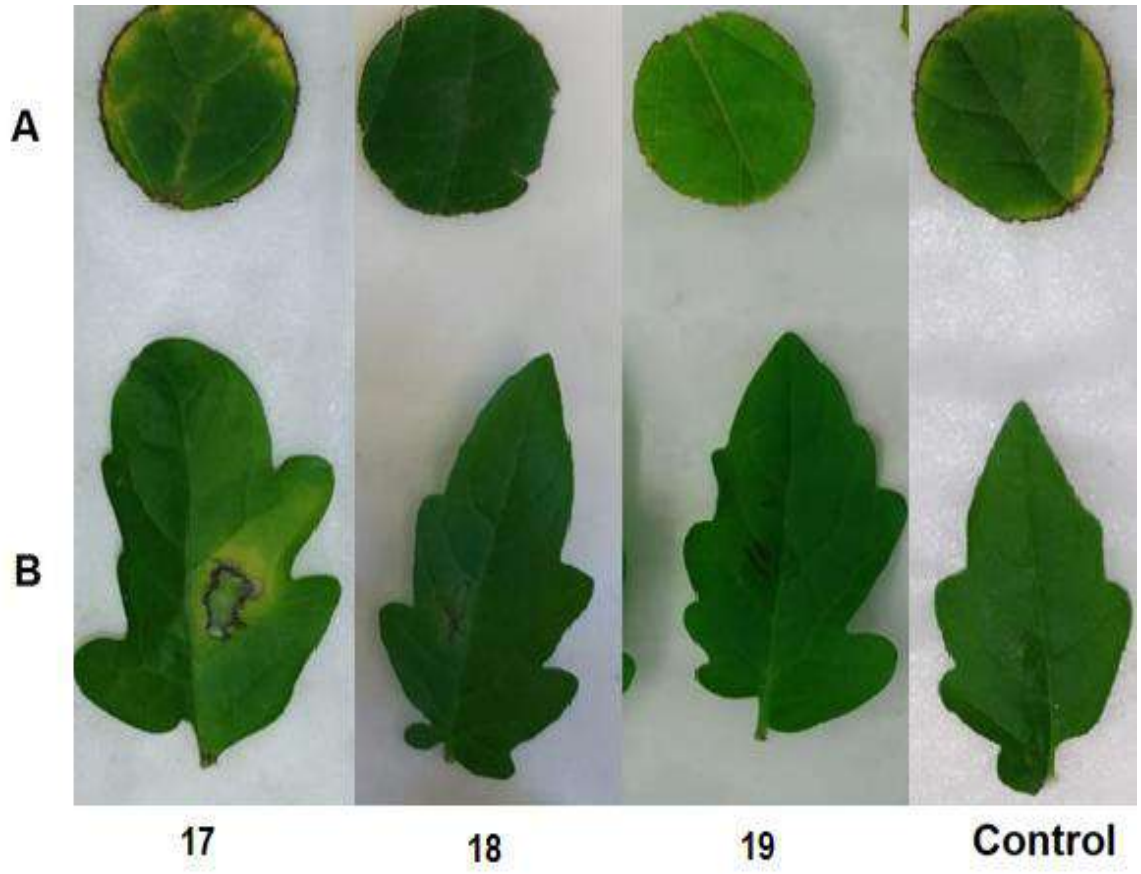

Figure 68. Phytotoxic activity induced by compounds (**17-19**) when tested at 10^{-3} M by leaf-puncture assay on soya (A: *Glycine max* L.) and on tomato (B: *Solanum lycopersicum* L.); control 4% MeOH in distilled water.

General Discussion

4. General Discussion

The objective of this PhD project was to investigate the isolation of bioactive compounds produced by Mediterranean fungi and plants. These bioactive metabolites could play an interesting role in agriculture as agents of biological control for weeds or specific plant diseases (Scharf *et al*., 2014; Cimmino *et al*., 2015; Masi *et al*., 2018b). Among them, phytotoxins could be also a useful tool, to develop specific and rapid diagnostic methods, in order to select plants naturally resistant to the pathogen identifying the genes of innate resistance (Evidente *et al*., 2014, *Cimmino et al*., 2015; Masi *et al*., 2018a; Evidente *et al*., 2019).

For this reason, it could be valuable to compare the isolated phytotoxins metabolites from edible macrofungus *Agaricus litoralis*, and the plant *Dittrichia viscosa* of different Mediterranean Basin ecosystems with those obtained from the two phytopathogenic fungi: *Dreschlera gigantea* and *Macrophomina phaseolina* as model microorganisms producing phytotoxins. For instance, a well-known phytotoxic metabolite, named tyrosol produced by *Agaricus litoralis*, an edible macrofungus, has been previously isolated from microorganisms, macrofungi, and plants, but this is the first record from *A. litoralis* as a phytotoxic metabolite. Besides, it is important to highlight that the macrofungus *A. litoralis* was collected and identified for the first time in this investigation, in Constantine region, Eastern Algeria. Its identification was based on morphological and molecular techniques, the second aim of this chapter.

The two sesquitepenoids, inuloxin D and E, isolated from *Dittrichia viscosa* plant showed an interested herbicidal activity against *Orobanche cumana.* This result could be compared by that obtained in a previous study (Andolfi *et al*., 2013), in which the sesquiterpene lactones produced by *D. viscosa* namely inuloxins A, C, and D have statistically significant herbicidal activity against broomrapes *Orobanche crenata* and field dodder *Cuscuta campestris.* Moreover, the two novel sesterpenoids; drophiobiolins A and B, as well as the ophiobiolin A obtained from *D. gigantea* revealed a remarkable phytotoxic effect against *Digitaria sanguinalis*. These interesting findings are similar to those reported by many researchers (Kim *et al*., 1999; Evidente *et al*., 2006; Tian et *al*., 2017) showing that ophiobolin metabolites produced by pathogenic fungi, attacking agricultural crops, have significant phytotoxic properties.

The evaluation of the antiproliferative activity revealed that drophiobolins A and B exhibited cytotoxicity against Hela B cells with an IC_{50} value of 10 μM. However, they had less or no

effect against Hacat, H1299 and A431 cells when compared to ophiobolin A. Our results could be comparable with those of other studies (Evidente *et al*., 2014; Ebada and Proksch, 2015; Tommonaro *et al*., 2015; Tian *et al.*, 2017) that confirmed the biological activities of ophiobolins, including cytotoxic and antimicrobial ones.

Besides, the different bioassays of phaseocyclopentenones A and B, isolated from *M. phaseolina* collected in Argentina, showed interesting phytotoxic properties on non-host plant *Solanum lycopersicum* L., while guignardone A resulted to be inactive in a cutting assay. The three compounds phaseocyclopentenones A and B and guignardone A were inactive on the host plant soybean, *Glycine max* L. The latter was isolated for the first time from *M. phaseolina* which previously showed to produce only the toxic sesquiterpene eremophilane phaseolinone (Dhar *et al*., 1982), and the polyketide botryodiplodin, that is a toxin also produced by other phytopatogenic fungi phaseolinone (Ramezani *et al*., 2007; Sen Gupta *et al*., 1966).

Fungal metabolites containing a dihydroxycyclopentenone core are already known as natural occurring compounds such as kodaistatins A–D produced by *Aspergillus terreus* with antidiabetic activity which are similar to phaseocyclopentenone A but they differed for the position of the substituents attached to the core (Peter and Brückner, 2018). However, the closest compound to phaseocyclopentenone A is a synthetic compound prepared by a gold-catalyzed oxidative reaction of propargylic carbonates or acetates using 3,5-dichloropyridine (Sun *et al*., 2014). Two fungal metabolites, named involutin and chamonixin, are the natural compounds closest to phaseocyclopentenone B but they differed for the position and the nature of the substituents on cyclopentenone core (Feling *et al*., 2001a).

For the antifungal activity, the three compounds were inactive against both *Cercospora nicotiane* and *Colletotrichum truncatum*.

Conclusion and Perspectives

5- Conclusion and Perspectives

In this thesis project, different bioactive metabolites with a potential herbicidal and fungicidal activity, producing by Mediterranean fungi and plants, have been isolated and characterized as reported below:

An edible macro-fungus *Agaricus litoralis* collected in Constantine region (Eastern Algeria), was identified based on both morphological observation and DNA sequence analyses of the ITS region. From its EtOAc extract, its main phytotoxic metabolite was isolated and identified as tyrosol. When it was tested using the leaf puncture assay, it showed a strong phytotoxicity on grapevine (*Vitis vinifera* L.), apricot (*Prunus armeniaca* L.), peach (*Prunus persica* (L.) *Batsch*), *Cucurbita* (*Cucurbita* L.), and blackberry (*Rubus fruticosus* L.), while moderate and low phytotoxicity was recorded on eggplant (*Solanum melongena* L.), fig (*Ficus carica* L.) and lemon (*Citrus limon* (L.) *Osbeck*); respectively.

A new sesquitepenoid named inuloxin E and four known metabolites; α-costic acid, inuloxins A, C and D, were isolated and identified from the aerial part of *Dittrichia viscosa*. In which, the two inuloxins D and E, as well as the four derivatives of inoluxin D did not induce the germination of the two parasitic weeds *Orobanche minor* and *Phelipanche ramosa* but they were active on the seeds of *Orobanche cumana,* inducing their germination.

Two new ophiobolan sesterterpenoids named drophiobiolins A and B, as well as four well-known sesterterpenoids; ophiobolin A, 6-*epi*-ophiobolin A, 3-anhydro-6-*epi*-ophiobolin A, and ophiobolin I, were isolated from the liquid culture of *D. gigantea,* then identified using spectroscopic analyses; NMR and ESI-MS. The phytotoxicity activity of these previous molecules, on cultivated plant (*Lycopersicon esculentum* L.), host weed plant (*Digitaria sanguinalis* L.) and non-host weed plant (*Chenopodium album* L.), was also detected; whereby the two new drophiobiolins A and B showed a strong phytotoxicity as ophiobolin A on both cultivated and host plants. However, a lower toxicity was observed on non-host plant compared to that of ophiobolin A. Furthermore, the drophiobiolins A and B showed the highest cytotoxicity effect against Hela B cells, but they had less important effect against Hacat, H1299 and A431 cells.

Besides, two new penta- and tetra-substituted cyclopentenones, named phaseocyclopentenones A and B, were isolated from the liquid culture of *M. phaseolina* together with the well-known

fungal meroterpenoid guignardone A, then identified by spectroscopic analyses. In the different phytotoxic bioassays, phaseocyclopentenones A and B showed a strong phytotoxicity on non-host plant (*Solanum lycopersicum* L.). Conversely, these three compounds; phaseocyclopentenones A and B and guignardone A were inactive on the host plant soybean (*Glycine max* L.).

In conclusion, the isolated bioactive metabolites could be exploited to use them in developing a rapid and specific method for plant disease diagnosis and understand their role in induction of disease symptoms. Furthermore, these metabolites could be used in agriculture as biopesticides (natural safe herbicides, fungicides, insecticides etc.) and in medicine as pro-drug (anticancer, antibiotic, antimalaria, anti-inflammatory etc.) with new mode of action.

Perspectives

As a result, several perspectives can emerge from this research:

- Confirmation of the effects observed on larger samples (field study);
- Study of the combinatorial effect of the different active substances produced in this work;
- Improvement of the biological activity of molecules identified by the production of products derived from these substances by organic synthesis.

Publications and Manuscripts Arising from the Research

Publications and Manuscripts Arising from the Research

Refereed Journal Articles:

Paper 1

Zatout, R., Cimmino, A., Cherfia, R., Kacem Chaouche, N. (2021). Isolation of tyrosol the main phytotoxic metabolite produced by the edible fungus *Agaricus litoralis*. *Egyptian journal of chemistry*, 64, 5741 – 5745.

Paper 2

Masi, M., Fernández-Aparicio, M., **Zatout, R**., Boari, A., Cimmino, A., Evidente, A. (2019). Inuloxin E, a new seco-eudesmanolide isolated from *Dittrichia viscosa*, stimulating *Orobanche cumana* seed germination. *Molecules*, 24, 19, 3479.

Paper 3

Johnson J.L., Santoro, E., **Zatout, R**., Petrovic, A.G., Cimmino, A., Superchi, S., Evidente, A., Nina D. Berova, N.D., Polavarapu, P.L. (2021). Absolute configuration of seco-eudesmanolide inuloxin D from experimental and predicted chiroptical studies of its 4-*O*-acetyl derivative. *Chirality*, 33, 5, 233-241.

Paper 4

Zatout, R., Masi, M., Sangermano, F., Vurro, M., Zonno, M. C., Santoro, E., Evidente, A. (2020). Drophiobiolins A and B, bioactive ophiobolan sestertepenoids produced by *Dreschslera gigantea*. *Journal of Natural Products*, 83, 11, 3387–3396

Paper 5

Masi, M., Sautua, F., **Zatout, R**., Castaldi, S., Arrico, L., Isticato, R., Pescitelli, G., Carmona, M. A., Evidente, A. (2021). Phaseocyclopentenones A and B, phytotoxic penta- and tetrasubstituted cyclopentenones produced by *Macrophomina phaseolina*, the causal agent of charcoal rot of soybean in Argentina. *Journal of Natural Products*, 84, 2, 459–465.

Appendix

Appendix 1

DNA Sequences of *Agaricus litoralis*

ATGCGAGAGCCAAGAGATCCGTTGCTGAAAGTTGTATTACAATTTTC
ATAGGCATACAAGCCCATGTAAAGACATTCAATAACATTCGATAGG
GTATAATGAATGACATAGACTCTGGTGAGAAAACAAATCCGTGGCC
AAGTAAAGGACAGCAAAGCTTTCACACTGCAAGTCCTCACATCCAG
CAAGTGCTGATAGGCTGACCACTTCATCGATACCCAACCAAAGACTA
CAATAGGTGCACAGGTGGATGAAGATGAAATCCAAACAGGCGTGCA
CATGCTCTAAAGAGCCAGCTACAACCCATCTAGAAACATAATTCAAT
AATGATCCTTCCGCAGGTTCACCTACGGAAACCTTGTTACGACTTTT
ACTTCCTCTA

ملخـــص

ملخــص

الهدف الرئيسي من هذه الأطروحة هو دراسة المستقلبات ذات النشاط المحتمل كمبيد للأعشاب والفطريات التي تنتجها الفطريات والنباتات. تم وصف المستقلبات النشطة بيولوجيًا و كيميائيًا. باستخدام طرق كروماتوغرافيا. حيث تم جمع الفطر الكبير *Agaricus litoralis* من غابة جبل الوحش ، في الشرق القسنطيني ، الجزائر وتم التعرف عليه باستخدام البيانات المورفولوجية والجزيئية. في الواقع، تم اظهار سمية نباتية عالية لمستخلص EtOAc على أوراق *Lycopersicon esculentum* L. ؛ حيث تم عزل جزيء معروف سمي للنبات يسمى التيروزول وتم تحديده بواسطة طرق التحليل الطيفي. تم اختبار النشاط السام للنبات لهذا الأخير، التيروزول ، على سبعة نباتات زراعية واثنين من النباتات البرية باستخدام اختبار ثقب الأوراق. أظهرت النتائج التي تم الحصول عليها أن أعلى تأثير سمي لوحظ على *Vitis vinifera* L.، *Prunus armeniaca* L. *Batsch*، *Prunus persica* L.، *Cucurbita* L. و *Rubus fruticosus* L. عند تركيز 1مجم / مل. بينما لوحظت تأثيرات سمية معتدلة على أوراق نبات *Solanum melongena L*. وأقل سمية نباتية على أوراق *Ficus carica* L. و *Osbeck Citrus limon* L. بالإضافة إلى ذلك، تم عزل *sesquiterpenoid* جديد ينتمي إلى المجموعة الفرعية *seco eudesmanolides*، تسمى inuloxin E، من *Dittrichia viscosa*، بالإضافة إلى sesquiterpenoids inuloxins A-D المعروف وحمض α-costic. تم التعرف على Inuloxin E بالبيانات الطيفية، وخاصة الرنين المغناطيسي النووي و ESIMS. تسبب inuloxin D و E في إنبات الحشائش الطفيلية *Orobanche cumana* ولكنهما كانا غير فعالين على بذور *Orobanche Minor* و *Phelipanche ramosa*. بالإضافة إلى ذلك، تمت دراسة نشاط إنبات بعض الاسترات شبه الاصطناعية ل inuloxin D. وبالمثل، تم عزل اثنين من مركبات الأفيوبولان الجديدة النشطة بيولوجيًا ، المسمى drophiobiolins A و B مع ophiobolin A وهو المستقلب الرئيسي ، epi-ophioboline A -6 ، 3-anhydro-6-epi-ophioboline A و ophioboline I أيضًا من *Drechslera gigantea* ،هذا الفطر مقترح كمبيد فطري للمكافحة البيولوجية ضد *Digitaria sanguinalis*. تم التعرف على Drophiobolins A و B بشكل أساسي بالرنين المغناطيسي النووي و HRESIMS. كما تم اختبار نشاطها السام للنبات من خلال اختبار انثقاب الأوراق على الأعشاب المزروعة (*Lycopersicon esculentum* L) ، وكذلك على المضيف (*Digitaria sanguinalis* L) والأعشاب غير المضيفة (*Chenopodium Album* L) مقارنة بتلك الموجودة في ophiobolin C: أظهر الاثنان اللذان تم تحديدهما حديثًا سمية نباتية كبيرة ، عند أعلى تركيز مستخدم. كما أظهر تقييم النشاط المضاد للتكاثر أيضًا أن دروفيوبولين A و B أظهروا سمية خلوية ضد خلايا Hela B بقيمة IC50 تبلغ 10 M. ومع ذلك، كان تأثيرهم أقل أو معدومًا ضد الخلايا الاخرى. تم عزل اثنين من البنتينونات الجديدة المستبدلة بخماسي ورباعي، تسمى phaseocyclopentenones A و B ، بالإضافة إلى guignardone A ، من مزارع *Macrophonina phaseolina*. تم عزل هذا الفطر الممرض للنبات من أنسجة فول الصويا المصابة التي تظهر أعراض الجمرة الخبيثة في الأرجنتين. تم تحديد Phaseocyclopentenones A و B بالطرق الطيفية (بشكل أساسي 1H1" D و 13 C" و 2 D NMR و HR-ESIMS). في اختبار على نبات غير مضيف (*Solanum lycopersicum* L.) عن طريق ثقب الأوراق، أظهر Phaseocyclopentenones A و B و guignardone A نشاطًا مثيرًا للاهتمام للنباتات. تنشط المركبات الجديدة أيضًا في تجربة على نفس النبات. في المقابل، لم يتم الكشف عن أي سمية نباتية أو نشاط مضاد للفطريات بواسطة المركبات الثلاثة الموجودة على نبات فول الصويا المضيف (*Glycine max* L) وضد بعض مسببات الأمراض الفطرية، وهي *Cercospora nicotiane* و *Colletotrichum truncatum* ، والتي عزلت أيضًا من نباتات فول الصويا المصابة في الأرجنتين.

الكلمات المفتاحية: الفطريات ؛ نباتات ؛ inuloxine E ؛ drophiobiolins A et B ؛ phaseocyclopenténones A et B؛ نشاط مبيدات الفطريات والأعشاب.

Bibliographic references

6- Bibliographic references

Abdullah, B., Abd Ghani, N.A. and Vo, D.V.N. (2017). Recent advances in dry reforming of methane over Ni-based catalysts. *Journal of Cleaner Production*, 162, 170-185.

Albuquerque, P., Casadevall, A. (2012). Quorum sensing in fungi–a review. *Medical mycology*, 50(4), 337-345.

Abbas, H. K., Bellaloui, N., Accinelli, C., Smith, J. R., Shier, W. T. (2019). Toxin production in soybean (*Glycine max* L.) plants with charcoal rot disease and by *Macrophomina phaseolina*, the fungus that causes the disease. Toxins, 11(11), 645.

Abrham, G., Dovrat, S., Bessler, H., Grossman, S., Uri, N., Bergman, M. (2010). Inhibition of inflammatory cytokine secretion by plant-derived compounds inuviscolide and tomentosin: the role of NFκB and STAT1. *The Open Pharmacology Journal*, 4(1).

Al-Thani, R. F. (2010). Survey of macrofungi (including truffles) in Qatar. *Atlas Journal of Biology*, 1(2), 26-29.

An, Q., Li, C., Chen, Y., Deng, Y., Yang, T., Luo, Y. (2020). Repurposed drug candidates for antituberculosis therapy. *European journal of medicinal chemistry*, 192, 112175.

Anderberg, A. A. (1991). Taxonomy and phylogeny of the tribe *Inuleae* (*Asteraceae*). *Plant Systematics and Evolution*, 176(1), 75-123.

Andolfi, A., Evidente, A., Santini, A., Tuzi, A. (2006). Ophiobolin A. *Acta Crystallographica Section E: Structure Reports Online*, 62(6), o2195-o2197.

Andolfi, A., Zermane, N., Cimmino, A., Avolio, F., Boari, A., Vurro, M., Evidente, A. (2013). Inuloxins A – D, phytotoxic bi-and tri-cyclic sesquiterpene lactones produced by *Inula viscosa*: Potential for broomrapes and field dodder management. *Phytochemistry*, 86, 112-120.

Andolfi, A., Ferrante, P., Petriccione, M., Cimmino, A., Evidente, A., Scortichini, M. (2014). Production of phytotoxic metabolites by *Pseudomonas syringae* pv. *actinidiae*, the causal agent of bacterial canker of kiwifruit. *Journal of Plant Pathology*, 96(1), 169-176.

Andrey, J., Mills, B., Leahy, M., Suggett, J. (2003). Weather as a chronic hazard for road transportation in Canadian cities. *Natural hazards*, 28(2), 319-343.

Aşkin Çelik, T., and Aslantürk, Ö. S. (2010). Evaluation of cytotoxicity and genotoxicity of *Inula viscosa* leaf extracts with Allium test. *Journal of biomedicine and biotechnology*, 2010.

Au, T. K., Chick, W. S., Leung, P. C. (2000). The biology of ophiobolins. *Life sciences*, 67(7), 733-742.

Autschbach, J. (2012). Perspective: relativistic effects. *The Journal of chemical physics*, 136(15), 150902.

Badalyan, S., and Rapior, S. (2020). Agraricomycetes medicinal mushrooms with potential neuroprotective activity growing in *Armenia*. *Proceedings of the Yerevan State University, Chemistry and Biology*, 54(3).

Balasundram, N., Sundram, K., Samman, S. (2006). Phenolic compounds in plants and agri-industrial by-products: Antioxidant activity, occurrence, and potential uses. *Food chemistry*, 99(1), 191-203.

Ballio, A., Barra, D., Bossa, F., Collina, A., Grgurina, I., Marino, G., Simmaco, M. (1991). Syringopeptins, new phytotoxic lipodepsipeptides of *Pseudomonas syringae* pv. *syringae*. *FEBS letters*, 291(1), 109-112.

Békési, P., Szani, Sz. és, Zalka, A. (1995): A *Macrophomina phaseolina* (Tassi) Goid. hazai előfordulása dinnyén. *Integrált termesztés a kertészetben* (16.). Budapest, 107.

Benazza-Bouregba M. (2017). Inventaire et identification des Basidiomycetes de la forêt de M'sila, Oran, Thèse Doctorat en Biotechnologie, Option: Microbiologie, Université d'Oran, faculté des sciences de la nature et de la vie, Département de Biotechnologie, 150-152.

Berger, S., and S. Braun (2004). 200 and More NMR Experiments: A Practical Course, WileyVch Weinheim.

Bhattacharya, D., Dhar, T. K., Ali, E. S. A. H. A. K. (1992). An enzyme immunoassay of phaseolinone and its application in estimation of the amount of toxin in *Macrophomina phaseolina*-infected seeds. *Applied and environmental microbiology*, 58(6), 1970-1974.

Boa, E. R. (2004). Wild edible fungi: a global overview of their use and importance to people.

Bouallagui, Z., and Sayadi, S. (2006). Production of high hydroxytyrosol yields via tyrosol conversion by *Pseudomonas aeruginosa* immobilized resting cells. *Journal of agricultural and food chemistry*, 54(26), 9906-9911.

Boari, A., Vurro, M., Calabrese, G. J., Mahmoud, M. N. Z., Cazzato, E., Fracchiolla, M. (2021). Evaluation of *Dittrichia viscosa* (L.) Greuter Dried Biomass for Weed Management. *Plants*, 10(1), 147.

Boudy P. 1955. African economy. Tom IV. Forest description of Algeria and Tunisia. Paris: Larose. p. 481.

Breitmaier, E; Voelter, W. Carbon. (1987). ^{13} NMR Spectroscopy; VCH: Weinheim, Germany, 183-280. 13.

Bruhn, T., Schaumlöffel, A., Hemberger, Y., Bringmann, G. (2013). SpecDis: Quantifying the comparison of calculated and experimental electronic circular dichroism spectra. *Chirality*, 25(4), 243-249.

Brullo, S., and de Marco, G. (2000). Taxonomical revision of the genus *Dittrichia* (Asteraceae). *Portugaliae Acta Biologica*, 19(1), 341-354.

Bury, M., Girault, A., Megalizzi, V., Spiegl-Kreinecker, S., Mathieu, V., Berger, W., Evidente, A., Kornienko, A., Gailly, P., and Vandier, C. (2013). Ophiobolin A induces paraptosis-like cell death in human glioblastoma cells by decreasing BKCa channel activity. *Cell Death* and *Disease*, 4, e561.

Cai, R., Jiang, H., Mo, Y., Guo, H., Li, C., Long, Y., She, Z. (2019). Ophiobolin-type sesterterpenoids from the mangrove endophytic fungus *Aspergillus* sp. ZJ-68. *Journal of natural products*, 82(8), 2268-2278.

Callac, P., and Chen, J. (2018). Tropical species of Agaricus. *Updates on tropical mushrooms. Basic and applied research. San Cristobal de Las Cascaas, Chiapas*, 25-38.

Canales, M. W., Gray, G. R. (1988). 6-*epi*-ophiobolin A and 3-anhydro-6-*epi*-ophiobolin A, host specific phytotoxins of *Drechslera maydis* (race T). *Phytochemistry*, 27: 1653-1663.

Canonica, L., A. Fiecchi, M. Galli Kienle, and A. (1966) Scala. The constitution of cochliobolin. *Tetrahedron Letters*, 7(11), 1211-1218.

Capasso, R., Iacobellis, N. S., Bottalico, A., Randazzo, G. (1984). Structure-toxicity relationships of the eremophilane phomenone and PR-toxin. *Phytochemistry*, 23(12), 2781-2784.

Capasso, R., Cristinzio, G., Evidente, A., Scognamiglio, F. (1992). Isolation, spectroscopy and selective phytotoxic effects of polyphenols from vegetable waste waters. *Phytochemistry*, 31(12), 4125-4128.

Cappelli, A. (1984). *Agaricus* L.Fr. (*Psalliota* Fr.) Fungi Europaei, Vol. 1. *Libreria editrice Biella Giovanna*, Italy Saronno. p. 42e47.

Chandramohan, S., and Charudattan, R. (2001). Control of seven grasses with a mixture of three fungal pathogens with restricted host ranges. *Biological control*, 22(3), 246-255.

Chandramohan, S., and Charudattan, R., Sonoda, R. M., Singh, M. (2002). Field evaluation of a fungal pathogen mixture for the control of seven weedy grasses. *Weed Science*, 50(2), 204-213.

Chang, S. T., and Miles, P. G. (1989). Edible mushrooms and their cultivation. *Edible mushrooms and their cultivation.*

Chang, C. H., Qiu, J., O'Sullivan, D., Buck, M. D., Noguchi, T., Curtis, J. D. Pearce, E. L. (2015). Metabolic competition in the tumor microenvironment is a driver of cancer progression. *Cell*, 162(6), 1229-1241.

Chavan, S. V., Jadhav, P. V., Madke, M. S., Mane, S. S., Nandanwar, R. S. (2019). Molecular Characterization of Soybean Genotypes in Response to Charcoal Rot Disease by using SSR Markers. *International Journal* of *Current Microbiology* and *Applied* Sciences, 8(10), 393-400.

Chen, J., Callac, P., Parra, L. A., Karunarathna, S. C., He, M. Q., Moinard, M., Zhao, R. L. (2017). Study in *Agaricus* subgenus *Minores* and allied clades reveals a new American subgenus and contrasting phylogenetic patterns in Europe and Greater Mekong Subregion. *Persoonia: Molecular Phylogeny and Evolution of Fungi*, 38, 170-196.

Chen, C., Chen, H. Y., Chen, X., & Huang, Z. (2019). Meta-analysis shows positive effects of plant diversity on microbial biomass and respiration. *Nature communications*, 10(1), 1-10.

Cheng, C., Maggiora, G., Lajiness, M., Johnson, M. (1996). Four association coefficients for relating molecular similarity measures. *Journal of chemical information and computer sciences*, 36(4), 909-915.

Cimmino, A., Fernández-Aparicio, M., Andolfi, A., Basso, S., Rubiales, D., and Evidente, A. (2014). Effect of fungal and plant metabolites on broomrapes (*Orobanche* and *Phelipanche* spp.) seed germination and radicle growth. *Journal of Agriculture Food Chemistry*, 62, 10485-10492.

Cimmino, A., Masi, M., Evidente, M., Superchi, S., Evidente, A. (2015a). Fungal phytotoxins with potential herbicidal activity: chemical and biological characterization. *Natural product reports*, 32(12), 1629-1653.

Cimmino, L., Dolgalev, I., Wang, Y., Yoshimi, A., Martin, G. H., Wang, J., Aifantis, I. (2017). Restoration of TET2 function blocks aberrant self-renewal and leukemia progression. *Cell*, 170(6), 1079-1095.

Christenhusz, M. J., and Byng, J. W. (2016). The number of known plants species in the world and its annual increase. *Phytotaxa*, 261(3), 201-217.

Coronado-Aceves, E. W., Gigliarelli, G., Garibay-Escobar, A., Zepeda, R. E. R., Curini, M., Cervantes, J. L., Marcotullio, M. C. (2017). New Isoflavonoids from the extract of *Rhynchosia precatoria* (Humb. & Bonpl. ex Willd.) DC. and their antimycobacterial activity. *Journal of ethnopharmacology*, 206, 92-100.

Courtecuisse R. and Duhem B. (1994). Guide des champignons de France et d'Europe, Ed.Delachaux Niestle, Paris. 480.

Courtecuisse, R., and Duhem, B. (2013). *Champignons de France et d'Europe*. Delachaux et Niestlé.

Covington, C. L., and Polavarapu, P. L. (2016). CDSpecTech: Computer Programs for Calculating Similarity Measures for Experimental and Calculated Dissymmetry Factors and Circular Intensity Differentials. https://sites.google.com/site/cdspectech1/; 2016. 21.

Covington, C. L., and Polavarapu, P. L. (2017). CDSpecTech: A single software suite for multiple chiroptical spectroscopic analyses. *Chirality*, 29(5), 178-192.

Dasari, S., Wudayagiri, R., Valluru, L. (2015). Cervical cancer: Biomarkers for diagnosis and treatment. *Clinica chimica acta*, 445, 7-11.

Décamps, H., and Tabacchi, E. R. I. C. (1994). Species richness in vegetation along river margins. *Species richness in vegetation along river margins*, 1-20.

Deshmukh, H. S., Liu, Y., Menkiti, O. R., Mei, J., Dai, N., O'leary, C. E., Worthen, G. S. (2014). The microbiota regulates neutrophil homeostasis and host resistance to Escherichia coli K1 sepsis in neonatal mice. *Nature medicine*, 20(5), 524-530.

Dewick, P. M. (2009). The shikimate pathway: aromatic amino acids and phenylpropanoids. *Medicinal Natural Products*, 137, 86.

Dhar, T. K., Siddiqui, K. A., Ali, E. (1982). Structure of phaseolinone, a novel phytotoxin from *Macrophomina phaseolina*. *Tetrahedron letters*, 23(51), 5459-5462.

Di Benedetto, D. (2007). *Spectrophotometrie D'Absorption dans I'Ultraviolet et le Visible*. Ed. Techniques Ingénieur.

Didukh, M., Vilgalys, R., Solomon, P., Isikhuemhen, O. S., Eviatar, N. E. V. O. (2005). Notes on Agaricus section Duploannulati using molecular and morphological data. *Mycological Research*, 109(6), 729-740.

Dor, E., and Hershenhorn, J. (2012). Allelopathic effects of *Inula viscosa* leaf extracts on weeds. *Allelopathy Journal*, 30(2), 281-289.

DPIPWE (Department of Primary Industries, Parks, Water and Environment). (2011). False Yellow Head Weed Management Plan. Statutory Weed Management Plan. June 2011. Tasmania/Australia.http://www.dpiw.tas.gov.au/inter.nsf/Attachments/LBUN-8EZ5HA? Open, last access June 2011.

Duan, X., Tan, X., Gu, L., Liu, J., Hao, X., Tao, L., Zhang, Y. (2020). New secondary metabolites with immunosuppressive activity from the phytopathogenic fungus *Bipolaris maydis*. *Bioorganic chemistry*, 99, 103816.

Durbin, R., Rumelhart, D. E. (1989). Product units: A computationally powerful and biologically plausible extension to backpropagation networks. *Neural computation*, 1(1), 133-142.

Ebada, S.S., and Proksch, P. (2015). Marine-derived fungal metabolites. In *Springer Handbook of Marine Biotechnology*, Berlin, Heidelberg, 759-788.

Ebert, M. K., Spanner, R. E., de Jonge, R., Smith, D. J., Holthusen, J., Secor, G. A., Bolton, M. D. (2019). Gene cluster conservation identifies melanin and perylenequinone biosynthesis pathways in multiple plant pathogenic fungi. *Environmental microbiology*, 21(3), 913-927.

El-Kholfy, S., Aguil, F. A., Touhami, A. O., Benkirane, R., Douira, A. (2011). Bibliographic inventory of Moroccan Rif's fungi: catalog of rifain fungal flora. *Journal of Animal and Plant Sciences* (JAPS), 12(1), 1493-1526.

Ellestad, G. A; Kunstmann, M. P; Mirando, P; Morton, G. O. (1972). Structures of fungal diterpene antibiotics LL-S491. beta and- gamma. *Journal of the American Chemical Society*, 94, 6206-6208.

Enow, E., Kinge, T. R., Tabi, E. M., Thiobal, N., Mih, A. M. (2013). Diversity and distribution of macrofungi (mushrooms) in the Mount Cameroon Region. *Journal of Ecology and the Natural Environment*, 5(10), 318-334.

Ersek, T. (1979). Occurrence of charcoal rot and anthracnose of soybeans in Hungary. *Acta Phytopathologica Academiae Scientiarum Hungaricae*, 14(1/2), 17-21.

Evidente, A., Lanzetta, R., Capasso, R., Andolfi, A., Bottalico, A., Vurro, M., Zonno, M. C. (1995). Putaminoxin, a phytotoxic nonenolide from *Phoma putaminum*. *Phytochemistry*, 40(6), 1637-1641.

Evidente, A., Sparapano, L., Fierro, O., Bruno, G., Giordano, F., Motta, A. (1997). Sphaeropsidins B and C, phytotoxic pimarane diterpenes from *Sphaeropsis sapinea* f. sp. *cupressi* and *Diplodia mutila*. *Phytochemistry*, 45, 705-713

Evidente, A., Motta, A. (2001). Phytotoxins from fungi, pathogenic for agrarian, forestal and weedy plants. *Bioactive compounds from natural sources*, 473.

Evidente, A., Andolfi, A., Vurro, M., Zonno, M. C., Motta, A. (2002). Cytochalasins Z1, Z2 and Z3, three 24-oxa [14] cytochalasans produced by *Pyrenophora semeniperda*. *Phytochemistry*, 60(1), 45-53.

Evidente, A., Andolfi, A., Cimmino, A., Vurro, M., Fracchiolla, M., and Charudattan, R. (2006a). Herbicidal potential of ophiobolins produced by *Drechslera gigantea*. *Journal of Agricultural* and *Food Chemistry*, 54(5), 1779-1783.

Evidente, A., Andolfi, A., Cimmino, A., Vurro, M., Fracchiolla, M., Charudattan, R., and Motta, A. (2006b). Ophiobolin E and 8-epi-ophiobolin J produced by *Drechslera gigantea*, a potential mycoherbicide of weedy grasses. Phytochemistry, 67(20), 2281-2287.

Evidente, A., Andolfi, A., Cimmino, A. (2011). Relationships between the stereochemistry and biological activity of fungal phytotoxins. *Chirality*, 23(9), 674-693.

Evidente, A., Cimmino, A., Andolfi, A. (2013). The effect of stereochemistry on the biological activity of natural phytotoxins, fungicides, insecticides and herbicides. *Chirality*, 25(2), 59-78.

Evidente, A.; Kornienko, A.; Cimmino, A.; Andolfi, A.; Lefranc, F.; Mathieu, V.; Kiss, R. (2014). Fungal metabolites with anticancer activity. *Natural Product Reports*, 31(5), 617-627.

Evidente, M., Cimmino, A., Zonno, M.C., Masi, M., Berestetskyi, A., Santoro, E., Superchi, S., Vurro, M., and Evidente, A. (2015). Phytotoxins produced by *Phoma chenopodiicola*, a fungal pathogen of *Chenopodium album*. *Phytochemistry*,117, 482-488.

Evidente, A., Cimmino, A., Masi, M. (2019). Phytotoxins produced by pathogenic fungi of agrarian plants. *Phytochemistry Reviews*, 18(3), 843-870.

Farr, D. F., Bills, G. F., Chamuris, G. P., Rossman, A. Y. (1989). *Fungi on plants and plant products in the United States*. APS press.

Farooq, M. S., Riaz, S., Abid, A., Abid, K., Naeem, M. A. (2019). A Survey on the Role of IoT in Agriculture for the Implementation of Smart Farming. *IEEE Access*, 7, 156237-156271.

Fayzalla, E. A., Abdalla, M. E., Zaghloul, M. G., Gedara, S. R., Elsherbiny, E. A. (2010). Antifungal Potential of Extracellular Metabolites Produced by *Drechslera* spp. against Phytopathogenic Fungi.

Feling, R., Polborn, K., Steglich, W., Mühlbacher, J., Bringmann, G. (2001a). The absolute configuration of the mushroom metabolites involutin and chamonixin. *Tetrahedron*, 57(37), 7857-7863.

Fernández-Aparicio, M., Flores, F., Rubiales, D. (2009). Recognition of root exudates by seeds of broomrape (*Orobanche* and *Phelipanche*) species. *Annals of botany*, 103(3), 423-431.

Fernández-Aparicio, Mónica, Koichi Yoneyama, and Diego Rubiales. (2011). The role of strigolactones in host specificity of *Orobanche* and *Phelipanche* seed germination. *Seed Science Research*, 21(1), 55-61.

Fernández-Aparicio, M., Cimmino, A., Evidente, A., Rubiales, D. (2013). Inhibition of *Orobanche crenata* seed germination and radicle growth by allelochemicals identified in cereals. *Journal of agricultural and food chemistry*, 61(41), 9797-9803.

Fernández-Aparicio, M.; Masi, M.; Maddau, L.; Cimmino, A.; Evidente, M.; Rubiales, D.; Evidente, A. (2016). Induction of haustorium development by sphaeropsidones in radicles of the parasitic weeds Striga and *Orobanche*. A structure–activity relationship study. *Journal of Agriculture Food Chemistry*, 64(25), 5188-5196.

Fischl, G., Kadlicsko, S., Kovacs, J. (1995). Wilting of paprika plants caused by Macrophomina phaseolina (Tassi) Goid. *NOVENYVEDELEM, 31*, 589-592.

Fischl, G., Csöndes, I., Kadlicsko, S., Józsa, A. (2008). Study on the factors provoking the reddening and decline of blue spruce (*Picea pungens Engelm*.). *Növényvédelem*, 44(8), 401-402.

Frisch, A. (2009). Gaussian 09W Reference. *Wallingford, USA, 25p*.

Fukushima, T., Tanaka, M., Gohbara, M., Fujimori, T. (1998). Phytotoxicity of three lactones from Nigrospora sacchari. *Phytochemistry*, 48(4), 625-630.

Gamboa-Angulo, M. M., García-Sosa, K., Alejos-González, F., Escalante-Erosa, F., Delgado-Lamas, G., Peña-Rodríguez, L. M. (2001). Tagetolone and tagetenolone: two phytotoxic polyketides from Alternaria tagetica. *Journal of agricultural and food chemistry*, 49(3), 1228-1232.

Gardes, M., Bruns, T. D. (1993). ITS primers with enhanced specificity for basidiomycetes-application to the identification of mycorrhizae and rusts. *Molecular ecology*, 2(2), 113-118.

Gerhauser, H., Claassen, H. A., Lehnen, M., & Zagorski, R. (2000). Improved 2D edge modelling and comparison with measurements in TEXTOR-94. *Contributions to Plasma Physics*, 40.

Giannenas, I., Tsalie, E., Chronis, E. F., Mavridis, S., Tontis, D., Kyriazakis, I. (2011). Consumption of *Agaricus bisporus* mushroom affects the performance, intestinal microbiota composition and morphology, and antioxidant status of turkey poults. *Animal Feed Science and Technology*, 165(3-4), 218-229.

Govorushko, S., Rezaee, R., Dumanov, J., Tsatsakis, A. (2019). Poisoning associated with the use of mushrooms: A review of the global pattern and main characteristics. *Food and chemical toxicology*, 128, 267-279.

Grande, M., Bellido, I. S., Torres, P., Piera, F. (1992). 9-Hydroxynerolidol esters and bicyclic sesquiterpenoids from *Dittrichia viscosa*. *Journal of natural products*, 55(8), 1074-1079.

Grauso, L., Teta, R., Esposito, G., Menna, M., Mangoni, A. (2019). Computational prediction of chiroptical properties in structure elucidation of natural products. *Natural product reports*, 36(7), 1005-1030.

Grindberg, R. V., Ishoey, T., Brinza, D., Esquenazi, E., Coates, R. C., Liu, W. T., Gerwick, W. H. (2011). Single cell genome amplification accelerates identification of the apratoxin biosynthetic pathway from a complex microbial assemblage. *PloS one*, 6(4), e18565.

Gui, J., Pan, C. M., Jin, Y., Qin, T., Lo, J. C., Lee, B. J., Baran, P. S. (2015). Practical olefin hydroamination with nitroarenes. *Science*, 348(6237), 886-891.

Gum, G., Spadaro, A.N., Gallo, R. and Citraro, T. (2007). *Inula viscosa* (L.) Aiton—part IV: characterization based on chemical composition. *Revista Italiana EPPOS*, 44: 23-32.

Hallock, Y. F., Lu, H. S., Clardy, J., Strobel, G. A., Sugawara, F., Samsoedin, R., Yoshida, S. (1993). Triticones, spirocyclic lactams from the fungal plant pathogen *Drechslera tritici-repentis*. *Journal of Natural Products*, 56(5), 747-754.

Harada, T., Mimura, T., Ito, K., Nakanishi, Y., Senoo, T., Hosoda, Y., Tsukayama, C. (1983). Divergent histology in the primary and metastatic lesions of thyroid carcinoma. *Nihon Geka Gakkai zasshi*, 84(9), 758-761.

Harada, N., Nakanishi, K., Berova, N. (2012). Electronic CD exciton chirality method: principles and applications. *Comprehensive chiroptical spectroscopy*, 2, 115-166.

He, X., Du, X., Wang, X., Tian, F., Tang, J., Chua, T. S. (2018). Outer product-based neural collaborative filtering. *arXiv preprint arXiv*, 1808, 03912.

Hussain, M. S., Monkaresi, H., Calvo, R. A. (2012). Combining classifiers in multimodal affect detection. In Proceedings of the Tenth Australasian Data Mining Conference-Volume 134, 103-108.

Hongyun, L., Hanghang, Lou., Jingjin, H., Zhengjie, L., Qihe, C. (2020). Macrofungi: A review of cultivation strategies, bioactivity, and application of mushrooms." *Comprehensive Reviews in Food Science and Food Safety*, 19(5), 2333-2356.

Hussain, M. S., Fareed, S., Saba Ansari, M., Rahman, A., Ahmad, I. Z., Saeed, M. (2012). Current approaches toward production of secondary plant metabolites. *Journal of pharmacy and bioallied sciences*, 4(1), 10.

Irvine, C. A. (2002). USA: Wavefunction Inc.

Johnson, J. L., Raghavan, V., Cimmino, A., Moeini, A., Petrovic, A. G., Santoro, E., Polavarapu, P. L. (2018). Absolute configurations of chiral molecules with multiple stereogenic centers without prior knowledge of the relative configurations: A case study of inuloxin C. *Chirality*, 30(11), 1206-1214.

Karunarathna SC, Guinberteau J, Chen J, Vellinga EC, Zhao RL, Chukeatirote E, Callac P. (2014). Two new species in *Agaricus* tropical clade I. Chiang Mai J Sci, 41, 771-780.

Kaur, S., Jobling, S., Jones, C. S., Noble, L. R., Routledge, E. J., Lockyer, A. E. (2015). The nuclear receptors of *Biomphalaria glabrata* and *Lottia gigantea*: implications for developing new model organisms. *PloS one*, 10(4), e0121259.

Kavallieratos, N. G., Stathas, G. J., Athanassiou, C. G., Papadoulis, G. T. (2002). *Dittrichia viscosa* and *Rubus ulmifolius* as reservoirs of aphid parasitoids (Hymenoptera: Braconidae: Aphidiinae) and the role of certain coccinellid species. *Phytoparasitica*, 30(3), 231-242.

Kerrigan, S., Savage, M., Cavazos, C. Bella, P. (2016). Thermal degradation of synthetic cathinones: implications for forensic toxicology. *Journal of analytical toxicology*, 40(1), 1-11.

Kim, I. H., Prusti, R. K., Song, P. S., Häder, D. P., Häder, M. (1984). Phototaxis and photophobic responses in Stentor coeruleus action spectrum and role of $Ca2^{+}$ fluxes. *Biochimica et Biophysica Acta (BBA)-General Subjects*, 799(3), 298-304.

Kim, H.J., Kim, J.C., Kim, B.S., Kim, H.G., Cho, K.Y. (1999). Antibiotic and phytotoxic activities of Ophiobolins from *Helminthosporium* species. *Journal of Plant Pathology*, 15(1), 14-20.

Kimura, Y., Tamura, S. (1973). Isolation of l-β-phenyllactic acid and tyrosol as plant growth regulators from *Gloeosporium laeticolor*. *Agricultural and Biological Chemistry*, 37(12), 2925-2925.

Kong, L., Li, S., Liao, Q., Zhang, Y., Sun, R., Zhu, X., Zhu, Y. (2013). Oleanolic acid and ursolic acid: novel hepatitis C virus antivirals that inhibit NS5B activity. *Antiviral research*, 98(1), 44-53.

Kozarski, M., Klaus, A., Jakovljevic, D., Todorovic, N., Vunduk, J., Petrović, P. Van Griensven, L. (2015). Antioxidants of edible mushrooms. *Molecules*, 20(10), 19489-19525.

Kumar, P., Nagarajan, A., Uchil, P. D. (2018). Analysis of cell viability by the lactate dehydrogenase assay. *Cold Spring Harbor Protocols*, 2018(6), pdb-prot095497.

Lauro, L., Rolih, C., (1990). Observations and research on an extract of *Inula viscosa* Ait. *Bollettino della Societa Italiana di Biologia Sperimentale*, 66(9), 829-834.

Li, E., Clark, A.M., Rotella, D.P., Hufford, C.D., (1995). Microbial metabolites of ophiobolin A and antimicrobial evaluation of ophiobolins. *Journal of Natural Products*, 58, 74-81.

Li, B., Ding, Y., Tang, X., Wang, G., Wu, S., Li, X., Tang, X. (2019). Effect of l-arginine on maintaining storage quality of the white button mushroom (*Agaricus bisporus*). *Food and bioprocess technology*, 12(4), 563-574.

Loria-Kohen, V., Lourenço-Nogueira, T., Espinosa-Salinas, I., Marín, F. R., Soler-Rivas, C., Ramirez de Molina, A. (2014). Nutritional and functional properties of edible mushrooms: A food with promising health claims. *Journal of pharmacy and Nutrition Sciences*, 4, 187-198.

Liu, M., I. U., Yan, H. E., Ling, S. H. E. N., Zheng-Xi, H. U., Zhang, Y. H. (2019). *Bipolarins A–H, eight new ophiobolin-type sesterterpenes with antimicrobial activity from fungus Bipolaris* sp. TJ403-B1. *Chinese Journal of Natural Medicines*, 17(12), 935-944.

Locato, V., Uzal, E.N., Cimini, S., Zonno, M.C., Evidente, A., Micera, A., Foyer, C.H., and De Gara, L. (2015). Low concentrations of the toxin ophiobolin A, lead to an arrest of the cell cycle and alter the intracellular partitioning of glutathione between the nuclei and cytoplasm. J. Exp. Bot 66, 2991-3000.

Lucas, F., Niravong, M., Villeminot, S., Kaaks, R., Clavel-Capelon, F. (1995). Estimation of food portion size using photographs: validity, strengths, weaknesses, and recommendations. *Journal of Human Nutrition and Dietetics*, 8(1), 65-74.

Malençon G, Bertault R. (1970). Champignons superieurs du Maroc. Travaux of the Institut Scientifique Chérifien et Faculté des Sciences de Rabat. *Series Botanique et Biologie Vegetale*, (32).

Mándi, A., and Kurtán, T. (2019). Applications of OR/ECD/VCD to the structure elucidation of natural products. *Natural product reports*, 36(6), 889-918.

Masi, M., Cimmino, A., Reveglia, P., Mugnai, L., Surico, G., and Evidente, A. (2018a). Advances on fungal phytotoxins and their role in grapevine trunk diseases. *Journal of Agricultural* and *Food Chemistry*, *66*(24), 5948-5958.

Masi, M., Maddau, L., Linaldeddu, B.T., Scanu, B., Evidente, A., and Cimmino, A. (2018b). Bioactive metabolites from pathogenic and endophytic fungi of forest trees. *Current Medicinal Chemistry,* 25(2), 208-252.

Masi, M., Dasari, R., Evidente, A., Mathieu, V., Kornienko, A. (2019). Chemistry and biology of ophiobolin A and its congeners. *Bioorganic & medicinal chemistry letters*, 29(7), 859-869.

Masi, M., Reveglia, P., Baaijens-Billones, R., Górecki, M., Pescitelli, G., Savocchia, S., Evidente, A. (2020). Phytotoxic metabolites from three *Neofusicoccum* species causal agents of *Botryosphaeria dieback* in Australia, luteopyroxin, neoanthraquinone, and luteoxepinone, a disubstituted furo-α-pyrone, a hexasubstituted anthraquinone, and a trisubstituted oxepi-2-one from *Neofusicoccum luteum*. *Journal of natural products*, 83(2), 453-460.

Meenu, M., Xu, B. (2019). Application of vibrational spectroscopy for classification, authentication and quality analysis of mushroom: A concise review. *Food chemistry*, 289, 545-557.

Molinski, T. F., and Morinaka, B. I. (2012). Integrated approaches to the configurational assignment of marine natural products. *Tetrahedron*, 68(46), 9307.

Møller, F. H. (1950). Danish Psalliota species. Preliminary studies for a monograph of the Danish Psalliotae. *Friesia*, 4(1-2).

Morrison, R., Gardiner, C., Evidente, A., Kiss, R., Townley, H. (2014). Incorporation of ophiobolin A into novel chemoembolization particles for cancer cell treatment. *Pharmaceutical research*, 31 (10), 2904-2917.

Morita, S., Giessibl, F. J., Meyer, E., Wiesendanger, R. (Eds.). (2015). *Noncontact Atomic Force Microscopy: Volume 3*. Springer.

Mueller, L. N., Rinner, O., Schmidt, A., Letarte, S., Bodenmiller, B., Brusniak, M. Y., Müller, M. (2007). SuperHirn–a novel tool for high resolution LC-MS-based peptide/protein profiling. *Proteomics*, 7(19), 3470-3480.

Mukaiyama, T., Banno, K., Narasaka, K. (1974). New cross-aldol reactions. Reactions of silyl enol ethers with carbonyl compounds activated by titanium tetrachloride. *Journal of the American Chemical Society*, 96(24), 7503-7509.

Mullis KB, Faloona FA. (1987). Specific synthesis of DNA in vitro via a polymerase-catalyzed chain reaction. Methods in enzymology, 155, 335-350.

Murray, M. G., Thompson, W. F. (1980). Rapid isolation of high molecular weight plant DNA. *Nucleic acids research*, 8(19), 4321-4326.

Muzio, F. M., Agaras, B. C., Masi, M., Tuzi, A., Evidente, A., Valverde, C. (2020). 7-hydroxytropolone is the main metabolite responsible for the fungal antagonism of *Pseudomonas donghuensis* strain SVBP6. *Environmental microbiology*, 22(7), 2550-2563.

Nakanishi, K., and Solomon, P. H. (1977). Infrared Absorption Spectroscopy, 2nd edition. Holden Day, Oakland, 17-44.

Niego, A. G., Rapior, S., Thongklang, N., Raspé, O., Jaidee, W., Lumyong, S., Hyde, K. D. (2021). Macrofungi as a Nutraceutical Source: Promising Bioactive Compounds and Market Value. *Journal of Fungi*, 7(5), 397.

Nielsen, M. M., Witherden, D. A., Havran, W. L. (2017). γδ T cells in homeostasis and host defence of epithelial barrier tissues. *Nature Reviews Immunology*, 17(12), 733-745.

Nouguier, R., Gastaldi, S., Stien, D., Bertrand, M., Villar, F., Andrey, O., Renaud, P. (2003). Synthesis of (±)-and (−)-botryodiplodin using stereoselective radical cyclizations of acyclic esters and acetals. *Tetrahedron: Asymmetry*, 14(19), 3005-3018.

Nozoe, S., Morisaki, M., Tsuda, K., Iitaka, Y., Takahashi, N., Tamura, S., Shirasaka, M. (1965). The structure of ophiobolin, a C25 terpenoid having a novel skeleton. *Journal of the American Chemical Society*, 87(21), 4968-4970.

Nugroho, A. E., and Morita, H. (2014). Circular dichroism calculation for natural products. *Journal of natural medicines*, 68(1), 1-10.

Palacios, G., da Rosa, A. T., Savji, N., Sze, W., Wick, I., Guzman, H., Lipkin, W. I. (2011). Aguacate virus, a new antigenic complex of the genus *Phlebovirus* (family Bunyaviridae). *The Journal of general virology*, 92(Pt 6), 1445.

Parolin, P., Scotta, M. I., Bresch, C. (2014). Biology of *Dittrichia viscosa*, a Mediterranean ruderal

plant: a review. *Phyton, International Journal of Experimental Botany*, 83, 251-262.

Parra, L. A. (2008). *Agaricus* L. *Allopsalliota, Nauta Bas. In: Fungi Europaei* 1. Edizioni Candusso, Alassio, Italy, 824.

Parra, L. A., Angelini, C., Ortiz-Santana, B., Mata, G., Billette, C., Rojo, C., Chen, J., Callac, P. (2018). The genus *Agaricus* in the Caribbean. Nine new taxa mostly based on collections from the Dominican Republic. *Phytotaxa*, 345(3), 219-271.

Parsaeimehr, A., Sargsyan, E., Vardanyan, A. (2011). Expression of secondary metabolites in plants and their useful perspective in animal health. *Parsaeimehr A., Sargsyan E., Vardanyan A*, 115-124.

Paulitz, T. C., and Bélanger, R. R. (2001). Biological control in greenhouse systems. *Annual review of phytopathology*, 39(1), 103-133.

Pearson, P. B., Darnell, A. L., Weir, J. (1946). The thiamine, riboflavin, nicotinic acid and pantothenic acid content of colostrum and milk of the cow and ewe. *The Journal of Nutrition*, 31(1), 51-57.

Pagano, M. C., and Miransari, M. (2016). The importance of soybean production worldwide. In *Abiotic and biotic stresses in soybean production*. Academic Press, 1-26.

Pelser, P. B., Kennedy, A. H., Tepe, E. J., Shidler, J. B., Nordenstam, B., Kadereit, J. W., Watson, L. E. (2010). Patterns and causes of incongruence between plastid and nuclear *Senecioneae* (Asteraceae) phylogenies. *American Journal of Botany*, 97(5), 856-873.

Pena-Rodriguez, L. M., and Chilton, W. S. (1989). 3-anhydro-ophiobolin A and 3-anhydro-6-*epi*-ophiobolin A, phytotoxic metabolites of the johnson grass pathogen *Bipolaris sorghicola*. *Journal of Natural Products*, 52(5), 1170-1172.

Peng, L., Shang, Y., Gao, B., Xu, X. (2021). Co_3O_4 anchored in N, S heteroatom co-doped porous carbons for degradation of organic contaminant: role of pyridinic N-Co binding and high tolerance of chloride. *Applied Catalysis B: Environmental*, *282*, 119484.

Pena-Rodriguez, L. M., Chilton, W. S. (1989). Victoxinine and prehelminthosporolactone, two minor phytotoxic metabolites produced by *Bipolaris* sp., a pathogen of Johnson grass. *Journal of Natural Products*, 52(4), 899-901.

Perotti, V. E., Larran, A. S., Palmieri, V. E., Martinatto, A. K., Permingeat, H. R. (2020). Herbicide resistant weeds: A call to integrate conventional agricultural practices, molecular biology knowledge and new technologies. *Plant Science*, *290*, 110255.

Pescitelli, G., and Bruhn, T. (2016). Good computational practice in the assignment of absolute configurations by TDDFT calculations of ECD spectra. *Chirality*, 28(6), 466-474.

Pescitelli, G., and Di Bari, L. (2017). Revision of the absolute configuration of preussilides A–F established by the exciton chirality method. *Journal of natural products*, 80(10), 2855-2859.

Peter, D., and Brückner, R. (2018). Syntheses of a Pair of Simplified Model Compounds of the Dihydroxycyclopentenone Core of the Kodaistatins A–D. *European Journal of Organic Chemistry*, 2018(45), 6256-6273.

Petrak, F. (1923). Mykologische Notizen, 289. Ann. *Mycol*, *XXI*, 314-315

Pilát, A. (1954). Pecárka Moškova. *Agaricus Maskae* Pilát, nový druh z blizkého príbuzenstva pecárky velkovytrusé. *Ceská Mykologie*, 8, 165.

Pinkerton, F., Strobel, G. A. (1976). Serinol as an activator of toxin production in attenuate cultures of *Helminthosporium sacchari*. *Proceeding of the National Academy of Science U.S.A.*, *73*(11), 4007-4011.

Polavarapu, P. L., Covington, C. L., Raghavan, V. (2017). To avoid chasing incorrect chemical structures of chiral compounds: Raman optical activity and vibrational circular dichroism spectroscopies. *ChemPhysChem*, 18(18), 2459-2465.

Poucheret, P., Fons, F., Rapior, S. (2006). Biological and pharmacological activity of higher fungi: 20-year retrospective analysis. *Cryptogamie Mycologie*, 27(4), 311.

Pretsch, E., Bühlmann, P., Affolter, C. (2000). Structure Determination of Organic Compounds – Tables of Spectral Data. Springer-Verlag, Berlin, 161-244.

Pretsch, E., Buhlmann, P., Affolter, C. (2000). Structure Determination of Organic Compounds Tables of Spectral Data, 3rd ed.; Springer- Verlag: Berlin, Germany, 161−243.

Polavarapu, P. L., Covington C. L., Raghavan, V (2017). To avoid chasing incorrect chemical structures of chiral compounds: Raman optical activity and vibrational circular dichroism spectroscopies. *ChemPhysChem*, 18(18):2459-2465.

Ramezani, M., Shier, W. T., Abbas, H. K., Tonos, J. L., Baird, R. E., Sciumbato, G. L. (2007). Soybean charcoal rot disease fungus *Macrophomina phaseolina* in Mississippi produces the phytotoxin (−)-botryodiplodin but no detectable phaseolinone. *Journal of natural products*, 70(1), 128-129.

Ramos, B., Miller, F. A., Brandão, T. R. S., Teixeira, P., Silva, C. L. M. (2013). Fresh fruits and vegetables—an overview on applied methodologies to improve its quality and safety. *Innovative Food Science & Emerging Technologies*, 20, 1-15.

Reveglia, P., Savocchia, S., Billones-Baaijens, R., Masi, M., Cimmino, A., Evidente, A. (2019). Phytotoxic metabolites by nine species of Botryosphaeriaceae involved in grapevine dieback in Australia and identification of those produced by *Diplodia mutila*, *Diplodia seriata*, *Neofusicoccum australe* and *Neofusicoccum luteum*. *Natural product research*, 33(15), 2223-2229.

Ribera, A. E., and Zuñiga, G. (2012). Induced plant secondary metabolites for phytopatogenic fungi control: a review. *Journal of soil science and plant nutrition*, 12(4), 893-911.

Rozenblat, S., Grossman, S., Bergman, M., Gottlieb, H., Cohen, Y., Dovrat, S. (2008). Induction of G2/M arrest and apoptosis by sesquiterpene lactones in human melanoma cell lines. *Biochemical pharmacology*, 75(2), 369-382.

Rukaibaa, A.C.; Mohammed, O.M. and Ziena, M.A. (2017). Evaluation of new local media (Cumin media) to prepare mother culture of Oyster Mushroom and its role to raise the productivity patent 5010, *the republic of Iraq, the ministry of planning, cent.*

Russell, R. E., Halstead, B. J., Mosher, B. A., Muths, E., Adams, M. J., Grant, E. H., Hossack, B. R. (2019). Effect of amphibian chytrid fungus (*Batrachochytrium dendrobatidis*) on apparent survival of frogs and toads in the western USA. *Biological Conservation*, 236, 296-304.

Salvatore, M. M., Félix, C., Lima, F., Ferreira, V., Naviglio, D., Salvatore, F., Esteves, A. C. (2020). Secondary metabolites produced by *Macrophomina phaseolina* isolated from *Eucalyptus globulus*. *Agriculture*, 10(3), 72.

Santoro E, Mazzeo, G., Petrovic, A. G., Cimmino, A., Koshoubu, J., Evidente, A., Superchi, S. (2015). Absolute configurations of phytotoxins seiricardine A and inuloxin A obtained by chiroptical studies. *Phytochemistry*, 116, 359-366.

Sautua, F. J., Doyle, V. P., Price, P. P., Porfiri, A., Fernandez, P., Scandiani, M. M., Carmona, M. A. (2020). Fungicide resistance in *Cercospora* species causing cercospora leaf blight and purple seed stain of soybean in Argentina. *Plant Pathology*, 69(9), 1678-1694.

Scharf, D. H., Heinekamp, T., Brakhage, A. A. (2014). Human and plant fungal pathogens: the role of secondary metabolites. *PLoS pathogens*, 10(1), e1003859.

Schinella, G. R., Tournier, H. A., Prieto, J. M., De Buschiazzo, P. M., Rıos, J. L. (2002). Antioxidant activity of anti-inflammatory plant extracts. *Life sciences*, 70(9), 1023-1033.

SenGupta, R., Chandran, R.R., Divekar, P.V. (1966). Botryodiplodin, a new antibiotic from *Botryodiplodia theobromae* I. Production, isolation, and biological properties. *Indian Journal of Experimental Biology*, 4, 152-153.

Shen, J., Zhu, C., Reiling, S., Vaz, R (2010). A novel computational method for comparing vibrational circular dichroism spectra. *Spectrochim Acta A Mol Biomol Spectrosc*, 76(3–4): 418-422.

Shtacher, G. and Kashman, Y. (1970). 12-Carboxyeudesma-3, 11 (13)-diene. Novel sesquiterpenic acid with a narrow antifungal spectrum. *Journal of Medicinal chemistry*, 13(6), 1221-1223.

Sladonja, B., Poljuha, D., Krapac, M., Uzelac, M., Mikulic-Petkovsek, M. (2021). *Dittrichia viscosa*: Native-Non Native Invader. *Diversity*, 13(8), 380.

Simay, E. I. (1987). Three new hosts of Macrophomina phaseolina (Tassi) Goid. in Hungary. *Novenytermeles (Hungary)*.

Simay, E. I. (1991). A *Macrophomina phaseolina* (Tassi) Goid. előfordulása dísznövényeken. 37. *Növényvédelmi Tudományos Napok, Budapest. Összefoglaló*, 111.

Simay, E. J., and Kadlicskd, S. (1993). New host plants of *Macrophomina phaseolina* in Hungary. *Nov6nyv6de1 em*, 26, 27-28.

Simonetti, E., Viso, N. P., Montecchia, M., Zilli, C., Balestrasse, K., Carmona, M. (2015). Evaluation of native bacteria and manganese phosphite for alternative control of charcoal root rot of soybean. *Microbiological research*, 180, 40-48.

Sivanesan, A. (1992). *Drechslera gigantea*. *Mycopathologia (1975)*, *119*(1), 49-50.

Staurianakou, S., Liakoura, V., Levizou, E., Karageorgou, P., Delis, C., Liakopoulos, G., Karabourniotis, G., Manetas, G. and Manetas, Y. (2004). Allelopathic effects of water-soluble leaf epicuticular material from *Dittrichia viscosa* on seed germination of crops and weeds. *Allelopathy Journal*, 14:35-41.

Steyn, J. H., Smith, F. W. (1982). Nuclear magnetic resonance imaging of the prostate. *British journal of urology*, 54(6), 726-728.

Strobel, M. (1991). *European women and the second British empire*. Indiana University Press.

Sugawara, F., and Strobel, G. A. (1986). (−)-Dihydropyrenophorin, a novel and selective phytotoxin produced by *Drechslera avenae*. *Plant science*, 43(1), 1-5.

Sugawara, F., Strobel, G., Stange, N. R., Siedow, J. N., Van Duyne G. D., Clardy, J. (1987). Phytotoxins from the pathogenic fungi *Drechslera maydis* and *Drechslera sorghicola*. *Proceeding of the National Academy of Sciences U.S.A.*, 84, 3081-3085.

Sugawara, I., Kataoka, I., Morishita, Y., Hamada, H., Tsuruo, T., Itoyama, S., Mori, S. (1988). Tissue distribution of P-glycoprotein encoded by a multidrug-resistant gene as revealed by a monoclonal antibody, MRK 16. *Cancer research*, 48(7), 1926-1929.

Sugawara, F., Strobel, G., Yoshida, S. (1993). Phytoactive eremophilanes produced by the weed pathogen *Drechslera gigantea*. *Bioscience, biotechnology, and biochemistry*, 57(2), 236-239.

Sun, N., Chen, M., Liu, Y. (2014). Gold-catalyzed oxidative reactions of propargylic carbonates involving 1, 2-carbonate migration: stereoselective synthesis of functionalized alkenes. *The Journal of organic chemistry*, 79(9), 4055-4067.

Superchi, S., Scafato, P., Gorecki, M., Pescitelli, G. (2018). Absolute configuration determination by quantum mechanical calculation of chiroptical spectra: basics and applications to fungal metabolites. *Current medicinal chemistry*, 25(2), 287-320.

Strobel, G., Kenfield, D., Bunkers, G., Sugawara, F., Clardy, J. (1991). Phytotoxins as potential herbicides. *Experientia*, 47(8), 819-826.

Tamura, K., and Nei, M. (1993). Estimation of the number of nucleotide substitutions in the control region of mitochondrial DNA in humans and chimpanzees. *Molecular biology and evolution*, 10(3), 512-526.

Tanimoto, T. T. (1958). An Elementary Mathematical Theory of Classification and Prediction. *New York: International Buisiness Machine Corporation*.

Tian, W., Deng, Z., Hong, K. (2017). The biological activities of sesterterpenoid-type ophiobolins. *Marine drugs*, 15(7), 229.

Tomasi, J., Mennucci, B., Cammi, R. (2005). Quantum mechanical continuum solvation models. *Chemical reviews*, 105(8), pp.2999-3094.

Tommonaro, G., Pejin, B., Iodice, C., Tafuto, A., De Rosa, S. (2015). Further in vitro biological activity evaluation of amino-, thio-and ester-derivatives of avarol. *Journal of enzyme inhibition and medicinal chemistry*, 30(2), 333-335.

Tscharntke, T., Tylianakis, J. M., Rand, T. A., Didham, R. K., Fahrig, L., Batáry, P., Westphal, C. (2012). Landscape moderation of biodiversity patterns and processes-eight hypotheses. *Biological reviews*, 87(3), 661-685.

Vajna, L, and Rozsnyai, Zs. (1995). *Macrophomina phaseolina* (Tassi) Goid. és a Diaporthe eres Nitschke, mint a fiatal kajszifák elhalásában szerepet játszó gombák Magyarországon. *Növényvédelem*, 31(2), 81-83.

Venkatasubbaiah, P., Dyke, C. V., Chilton, W. S. (1992). Phytotoxic metabolites of *Phoma sorghina*, a new foliar pathogen of pokeweed. *Mycologia*, 84(5), 715-723.

Vörös, J., and Manninger, I. (1973). A *Macrophomina phaseolina* (Tassi) Goid. előfordulása kukoricán, Magyarországon. *Növényvédelem*, 9, 193-195.

Vu, H. T., Scarlett, C. J., Vuong, Q. V. (2019). Maximising recovery of phenolic compounds and antioxidant properties from banana peel using microwave assisted extraction and water. *Journal of food science and technology*, 56(3), 1360-1370.

Wang, Q., Rowan, M. J., Anwyl, R. (2004). β-amyloid-mediated inhibition of NMDA receptor-dependent long-term potentiation induction involves activation of microglia and stimulation of inducible nitric oxide synthase and superoxide. *Journal of Neuroscience*, 24(27), 6049-6056.

White, T. J, Bruns, T. D, Lee, S., Taylor, J. W. (1990). Amplification and direct sequencing of fungal ribosomal RNA genes for phylogenetics. PCR protocols: a guide to methods and applications. *Academic, San Diego*, 482.

Wu, K., Su, D., Liu, J., Saha, R., Wang, J. P. (2019). Magnetic nanoparticles in nanomedicine: a review of recent advances. *Nanotechnology*, 30(50), 502003.

Yuan, W. H., Liu, M., Jiang, N., Guo, Z. K., Ma, J., Zhang, J, Tan, R. X. (2010). Guignardones A–C: Three meroterpenes from *Guignardia mangiferae*.

Yourman, L. F., and Jeffers, S. N. (1999). Resistance to benzimidazole and dicarboximide fungicides in greenhouse isolates of Botrytis cinerea. *Plant disease*, 83(6), 569-575.

Zhang J, Chen Q, Huang C, Gao W, Qu J. (2015). History, current situation and trend of edible mushroom industry development. *Mycosystema*, 34(4), 524-540.

Zeb, M., Lee, C. H. (2021). Medicinal properties and bioactive compounds from wild mushrooms native to North America. *Molecules*, 26(2), 251.

Zhang, J., Chen, Q., Huang, C., Gao, W., Qu, J. (2015). History, current situation and trend of edible mushroom industry development. *Mycosystema* 34(4), 524-540.

Zhao, Y., Tanaka, S., Pan, C. C., Fujito, K., Feezell, D., Speck, J. S., Nakamura, S. (2011). High-power blue-violet semipolar InGaN/GaN light-emitting diodes with low efficiency droop at 200 A/cm^2. *Applied physics express*, 4(8), 082104.

Zhao, R. L., Zhou, J. L., Chen, J., Margaritescu, S., Sánchez-Ramírez, S., Hyde, K. D., Moncalvo, J. M. (2016). Towards standardizing taxonomic ranks using divergence times–a case study for reconstruction of the *Agaricus* taxonomic system. *Fungal diversity*, 78 (1), 239-292.

République Algérienne Démocratique et Populaire
Ministère de l'Enseignement Supérieur et de la Recherche Scientifique
Université Mentouri Constantine 1
Faculté des Sciences de la Nature et de la Vie
Département de Biologie Appliquée
En cotutelle avec l'Université Napoli Federico II (Italie)
Département Sciences chimiques

Thèse en vue de l'obtention du diplôme de Doctorat troisième cycle
En Biotechnologie Microbiennes et Bioprocédés

Résumé en Français de la thèse de doctorat LMD

Présenté par **Zatout Roukia**

Potentiel de biocontrôle des substances bioactives produites par des champignons et des plantes de différents écosystèmes du bassin méditerranéen

2021-2022

Introduction générale

L'agriculture joue un rôle central dans l'augmentation de la disponibilité alimentaire, nécessaire pour nourrir la population humaine en constante augmentation dans le monde qui atteindra près de 10 milliards en 2050. Ce secteur a également un rôle essentiel dans le domaine de la santé (FAO, 2017 ; Evidente et *al*., 2019). C'est un facteur clé pour améliorer à la fois la sécurité alimentaire et nutritionnelle, en soutenant les moyens de subsistance et en contribuant à l'économie globale. Elle a également un impact direct sur la déforestation, la pollution de l'air et de l'eau et les maladies d'origine alimentaire.

Malgré les progrès importants réalisés par l'introduction de nouvelles technologies dans les pratiques agricoles (Mintesno, 2016 ; FAO, 2017 ; Evidente et *al*., 2019), les stress biotiques et abiotiques sont des contraintes majeures pour la croissance des plantes, le rendement des cultures, la qualité des aliments, et la sécurité alimentaire mondiale depuis le stade de la germination des graines jusqu'à celui de la récolte.

Les agents biotiques responsables des maladies infectieuses des plantes comprennent les champignons, les bactéries, les virus, les nématodes, les insectes, les mauvaises herbes et les plantes supérieures parasites. D'autre part, le stress biotique est totalement différent du stress abiotique, qui est imposé aux plantes par des facteurs non vivants tels que la salinité, l'ensoleillement, la température, le froid, les inondations et la sécheresse qui ont des impacts négatifs sur les plantes cultivées. Les deux stress peuvent déterminer de lourdes pertes en qualité et en quantité de la production agraire (Oerke, 2006 ; Kenawy et *al*., 2019 ; Suryadi, 2019). Différentes méthodes biologiques, physiques et/ou chimiques ont été utilisées pour contrôler les pertes de récoltes causées par les ravageurs au champ et pendant le stockage (Droby et *al.*, 1989 ; Sharma et *al*., 2009). Cependant, la principale méthode de contrôle est l'utilisation massive de pesticides chimiques avec un impact environnemental important et un risque conséquent pour la santé humaine et animale en raison de leur transmission le long de la chaîne alimentaire (Tscharntke et *al*., 2012).

Une alternative aux pesticides chimiques pourrait être l'utilisation de pesticides à base de composés naturels, qui sont respectueux de l'environnement et idéaux pour une production agricole durable avec un minimum de dommages pour l'environnement et sans risque pour la santé humaine et animale. De plus, ces produits naturels jouent un rôle important dans l'écologie de nombreux types d'organismes dont l'étude peut conduire à la découverte de nouveaux

produits naturels avec des bioactivités d'importance pratique (Godfray et *al*., 2010; Cimmino et *al*., 2015a ; Evidente et *al*., 2019).

Les principaux objectifs de la présente thèse ont été l'isolement ainsi que la caractérisation chimique et biologique de métabolites bioactifs ; avec des activités herbicides et fongicides potentielles ; produits par des champignons et des plantes de différents écosystèmes du bassin méditerranéen en comparaison de deux champignons phytopathogènes d'Argentine ; *Dreschlera gigantea* et *Macrophomina phaseolina*.

Cette thèse a d'abord été consacrée à l'introduction générale qui a porté sur les recherches antérieures. Ensuite, le premier chapitre a été consacré à la collecte et à l'identification d'un macro-champignon comestible de la forêt du Djebel El Ouahch de la région de Constantine à l'est de l'Algérie, suivi de l'extraction et de la purification de ses métabolites bioactifs. Par ailleurs, le deuxième chapitre a été focalisé sur la collecte d'une plante allélopathique (*Dittrichia viscosa*) d'Italie, avec l'extraction et la purification de ses substances bioactives. En outre, le troisième chapitre a été réuni la production, l'extraction et la purification des métabolites bioactifs des deux champignons phytopathogènes sélectionnés d'Argentine ; *D. gigantea* et *M. phaseolina*. Cette thèse se termine par une conclusion générale qui ouvre d'autres perspectives de recherche sur le sujet étudié.

Chapitre 1 : Collecte, extraction et purification des métabolites bioactifs d'*Agaricus litoralis*

1.1- Introduction

Les macrochampignons sauvages comestibles sont utilisés depuis longtemps pour leurs propriétés médicinales et nutritionnelles (Wu et *al*., 2019 ; Zeb et Lee, 2021). En fait, de nombreuses études ont démontré que les macrochampignons sont de bons producteurs d'un large spectre de composés bioactifs tels que les protéines, les composés phénoliques et les vitamines ; possèdent de fortes activités biologiques (Badalyan et Rapior, 2020 ; Niego et al., 2021).

En raison des conditions climatiques spécifiques, la zone forestière d'Algérie est l'une des régions d'Afrique du Nord avec une plus grande diversité de macrochampignons comestibles. Malgré ces importances crédibles, seuls quelques rapports sont connus (Benazza-Bouregba, 2017). En effet, trop peu de travaux ont été menés sur la composition chimique et les composés bioactifs des macrochampignons sauvages comestibles en Algérie, notamment dans les forêts

du Djebel el Ouahech de la région de Constantine. Les deux objectifs principaux de ce chapitre étaient : tout d'abord de collecter et d'identifier un macrochampignon sauvage comestible, *Agaricus* spp. des forêts du Djebel el Ouahech de la région de Constantine-Algérie, et d'autre part, d'isoler les composés phytotoxiques de ces espèces identifiées.

1.2- Revue bibliographique

1.2.1- Macrochampignons

Les macrochampignons présentent une section importante du royaume des champignons, contenant les organismes eucaryotes et hétérotrophes les plus divers sur terre (Boa, 2004; Mueller et al., 2007). Ils jouent un rôle essentiel dans la vie des plantes, des animaux et des êtres humains ; pourtant leur diversité est négligée (Govorushko et *al*., 2019 ; Hongyun et *al*., 2020).

La plupart des macrochampignons produisent des fructifications charnues et colloïdales représentant des structures de reproduction sexuée ; cependant, peu d'espèces représentent le stade de reproduction asexuée. En effet, la plupart de ces macrochampignons appartenant au phylum des Basidiomycota ou des Ascomycota tandis que les autres, à quelques chiffres, sont des Zygomycota. Leurs fructifications peuvent être situées au-dessus ou au-dessous du sol (Mueller et *al*., 2007; Govorushko et *al*., 2019).

Sur le plan écologique, les macrochampignons sont soit des saprophytes, soit des parasites, soit des symbiotiques. Les principaux de ces derniers, les symbiotiques, sont des ectomycorhizes qui ne peuvent pas être reproduites indépendamment. Au lieu de cela, leurs partenaires hôtes sont nécessaires pour aider à leur dispersion et à leur reproduction (Al-Thani, 2010). Près de 14 000 espèces macrofongiques ont été identifiées dans le monde, parmi lesquelles plus de 2000 macrochampignons comestibles et/ou médicinaux ont été caractérisés (Meenu et Xu, 2019 ; Hongyun et *al*., 2020) comme le genre Agaricus.

1.2.1.1- *Agaricus*

Agaricus L. est un genre de champignons saprophytes de l'ordre des Agaricales (Basidiomycota) comprenant plus de 500 espèces dans le monde en particulier dans les pays asiatiques, en Amérique du Nord, en Europe ainsi que dans certaines parties de l'Afrique (Gui et *al*., 2015 ; Kerrigan 2016 ; Zhao et al., 2016, Chen et *al*. 2019, An-Qi et al. 2020). Le genre *Agaricus* se caractérise par un stipe détachable du chapeau pourvu d'un ou plusieurs anneaux et de lamelles libres qui produisent des basidiospores brunes, à odeur souvent faible ou fongique,

des cheilocystides fréquemment absentes ou peu différentes des basides immatures (Parra 2008 ; Zhao et *al*. , 2011). Au cours de la dernière décennie, la taxonomie d'*Agaricus* a été bien développée en utilisant des méthodes phylogénétiques basées sur l'ADN (Zhao et *al*., 2016; Chen et *al*., 2019). *A. litoralis* fait partie du genre *Agaricus*.

1.2.1.2- Agaricus litoralis

A. litoralis (Fig. 1), également connu sous le nom de champignon côtier, est une espèce de champignon du genre *Agaricus*. Il a été décrit pour la première fois par Wakefield et Pearson sous le nom de *Psalliota litoralis* en 1946 (Møller, 1950). L'espèce *A. litoralis* pousse le plus souvent dans les endroits herbeux, dunes, steppes, elle est originaire de toute l'Europe et le long des côtes ; Angleterre et Danemark. Bien qu'il puisse être assez commun localement, comme sur l'île d'Öland (Cappelli, 1984a ; Courtecuisse et Duhem, 1994). *A. litoralis* est un champignon blanc ou gris-blanc avec un chapeau compact qui peut atteindre une largeur de 12 centimètres. Son capuchon est souvent déprimé lorsqu'il vieillit et des restes de l'anneau peuvent se produire sur le bord extérieur. Bien que de couleur rose à un jeune âge, les branchies deviennent brun foncé à mesure que le champignon vieillit. En outre, la tige atteint 5 à 6 centimètres de hauteur et 1,5 à 2 centimètres de largeur. Il est souvent remarquablement plus court que le capuchon. Ses spores sont généralement brun foncé et en forme d'œuf. Le champignon est saprotrophe ; il se nourrit de matières en décomposition et préfère les prairies sèches herbacées (Cappelli, 1984b ; Møller, 1950 ; Parra, 2008-2013).

Figure 1. *Agaricus litoralis*, Sociedad Micológicas (2017).

1.2.2- Champignons comme source de composés bioactifs

Les champignons sont l'une des sources les plus riches de métabolites secondaires qui ont le potentiel pour la découverte de nouveaux médicaments et produits agrochimiques, y compris toutes les catégories importantes de produits naturels ; terpènes, phénylpropanoïdes, polycétides, alcaloïdes, etc. (Cimmino et *al*., 2015a ; Deshmukh et *al*., 2014 ; Evidente et *al*.,

2019). Ces métabolites fongiques pourraient être utilisés pour formuler des bio-pesticides naturels et plusieurs études ont déjà été menées pour comprendre le rôle des métabolites fongiques bioactifs et donc les utiliser contre des maladies spécifiques. En conséquence, de nombreux nouveaux phytotoxines, fongicides, antibiotiques et régulateurs de croissance des plantes ont déjà été rapportés (Ballio et *al*., 1991 ; Décamps et Tabacchi, 1994 ; Evidente et Motta, 2001; Evident et *al*., 2019).

1.2.3- Métabolites bioactifs produits par les macrochampignons

Les macrochampignons peuvent jouer un rôle important dans la régulation du microbiome intestinal humain (Chang et *al*., 2015 ; Giannenas et *al*., 2011 ; Li et *al*., 2019). Cette caractéristique ouvre de nouvelles perspectives pour l'application des macrochampignons et de leurs ingrédients bioactifs.

Ils produisent des composés naturels avec un large spectre d'activités biologiques, notamment ; propriétés antimicrobiennes, antifongiques, antivirales, anti-inflammatoires, antioxydantes, antidiabétiques, antithrombotiques, antitumorales, anticancéreuses, anticomplémentaires, anticoagulantes, hypolipidémiques, hépatoprotectrices, immunostimulantes et immunologiques ; ce qui les a rendus adaptés à leur utilisation dans l'alimentation, la cosmétique, la biomédecine, l'agriculture, la protection de l'environnement et la gestion des eaux usées (Chang et Miles, 1989 ; Ha, Gerhauser et *al*., 2000 ; Loria-Kohen, Lourenco-Nogueira et *al*., 2014 ; Kozarski et *al*., 2015, Abdullah, 2017).

Les plus importantes substances biologiquement actives, présentes dans les macrochampignons, sont des composés phénoliques. Ils sont des métabolites secondaires qui ont un cycle aromatique portant un ou plusieurs groupes hydroxyles (Balasundram, Sundram et Samman, 2006 ; Palacios, da Rosa et al., 2011). Ces composés phénoliques jouent un rôle important dans l'écologie de différents organismes. Les phytotoxines sont un exemple de composés phénoliques naturels avec une application potentielle en agriculture en tant qu'herbicides, fongicides, bactéricides, insecticides, etc.

1.3- Matériel et méthodes

1.3.1- Collection de Macrochampignons

Des macrochampignons frais ont été collectés en décembre 2017 et mai 2018 dans la forêt de Djebel el Ouahch de la région de Constantine dans l'est de l'Algérie, qui couvre une superficie de 66 535 ha. Elle est comprise entre 36°14'20, 19" et 36°33'55,81" de latitude nord et entre 6°38'0,82" et 6°58'37,65" de longitude Est (Boudy, 1955). Un spécimen de référence a été

déposé à l'Herbier de l'Université de Montpellier 2, Institut de Botanique, France. Les fructifications ont été séchées à l'ombre, puis coupées en petits morceaux à l'aide de scalpels et ensuite broyées à l'aide d'un pistil et d'un moteur pour obtenir poudre fine.

1.3.2- Identification d'*Agaricus* spp.

L'identification d'*Agaricus* spp a été réalisée basant sur deux point principaux ; ses caractères morphologiques (forme, taille et couleur du chapeau, etc) (Cappelli 1984, Zhao et *al*., 2011, Courtecuisse et Duhem, 2013) et sa identification moléculaire (extraction, amplification et séquençage d'ADN) (Murray et Thompson, 1980), où ses séquences obtenues ont été déposées dans GenBank et un arbre phylogénétique, en utilisant la méthode du maximum de vraisemblance et le modèle Tamura-Nei (Tamura et Nei, 1993), était affichée.

1.3.3- Extraction et purification des métabolites secondaires d'*Agaricus* spp.

La macération dans le MeOH-H_20 (1:1, v/v), selon la méthode de Kimura et Tamura (1973), a été utilisée pour extraire les métabolites secondaires d'*Agaricus* spp. (500 g).

Ensuite, l'extrait d'EtOAc (170 mg) a été purifié par Chromatographie sur colonne en utilisant le gel de silice, élue avec CHCl3-i-PrOH (8:2, v/v), donnant le métabolite principal sous forme de solide blanc (1,5 mg).

1.3.4- Test de phytotoxicité

L'activité phytotoxique du métabolite purifié, tyrosol (1 mg/mL), a été réalisée en utilisant deux tests différents ; bouturage ( ) sur les feuilles de tomate (*Lycopersicon esculentum* L.) et perforation foliaire ( ) sur les feuilles de sept plantes agraires : *Solanum melongena* L., *Ficus carica* L., *Prunus armeniaca* L., *Prunus persica* (L.) Batsch, *Citrus limon* (L.) Osbeck, *Cucurbita* L. et *Vitis vinifera* L., ainsi que sur les feuilles de plantes sauvages : *Quercus phellos* L. et *Rubus fruticosus* L.).

1.4- Résultats et discussions

1.4.1- Identification d'*Agaricus* spp.

Les caractéristiques antérieures peuvent suggérer le genre *Agaricus* à notre macro-champignon qui est hémisphérique puis plan-convexe à maturité, avec une surface blanchâtre, puis rapidement gris-ochracé-brunâtre. Bord d'abord involué puis appendiculaire, entier, dépassant nettement les lamelles quand il est jeune. Lamelles libres, serrées, pâles, puis de couleur chair, enfin brun foncé à maturité. Stipe court, robuste, ventriceux, presque lisse, à base généralement prolongée par un ou plusieurs rhizoïdes. Anneau membraneux, blanc, fragile, persistant, assez

ample, face supérieure striée, face inférieure lisse, souvent déchirée et appendiculaire au bord du chapeau. Contextes compacts, épais, blanchâtres, légèrement rougissant lorsqu'on les coupe surtout vers la base du stipe. Odeur d'amande amère. Goût doux, fongique avec spore brunâtre imprimée.

Le résultat de BLAST après l'analyse de la séquence d'ADN de la région ITS montre aussi que les séquences correspondaient à celles *d'Agaricus litoralis* ; % d'identité 99.72 (i.e. JF727867.1) de France. L'analyse phylogénétique confirme la monophylie du clade englobant la séquence algérienne et la séquence MW165560.1 identifiée comme *A. litoralis* dans GenBank.

Il s'agit du premier signalement publié d'*Agaricus litoralis* dans la forêt du Djebel el Ouahch (Constantine, Est Algérien). Le genre Agaricus est très diversifié en Europe et peu documenté à ce jour dans les régions méditerranéennes. L'espèce *Agaricus litoralis*, morphologiquement similaire à *Agaricus arvensis* et *Agaricus crocodilinus*, a déjà été collectée mais mal identifiée en Afrique du Nord (Malencon et Bertault, 1970 ; El Kholfy et *al*., 2011) l'a signalée au Maroc (sous le nom *d'Agaricus spissicaulis*).

1.4.2- Identification structurale des métabolites secondaires *d'Agaricus litoralis*

L'extrait d'AcEtO obtenu à partir *d'A. litoralis* a été purifié par combinaison de chromatographie sur colonne et de CCM, donnant un métabolite connu qui a été identifié comme le tyrosol (Fig. 5). **Le tyrosol**, obtenu sous forme de solide amorphe, avait : RMN 1H (400 MHz, dans CDCl3) δ 7,10 (d, J=8,2 Hz, H-2 et H-6), 6,79 (d, J=8,2 Hz, H-3 et H-5), 3,82 (t, J=6,6 Hz, H2-8), 2,80 (t, J=6,6 Hz, H2-7); ESIMS (+) m/z 299 [2M+Na]+, 161 [M+Na]+. Sa structure chimique a été confirmée en comparant ses données d'analyses spectroscopiques (1H-RMN et ESI-MS) avec celles rapportées dans la littérature (Kimura et Tamura 1973 ; Capasso et *al*. 1992 ; Cimmino et *al*. 2017 ; Masi et *al*., 2020) .

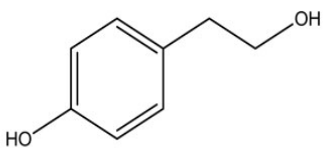

Figure 5. Tyrosol (1) un métabolite secondaire isolé *d'Agaricus litoralis.*

Le tyrosol est un métabolite secondaire omniprésent qui a été trouvé dans les plantes (Capasso et *al*., 1992), les bactéries (Bouallagui et Sayadi, 2006) et les champignons (Masi et *al*., 2018). De plus, le tyrosol a été considéré comme un métabolite bien connu qui a diverses activités

biologiques (Di Benedetto, 2007), y compris la phytotoxicité. Récemment, le tyrosol a également été identifié comme un métabolite phytotoxique produit par plusieurs champignons qui agissent comme agents pathogènes pour les plantes agraires (Evidente et *al*., 2019) et forestières (Masi et *al*., 2018). En effet, son activité phytotoxique sur la féverole, la légumineuse, la tomate (Evidente et al., 2010), la vigne (Reveglia, 2019), le souci, le pricklysida et le chénopode blanc a déjà été rapportée (Gamboa-Angulo, 2001 ; Venkatasubbaiah et *al*., 1992). Le tyrosol est également signalé comme une molécule de détection de quorum chez *Candida albicans*, contrôlant la croissance, la morphogenèse et la formation de biofilm (Albuquerque et Casadevall, 2012).

1.4.3- Test de phytotoxicité

Deux essais biologiques, bouturage et perforation foliaire, ont été utilisés pour étudier l'activité phytotoxique de l'extrait organique d'*A. litoralis* et du tyrosol.

En effet, l'extrait d'AcOEt à 1 mg/mL par les deux tests sur les feuilles de tomate (*Lycopersicon esculentum* L.) a présenté une forte activité de phytotoxicité. En outre, le tyrosol à 1 mg/mL par le test de perforation foliaire sur sept plantes agraires (aubergine, figuier, abricot, pêcher, citron, cucurbitacée et vigne) et deux plantes sauvages (chêne saule et mûre) était actif en provoquant une nécrose chez toutes les plantes à l'exception du chêne des saules dans les feuilles des plantes sauvages. Ce composé a montré l'effet toxique le plus élevé sur la vigne, l'abricot, la pêche, la cuccurbita et la mûre, tout en étant modérément toxique sur les feuilles d'aubergine. Le tyrosol est également apparu avec une faible phytotoxicité sur les feuilles de figuier et de citronnier (Fig. 6 et Tableau 2).

Chapitre 2 : Collecte, extraction et purification des métabolites bioactifs de *D. viscosa*

2.1- Introduction

Les mauvaises herbes sont l'une des principales raisons affectant l'agriculture moderne et leur gestion (Boari et *al*., 2021). Les orobanches (*Orobanche* et *Phelipanche* spp.) sont des adventices obligatoires, dépourvues de chlorophylle, parasites des racines qui obtiennent toutes leurs ressources nutritives en attaquant les cultures, infligeant des pertes de rendement élevées dans de nombreuses régions d'Europe, d'Asie et d'Afrique.

L'Orobanche cumana est l'une des adventices les plus virulentes de l'orobanche hautement spécialisée dans l'attaque du tournesol. Par ailleurs, *Phelipanche ramosa* et *Orobanche minor* ont aussi des gammes d'hôtes plus larges, infectant non seulement de nombreuses cultures, mais aussi les mauvaises herbes non parasites et autres plantes sauvages associées.

De plus, lorsque la plante cultivée est déjà infectée par ces mauvaises herbes, l'utilisation d'herbicides est la seule option ; mais l'utilisation répétée d'herbicides chimiques traditionnels peut réduire la valeur sanitaire des cultures et augmenter le risque d'émergence de résistances aux herbicides dans la mauvaise herbe. Par conséquent, il est nécessaire de diversifier les alternatives efficaces à la lutte conventionnelle contre l'orpin pour réaliser des programmes de protection des plantes durables (Perotti et *al*., 2015 ; Fernández-Aparicio et *al*., 2016).

En effet, *Dittrichia viscosa* (L.) *Greuter*, une plante méditerranéenne indigène et spontanée, produit plusieurs composés bioactifs, dont certains ont des effets phytotoxiques et allélopathiques provoquant une inhibition de la germination des graines et de la croissance des plantes, ou une nécrose des feuilles (Andolf et *al*., 2013 ; Boari et *al*., 2021). Quatre lactones sesquiterpéniques bi- et tricycliques nommées inuloxines A, B, C et D, ainsi que l'acide α-costique isolés de *Dittrichia viscosa*, ont une activité herbicide potentielle contre les mauvaises herbes parasites *O. crenata*, et *C. campestris*. De plus, l'acide α-costique avait un effet suppresseur sur la germination des graines de cuscute mais avait une action stimulante sur la germination des graines d'orpin. Compte tenu de leur activité intéressante, d'autres études sont également prévues sur la configuration absolue (CA) des inuloxines A, B, C et D.

Les objectifs principaux de ce chapitre sont l'extraction et la purification des métabolites bioactifs de *Dittrichia viscosa* ; ainsi la caractérisation chimique et biologique de nouveaux métabolites ; affectation de configurations relatives et absolues et même préparation de dérivés hémisynthétiques de certains métabolites ont des activités biologiques.

2.2- Revue bibliographique

2.2.1- Plantes comme source de composés bioactifs

Les plantes produisent un assortiment vaste et diversifié de métabolites secondaires. Ces substances sont souvent réparties différemment entre des groupes taxonomiques limités au sein du règne végétal. L'estimation du nombre d'espèces végétales identifiées est désormais d'environ 374 000, dont 295 383 espèces de plantes à fleurs (Christenhusz, 2016).

Les principaux métabolites tels que les phytostérols, les lipides acyles, les nucléotides, les acides aminés et les acides organiques se trouvent dans toutes les plantes et remplissent des rôles métaboliques essentiels et généralement évidents (Hussain et *al*., 2012). En revanche, les métabolites secondaires dans les plantes sont une source importante pour la découverte de composés bioactifs avec un large éventail d'applications telles que les médicaments ou les produits agrochimiques (Grindberg et *al*., 2011 ; Jimenez-Garcia et *al*., 2013).

2.2.1.1- *Dittrichia viscosa*

Dittrichia viscosa (L.) Greuter (sin. *Inula viscosa* (L.) Aiton) (Fig. 7) est un arbre à feuilles persistantes, appartenant à la famille des Composées (Asteraceae). *D. viscosa* est un petit arbuste très ramifié commun dans tout le bassin méditerranéen, originaire des côtes du sud de l'Europe (France, Espagne, Grèce, Italie, Bulgarie) et de la Turquie, du Moyen-Orient (Israël, Jordanie et Syrie) ainsi que de l'Afrique du Nord (Algérie, Egypte, Libye). Il est bien adapté aux situations ouvertes perturbées et aux écosystèmes secs.

Elle est considérée comme une mauvaise herbe environnementale grave marquée pour l'éradication et l'importation interdite en Australie (DPIPWE, 2011 ; Daissie, 2012 ; Parolin et *al*., 2014 ; Sladonja et al., 2021). C'est une plante arbustive vivace, aux feuilles longues et étroites pointues aux deux extrémités de couleur verte. L'exsudat collant des poils glandulaires diffuse une odeur désagréable. Cet exsudat collant contient de l'huile essentielle. L'inflorescence pyramidale est composée de nombreux capitules aux fleurs jaune doré.

La floraison a lieu en automne, tandis que les fruits sont constitués d'akènes. L'espèce est très résistante aux conditions abiotiques défavorables courantes dans les environnements dégradés comme les coupes fréquentes, les incendies, la sécheresse et les sols pauvres en nutriments (Parolin et *al*., 2014). Elle est important comme nourriture pour les chenilles de certains papillons, mites ainsi que plusieurs parasitoïdes de ravageurs économiquement importants (Kavallieratos et *al*., 2002).

Figure 7. *Dittrichia viscosa*

2.2.2- Métabolites de *Dittrichia viscosa*

Dittrichia viscosa est une espèce connue pour la présence de plusieurs classes de métabolites responsables des propriétés biologiques telles que les flavonoïdes, les lactones

sesquiterpéniques, les triterpénoïdes et les acides (Staurianakou et *al*., 2004 ; Gum et al., 2007 ; Dor et Hershenhorn et *al*., 2012 ; Sladonja et *al*., 2021). Parmi ceux-ci, l'acide α-costique a montré différentes activités tandis que les sesquiterpènes, inuviscolide et tomentosine induisaient l'apoptose des cellules de mélanome humain (Rozenblat et *al*., 2008) ainsi qu'une activité anti-inflammatoire, antioxydante, antibactérienne et antifongique (Abrham et al., 2010 ; Schinella et *al*., 2002). De plus, l'acide α-costique et les inuloxines A-D isolés des feuilles, des parties aériennes et des plantes entières de la plante *D. viscosa* ont démontré leur capacité à inhiber la germination des graines *d'Orobanche crenata* et de *Cuscuta campestris*. Successivement, l'inuloxine A et l'acide α-costique ont induit une germination significative des graines *d'O. cumana* tandis que l'inuloxine C a induit un effet phytotoxique sur quatre romarins (Andolfi et *al*., 2013 ; Cimmino et *al*., 2014).

Considérant que la configuration absolue (CA) des composés naturels est étroitement liée à leur activité biologique (Evidente et *al*., 2011; Evidente et *al*., 2013;) l'CA de l'inuloxine A, le principal germacrane sesquiterpène isolé de *D. viscosa* , a été déterminé par des méthodes chiroptiques et informatiques (Santoro et *al*., 2015). Des études ont été menées pour étudier le potentiel fongicide de *D. viscosa* contre certains agents pathogènes d'intérêt agricole, notamment le concombre, la tomate, la pomme de terre, le blé et le tournesol (Wang et *al*., 2004 ; Hernandez et *al*., 2007). Cette plante a également potentiel allélopathique et, en particulier, ses extraits ont provoqué des effets phytotoxiques sur plusieurs espèces, inhibant les racines et provoquant des anomalies anatomiques racinaires (Aşkin Çelik et Aslantürk, 2010).

2.3- Matériel et méthodes

2.3.1- Collecte de *Dittrichia viscosa*

L'espèce *D. viscosa* a été collectée fraîche dans le sud de l'Italie. Un spécimen de référence a été déposé à la Colletion of Istituto di Scienze delle Produzioni Alimentari, CNR, Bari, Italie. Après la récolte, les feuilles ont été détachées des tiges et séchées dans une étuve ventilée à 50 °C pendant deux jours. Le matériel végétal a ensuite été broyé pour obtenir une poudre fine et emballé dans des sacs en plastique sous vide jusqu'à son utilisation.

2.3.2- Procédures expérimentales générales

Plusieurs méthodes analytiques ont été appliquées pour l'isolement et la caractérisation des métabolites séparés dans ce chapitre ; la rotation optique, les spectres IR, les spectres UV, les spectres RMN, l'HR ESIMS et ESIMS ont été enregistrés en utilisant le système LC/MS

ESIMS-TOF. La séparation par HPLC, les CCM analytiques, préparatives et en phase inverse, ainsi la Chromatographie sur colonne a été réalisée en utilisant du gel de silice.

2.3.3- Extraction et purification des métabolites secondaires de *Dittrichia viscosa*

La méthode d'Andolfi (2013), a été utilisée pour extraire les métabolites secondaires de *Dittrichia viscosa* (450 g).

Ensuite, un résidu huileux brun-rouge (17 g) a été séparé en utilisant une chromatographie sur colonne de gel de silice éluée avec CHCl3-i-PrOH (95:5, v/v), donnant à la fin le principal métabolite identifié sous forme d'huile jaune homogène comme l'acide α-costique (2 400 mg, Fig. 9), un autre métabolite huileux homogène, nommé inuloxine A (3, 105 mg, 9). Le résidu (36,8 mg) de la première fraction de cette dernière colonne a été purifié par CCM préparative en utilisant EtOAc-n-hexane (6:4, v/v) donnant à la fois des inuloxines E et D sous forme d'huiles pures (6, 11,6 mg, Rf 0,65 et 5, 5,8 mg, Rf 0,48, Fig. 9) et inuloxine C (4, 11,0 mg, Rf 0,40).

2.3.3.1- Préparation des dérivés hémisynthétiques de l'inuloxine D

Quatre dérivés de l'inuloxine D ont été synthétisées suivant des méthodes précises ;

- Dérivé 4-O-acétyle de l'inuloxine D (7) avait : Rf 0,75; RMN 1H :; ESIMS (+), m/z 315 [M + Na]+, 293 [M + H]+. (),

- Dérivé 4-O-Azidopentanoyl Ester d'Inuloxine D (8) avait : Rf 0,70 ; RMN 1H; ESIMS (+), m/z 398 [M + Na]+, 376 [M + H]+ (),

- Dérivé 4-O-Mesyl Ester d'Inuloxine D (9) avait : RMN 1H; ESIMS (+), m/z 351 [M + Na]+, 329 [M + H]+ (),

- Dérivé 4-O-p-bromobenzoylester d'inuloxine D (10) avait : RMN 1H; ESIMS (+), m/z 454 et 452 [M + Na]+ 432 et 430 [M + H]+.

2.3.4- Activités biologiques

2.3.4.1- Induction de germination

L'activité germinative de l'inuloxine D, de l'inuloxine E et des dérivés de l'inuloxine D a été testée sur des graines *d'O. cumana*, *O. minor* et *P. ramosa*. Cette activité a été réalisée selon la méthode décrite par (), où le pourcentage de germination a été établi.

2.3.4.2- Inhibition de la germination et de la croissance

L'activité inhibitrice des inuloxines D et E sur la germination des graines et la croissance des radicules *d'O. cumana*, *O. minor* et *P. ramosa* a été analysée comme indiqué précédemment

(Fernández-Aparicio et *al*., 2013). Le pourcentage de germination a été déterminé en notant le nombre de graines avec une radicule émergée à travers le tégument dans un total de 100 graines par disque. La longueur de la radicule a été mesurée dans 15 graines germées sélectionnées au hasard à partir de chaque disque.

2.3.5- Analyse statistique

Les tests biologiques ont été effectués deux fois avec trois répétitions. Les données de pourcentage ont été rapprochées de la distribution de fréquence normale au moyen d'une transformation angulaire (180/π × arcsinus (sqrt [%/100])) et ont été soumises à une analyse de variance (ANOVA) à l'aide du logiciel SPSS pour Windows, version 21.0 (SPSS Inc. Chicago, Illinois, États-Unis). La signification des différences moyennes entre chaque traitement par rapport à son témoin respectif a été évaluée par le test de Dunnett bilatéral.

2.3.6- Configuration absolue de l'inuloxine D

ECD, VCD et ORD ont été mesurés pour le dérivé 4-O-acétyle (7) qui a été obtenu par acétylation commune de l'inuloxine D (5) avec de la pyridine et de l'anhydride acétique comme détaillé précédemment (Fernández-Aparicio et *al*., 2011). La comparaison quantitative entre l'ORD expérimental et calculé est obtenue (Polavarapu et *al*., 2021) en calculant la déviation quadratique moyenne (RMSD) comme suit :

$$\mathrm{RMSD} = \sqrt{\frac{\sum_i \left(Y_{i,\mathrm{calc}} - Y_{i,\mathrm{obs}}\right)^2}{N}}$$

Les analyses spectrales ECD et VCD ont été réalisées à l'aide du programme CDSpecTech (Covington et Polavarapu, 2017) qui implémente la fonction de similarité de Tanimoto (Tanimoto 1958; Cheng et *al*., 1996) comme proposé par Shen et *al*. (2010).

2.4- Résultats et discussion

2.4.1- Identification structurale des métabolites secondaires de *Dittrichia viscosa*

L'extrait organique de la partie aérienne de *D. viscosa*, obtenu comme décrit dans la section expérimentale, a été fractionné par une combinaison de chromatographie sur colonne et de CCM pour donner un nouveau sesquitepenoid, nommé inuloxin E (6, Fig. 9) et quatre métabolites connus ; l'acide α-costique et les inuloxines A, C et D (2 -5).

2.4.1.1- Acide α-costique (2)

Il a été obtenu sous la forme d'une huile jaune homogène, avait : [a]25D +48,6° (c 1,0, CHCl3) ; IR max 3450, 1680, 1657, 1613 cm-1]; Le spectre RMN 1H est très similaire à celui rapporté dans la littérature (Andolfi et *al*., 2013). ESIMS (+) m/z 235[M+H]+, 189 [M-COOH]+. Ces données concordent avec celles précédemment rapportées (Shtacher et Kashman, 1970 ; Andolfi et *al*., 2013).

2.4.1.2- Inuloxine A (3)

Elle a été obtenue sous forme d'un homogène huileux, avait : [α] 25D +8:5 (c 1,9); Le spectre RMN 1H est similaire à celui rapporté dans la littérature (Andolfi et al., 2013). HR ESIMS (+) m/z 519 [2M+Na]+, 287 [M+K]+, 271.1321 [calculé. pour C15H20NaO3 271.1310, M+Na]+, 249 [M+H]+, 231 [M+H-H2O]+. Ces données concordent avec celles précédemment rapportées (Shtacher et Kashman, 1970 ; Andolfi et *al*., 2013).

2.4.1.3. Inuloxine C (4)

Elle a été obtenue sous forme d'un homogène huileux, avait : [α]25D +13,1 (c 0,3) ; IR max 3428, 1758, 1662, 1635, 1152 cm-1; UV max nm (log) 262 (1,07); Le spectre RMN 1 H est similaire à celui rapporté dans la littérature (Andolfi et al., 2013) ; HR ESIMS (+) m/z 519 [2M+Na]+, 287 [M+K]+, 271.1319 [calculé. pour C15H20NaO3 271.1310, M+Na+], 253 [M+Na=H2O]+. Ces données concordent avec celles précédemment rapportées (Shtacher et Kashman, 1970 ; Andolfi et *al*., 2013).

2.4.1.4- Inuloxine D (5)

Le spectre RMN 1H est similaire à celui rapporté dans la littérature (Andolfi et al., 2013). HR ESIMS (+) m/z : 251,1658 [calculé. pour C15H23O3 251.1647, M+H]+, 233 [M+H-H2O]+. Ces données spectroscopiques et optiques de l'inuloxine D similaires à celles précédemment rapportées dans la littérature (Andolfi et *al*., 2013).

2.4.1.5- Inuloxine E (6)

L'inuloxine E a été obtenue sous forme d'huile pure, avait : [α] 25D + 21,4 (c 0,4); IR max 1762, 1714, 1660 cm-1 (Fig. 16). Les RMN 1H et 13C (figure 10 et figure 11) sont rapportées dans le tableau 3; HR ESIMS (+), m/z 519 [2M + Na]+, 271.1321 (C15H20NaO3, calculé 271.1310 [M + Na]+), 249 [M + H]+.

2.4.2- Hémisynthèse et caractérisation chimique des dérivés de l'inuloxine D

Les inuloxines E et D ont été dosées en comparaison avec quatre dérivés esters différents préparés à partir d'inuloxine D (7-10). En particulier le dérivé acétylé de 5 (7) a été préparé par acétylation usuelle. Son ESIMS a montré les formes sodiées [M + Na]+ et protonées [M + H]+ à m/z 315 et 293. L'ester 4-O-azidopentanoyle de 5 (8) préparé par déshydratation entre (5) et 5 L'acide -azidopentanoyle a montré un spectre RMN 1H qui différait de celui de (5). Le spectre ESI-MS a montré les formes sodiées [M + Na]+ et protonées [M + H]+ à m/z 398 et 376. L'ester 4-O-mésylique de 5 (9) a été préparé par réaction de l'inuloxine D avec du chlorure de mésyle. Son spectre RMN 1H (tableau 4) différait de celui de (5). Son ESIMS a montré les formes sodiées [M + Na]+ et protonées [M + H]+ à m/z 351 et 329. Enfin, le p-bromobenzoyl ester de 5 (10) a été préparé par réaction entre l'inuloxine D et p -chlorure de bromobenzoyle. Le spectre RMN 1H (tableau 4) différait de celui de (5). Son ESIMS a montré les formes isotopiques typiques sodiées [M + Na]+ et protonées [M + H]+ à m/z 454 et 452 et 432 et 430, respectivement. Ces données sont les mêmes que celles déjà rapportées dans Andolfi et *al*. (2013)

3.4.3- Tests biologiques

3.4.3.1- Induction de germination

L'activité de stimulation des inuloxines D et E a été étudiée chez trois espèces d'herbes : *O. cumana, O. minor et P. ramosa* (Figure 17). Aucune de ces inuloxines n'était active dans l'induction de la germination *d'O. minor et de P. ramosa*, deux espèces d'orpins connues pour leur faible niveau de spécialisation dans la reconnaissance des exsudats racinaires (Fernández-Aparicio et *al*., 2009-2011). Au contraire, les deux inuloxines ont induit la germination des graines hautement sélectives *d'O. cumana,* où l'effet de l'inuloxine D était plus fort que celui induit par l'inuloxine E. Par conséquent, les quatre dérivés esters rapportés ci-dessus ont été préparés à partir d'inuloxine D et testés chez toutes les espèces d'orpin (tableau 5). Où, les modifications structurelles apportées à l'inuloxine D ne portaient pas d'activité d'induction sur les graines *d'O. minor* et *P. ramosa* induisant leur germination.

En effet, le niveau de germination *d'O. cumana* a été réduit en (8 et 10), à toutes les concentrations testées en comparaison avec l'inuloxine D. A 10-4 M les niveaux de germination *d'O. cumana* induits par (7 et 9) étaient comparables à celui induite par (5), mais à des concentrations plus faibles, l'activité germinative a été réduite dans ces dérivés par rapport à l'inuloxine D. L'activité d'inhibition de l'inuloxine E et de l'inuloxine D dans les graines de trois espèces d'herbes : *O. cumana, O. minor et P. ramosa* a été étudié en mélangeant ces métabolites

avec du GR24, un stimulant synthétique de la germination actif dans les trois adventices de l'ortie étudiées dans ce travail. Aucune action inhibitrice n'a été observée dans l'inuloxine D et l'inuloxine E car l'activité germinative du GR24 mélangé à chaque inuloxine n'était pas différente de celle induite par le contrôle GR24. Cet effet a été observé pour O. cumana ainsi que pour les espèces *O. minor et P. ramosa*, et a donc confirmé que l'effet rapporté sur la figure 18 pour *O. minor et P. ramosa* est un manque d'activité stimulatrice et non une action inhibitrice. Fait intéressant, les graines *d'O. cumana* et de P. ramosa qui ont germé avec du GR24 mélangé à de l'inuloxine D ont développé des radicules plus courtes. Cette inhibition de la croissance radiculaire n'a pas été observée dans les graines d'O. minor. L'inuloxine E n'a inhibé la croissance des radicules chez aucune des espèces d'orpin à balais testées.

2.4.4- Configuration absolue de l'inuloxine D

Puisqu'il n'y a aucune possibilité de liaison hydrogène intramoléculaire dans (5), la recherche conformationnelle est moins compliquée. Néanmoins, il existe un grand nombre de conformères en raison de la flexibilité de la chaîne latérale contenant C1-C4.
Pour chaque diastéréoisomère, les nombres de conformères dans une différence d'énergie électronique de 2 kcal/mol, qui ont été utilisés pour la fréquence vibratoire finale et les calculs spectraux, sont répertoriés dans le tableau 16.

Étant donné que les spectres ECD prédits pour tous les diastéréomères présentent des correspondances relativement fortes avec les spectres ECD expérimentaux, ayant le modèle négatif-positif-négatif des effets sur le coton (CE), il est difficile de discerner qualitativement si un diastéréomère particulier peut être favorisé pour attribuer la CA. L'analyse quantitative utilisant la similitude entre les spectres calculés et expérimentaux permet une discrimination dans une certaine mesure (tableau 6). Comme on le verra plus loin, la conclusion basée sur les analyses ECD sera contredite par les analyses VCD et ORD.

Les spectres VA et VCD prédits pour les diastéréoisomères de (5) sont comparés aux spectres expérimentaux correspondants sur les figures 65. Comme on peut le voir sur ces figures, les spectres VA pour les quatre diastéréoisomères semblent qualitativement identiques. Les spectres VCD des diastéréoisomères montrent quelques différences qualitatives, mais il est difficile de juger quels spectres prédits de diastéréomères correspondent le mieux aux spectres expérimentaux. L'amplitude de SimVCD pour 5C est proche du seuil de confiance, mais celles des autres diastéréoisomères sont bien en dessous du seuil de confiance (Polavarapu et al., 2017). Ainsi, l'analyse VCD favorise clairement le diastéréoisomère (1R,4S,7R,8R) pour

attribuer le CA de (S6). Ce type d'analyse de similarité quantitative se présente comme un outil indispensable pour déterminer l'AC dans les situations où la comparaison visuelle n'indique pas une préférence évidente.

Les mesures expérimentales de l'ORD ont révélé des valeurs SOR très faibles, avec un changement de signe à une longueur d'onde plus courte (Fig. 66). L'inversion de signe à la longueur d'onde la plus courte n'est reproduite dans les calculs pour aucun des diastéréomères, mais les signes positifs observés dans l'expérience à des longueurs d'onde plus longues sont reproduits dans les valeurs prédites pour ent-2A et ent-2D et pour les diastéréomères 2B et 2C . L'analyse quantitative (voir l'équation 1) indique que les valeurs RMSD pour 2A-2D sont, respectivement, 272, 320, 244 et 370. Sur la base de ces valeurs RMSD, 2C est le diastéréoisomère préféré pour l'affectation AC.

Pour résumer les analyses, les données VCD et ORD favorisent le diastéréoisomère (1R,4S,7R,8R) (6C) pour attribuer l'AC de (5). Ainsi, l'AC de (5), l'inuloxine D acétylée, et par extension l'inuloxine D, peut raisonnablement être attribuée comme (1R,4S,7R,8R), tandis que celle de l'inuloxine E peut raisonnablement être attribuée comme (1R,7R,8R) (Fig. 67).

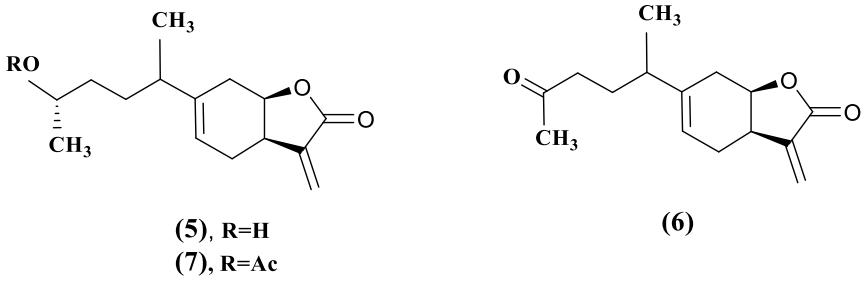

Figure 22. Inuloxine D (5), inuloxine D acétylée (7) et inuloxine E (6), avec CA assigné.

Chapitre 3 : Production, extraction et purification de métabolites bioactifs à partir de deux champignons phytopathogènes Dreschlera gigantea et Macrophomina phaseolina

3.1- Introduction

Les champignons phytopathogènes constituent l'une des principales maladies infectieuses des plantes cultivées, jouant un rôle important dans les pertes annuelles persistantes et significatives des récoltes, avec de lourds problèmes économiques. En effet, ils sont contrôlés par des fongicides de synthèse pour éviter les pertes de production agraire (Paulitz et Bélanger, 2001 ; Ribera et Zuñiga, 2012 ; Evidente, Cimmino et Masi, 2019). Cependant, l'utilisation intensive de ces pesticides a entraîné une série de problèmes environnementaux et écologiques, tels que

l'augmentation des populations de mauvaises herbes résistantes, le compactage des sols et la pollution de l'eau, qui affectent gravement le développement durable de l'agriculture.

Par conséquent, il existe une forte demande de nouveaux fongicides naturels (Tscharntke et al., 2012 ; Cimmino et *al*., 2015a ; Peng et *al*., 2021). Ainsi, de nombreuses études ont été menées sur les phytotoxines produites à partir de champignons phytopathogènes et la connaissance des processus de pathogenèse des plantes peut aider à trouver le meilleur remède rapide pour contrôler les maladies des plantes. Au vu de ces résultats, il semble intéressant de trouver de nouveaux métabolites bioactifs produits par deux champignons phytopathogènes *Dreschlera gigantea* et *Macrophomina phaseolina*, lors de leur croissance en cultures liquides.

Le but de ce chapitre a été l'isolement et la caractérisation chimique et biologique de métabolites bioactifs avec une activité herbicide et fongicide potentielle produits par deux champignons phytopathogènes d'Argentine : *D. gigantea* et *M. phaseolina*.

3.2- Revue bibliographique

3.2.1- Champignons phytopathogènes

3.2.1.1- *Drechslera gigantea*

D. gigantea (Fig. 23A) est un pathogène fongique cosmopolite présent dans toute l'Amérique du Nord et du Sud, au Japon et dans d'autres régions (Evidente Andolfi et al. 2006, Sivanesan, 1992). Il provoque une maladie des taches oculaires zonée de nombreuses graminées et mauvaises herbes couramment cultivées, y compris *Digitaria* spp., *Agropyron repens* et *Cynodon dactylon* (Strobel, Kenfield et al., 1991; Evidente et al. , 2006, Sivanesan, 1992, Farr et al., 1989).

Le *D. gigantea* seul et en combinaison avec deux autres pathogènes des graminées, *Exserohilum longirostratum* et *E. rostratum* est efficace pour la gestion des graminées dans des conditions de terrain (Chandramohan et Charudattan, 2001 ; Chandramohan et al., 2002). En règle générale, les symptômes de la brûlure des feuilles par *D. gigantea* (figure 24B) apparaissent environ une semaine après la pulvérisation du champignon sur le feuillage des graminées et la maladie progresse régulièrement au cours des deux à trois semaines suivantes. De plus, certaines évaluations ont confirmé que ces champignons sont efficaces pour la gestion des graminées dans des conditions de terrain (Chandramohan et Charudattan, 2001 ; Chandramohan et *al.*, 2002 ; Evidente et *al*., 2006).

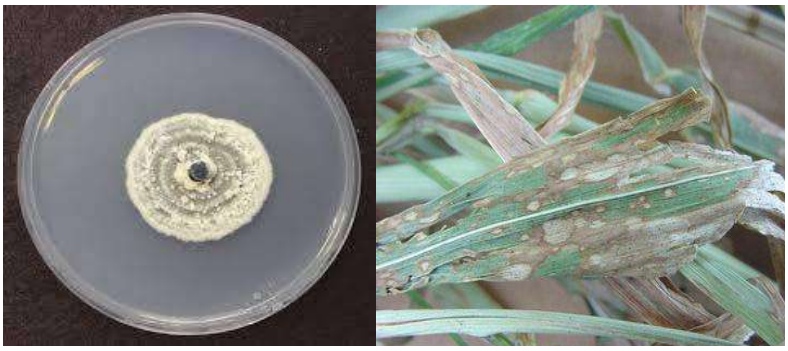

Figure 23. A. Colonie de *D. gigantea* poussant sur PDA après 7 jours (Lane et al., 2020). B. brûlure des feuilles (Drechslera gigantea) par Paul Bachi.

3.2.1.2- *Macrophomina phaseolina*

M. phaseolina (Tassi) Goid. (Fig. 24A), est un champignon pathogène de la famille des Botryosphaeriaceae que l'on trouve partout dans le monde, en particulier dans les pays tropicaux et subtropicaux aux climats arides à semi-arides en Afrique, en Asie, en Amérique du Nord et du Sud et en Europe. Il provoque le chancre des tiges, la brûlure des semis, la pourriture charbonneuse, le flétrissement, la brûlure des feuilles (Fig. 24B), la brûlure des tiges et la fonte des semis en prélevée et en post levée, la pourriture sèche des racines et la pourriture de la tige des arbres forestiers, des arbres fruitiers et des espèces de mauvaises herbes. En fait, *M. phaseolina* attaque un large éventail d'hôtes dans plus de 500 espèces de plantes cultivées et sauvages (Kaur et al., 2012 ; Abbas et al., 2020). Les principaux hôtes cultivés comprennent l'arachide, le chou, le poivre, le pois chiche, le soja, le tournesol, la patate douce, la luzerne, le sésame, la pomme de terre, le sorgho, le blé et le maïs.

M. phaseolina continue de causer d'énormes pertes économiques dans de nombreuses cultures (Kaur, 2012; Chavan et al., 2019). Parmi les nombreuses cultures importantes et économiques infectées, il y a aussi le soja, une légumineuse qui est l'une des cultures les plus importantes au monde pour son utilisation dans l'agro-alimentaire et comme industrie pétrolière biosourcée. Il n'est pas seulement utilisé pour la consommation humaine, mais aussi pour produire à faible coût et à haute teneur en protéines produites en vrac en tant qu'ingrédients dans plusieurs aliments (Lusas et al., 1995). Le soja a également été génétiquement modifié, et il représente 40 % de la production totale dans le monde et il est essentiellement cultivé en Asie, au Brésil, aux États-Unis, en Inde et en Argentine (Pagano et Miransari, 2016). Le genre *Macrophomina* a été établi pour la première fois par Petrak (1923) avec la description de *M. philippinensis*. *M. phaseolina* a également été identifié dans le maïs (Vörös – Manninger, 1973).

Simay en 1991 a trouvé ce champignon chez *Solanum tuberosum, Helianthus tuberosus, Phaseolus vulgaris, Vicia faba, Allium sativum*, de plus il a également été identifié chez *Beta vulgaris* (Koppányi, 1993), *Cannabis sativa, Valeriana officinalis* (Simay-Kadlicskó, 1993) , *Capsicum annuum* (Fischl et al., 1995), *Citrullus lanatus* (Békési et al., 1995) *Prunus armeniaca* (Vajna-Rozsnyai, 1995) et *Picea pungens* (Fischl et al., 2008).

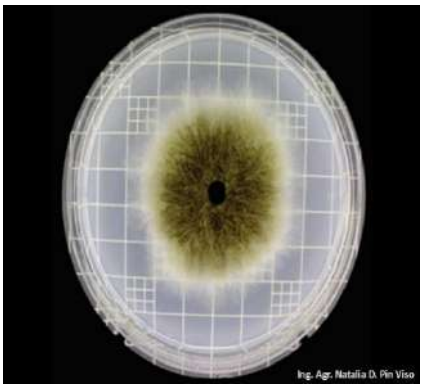

Figure 24. A. Colonie de *M. phaseolina* poussant sur PDA après 7 jours (Lane et *al*., 2020).

3.2.2- Métabolites bioactifs produits par les champignons phytopathogènes

Les champignons phytopathogènes produisent plusieurs métabolites bioactifs qui ont une grande diversité fonctionnelle. Ils pourraient être impliqués dans l'interaction avec l'hôte, la virulence, la protection contre le stress biotique ou abiotique et dans certains cas, ils pourraient être impliqués dans des relations symbiotiques (Nielsen et *al*., 2017, Ebert et *al*., 2019).

3.2.2.1- Métabolites des espèces *Drechslera*

Drechslera est un genre fongique bien connu pour produire de nombreux métabolites secondaires phytotoxiques. La plupart des espèces phytopathogènes de *Drechslera* et leurs phytotoxines ont été largement étudiées comme agents de maladies très graves des cultures céréalières telles que le riz, le maïs et le sorgho, en provoquant des lésions de taches brunes sur les feuilles (Au et al., 2000 ; Bury et *al*., 2013a ; Evidente et *al*., 2006 ; Fayzalla et *al*., 2010).

L'ophioboline A a été le premier et le plus représentatif composé isolé des espèces de *Drechslera* (Fig. 25). Ce métabolite était la principale phytotoxine produite par le pathogène du riz *Helminthosporium orizae* (ou *Cochliobolus orizae*, ou *Drechslera orizae*, ou *Bipolaris orizae*) (Nozoe et al., 1965; Canonica et al., 1966). Plusieurs ophiobolines proches de l'ophioboline A ont été isolées de différents champignons et ont montré des activités biologiques différentes, telles que revues par Au et al., (2000) et la plus récente par Masi et al., (2019).

3.2.2.2- Métabolites secondaires produits par *Macrophomina phaseolina*

Il a été rapporté que *M. phaseolina* produisait différents métabolites secondaires (Salvatore et *al.*, 2020). En effet, des études ont été menées pour étudier les phytotoxines produites par l'agent pathogène et potentiellement impliquées dans la pourriture charbonneuse (Evidente et *al*., 2019). La phaséolinone, un séquiterpénoïde érémophilane, qui inhibe la germination des graines de gram noir (*Phaseolus mungo* L.), a d'abord été isolée à partir de filtrats de culture de *M. phaseolina* et sa structure a été déterminée par des méthodes spectroscopiques et chimiques (Dahr et *al*., 1982). La phaséolinone a été isolée en Inde à partir des filtrats couture de *M. phaseolina* avec l'asperline, l'isoasperline, l'acide phaséolinique et l'acétylphomalactone. Tous ces métabolites ont pu provoquer une nécrose foliaire non spécifique sur plusieurs plantes, mais seule la phaséolinone a induit des symptômes de maladie chez les plantes similaires à ceux causés par l'agent pathogène (Bhattacharya et *al*., 1992).

Lorsque *M. phaseolina* a été cultivée dans le Mississippi, la phaséolinone n'a pas été produite. mais la principale phytotoxine semble être la (-)-botryodiplodine (Ramezani et al., 2007), une mycotoxine précédemment isolée de *Botryodiplodia theobromae*, un champignon qui provoque la pourriture des fruits tropicaux (Sen Gupta et al., 1966).Récemment, les métabolites produits par une souche de *M. phaseolina* isolée *d'Eucalyptus globulus* ont été étudiés et identifiés comme les métabolites fongiques bien connus (3R,4S)-botryodiplodine, acide succinique, tyrosol, (R)-melleine, et cis-(3R,4R)-4-hydroxymelleine et acide azélaïque. Cependant, aucune activité biologique n'a été signalée pour ces métabolites (Salvatore et *al*., 2020).

Le soja devient une culture très importante pour l'agriculture en Argentine. Cependant, les conditions de croissance en monoculture et en semis direct ont favorisé l'apparition et la sévérité d'un grand nombre de maladies, qui constituent une contrainte sérieuse à la production et à la qualité de la légumineuse. Ainsi, de nombreuses études ont été menées pour développer des méthodes basées sur leur biocontrôle. Certaines bactéries ont été évaluées en double test *in vitro* pour leur activité antifongique associée au phosphate de manganèse. Deux souches ont été sélectionnées comme *Pseudomonas fluorescens* et *Bacillus subtilis*. Par conséquent, l'expérience en serre démontre que les plus grandes réductions de la gravité de la maladie du soja induite par *M. phaselina* ont été obtenues lorsque la souche *P. fluorescens* a été appliquée seule ou lorsque la souche *B. subtilis* a été combinée avec du phosphite de manganèse, atteignant 82 % de contrôle dans les deux cas (Simonetti et *al*., 2015). Récemment, une souche de *Pseudomonas donghensis* SVBP6, isolée d'une parcelle agricole en Argentine, a montré une activité antifongique à large spectre et diffusible. À partir de ses filtrats de culture, le principal

métabolite antifongique a été isolé et identifié comme étant la 7-hydroxytropolone qui a montré une activité antifongique significative contre M. phaseolina. Ce résultat est très important pour son application pratique potentielle en tant que fongicide naturel facilement synthétisé et bioformable et en tant que précurseur de nouveaux composés tropolonoïdes bioactifs (Muzio et *al*., 2020).

3.3- Matériels et méthodes

3.3.1- Production, extraction et purification de métabolites bioactifs de *D. gigantea*

3.3.1.1- Production de *Dreschlera gigantea*

La souche *D. gigantea* N. 7004 a été isolée par Prof. R. Charudattan, lors de vastes prospections sur le terrain en Floride, à partir de *Digitaria sanguinalis* naturellement infectée (Chandramohan et Charudattan, 2001), la production a été faite.

3.3.1.2- Procédures générales

Différentes analyses ont été réalisées pour isoler et confirmer les structures chimiques des composés obtenus ; à savoir RMN 1D et 2D, HRESIMS, ESIMS, LC/MS, HPLC, Chromatographie sur colonne et CCM analytiques.

3.3.1.3- Extraction et purification des métabolites secondaires du filtrat de culture de *Drechslera gigantea*

Le matériel lyophilisé obtenu à partir des filtrats de culture (4 L) a été dissous dans de l'eau distillée (400 ml, pH final de 4,5) et extrait avec EtOAc (3 x 400 ml). Les extraits organiques ont été combinés, séchés avec Na2S04, filtrés et évaporés sous pression réduite pour obtenir un résidu huileux brun (1,2 g). Ce dernier a été purifié sur gel de silice élué avec CHCl3-i-PrOH (96:4, v/v) obtenant onze groupes de fractions homogènes.

La purification donnant des cristaux blancs d'ophioboline A (11, 448,2 mg, figure 27), deux solides amorphes homogènes identifiés comme étant la 3-anhydre-6-épi-ophioboline A (13, 13,2 mg, Fig. 27) et la 6-épi-ophioboline A (12, 7,9 mg). Un solide amorphe, qui étant nouveau nommé drophiobolin B (16, 1,9 mg, Fig. 27), un autre solide amorphe identifié comme l'ophioboline I (14, 8,9 mg, Fig. 27) et un autre le solide amorphe, qui étant nouveau nommé drophiobolin A (15, 1,2 mg, Fig. 27) ont aussi été obtenus.

3.3.1.4- Tests biologiques

- Activité phytotoxique

L'activité phytotoxique des drophiobolins A et B et de l'ophioboline A a été testée à 10-3 et 10-4 M par un test de perforation des feuilles sur des adventices (*Digitaria sanguinalis* L. et *Chenopodium album* L) et des plantes cultivées (*Lycopersicon esculentum* L.), comme précédemment rapporté (Liu et al., 2019). Les composés ont été dissous dans une petite quantité de MeOH puis dilués à la concentration souhaitée avec de l'eau distillée (concentration finale de MeOH 2%).

- Test d'activité cytotoxique MTT

L'effet des drophiobiolins A et B sur la viabilité cellulaire a été évalué sur des kératinocytes cutanés Hacat humains immortalisés et des lignées cellulaires dérivées de tumeurs A431 (carcinome épidermoïde), H1299 (carcinome pulmonaire non à petites cellules) et HeLa B (adénocarcinome du col de l'utérus). La cytotoxicité des drophobiolines A et B a été comparée à celle de l'ophioboline A.

Toutes les expériences ont été réalisées trois fois et présentées sous forme de moyenne ± écart type calculé à l'aide du logiciel GraphPad Prism8. L'analyse de la variance a été réalisée par ANOVA à un facteur et des comparaisons multiples. *P < 0,5 par rapport au témoin.

3.3.2- Production, extraction et purification de métabolites bioactifs à partir de *Macrophomina phaseolina*

3.3.2.1- Production de *Macrophomina phaseolina*

La souche *M. phaseolina* 2013-1 a été obtenue à partir de racines de soja infectées poussant à Pergamino, province de Buenos Aires, Argentine et maintenue sur gélose pomme de terre dextrose (PDA) dans une boîte de Pétri. L'isolat a été déposé dans la collection de cultures fongiques du Département de pathologie végétale de l'Université de Buenos Aires (FAUBA, Argentine). Plus tard, l'isolat a été cultivé dans des conditions stationnaires dans des flacons de 2 L contenant 1 L de PDB. Chaque flacon a été inoculé avec 15 bouchons mycéliens et incubé à 25 °C dans l'obscurité pendant 15 jours. Ensuite, les tapis mycéliens ont été éliminés par centrifugation (7000 rpm pendant 30 min) et filtration successive du surnageant à l'aide de membranes de diamètre de pores de 0,22 µm (Whatman, Maidstone, UK).

3.3.2.2- Extraction et purification des métabolites secondaires de *M. phaseolina*

Les filtrats de culture (4 L), montrant une activité phytotoxique significative sur tomate (*S. lycopersicum* L.), ont été réunis, et concentrés sous vide à température ambiante jusqu'à 400

mL. Ensuite, la culture a été acidifiée à pH 2 avec de l'acide formique et extraite de manière exhaustive avec EtOAc (3 x 400 mL). Les extraits organiques combinés ont été séchés, filtrés et évaporés sous pression réduite. Le résidu organique (109,7 mg) a été purifié par CC sur gel de silice élue avec EtOAc-MeOH-H20 (85:10:5, v/v/v) obtenant huit groupes de fractions homogènes. Le résidu de la seconde fraction (8,3 mg) a été purifié sur TLC élue avec CH2C12-MeOH, (1:1, v/v), donnant la guignardone A (8, 3,6 mg, figure 37) sous la forme d'un solide amorphe. Le résidu de la septième fraction (20,2 mg) a été encore purifié sur TLC élue avec CHCl3-EtOAc-MeOH-H2O (2:2:1, v/v/v) donnant les phaseocyclopenténones A (9, 10,2 mg, Fig. 37) et B (10, 7,5 mg, fig. 37) sous forme de deux huiles jaunâtres.

- Dérivé 3,5-Di-O-acétyle de la phaséocyclopenténone A (20)

La phaseocyclopenténone A (9, 1 mg) a été acétylée avec de la pyridine (20 L) et de l'Ac2O (20 L). La réaction a été laissée à température ambiante dans l'obscurité pendant 48 h et arrêtée par évaporation sous flux de N2. Le résidu (1,2 mg) a été purifié par CCM, élue avec CH2C12-MeOH (9:1, v/v) pour donner (11) sous la forme d'un composé homogène.

3.3.2.3- Tests biologiques

- Activité phytotoxique

Les mêmes deux tests de phytotoxicité du 1 ^{er} chapitre ; bouturage sur la tomate et perforation des feuilles sur la tomate et le soja, ont été réalisés pour l'extrait organique et les métabolites obtenus ; phaséocyclopenténones A et B et les composés 17 et 19 ; dans ce chapitre 3.

- Activité antifongique

Le potentiel antagoniste des composés (17-19) a été testé contre deux souches de champignons pathogènes du soja, *Cercospora nicotiane* (Sautua et *al*., 2020) et *Colletotrichum truncatum* (Ramos et *al*., 2013) isolées en Argentine, en tant qu'inhibition de la croissance radiale mycélienne. En bref, des bouchons mycéliens de 6 mm de diamètre provenant d'une culture de 4 jours de *C. nicotianae* ou *C. truncatum* ont été placés au centre des plaques PDA.

3.4- Résultats et discussion

3.4.1- Caractérisation structurale des métabolites secondaires de *Dreschslera gigantea*

L'extrait organique obtenu à partir des filtrats de culture de *D. gigantea* a été purifié, comme détaillé dans la section expérimentale, l'obtention de quatre composés se sont avérés être des ophiobolines bien connues, ophioboline A, 6-epi-ophioboline A, 3-anhydro-6-epi -ophioboline A et ophioboline I (11-14, Fig. 27). Ils ont été identifiés en comparant leurs données

spectroscopiques (RMN 1H et ESIMS) avec les données rapportées (Evidente et al., 2006). Les deux autres nouveaux sesterterpénoïdes ophiobolan, nommés drophiobiolins A et B (15 et 16, Fig. 27). L'enquête RMN 1H et 13C préliminaire a montré que la drophiobolin A (15) était proche de la 3-anydrophiobolin A (Kim et al., 1984; Pena-Rodriguez et Chilton, 1989) tandis que les drophiobiolins B (16) apparaissaient proches de l'ophiobolin I (14) (Evidente et al., 2006).

- L'ophiobolin A (11) a été obtenue sous forme de cristaux blancs, le spectre 1H-RMN est très similaire à ceux précédemment rapportés (Li et al., 1995 ; Sugawara et al., 1987 ; Canales et al., 1988 ; Evidente et al., 2006) ESIMS m/z : 385 [M+H]+, 407 [M+Na]+, 423 [M+K]+. Ces données sont en accord avec celles précédemment rapportées (Sugawara et al., 1988).

- La 6-épi-ophioboline A (12) a été obtenue sous la forme d'un solide amorphe homogène, le spectre 1H RMN était très similaire à ceux précédemment rapportés (Sugawara et al., 1987; Canales et al., 1988; Evidente et al., 2006). ESIMS (+) m/z : 401 [M+H]+, 423 [M+Na]+, 439 [M+K]+.

- La 3-anhydre-6-épi-ophioboline A (13) a été obtenue sous la forme d'un solide amorphe homogène, Le spectre 1H-RMN est très similaire à ceux précédemment rapportés (Sugawara et al., 1987; Canales et al., 1988 ; Evidente et al., 2006) uniquement pour les signaux suivants, : 2,24 (1H, dd, J=6,7 et 3,8 Hz, H-15), 1,99 (1H, dd, J=13,2, 2,5 Hz , H-13A), 1,80 (H, m, H-12A), 1,42 et 1,77 (1H chacun, m H2C-1); ESIMS (+) m/z : 383 [M+H]+, 405 [M+ Na]+, 421 [M+K]+.

- L'ophiobolin I (14), obtenue sous forme de cristaux blancs. Le spectre 1H RMN et ESIMS m/z : 385 [M+H]+, 407 [M+Na]+, 423 [M+K]+ sont très similaires à ceux précédemment rapportés (Li et al., 1995 ; Sugawara et al., 1987 ; Sugawara et al. , 1988 ; Evidente et al., 2006).

- La drophiobolin A (15) a été obtenue sous la forme d'un solide amorphe, avait : IR max 3422, 1734, 1615 cm-1; UV max (log □) 275 (3,6) nm; Les RMN 1H et 13C (figures 13 et 14) sont rapportées dans le tableau 3; HR ESIMS (+) : m/z 1229 [3 M+ Na]+, 805 [2 M + H]+, 425 [M + Na]+, 403,2858 [calculé pour C25H39O4 403,2848 M + H]+, 385 [M + H - H2O]+, 367 [M + H - 2x H2O]+.

- La drophiobolin B (16) a été obtenue sous la forme d'un solide amorphe, avait : IR max 3421, 1737, 1646, 1614 cm-1; UV max (log □) 276 (3,6) nm; Les RMN 1H et 13C (figures 20 et 21)

sont rapportées dans le tableau 3; HR ESIMS (+) : m/z 819 [2M + Na]+, 797 [2M + H]+, 399,2526 [calculé pour C25H35O4 399,2535, M + H]+, 381 [M + H - H2O]+ (Fig. 26) .

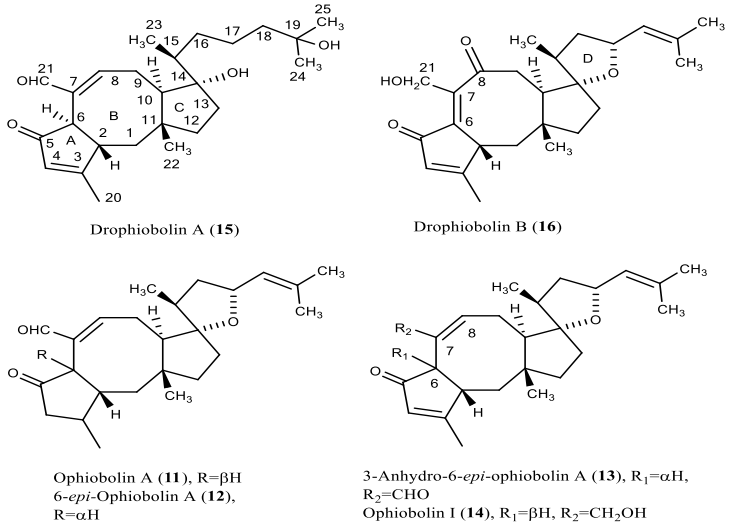

Figure 27. Structures de la drophiobolin A et B (15-16), de l'ophioboline A, de la 6-épi-ophioboline A, de la 3-anhydro-6épiophioboline A et de l'ophioboline I (11-14).

La configuration relative des drophiobolins A et B (15 et 16) a été déduite des corrélations observées dans les spectres NOESY correspondants (Berger et Braun, 2004). La configuration absolue (CA) des drophiobolins A et B (15 et 16) a ensuite été attribuée par comparaison des spectres expérimentaux et calculés par TDDFT de dichroïsme circulaire électronique (ECD) (Autschbach, 2012),

3.4.1.1- Tests biologiques

- Activité phytotoxique

L'activité phytotoxique des drophiobolins A et B, comparée à celle de l'ophioboline A, a été testée par test de perforation foliaire sur la plante adventice hôte (*Digitaria sanguinalis* L.) et adventice non hôte (*Chenopodium album* L.) et cultivée (*Lycopersicon esculentum* L.) plantes. Lorsqu'ils ont été testés à 10-3 M (tableau 13, figure 35), les deux (15 et 16) ont montré la même forte phytotoxicité de l'ophioboline A sur la plante hôte et la tomate. Une toxicité plus faible a été observée sur *C. album* par rapport à (11). A 10-4 M, la toxicité de (15 et 16) diminue légèrement sur toutes les plantes testées, (15) étant inactif sur *C. album*.

- Activité cytotoxique MTT

L'évaluation de la cytotoxicité *in vitro* a été réalisée dans des cellules cancéreuses A431, Hela B, H1299 ainsi que dans des kératinocytes immortalisés Hacat. Les expérimentations avec les nouvelles ophiobolines, les drophiobolins A et B, ont été réalisées en parallèle avec

l'ophioboline A déjà décrite. Après 24h de traitement, des doses croissantes (de 0,5 à 10 M) de (15) ou (16) ont légèrement réduit la viabilité cellulaire de Hacat (jusqu'à 63%) et A431 (jusqu'à 72%) tandis que la viabilité des cellules Hela B était significativement réduite (jusqu'à 50%, IC_{50} 10 M). Ophiobolin A, à la place, a eu des effets dramatiques sur ces lignées cellulaires. H1299 avait un comportement très différent étant stimulé par la drophiobolin A à toutes les concentrations testées alors que la drophiobolin B était inefficace. Il est intéressant de noter que l'ophioboline A, dont il a été précédemment démontré qu'elle avait de puissants effets anticancéreux contre le glioblastome (Dasari et al., 2015), semble être presque inefficace sur les cellules cancéreuses du poumon H1299, montrant ainsi une spécificité des cellules tumorales.

Les données sont exprimées en absorbance et présentées comme moyenne ± SD de trois expériences indépendantes, chacune réalisée en triplicata. L'analyse de la variance a été réalisée par Anova à sens unique et des comparaisons multiples*P<0,5 par rapport au témoin.

3.4.2- Caractérisation structurale des métabolites secondaires de *M. phaseolina*

L'extrait organique des filtrats de culture de *M. phaseolina*, obtenu comme décrit dans la section expérimentale, a été fractionné par une combinaison de chromatographie sur colonne et CCM pour donner trois métabolites purs (17-19) qui ont été isolés et identifiés. Deux nouveaux métabolites, nommés phaséocyclopenténones A et B (18 et 19, Fig. 53) et un métabolite connu identifié comme la guignardone A (17, Fig.53).

Le méroterpénoïde (17) a été isolé pour la première fois en tant que métabolite de *M. phaseolina*. Il a montré les mêmes propriétés physiques (rotation optique spécifique) et spectroscopiques (1H, 13C, COSY, HSQC et HMBC RMN et ESIMS) par rapport à celles rapportées après son premier isolement à partir de *Guignardia mangiferae*, un champignon endophyte isolé des feuilles *d'Ilex cornuta* (Yuan et al., 2010). Le méroterpénoïde fongique bien connu guignardone A (17) a été isolé pour la première fois à partir de *M. phaseolina*, qui s'est montré auparavant ne produire que le sesquiterpène toxique eremophilane phaseolinone (Dhar et *al*., 1982) et le polykétide botryodiplodine, qui est également une toxine produit par d'autres champignons phytopatogènes (Capasso et *al*., 1984; Bhattacharya et *al*., 1992). Une étude préliminaire des spectres RMN ^{1}H et ^{13}C des deux métabolites spécialisés (18 et 19), isolés de la souche argentine de *M. phaseolina*, a montré qu'ils partageaient deux caractéristiques structurelles telles qu'un phényle monosubstitué et un résidu cyclopenténone.

La guignardone A (17), obtenue sous forme de solide amorphe. Les spectres RMN ^{1}H, ^{13}C, COSY, HSQC et HMBC et ESIMS étaient très similaires à ceux précédemment rapportés (Yuan et *al*., 2006).

La phaséocyclopenténone A (18) a été obtenue sous forme d'huile jaunâtre, avait : IR Amax, 3332 (OH) ; 1719 (C=O), 1676 (C=C); (1597, 1530, 1503 (Ar) ; UV λmax nm (log ε); 279 (4,54) 248 (4,45); les données RMN 1H et 13C; HR ESIMS (+), m/z 643 [2M + Na]+, 311.0927 [M+ H]+ [(calculé pour C18H15O5, 311.0919)] 293 [M + H - H2O]+ ; HR ESIMS (-), m/z 619 [2M - H]- ; 309.0773 [M – H]- (calculé pour C18H13O5, 309.0763).

La phaseocyclopenténone B (19) a été obtenue sous forme d'huile jaunâtre, avait IR Amax, 3309 (OH), 1705 (C=O), 1627 (C=C) 1598, 1524, 1496 (Ar); UV max nm (log), 277 (4,38); Les données RMN 1H et 13C sont rapportées dans le tableau 11; HRESIMS (+), m/z 555 [2M + Na]+, 533 [2M + H]+ 267.1023 [M + H]+ (calculé pour C17H14O3, 267.1021).

Dérivé 3,5-Di-O-acétyle de la phaséocyclopenténone A (20) had, RMN 1H : 8,04 (2H, d, J = 8,0 Hz, H-2',H-6'), 7,95 (2H, d, J = 8,0 Hz , H-2'', H-6''), 7,52 (1H, t, J = 8,0 Hz, H-4'), 7,44 (2H, t, J = 8,0 Hz, H-3',H-5'), 7,29 (2H, t, J = 8,0 Hz, H-3'', H-5''), 7,21 (1H, t, J = 8,0 Hz, H-4''), 6,14 (1H, s, H-5), 2,09 (3H, s, MeCO-C3), 1,92 (3H, s, MeCO-C5) ESIMS (+), m/z 395 [M + H]+.

- Configuration relative et absolue (CA) des phaséocyclopenténones A et B

La configuration relative aux carbones C-4 et C-5 a été attribuée par les corrélations observées dans le spectre NOESY entre leurs protons géminés (Berger et Braun, 2004). Ainsi, H-4 et H-5 étaient en position cis, et la configuration relative était (4R*,5S*). Les deux métabolites (18 et 19) ont résisté à la cristallisation, ainsi que le dérivé (17). Ainsi, la CA des phaséocyclopenténones A et B (18 et 19) a été déterminé au moyen du dichroïsme circulaire électronique (DCE), en utilisant une procédure standardisée (Pescitelli et Bruhn, 2016 ; Superchi et *al*., 2018 ; Grauso et *al*., 2019). Les spectres ECD de (18 et 19) ont été enregistrés dans MeCN et simulés à l'aide d'une procédure établie. La comparaison entre les spectres expérimentaux et calculés a permis d'attribuer la configuration absolue comme (4S,5R)- (18) et (4R,5S)- (19).

3.4.2.1- Tests biologiques

- Activité phytotoxique

L'activité phytotoxique a été testée à l'aide de deux essais biologiques différents. Le filtrat de culture, l'extrait organique (à une concentration de 1 mg/mL) et les composés (18 et 19) (à une concentration de 10-3 M) ont été testés sur tomate (*S. lycopersicum* L.) par bouturage. Une forte

phytotoxicité a été observée en testant le filtrat de culture et l'extrait organique et la phaseocyclopenténone B (19) qui a provoqué un fort flétrissement tandis que de légers symptômes ont été détectés pour les plantes traitées avec le composé (18). Les composés (18 et 19) ont également été testés par ponction foliaire sur tomate et sur soja (*Glycine max* L.), en association avec la guignardone A (17) (obtenue en moindre quantité), à une concentration de 10-3 et 10 -4 M. les composés (17-19) a montré une phytotoxicité sur tomate aux deux concentrations alors qu'aucune activité n'a été observée sur la plante hôte. Le composé (17) a induit une nécrose marquée par rapport à celle des composés (18 et 19) surtout à la concentration la plus élevée.

Ces résultats ont démontré l'importance des substituants présents en C-4 et C-5 dans les composés (18 et 19) pour conférer la phytotoxicité mais aussi un mécanisme d'action différent dans les deux bio-essais. Il s'agit du premier rapport sur l'activité phytotoxique de la guignardone A également par rapport aux autres méroterpénoïdes appartenant au même groupe de composés naturels.

- Activité antifongique

Les métabolites (17-19) n'ont présenté aucune activité antifongique contre *Colletotrichum truncatum* et *Cercospora nicotianae*, deux champignons pathogènes du soja.

4- Discussion générale

L'objectif de cette thèse était l'isolement de composés bioactifs produits par les champignons et les plantes méditerranéens. Ces métabolites bioactifs pourraient jouer un rôle intéressant en agriculture en tant qu'agents de lutte biologique contre les adventices ou des maladies spécifiques des plantes (Scharf et al., 2014 ; Cimmino et al., 2015 ; Masi et al., 2018b). Parmi elles, les phytotoxines pourraient également être un outil utile, pour développer des méthodes de diagnostic spécifiques et rapides, afin de sélectionner des plantes naturellement résistantes au pathogène identifiant les gènes de résistance innée (Evidente et *al*., 2014, Cimmino et al., 2015 ; Masi et *al*., 2018a ; Evidente et *al*., 2019).

Pour cette raison, il pourrait être intéressant de comparer les métabolites de phytotoxines isolés du macrochampignon comestible *Agaricus litoralis* et de la plante *Dittrichia viscosa* de différents écosystèmes du bassin méditerranéen avec ceux obtenus à partir des deux champignons phytopathogènes d'Argentine : *Dreschlera gigantea* et *Macrophomina phaseolina* en tant que micro-organismes modèles produisant des phytotoxines. Par exemple, un métabolite phytotoxique bien connu, nommé tyrosol, produit par *Agaricus litoralis*, un

macrochampignon comestible, a déjà été isolé à partir de micro-organismes, de macrochampignons et de plantes, mais il s'agit du premier signalement *d'A. litoralis* en tant que métabolite phytotoxique. Par ailleurs, il est important de souligner que le macrochampignon A. litoralis a été collecté et identifié pour la première fois dans cette enquête, dans la région de Constantine, à l'Est de l'Algérie. Son identification a été basée sur des techniques morphologiques et moléculaires, deuxième objectif de ce chapitre.

Les deux sesquitepenoids, inuloxine D et E, isolés de la plante *Dittrichia viscosa* ont montré une activité herbicide intéressante contre *Orobanche cumana*. Ce résultat pourrait être comparé à celui obtenu dans une étude précédente (Andolfi et al., 2013), dans laquelle les lactones sesquiterpéniques produites par *D. viscosa* à savoir les inuloxines A, C et D ont une activité herbicide statistiquement significative contre *l'Orobanche crenata* et *Cuscuta campestris*. De plus, les deux nouveaux sesterpénoïdes ; les drophiobiolines A et B, ainsi que l'ophiobioline A obtenue à partir de *D. gigantea* ont révélé un effet phytotoxique remarquable contre *Digitaria sanguinalis*. Ces découvertes intéressantes sont similaires à celles rapportées par de nombreux chercheurs (Kim et *al*., 1999 ; Evidente et *al*., 2006 ; Tian et *al*., 2017) montrant que les métabolites de l'ophioboline produits par des champignons pathogènes, attaquant les cultures agricoles, ont des propriétés phytotoxiques importantes.

L'évaluation de l'activité antiproliférative a révélé que les drophiobolins A et B présentaient une cytotoxicité contre les cellules Hela B avec une valeur IC50 de 10 M. Cependant, ils ont eu moins ou pas d'effet contre les cellules Hacat, H1299 et A431 par rapport à l'ophioboline A. Nos résultats pourraient être comparables à ceux d'autres études (Evidente et *al*., 2014 ; Ebada et Proksch, 2015 ; Tommonaro et *al*, 2015 ; Tian et *al*., 2017) qui ont confirmé les activités biologiques des ophiobolines, notamment cytotoxiques et antimicrobiennes.

Par ailleurs, les différents bioessais des phaséocyclopenténones A et B, isolées de *M. phaseolina* collectés en Argentine, ont montré des propriétés phytotoxiques intéressantes sur la plante non-hôte *Solanum lycopersicum* L., tandis que la guignardone A s'est révélée inactive dans un essai de bouturage. Les trois composés phaséocyclopenténones A et B et la guignardone A étaient inactifs sur la plante hôte de soja, *Glycine max* L. Cette dernière a été isolée pour la première fois de *M. phaseolina* qui s'est révélée auparavant ne produire que le sesquiterpène toxique eremophilane phaseolinone (Dhar et *al*., 1982) et le polykétide botryodiplodine, qui est une toxine également produite par d'autres champignons phytopatogènes phaséolinone (Ramezani et *al*., 2007; Sen Gupta et *al*., 1966).

Les métabolites fongiques contenant un noyau de dihydroxycyclopenténone sont déjà connus comme des composés naturels tels que les kodaistatines A–D produites par *Aspergillus terreus* avec une activité antidiabétique qui sont similaires à la phaseocyclopenténone A mais ils diffèrent par la position des substituants attachés au noyau (Peter et Brückner, 2018). Cependant, le composé le plus proche de la phaseocyclopenténone A est un composé synthétique préparé par une réaction d'oxydation catalysée par l'or de carbonates ou d'acétates propargyliques en utilisant la 3,5-dichloropyridine (Sun, Chen et Liu, 2014). Deux métabolites fongiques, nommés involutine et chamonixine, sont les composés naturels les plus proches de la phaseocyclopenténone B mais ils diffèrent par la position et la nature des substituants sur le noyau de cyclopenténone (Feling et *al*., 2001a).
Pour l'activité antifongique, les trois composés étaient inactifs contre *Cercospora nicotiane* et *Colletotrichum truncatum*.

5. Conclusion et perspectives

Dans le présent travail, différents métabolites bioactifs ayant une activité herbicide et fongicide potentielle, produits par des champignons et des plantes méditerranéens, ont été isolés et caractérisés comme indiqué ci-dessous :

Un macro-champignon comestible *Agaricus litoralis* collecté dans la région de Constantine (Est algérien), a été identifié sur la base à la fois d'observations morphologiques et d'analyses de séquences d'ADN de la région ITS. A partir de son extrait EtOAc, son principal métabolite phytotoxique a été isolé et identifié comme le tyrosol. Lorsqu'il a été testé par le test de perforation foliaire, il a montré une forte phytotoxicité *Vitis vinifera* L., *Prunus armeniaca* L., *Prunus persica* (L.) Batsch, *Cucurbita* L., et *Rubus fruticosus* L., tandis qu'une phytotoxicité modérée et faible a été enregistrée sur *Solanum melongena* L., *Ficus carica* L. et *Citrus limon* (L.) Osbeck ; respectivement.

Un nouveau sesquitpénoïde nommé inuloxine E et quatre métabolites connus ; L'acide α-costique, les inuloxines A, C et D, ont été isolés et identifiés à partir de la partie aérienne de *Dittrichia viscosa*. Dans laquelle, les deux inuloxines D et E, ainsi que les quatre dérivés de l'inoluxine D n'ont pas induit la germination des deux mauvaises herbes parasites *Orobanche minor et Phelipanche ramosa* mais ils étaient actifs sur les graines *d'Orobanche cumana*, induisant leur germination.

Deux nouveaux sesterterpénoïdes ophiobolan nommés drophiobiolins A et B, ainsi que quatre sesterterpénoïdes bien connus ; l'ophioboline A, la 6-épi-ophioboline A, la 3-anhydro-6-épi-ophioboline A et l'ophioboline I ont été isolées de la culture liquide de *D. gigantea*, puis identifiées à l'aide d'analyses spectroscopiques ; RMN et ESI-MS. L'activité de phytotoxicité de ces molécules précédentes, sur plante cultivée (*Lycopersicon esculentum* L.), plante adventice hôte (*Digitaria sanguinalis* L.) et plante adventice non hôte (*Chenopodium album* L.), a également été détectée ; où les deux nouvelles drophiobiolins A et B ont montré une forte phytotoxicité en tant qu'ophioboline A sur les plantes cultivées et hôtes. Cependant, une toxicité plus faible a été observée sur la plante non hôte par rapport à celle de l'ophioboline A. De plus, les drophiobiolins A et B ont montré l'effet cytotoxique le plus élevé contre les cellules Hela B, mais elles ont eu un effet moins important contre les cellules Hacat, H1299 et A431.

En outre, deux nouvelles cyclopenténones penta- et tétra-substituées, nommées phaséocyclopenténones A et B, ont été isolées de la culture liquide de *M. phaseolina* avec le méroterpénoïde fongique bien connu guignardone A, puis identifiées par des analyses spectroscopiques. Dans les différents bioessais phytotoxiques, les phaséocyclopenténones A et B ont montré une forte phytotoxicité sur la plante non hôte (*Solanum lycopersicum* L.). A l'inverse, ces trois composés ; les phaséocyclopenténones A et B et la guignardone A étaient inactives sur la plante hôte soja (*Glycine max* L.).

En conclusion, les métabolites bioactifs isolés pourraient être exploités pour les utiliser dans le développement d'une méthode rapide et spécifique de diagnostic des maladies des plantes et comprendre leur rôle dans l'induction des symptômes de la maladie. De plus, ces métabolites pourraient être utilisés en agriculture comme biopesticides (herbicides, fongicides, insecticides naturels sûrs, etc.) et en médecine comme pro-drogue (anticancéreux, antibiotique, antipaludique, anti-inflammatoire, etc.) avec un nouveau mode d'action.

De nombreuses perspectives se dégagent de cette recherche. En effet, des études plus approfondies s'imposaient sur plusieurs points, à savoir :

- Trouver de nouveaux métabolites bioactifs avec une application pratique potentielle en agriculture ;
- Obtenir d'une variété de plantes hôtes résistantes aux maladies fongiques ;
- Synthétiser des dérivés pour la relation structure-activité.

Nom et Prénom : Roukia Zatout	**Date de sustenance:**

Titre : Potentiel de bio-contrôle des substances bioactives produites par des champignons et des plantes de différents écosystèmes du bassin méditerranéen.

Résumé

L'objectif principal de cette thèse porte sur l'étude des métabolites, ayant une activité herbicide et fongicide potentielle, produits par des champignons et des plantes du bassin méditerranéen. Ces métabolites bioactifs ont été caractérisés chimiquement et biologiquement à l'aide de procédés chromatographiques bio-guidés. En effet, le macro-champignon *Agaricus litoralis*, collecté de la forêt du Djebel el Ouahch de la région de Constantine à l'Est Algérien, a été identifié à l'aide des données morphologiques et moléculaires. De ce fait, une phytotoxicité élevée de son extrait d'EtOAc sur les feuilles de *Lycopersicon esculentum* L, plante de test, a été révélée d'où un métabolite phytotoxique connu en l'occurrence, tyrosol a été isolé et identifié par des méthodes spectroscopiques. L'activité phytotoxique de ce dernier a été testée sur sept plantes agraires et deux plantes sauvages en utilisant le test de perforation des feuilles. Les résultats obtenus ont révélé que l'effet toxique le plus élevé a été observé sur *Vitis vinifera* L., *Prunus armeniaca* L., *Prunus persica* L., *Batsch*, *Cucurbita* L. et *Rubus fruticosus* L. à 1 mg/mL, en revanche, des effets toxiques modérés ont été observés sur les feuilles de *Solanum melongena* L. et une phytotoxicité moindre sur les feuilles de *Ficus carica* L. et *Citrus limon* L. *Osbeck*. Par ailleurs, un nouveau sesquiterpénoïde appartenant au sous-groupe des seco eudesmanolides, nommé inuloxine E, a été isolé de *Dittrichia viscosa*, en plus des sesquiterpénoïdes déjà connus comme ; inuloxines A-D et l'acide α-costique. L'inuloxine E a été caractérisée par des techniques spectroscopiques, essentiellement RMN et ESIMS. Les deux inuloxines D et E ont inhibé la germination des semences de la mauvaise herbe parasite *Orobanche cumana* mais étaient inactives sur les graines d'O*robanche minor* et de *Phelipanche ramosa*. En outre, l'activité germinative de certains esters hémisynthétiques de l'inuloxine D a, également, été étudiée révélant leurs effets antigerminatifs sur *O. minor* et *P. ramosa*. Sur un autre volet, deux nouveaux sestertépénoïdes ophiobolanes bioactifs ; drophiobiolins A et B, caractérisées par RMN et HRESIMS, ont été obtenus à partir de *Drechslera gigantea*, un champignon connu comme mycoherbicide dans la lutte biologique contre *Digitaria sanguinalis*. En outre, d'autres métabolites caractéristiques à ce même champignon ont été obtenus en l'occurrence, l'ophioboline A comme principal métabolite, la 6-épi-ophioboline A, la 3-anhydro-6-épi-ophioboline A et l'ophioboline I. En effet, l'activité phytotoxique des drophiobiolins A et B a été recherchée par un test de perforation des feuilles sur des plantes ; adventice cultivée (*Lycopersicon esculentum* L.), adventice hôte (*Digitaria sanguinalis* L.) et non-hôte (*Chenopodium album* L.), où, ces deux ophiobolines nouvellement identifiées ont montré une phytotoxicité significative, à la concentration élevée de 10^{-3} M, en comparaison à celle-ci d'ophioboline A. L'activité antiproliférative des drophiobolins A et B a également été évaluée en révélant que les deux molécules présentaient une cytotoxicité remarquable contre les cellules Hela B avec une valeur d'IC_{50} égale à 10 M. Cependant, ils ont eu moins d'effet contre les cellules Hacat, H1299 et A431 en comparaison toujours à l'ophioboline A. Dans un autre axe, deux nouvelles cyclopenténones penta- et tétra-substituées, nommées phaséocyclopenténones A et B, ainsi que la guignardone A ont été purifiées à partir de *Macrophonina phaseolina*. Ce champignon phytopathogène a été isolé à partir de tissus de soja infectés présentant des symptômes de pourriture charbonneuse en Argentine. Les deux phaséocyclopenténones A et B ont été identifiées par des méthodes spectroscopiques (essentiellement RMN 1D « ^{1}H et ^{13}C » et 2D et HR-ESIMS). Lors d'un essai de phytotoxicité sur une plante non-hôte (*Solanum lycopersicum* L.) par ponction foliaire, les phaseocyclopenténones A et B et la guignardone A ont montré une activité phytotoxique intéressante. Ces nouveaux composés sont également actifs dans un essai de bouturage sur la même plante. En revanche, aucune phytotoxicité n'a été détectée par les trois composés sur la plante hôte de soja (*Glycine max* L.). En outre, aucune activité antifongique n'a été développée par les mêmes molécules contre certaines moisissures phytopathogènes, à savoir *Cercospora nicotiane* et *Colletotrichum truncatum*, qui ont également été isolées de plantes de soja infectées en Argentine.

Mots clés: Champignons; plantes; inuloxine E ; drophiobiolins A et B ; phaseocyclopenténones A et B ; activité fongicide et herbicide.

Laboratories

1. Laboratoire de Mycologie, de Biotechnologie et de l'Activité Microbienne (LaMyBAM), Université des Frères Mentouri, Constantine1.
2. Laboratoire de Substances Naturelles & Activités Biologiques (SNAB), University of Naples Federico II, Italy.

President:	**Khedara Abdelkarim**	**Pr. Université Mentouri, Constantine1**
Thesis Supervisors:	**Noreddine Kacem Chaouche**	**Pr. Université Mentouri, Constantine1**
	Evidente Antonio	**Pr. Université de Napoli Federico II**
Examiners:	**Marina Della Greca**	**Pr. Université de Napoli Federico II**
	Lucia Panzella	**Pr. University of Naples Federico II**
	Rihab Boushaba	**Pr. Université Salah Boubnider, Constantine3**

Name and Last name: Roukia Zatout	**Viva date:**

Title: Potential biocontrol of bioactive substances produced by fungi and plants from different ecosystems of the Mediterranean basin.

Abstract

The main objective of this thesis is the study of metabolites with a potential herbicidal and fungicidal activity, produced by fungi and plants of the Mediterranean basin. These bioactive metabolites have been characterized chemically and biologically using bio-guided chromatographic methods. Indeed, the macro-fungus *Agaricus litoralis*, collected in the forest of Jebel el Ouahch in the Constantine region in eastern Algeria, was identified using morphological and molecular data. As a result, a high phytotoxicity of its EtOAc extract on the leaves of *Lycopersicon esculentum* L., test plant, has been revealed from which a well-known phytotoxic metabolite, tyrosol, was isolated and identified by spectroscopic methods. The phytotoxic activity of this latter molecule, tyrosol, was tested on seven agrarian plants and two wild plants using the leaf puncture test. The obtained results revealed that the highest toxic effect was observed on *Vitis vinifera* L., *Prunus armeniaca* L., *Prunus persica* L. *Batsch, Cucurbita* L., and *Rubus fruticosus* L. at 1 mg / mL; while moderate toxic effects were observed on *Solanum melongena* L. leaves and less phytotoxicity on both *Ficus carica* L. and *Citrus limon* L. *Osbeck* leaves. Besides, a new sesquiterpenoid belonging to the seco eudesmanolides subgroup, called inuloxin E, has been isolated from *Dittrichia viscosa*, as well as the already known sesquiterpenoids inuloxins A-D, and α-costic acid. Inuloxin E was characterized by spectroscopic data, mainly NMR and ESIMS. Both inuloxins D and E inhibited the seed germination of the parasitic weed *Orobanche Cumana*, but they were inactive on the seeds of *Orobanche minor* and *Phelipanche ramosa*. Moreover, the germination activity of certain semisynthetic esters of inuloxin D has also been studied, revealing their anti-germinating effects on *O. minor* and *P. ramosa*. On another aspect, two new bioactive ophiobolan sestertepenoids ; drophiobiolins A and B, characterized by NMR and HRESIMS, were obtained from *Drechslera gigantea*, a fungus known as a mycoherbicide in the biological control of *Digitaria sanguinalis*. In addition, other metabolites characteristic of this same fungus were likewise obtained; ophiobolin A as the main metabolite, 6-epi-ophioboline A, 3-anhydro-6-epi-ophioboline A, and ophioboline I. In fact, the phytotoxic activity of drophiobiolins A and B was sought by a leaf perforation test on plants; cultivated weed (*Lycopersicon esculentum* L.), host weed (*Digitaria sanguinalis* L.), and non-host one (*Chenopodium album* L.) , where, these two newly identified ophiobolins showed significant phytotoxicity, at the highest concentration of 10-3 M, in comparison with that of ophiobolin A. The antiproliferative activity of drophiobolins A and B was also evaluated revealing that the two molecules exhibited a remarkable cytotoxicity against Hela B cells with an IC_{50} value equal to 10 M. However, they had less effect against Hacat, H1299 and A431 cells, compared to ophiobolin A. In another axis, two new penta- and tetra-substituted cyclopentenones; named phaseocyclopentenones A and B, as well as guignardone A were purified from *Macrophonina phaseolina*. This phytopathogenic fungus was isolated from infected soybean tissues showing symptoms of anthrax in Argentina. The two phaseocyclopentenones A and B were identified by spectroscopic methods (essentially 1D NMR "1H and 13C", 2D NMR, and HR-ESIMS). During a phytotoxicity test on a non-host plant (*Solanum lycopersicum* L.) by leaf puncture, phaseocyclopentenones A and B, as well as guignardone A displayed interesting phytotoxic activity. These new compounds are also active in a cuttings trial on the same plant. In contrast, no phytotoxicity of the three compounds was detected on the soybean host plant (*Glycine max* L.). Besides, no antifungal activity was developed by the same molecules against certain phytopathogenic molds, namely *Cercospora nicotiane* and *Colletotrichum truncatum*, which were similarly isolated from infected soybean plants in Argentina.

Key words: Mushrooms; plants; inuloxin E; drophiobiolins A and B; phaseocyclopentenones A and B; fungicidal and herbicidal activity.

Laboratories

1. Laboratoire de Mycologie, de Biotechnologie et de l'Activité Microbienne (LaMyBAM), Université des Frères Mentouri, Constantine1
2. Laboratoire de Substances Naturelles & Activités Biologiques (SNAB), University of Naples Federico II, Italy

President: Abdelkarim Khedara	**Pr. Mentouri Brothers University of Constantine1**
Supervisor: Noreddine Kacem Chaouche	**Pr. Mentouri Brothers University of Constantine1**
Antonio Evidente	**Pr. University of Naples Federico II**
Examiners: Marina Della Greca	**Pr. University of Naples Federico II**
Lucia Panzella	**Pr. University of Naples Federico II**
Rihab Boushaba	**Pr. Salah Boubnider niversity, Constantine3**